OAK RIDGE NATIONAL LABORATORY LIBRARIES
3 4456 0548253 6

CENTRAL RESEARCH LIBRARY
DOCUMENT COLLECTION

ORNL-3831
UC-25 – Metals, Ceramics, and Materials

STATUS AND PROGRESS REPORT FOR THORIUM FUEL CYCLE DEVELOPMENT FOR PERIOD ENDING DECEMBER 31, 1964

Compiled by
R. G. Wymer and D. A. Douglas, Jr.

CENTRAL RESEARCH LIBRARY
DOCUMENT COLLECTION
LIBRARY LOAN COPY
DO NOT TRANSFER TO ANOTHER PERSON
If you wish someone else to see this document, send in name with document and the library will arrange a loan.

OAK RIDGE NATIONAL LABORATORY
operated by
UNION CARBIDE CORPORATION
for the
U.S. ATOMIC ENERGY COMMISSION

Printed in USA. Price $6.00. Available from the Clearinghouse for Federal Scientific and Technical Information, National Bureau of Standards, U.S. Department of Commerce, Springfield, Virginia

LEGAL NOTICE

This report was prepared as an account of Government sponsored work. Neither the United States, nor the Commission, nor any person acting on behalf of the Commission:

A. Makes any warranty or representation, expressed or implied, with respect to the accuracy, completeness, or usefulness of the information contained in this report, or that the use of any information, apparatus, method, or process disclosed in this report may not infringe privately owned rights; or

B. Assumes any liabilities with respect to the use of, or for damages resulting from the use of any information, apparatus, method, or process disclosed in this report.

As used in the above, "person acting on behalf of the Commission" includes any employee or contractor of the Commission, or employee of such contractor, to the extent that such employee or contractor of the Commission, or employee of such contractor prepares, disseminates, or provides access to, any information pursuant to his employment or contract with the Commission, or his employment with such contractor.

ORNL-3831

Contract No. W-7405-eng-26

CHEMICAL TECHNOLOGY DIVISION

METALS AND CERAMICS DIVISION

STATUS AND PROGRESS REPORT FOR THORIUM FUEL CYCLE DEVELOPMENT FOR PERIOD ENDING DECEMBER 31, 1964

Compiled by
R. G. Wymer and D. A. Douglas, Jr.

MAY 1966

OAK RIDGE NATIONAL LABORATORY
Oak Ridge, Tennessee
operated by
UNION CARBIDE CORPORATION
for the
U. S. ATOMIC ENERGY COMMISSION

OAK RIDGE NATIONAL LABORATORY LIBRARIES

3 4456 0548253 6

The following technical personnel contributed to the work reported here:

Chemical Technology Division

R. E. Brooksbank
W. D. Bond
J. M. Chandler
S. D. Clinton
O. C. Dean*
D. E. Ferguson
P. A. Haas
C. C. Haws, Jr.
A. R. Irvine
A. T. Kleinsteuber
J. Klitgaard**
J. L. Matherne
K. H. McCorkle
A. B. Meservey
F. W. Miles
J. R. Parrott
R. J. Shannon
W. A. Shannon
D. M. Shepherd
J. W. Snider
J. W. Ullmann
R. G. Wymer

Plant and Equipment Division

J. W. Anderson
F. C. Davis
J. P. Jarvis

Metals and Ceramics Division

D. A. Douglas, Jr.
W. S. Ernst, Jr.
R. B. Fitts
H. J. Flamm†
J. P. Hammond
R. L. Hamner
Y. Hirose††
A. L. Lotts
E. J. Manthos
C. S. Morgan
A. R. Olsen
R. L. Pilloton
J. W. Prados‡
R. B. Pratt
J. M. Robbins
J. L. Scott
J. D. Sease
A. J. Taylor

Reactor Chemistry Division

P. B. Bien
E. L. Compere
J. C. Griess
D. N. Hess
M. J. Kelly
W. T. Rainey
P. E. Reagan
C. H. Secoy
A. J. Shor
B. A. Soldano

---

*Deceased
**Guest scientist from Denmark
†EURATOM visitor
††Visitor from Japan
‡Consultant from the University of Tennessee

TABLE OF CONTENTS

Page

1. Process Demonstration 1
   Solvent Extraction 1
   Sol-Gel Process 2
      Description of Process and Facility 2
      Facility Operation 2
      Radiation-Measurement Program 7
   Rod Fabrication (Kilorod) 12
      Fuel Rod Design and Production Flowsheet 13
      Utilization of Material 15
      Operating Experience 15
      Fabrication of ^{233}U-Bearing Fuel Rods for Irradiation Tests 24
      Kilorod Program Conclusions and Recommendations 30
2. Thorium-Uranium Fuel Cycle Development Facility 33
   Building Design 33
   Preparation of Thoria-Base Solids 35
      Description of Sol-Gel Process 35
      Thoria and Uranyl Nitrate Feed Materials Properties 39
      Sol-Gel Process Equipment 39
      Oxide Fabrication Equipment 43
      Basis for Process and Equipment Design 44
      Equipment Design 46
      Summary of State of Oxide Fabrication Equipment 56
3. Process Development and Evaluation 57
   Extensions of the Sol-Gel Process 57
      Particle Sizing 57
      Formation of Microspheres from Oxide and Oxide-Carbon Sols. 64
   Effects of Irradiation on Thorium Oxide Fuels 82
      MTR-I and NRX-III 82
      ETR-I 103
      Pellet Fuel 112

CONTENTS (CONTINUED)

Page

Irradiation Testing of Pyrolytic-Carbon-Coated Sol-Gel ThO_2-UO_2 Microspheres 116
Experiment B9-19 117
AVR Capsule 01-8 119
ORR Loop 1, Element 14 124
Vibratory Compaction Studies 126
Permeability of Vibratorily Compacted Fuels 127
Theoretical Considerations 129
Experimental Studies 131
Results and Conclusions 131
Sintering of Sol-Gel Oxides 134
Thorium Metal Fuels 137
Fabrication and Economics of Fueled-Graphite Elements 139
Fluidized-Bed Studies 140
Rotating-Drum Studies 155
Experiments on Conversion of Sol-Gel Microspheres from ThO_2 to ThC_2 161
Pilot-Scale Microsphere Fabrication Line 168
4. Basic Studies 175
Preparation of Special Materials for Advanced Fuels 175
Control of Sol-Gel Particle Porosity 175
Preparation of Zirconia Sols 177
Preparation of Thorium Nitride 179
Sol Encapsulation Studies: Southwest Research Institute . 179
Fission-Gas Release from Thoria Fuels 181
Gas Evolution from Thoria-Urania Sol-Gel Material 183
Effects of Particle Size on Gas Evolution 184
Effect of Temperature on Gas Evolution 186
Reversible Gas Sorption on Sol-Gel Material 187
Moisture Adsorption Characteristics of Sol-Gel Material . . 189
Discussion 190

CONTENTS (CONTINUED)

Page

Separation of Protactinium from Irradiated Thorium Salts . . . 191

Basis of Studies 191

$AlCl_3$-$ZrCl_4$ Phase Studies 192

$AlCl_3$-$ThCl_4$ Phase Studies 196

Protactinium-233 Tracer Experiments 197

APPENDIX 201

1. PROCESS DEMONSTRATION

The process demonstration work for the Thorium Fuel Cycle program has been limited to studies in the Fuel Rod Facility (Kilorod Facility),[1] which is part of an engineering-scale demonstration of the preparation of thoria-based fuel rods containing ^{233}U. The facility was used to prepare approximately 1000 fuel rods containing ^{233}U and thorium oxides for Brookhaven National Laboratory (hence the name Kilorod Program). The Kilorod Program was completed in March 1964. The results obtained during 1963, at which time approximately 75% of the program was completed, have been reported.[2] Results of the remainder of the program are presented in this report.

The Kilorod Program consisted in (1) solvent extraction purification of the ^{233}U to remove ^{232}U daughters; (2) production of easily dispersible thoria by hydrothermal denitration of thorium nitrate; (3) preparation of the mixed thoria-urania oxides by the sol-gel process; (4) sizing the mixed oxides and loading the sized oxide into tubes by vibratory compaction; and (5) remotely welding the end closure of the tube, cleaning the finished rods, and inspecting them for homogeneity and integrity.

Solvent Extraction

The ^{233}U used in the Kilorod Program contained 38 ppm ^{232}U, the decay products and associated gamma activity of which necessitated purification by solvent extraction. A new single-cycle solvent extraction system using 2.5% di-*sec*-butylphenylphosphonate in diethylbenzene was used in the modified Thorex Pilot Plant.[3]

---

[1] A. L. Lotts, J. D. Sease, R. E. Brooksbank, A. R. Irvine, and F. W. Davis, "The Oak Ridge National Laboratory Kilorod Facility," pp. 351–383 in Proceedings of the Thorium Fuel Cycle Symposium, Gatlinburg, Tennessee, December 5–7, 1962, TID-7650, Bk 1 (July 1963).

[2] R. G. Wymer and D. A. Douglas, Jr., Status and Progress Report for Thorium Fuel Cycle Development for Period Ending December 31, 1963, ORNL-3611, pp. 1–31.

[3] *Ibid.*, pp. 2–8.

During 1964 two solvent extraction runs were made to purify approximately 11.5 kg to complete the ^{233}U requirement. Table 1.1 presents a summary of the pertinent results of all the solvent extraction runs.

Of particular significance are the results presented in Table 1.1 of the measurable ionic impurities in the uranium product. The major impurities noted were sodium, calcium, magnesium, and lithium. In an attempt to reduce these impurities in runs HJ-4 and HJ-5 the strip solution was treated with a mixed resin ion exchange column; however, no significant reduction was obtained.

To summarize, the solvent extraction process used to purify ^{233}U produced material that met all specifications imposed by the sol-gel process.

Sol-Gel Process

Description of Process and Facility

The sol-gel process consists of four operations: denitration, blending, drying (gelation), and calcination-reduction (Fig. 1.1). The facility and its initial operation have been reported in detail.[4]

Facility Operation

Denitration. More than enough ThO_2 was accumulated during 1963 to complete the Kilorod Program. The steam superheater that was burned out late in 1963 was replaced, and the denitration was operated to produce approximately 1000 kg of ThO_2 for other programs.

Sol-Gel Operations. During 1964 approximately 236 kg of (Th, $^{233}U)O_2$ product was prepared in the sol-gel cubicle bringing the total Kilorod Program production to approximately 989.9 kg. Table 1.2 presents a summary of the production from the entire program of seven campaigns.

---

[4] Ibid., pp. 8–22.

Table 1.1. Kilorod Program: Summary of Solvent Extraction Results

Run Number	^{233}U Recovered (g)	Decontamination Factors		NO_3^--to-U Ratio	Measurable Ionic Impurities (ppm in terms of ^{233}U)		
		Gross Gamma Activity	Thorium		Al	Na, Ca, Mg, Li	Total
			$\times 10^3$				
HJ-1[a]	4622	230	3.0	2.42	2490	2201.86	4744
HJ-2[a]	4527	380	5.0	2.25	52	<360.22	193
HJ-3[a]	3784	416	3.0	2.16	37	220.10	271
DC-1[a]	4358	185	2.0	2.12	28	296.46	310
DC-2[a]	7793	310	5.50	2.12	23	165.05	207
DC-3[a]	7918	258	5.50	2.12	16	75.59	113
DC-4[a]	5030	300	3.10	2.20	26	113.00	155
HJ-4[a]	5034	194	2.60	2.14	12	<234	193
HJ-5	6485	150	1.96	2.19	26	62	162
Specifications							
	4000–8000	≥100	1	2.50	<30		

[a]R. G. Wymer and D. A. Douglas, Status and Progress Report for Thorium Fuel Cycle Development for Period Ending December 31, 1963, ORNL-3611, p. 6.

Table 1.2. Quantities of ^{233}U and Thorium Charged and Product Removed from the Sol-Gel Process

Campaign Number	Input, kg			^{233}U-to-(Th + ^{233}U) Ratio	$(Th,^{233}U)O_2$ Prepared (kg)
	Thorium	^{233}U	Th + ^{233}U		
				$\times 10^{-2}$	
1[a]	104.693	3.196	107.889	2.969	118.562
2[a]	137.162	4.255	141.417	3.009	160.940
3[a]	102.468	3.166	105.634	2.997	118.468
4[a]	110.724	3.450	114.174	3.002	128.740
5[a]	195.530	6.056	201.586	3.004	226.845
6	145.182	4.521	149.703	3.019	167.7
7	59.972	1.873	61.845	3.029	68.6
Total	855.731	26.517	882.248	(3.006)	989.855

[a]R. G. Wymer and D. A. Douglas, Status and Progress Report for Thorium Fuel Cycle Development for Period Ending December 31, 1963, ORNL-3611, p. 18.

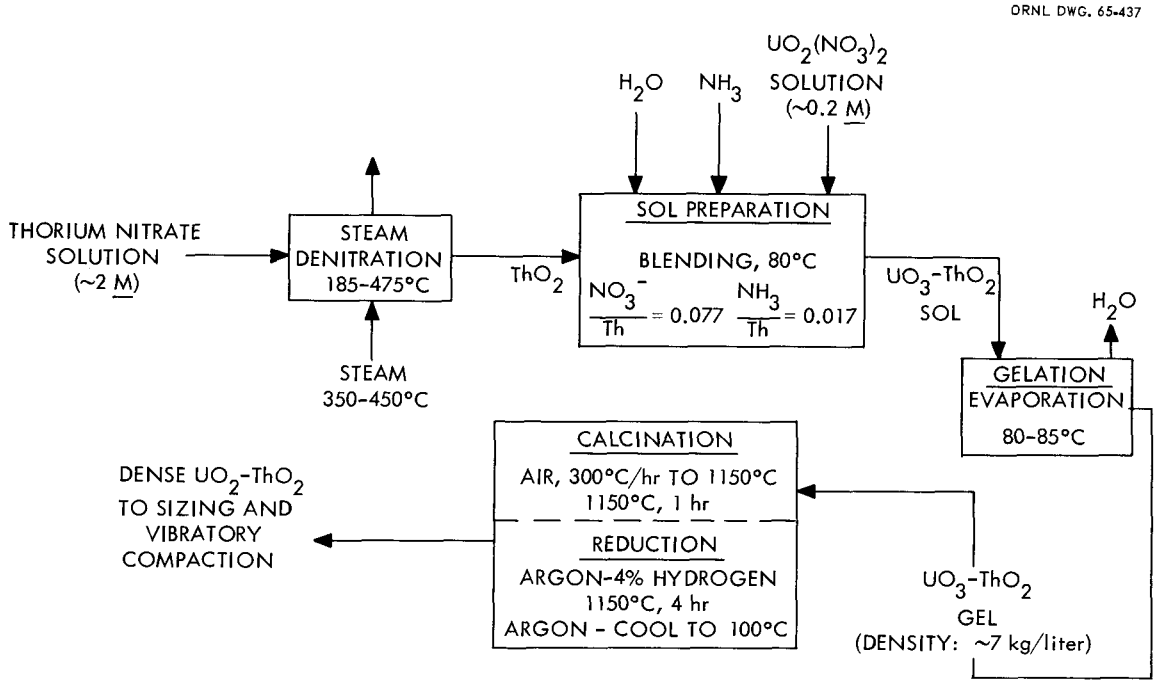

Fig. 1.1. Flowsheet for the Sol-Gel Process.

As will be noted, the control of the ^{233}U-to-(Th + ^{233}U) ratio continued to be excellent during 1964 (campaigns 6 and 7) meeting the target value of 3.00 ± 0.05 wt % ^{233}U.

The gas-release data of the calciner product continued to fall well within the expected maximum of 0.05 STD cm^3/g. as indicated in the complete data in the Appendix A.

Analyses of the gas released from the composite carrier samples (Table 1.3) show that the major constituent is hydrogen. Since the Kilorod fuel tubes were Zircaloy, hydrogen gas would be of concern if the elements were to be used in high burnup, high-temperature tests. As these rods are only for zero power experimental use there is no cause for concern. Using an assumed molecular weight of 35 for the gases and the average gas release for all carrier composite samples, the total hydrogen present in all forms would be only about 3 ppm in the fuel. From analysis of individual batches in Unit Operations and early Kilorod Program work,

Table 1.3. Composition of the Gas Released by the Kilorod Product

Carrier Composite Sample Number	Analytical Method[a]	Gas, wt %									
		H_2O	H_2	CH_4	HC[b]	N_2	CO	N_2 + CO	O_2	CO_2	NO
1	MS	23.9	21.3	0.4	0.2			31.5	0.2	19.4	3.1
		4.1	26.9	0.5	0.3			41.1	0.1	25.4	1.6
	MS		28.1	0.6	0.3			42.0	0.2	26.1	2.9
	GC		31.8	0.6		5.2	25.6	30.8	2.2	28.7	
2	MS	27.7	19.6	0.2	0.2			28.2	0.9	19.7	3.5
		22.1	21.2	0.2	0.2			30.7	0.6	21.9	3.1
	MS		27.2	0.3	0.3			39.3	1.0	27.8	4.4
	GC		27.1	0.5		5.0	32.3	37.3	2.0	25.6	
3	MS	10.8	29.3	0.3	0.5			40.2	<0.01	18.5	0.4
		35.9	19.7	0.3	0.3			27.5	0.03	13.0	3.0
	MS		31.8	0.5	0.5			44.0	0.3	20.5	2.5
	GC		36.9	0.6		4.72	30.7	35.4	2.2	21.2	
4	MS	2.2	33.7	0.2	0.1		50.4	50.4		13.2	0.1
		9.0	30.6	0.2	0.3			47.3	0.2	12.2	0.3
	MS		34.1	0.2	0.2			51.8	0.1	13.5	0.2
	GC		34.8	0.9		4.8	33.2	38.0	2.4	19.1	
5	MS	17.3[c]	11.8	0.3	0.3			36.6	4.2	28.9	0.6
	MS		14.3	0.3	0.4			44.3	5.1	34.9	0.7
	GC		31.8	0.6		12.8	12.9	25.7	5.9	38.3	
6	MS	20.6	28.2	0.2	0.4			25.3	0.1	24.6	0.6
		13.8	31.1	0.3	0.3			27.7	0.1	25.8	0.9
	MS		35.9	0.3	0.4			32.0	0.1	30.5	0.5
	GC		41.6	0.4		7.1	25.2	32.3	3.1	28.0	
7	MS	3.3	36.4	0.4	0.5			37.9	0.1	20.0	1.4
		6.9	33.6	0.5	0.4			37.2	0.1	19.9	1.4
	MS		36.8	0.5	0.5			39.7	0.2	21.0	1.5
	GC		40.6	0.8		4.5	29.9	34.4	1.5	21.9	
8	MS	2.02[c]	27.0	0.2	0.3			43.3	0.2	26.8	0.2
	MS		27.5	0.2	0.3			44.2	0.2	27.4	0.2
	GC		29.9	0.6		6.0	32.5	38.5	2.74	17.1	
9	MS	3.0	33.8	0.5	0.4			51.4	<0.05	10.7	0.2
		1.2	35.0	0.5	0.5			52.5	<0.05	10.2	0.1
	MS		35.1	0.5	0.5			53.1	<0.1	10.7	0.2
	GC		38.3	1.0		6.81	49.2	56.0	3.4	7.8	

[a]MS, mass spectrometer; GC, gas chromatograph.

[b]Other hydrocarbons.

[c]Duplicate sample lost.

a maximum hydrogen concentration of 50 wt % was expected. The present values are within this expectation. Other gases present in appreciable concentrations are CO and CO_2.

The gas composition results presented herein are unquestionably the best data obtained on any sol-gel product to date.

Mechanical reliability of the sol-gel equipment continued to be excellent, resulting in a program on-stream efficiency of better than 90%. This is considered to be an excellent maintenance record for a high-level alpha facility directly serviced.

Radiation-Measurement Program

During the last stages of the Kilorod Program the radiation exposures of workers continued to be consistently well below permissible levels and the accumulation of radioactivity in the equipment continued to be low.

Upon completion of the BNL fuel-rod commitment, a special run was made with aged ^{233}U to simulate operation with high ^{232}U content feed. In this run, ^{233}U containing 38 ppm of ^{232}U, which had been purified approximately six years before, was blended with recently purified material to obtain a radiation level equivalent to the level from daughter ingrowth in feed containing about 800 ppm of ^{232}U which was 14 days old. The principal objective was to obtain radiation data for use in scaling up the process for working with higher levels of ^{232}U than that encountered in the Kilorod Program. It should be recognized that since only one 10-kg batch of high-radiation-level oxide was prepared, the radiation background and exposure data were lower than that which would actually come from 800 ppm ^{232}U, since inventory equilibrium was not attained.

Table 1.4 presents the radiation background in operating areas or equipment during the 800-ppm-^{232}U content run. These data indicate that the radiation backgrounds were two or three times higher in the 800-ppm than in the 38-ppm work. Table 1.5 presents a summary of the radiation exposure experienced during the 800-ppm run.

When the exposures resulting from 800-ppm and 38-ppm batches are put on the same basis (millirems per 10-kg batch), it is indicated that

Table 1.4. Radiation Backgrounds at Various Locations in the Sol-Gel and Rod-Fabrication Cubicles During the 800-ppm-^{232}U Content Run

Location	Radiation Background (milirads/hr) Film Pack (Window)	G-M Survey Meter (Unshielded)
Sol-Gel Cubicle		
WS-1 (blend tank)	16.8	8
WS-1 (outside cubicle face, max.)	Not Available	~6[a]
(At work table above blend tank)	Not Available	~40
WS-2 (No. 1 bagout station)	27.9	<10
WS-3 (crucible station)	36.3	7
WS-3 (outside cubicle face, max.)	0.8	3[a]
(Bottom of tray dumper outside cubicle face, shields closed, loaded crucibles on table, max.)	Not available	60–65
WS-4 (No. 2 bagout station)	34.8	8
Tray of dried gel, near contact	3,200	2,500[b]
Crucible of fired oxide, near contact	6,400	4,000[b]
Rod-Fabrication Cubicle		
WS-5 (ball mill)	84.3	44
WS-5 (outside cubicle, face, max.)	12.6	1.8
WS-6 (blender)	52.9	40
WS-6 (outside cubicle, face, max.)	5.6	2.0
Against ball mill while in use	Not available	~600[b]
Against jaw crusher while in use	Not available	120
Against classifier while in use	Not available	180
WS-7 (rod loading)	91.3	250
WS-7 (outside cubicle face, max.)	1.3	1.4
Rod (at contact, 18 in. from threaded end)	600.0	~600[b]
Rod (at contact, 24 in. from threaded end)	600.0	~600[b]
Rod (at contact, 30 in. from threaded end)	657.0	~550[b]

[a]Shield closed.
[b]Cutie pie was used because of the 200 millirads/hr limit on G-M survey meter.

Table 1.5. Radiation Exposure During 800-ppm-^{232}U Content Run[a]

	Total Body Exposure[b]		Hand and Arm Exposure[b]	
	Shoulder Dosimeter	Pocket Meter	Sleeve Dosimeter	Film Ring
Sol-Gel Process				
Blending	<11	10	27	95
Crucible-table operation	< 7	20	53	155
Total	<18	30	80	250
Rod Fabrication				
Crushing	4		11	
Ball milling	6		18	
Blending	10		30	
Compacting	8		40	
Scanning	3		15	
Welding	5		20	
Clearing	2		5	
Leak Testing and weighing	2		10	
Smearing	3		15	
Supervision	4		10	
Total	47	87	174	700 (±30%)[c]

[a]One batch weighing 10 kg, producing 10 fuel rods.

[b]Millirems per operator

[c]Estimated

the total body exposure for the 800-ppm run was about 3 times greater (117 millirems, compared with 35). The hand and arm data for the 800-ppm run were about 5 times greater (950 millirems, compared with 190). Variation in the individual operations were about the same as the variation of the total.

As previously mentioned, because of the limited amount of high-level material processed, "steady-state" background levels were not attained, and the radiation exposures attained are conservative. It is estimated that with continuous operation, the Kilorod facility could process material having a ^{232}U content of about 500 ppm.

Table 1.6 presents the results of a study to estimate the radiation dose rates to operating personnel as a function of shielding and ^{232}U content.

It is estimated that with weekly chemical purification, the average elapsed time during sol-gel and rod-fabrication work can be reduced to about 7.5 and 12 days, respectively. If this time reduction were obtained, the use of 2 in. of lead shielding would permit operation with ^{233}U that contains 500 ppm of ^{232}U. Further, ^{233}U containing 50 ppm of ^{232}U could be processed with no shielding other than the walls of the vessels and glove boxes and from self-shielding in the fuel material.

By designing a plant to operate semicontinuously to minimize holdup times in all steps, the average elapsed time in sol-gel work can be reduced to 4.5 days and in rod-fabrication work to 6 days. Such a design becomes reasonable for a plant considerably larger than the Kilorod Facility. Much of the equipment in such a plant would be automated to minimize attendance by personnel, and an automatic conveyor belt tray-dryer and a gravity-fed tube furnace would be used. Under these assumed conditions at a rate of 100 kg of total oxide per day, ^{233}U containing 600 ppm of ^{232}U can be processed with 2 in. of lead shielding and that containing 50 ppm with only the shielding offered by the vessels and fuel.

In general, shadow shielding is required for working with a mixed-oxide fuel containing 3% ^{233}U if the uranium contains more than about 50 ppm of ^{232}U unless the glove box is well designed and extreme care is taken in its use. With 2-in. lead-equivalent shadow shields for the major pieces of process equipment, ^{232}U concentrations of about 500 ppm

Table 1.6. Estimated Radiation Dose Rates to Operating Personnel as a Function of Shielding and ^{232}U Content for Fuel Element Manufacture[a]

Type of Operation	Scale (kg oxide/day)	Shielding as Equivalent of Lead of Shadow Shield, in.	Average Post-Purification Time in Sol-Gel Process (days)	Average Post-Purification Time in Rod Fabrication (days)	Weekly Radiation Dose Rate to Operators (millirems)		^{232}U Content (ppm in ^{233}U)
					Hands	Body	
Kilorod facility	10	2	15	19	100	20	40
Batch facility	10	2	15	19	500	100	200
	10	2	7.5	12	500	100	500
	10	0	7.5	12	50	100	50
Semicontinuous facility	100	2	4.5	6	500	100	600
	100	0	4.5	6	50	100	50

[a]Glove-box line producing 97% ThO_2–3% $^{233}UO_2$ by sol-gel and vibratory compaction; ^{233}U purified by solvent extraction.

can be handled safely on a batch basis at a scale of about 10 kg of mixed oxide per day. At the larger scale of 100 kg of total oxide per day, a semicontinuous process is reasonable and ^{233}U containing 500 ppm of ^{232}U can be handled safely with shadow shields. Operation with higher levels of ^{232}U will require complete shielding and remote operation.

In the Kilorod Program, the solids-handling equipment and cubicles were decontaminated effectively with a vacuum cleaner; chemical treatment was not needed. This is contrary to previous experiments with ceramic-grade ThO_2 powders, which were difficult to remove from surfaces. This experiment indicates that equipment can be maintained in unshielded or lightly shielded glove boxes following relatively simple decontamination.

In the above discussion, operation with weekly radiation exposure to operators of 100 millirems per week has been assumed. However, routine operation at a level of 40 millirems per week is recommended; therefore, the permissible ^{232}U content levels suggested in Table 1.6 should be reduced 60%.

Rod Fabrication (Kilorod)

During the past year, the production of 1100 fuel rods for Brookhaven National Laboratory was completed. This terminated the Kilorod demonstration; however, the facility remains intact and has been used to produce additional rods for irradiation experiments — their fabrication is reported elsewhere.[5]

---

[5]"Fabrication of ^{233}U-Bearing Fuel Rods for Irradiation Tests," p. 23 this report.

The design of the equipment and facility, as well as portions of the operating experience, have been previously described.[6–11] The data collected and the analysis of the operating experience are presented in the following discussion.

Fuel Rod Design and Production Flowsheet

The configuration of the rods, which were fabricated for criticality experiments at Brookhaven National Laboratory, is shown in Fig. 1.2. Nine hundred of these rods and 200 shorter (18 in. long), but otherwise identical, rods were fabricated.

The nominal compaction density of the fuel rods was determined by early production rods at 90% of the theoretical particle density. The acceptable average density was specified as ±2% of this determined value,

---

[6]D. E. Ferguson, Status and Progress Report for Thorium Fuel Cycle Development for Period Ending December 31, 1962, ORNL-3385, pp. 73–89.

[7]J. D. Sease, A. L. Lotts, and F. C. Davis, "New Remote Facility and Equipment at the Oak Ridge National Laboratory for Fabrication of Fuel Rods Bearing Uranium-233 and Thorium Oxide," pp. 33–43 in Proceedings of the 11th Conference on Hot Laboratories and Equipment, ANS Winter Meeting, New York, November 18–21, 1963, American Nuclear Society, Hindsdale, Illinois, 1963.

[8]J. D. Sease, A. L. Lotts, and F. C. Davis, Thorium-Uranium-233 Oxide (Kilorod) Facility – Rod Fabrication Process and Equipment, ORNL-3539 (April 1964).

[9]J. E. Van Cleve, Jr., and A. L. Lotts, "Operation of a Lightly Shielded Facility at the Oak Ridge National Laboratory for Fabrication of Fuel Rods Bearing ^{233}U and Thorium Oxide," paper presented at the Symposium on Powder Filled Uranium-Dioxide Fuel Elements, Worcester, Massachusetts, November 5–6, 1963. Proceedings to be published.

[10]R. G. Wymer and D. A. Douglas, Status and Progress Report for Thorium Fuel Cycle Development for Period Ending December 31, 1963, ORNL-3611, pp. 23–31.

[11]J. E. Van Cleve, Jr., and A. L. Lotts, "Operating Experience in a Semi-Remote Facility for Fabrication of Fuel Rods Containing $(U^{233},Th)O_2$," pp. 257–71 in Proceedings of the 12th Conference on Remote Systems Technology, American Nuclear Society, Hindsdale, Illinois, 1964.

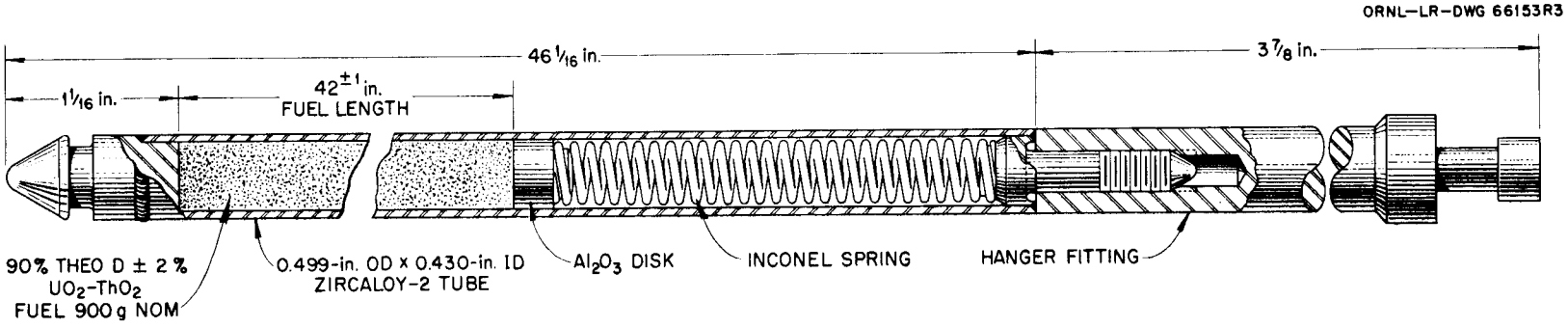

Fig. 1.2. Design Features of the Brookhaven National Laboratory Fuel Rod.

and the density variation within a rod could not exceed ±2% of the average density of the rod. The internal density variation was determined by a gamma scanner. The flowsheet used in fabrication is presented in Fig. 1.3.

Utilization of Material

The material balance data are presented in Table 1.7. The recoverable process losses represent the material that leaked out of the system or spilled during transfer or compaction operations. This material was reclaimed and dissolved for subsequent recovery of the uranium and thorium.

The net process loss represents the amount of material that remained unaccounted for at the end of each, and also the final, campaign. The system was remotely cleaned at the end of each campaign, using a vacuum cleaner; but even after cleaning, some powder was still visibly present on various surfaces and in inaccessible places.

The utilization of the powder in the comminution process was 100%, as no off-size material was produced. The overall utilization of the powder was 94.25%, 89.51% having been loaded into rods, and 4.74% having been removed from the system as analytical samples. The unused analytical samples can be reprocessed to recover the uranium and thorium.

The shipping cask had a capacity for 120 long or 240 short rods. The shipping data for the rods are presented in Table 1.8.

Operating Experience

During the Kilorod operation, process data were collected on the operating efficiency, equipment performance, and the radiation level experienced.

A time and motion study was performed to establish base-line data for evaluation of other facilities. The following information has been extracted from that study.[12]

---

[12] J. E. Van Cleve, Jr., J. J. Varagona, and A. L. Lotts, Time Study of Fuel Rod Fabrication in the Kilorod Facility, ORNL-3740 (October 1965).

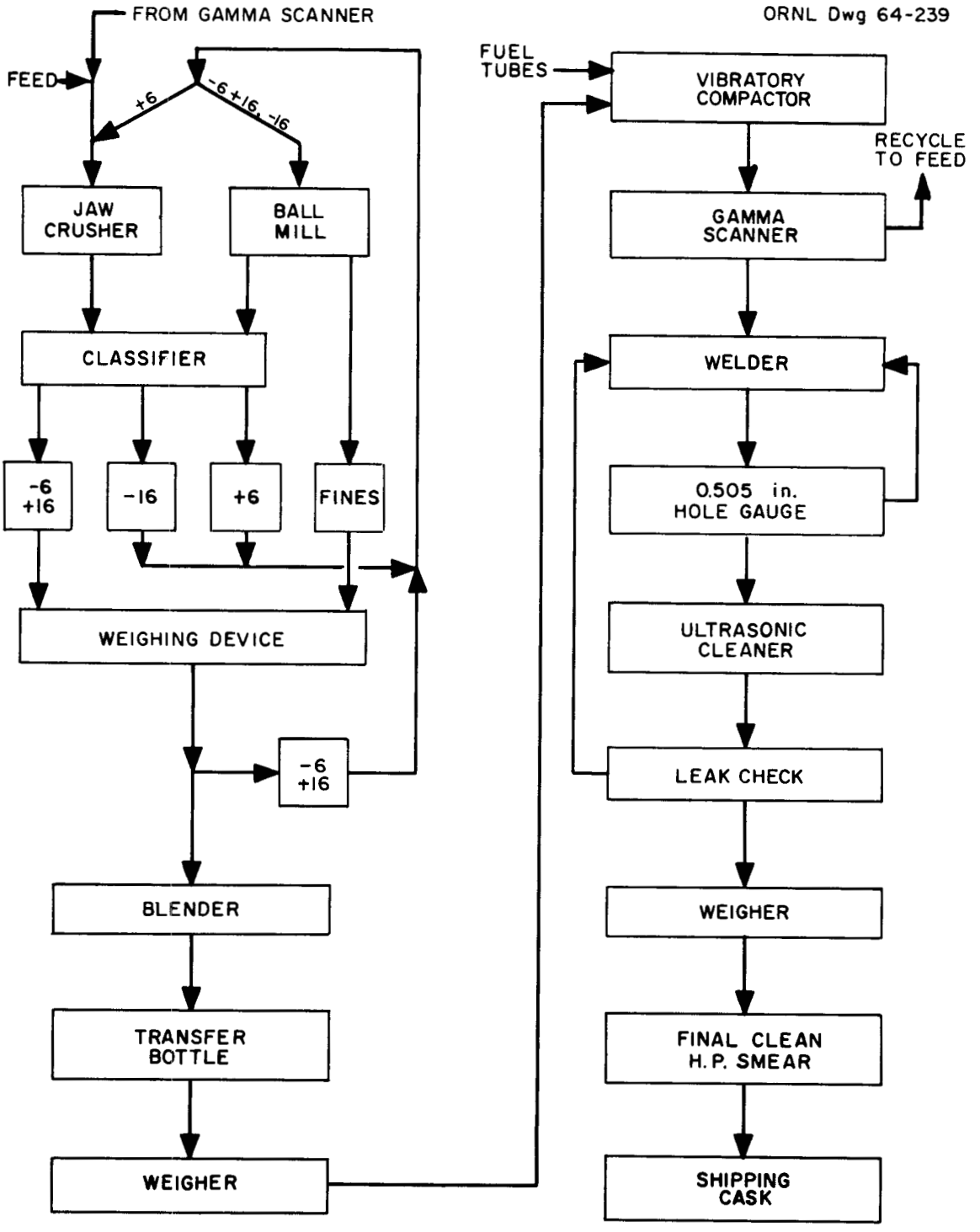

Fig. 1.3. Fuel Rod Fabrication Flowsheet.

Table 1.7. Fuel Utilization and Material Balance Data

Campaign Number	Fuel in Rods	Analytical Samples	Recoverable Process Losses	Process Hold Over	Net Unrecoverable Process Loss	Total[a] Material in Campaign
			$(Th,U)O_2$ Fuel, kg			
1	208.4	12.0	16.5	31.4		268.3
2	130.2	6.5	7.6	7.4		151.7
3	116.5	6.0	4.4	10.7		137.6
4	197.7	11.0	8.2	20.2		237.1
5	163.3	9.0	3.0	11.9		187.2
6	61.8	2.0	13.5		3.2	80.5
Total	877.9	46.5	53.2	81.6	3.2	1062.4
			$(Th,U)O_2$ Fuel, %			
Fuel utilization[b]	89.51	4.74	5.42		0.33	

[a]Total material charged to system = total material in campaign − process hold over; that is, for the total program, material charged to system = 1062.4 − 81.6 = 980.8 kg.

[b]Based on material charged to system (980.8 kg).

Table 1.8. Condensed Shipping Data

Shipment Number	$(Th,U)O_2$ in Shipment (g)	Average Density		$(Th,U)O_2$ (g/rod)
		In Shipment (g/cm^3)	Total (g/cm^3)	
1 (120 rods)	108,757	9.00	9.00	906
2 (240 rods)	108,576	8.93	8.97	905
3 (360 rods)	108,492	8.91	8.94	904
4 (480 rods)	109,287	8.98	8.95	908
5 (600 rods)	109,182	8.97	8.95	905
6 (720 rods)	108,525	8.94	8.95	904
7 (840 rods)	108,732	8.96	8.95	906
8 (900 rods)	54,541	8.99	8.96	909
9 (1100 rods)	62,626	9.04	8.97	313
Total	878,718			

The manpower required to operate the facility was one supervisor and three technicians. A total of 28 subroutines comprised of over 200 elements was divided among these men, and elemental time values were determined for each. Table 1.9 presents the subroutines and the time required for each. Calendar time is the length of time required to do an operation; work time is the number of minutes required for a man to work that operation.

The operating effectiveness was readily ascertained from data such as that in Fig. 1.4. Figure 1.4 shows that, for an operating force of 3.5 men, the maximum possible production rate was 15.5 rods per operating day. It is notable that, in calculating the operating effectiveness, an allowance of 108 min was made for reduction in work time caused by personal time, fatigue, and access limitations imposed by the contamination control area.

The analysis of the operating logbook is shown in Table 1.10. The table presents the causes of downtime experience as well as the length of each downtime period. The effectiveness values reflect the percent of the time actually spent producing 120 rods, taking into account a factor for the recycling of rods between the compaction and gamma-scanning steps. Several factors contribute to lowering the effectiveness, the major one being the time consumed in equipment maintenance or repair. A low effectiveness value does not necessarily reflect poorly on the performance of the crew or process; however, some cause of extended offstream time should be presented to explain the low value.

The process effectiveness ranged from a low value of 16% in the first shipment to a high value of 76% in the seventh. There were two major contributors to the low value: (1) frequent repair of the ball mill and (2) the large number of recycle rods, 43 required. The high value in the seventh shipment was characterized by a small amount of downtime and few recycle rods.

The normal radiation monitoring program was expanded to include the use of finger rings and film packs where the work was of such nature that the film badges or pocket dosimeters might not accurately reflect the dose to extremities. These cases arose when work was performed through the gloves and when close physical contact with the fuel occurred.

Table 1.9. Operational Subroutines and Time Values for Kilorod Rod Fabrication

Subroutine Number	Subroutine	Number of Rods[a]	Time in Minutes at 100% Effectiveness									
			Subroutine Cycle				Daily Time, Maximum Routine Included					
			Time per Subroutine		Per Rod		7-Rod Schedule		10-Rod Schedule		15-Rod Schedule	
			Calendar	Work	Calendar[b]	Work[b]	Calendar	Work	Calendar	Work	Calendar	Work
0	Energize equipment; pick up liquid nitrogen		12	12	1.71	1.71	12	12	12	12	12	12
1	Load in shipping cask											
	one man	120	12	12	0.1	0.1						
	second man	120	9	9	0.08	0.08						
3	Jaw crusher	11	8.45	5.95	0.77	0.54	8.45	5.95	8.45	5.95	16.9	11.9
4	Recycle	11	21.9	21.9	1.99	1.99	21.9	21.9	21.9	21.9	43.8	43.8
5	Ball Mill −16 fraction into fines[c]	8	145.2	10.2	9.10[d]	0.93			145.2	10.2	145.2	10.2
6	Ball Mill −6+16 fraction into fines	10	432.1	12.1	0.40	0.37	13.2	12.1	13.2	12.1	13.2	12.1
7	Blend; transfer bottle loading	1	11.2	8.2	11.2	8.2	78.4	57.4	112.0	82.0	168	123
8	Sample (−16 −6+16 fractions)	10	5	5	0.5	0.5	5	5	5.0	5	10	10
9	Seal samples	10	1	1	0.1	0.1	1	1	1	1	2	2
10	Dispose of old bag (powder preparation cubicle)	10	2.1	2.1	0.21	0.21	2.1	2.1	2.1	2.1	4.2	4.2
11	Seal old bag	10	1	1	0.1	0.1	1	1	1	1	2	2
12	Compacting	1	16.7	7.5	16.7	7.5	116.9	52.5	167	75	250.5	112.5
13	Transfer plugged rod for scanning	1	0.9	0.9	0.9	0.9	6.3	6.3	9	9	13.5	13.5
14	Scanner check	1	9.8	4.6	9.8	4.6	68.3	32.2	98	46	147	69
15	Welding	1	15.5	11.5	15.5	11.5	108.5	80.5	155	115	232.5	172.5
16	Ultrasonic cleaning	5	39.45	13.95	7.89	2.79	78.9	27.9	78.9	27.9	118.4	41.9
17	Dry, leak test, and weight	5	18.3	15.5	3.66	3.1	36.6	31	36.6	31	54.9	46.5
18	Rod cleaning	10	10.7	10.7	1.07	1.07	10.7	10.7	10.7	10.7	21.4	21.4

Table 1.9. (Continued)

Subroutine Number	Subroutine	Number of Rods[a]	Time in Minutes at 100% Effectiveness									
			Subroutine Cycle				Daily Time, Maximum Routine Included					
			Time per Subroutine		Per Rod		7-Rod Schedule		10-Rod Schedule		15-Rod Schedule	
			Calendar	Work	Calendar[b]	Work[b]	Calendar	Work	Calendar	Work	Calendar	Work
19	Smear — smear man	10	8.4	7.8	0.84	0.78	8.4	7.8	8.4	7.8	16.8	15.6
20	Smear — cubicle man	10	6.2	6.2	0.62	0.62	6.2	6.2	6.2	6.2	12.4	12.4
21	Assemble hanger and load in carrier											
	hanger man	10	13.1	8.65	1.31	0.87	13.1	8.65	13.1	8.65	26.2	17.3
22	carrier man	10	13.45	13	1.35	1.3	13.45	13	13.45	13	26.9	26
23	Mark, weight, and record empty rod	5	15	15	3	3	30	30	30	30	45	45
24	3-piece rod end assembly	20	6	6	0.3	0.3	6	6	6	6	6	6
25	Remove and dispose of cleaning pads	50	10	10	0.2	0.2	10	10	10	10	10	10
26	Load shipping cask											
	one man	120	12	12	0.1	0.1						
27	second man	120	9	9	0.08	0.08						
	Total Time (excluding routines 1, 2, 26, and 27) =				89.22	53.18	656.4	441.2	964.2	549.5	1398.8	840.8

[a]One day output.

[b]Based on 7 rod day.

[c]Ball milling done overnight and unattended.

[d]Ball milling attended maximum of twice a day (plus one −6 +16 fraction ball milling) to produce fines to meet maximum schedule.

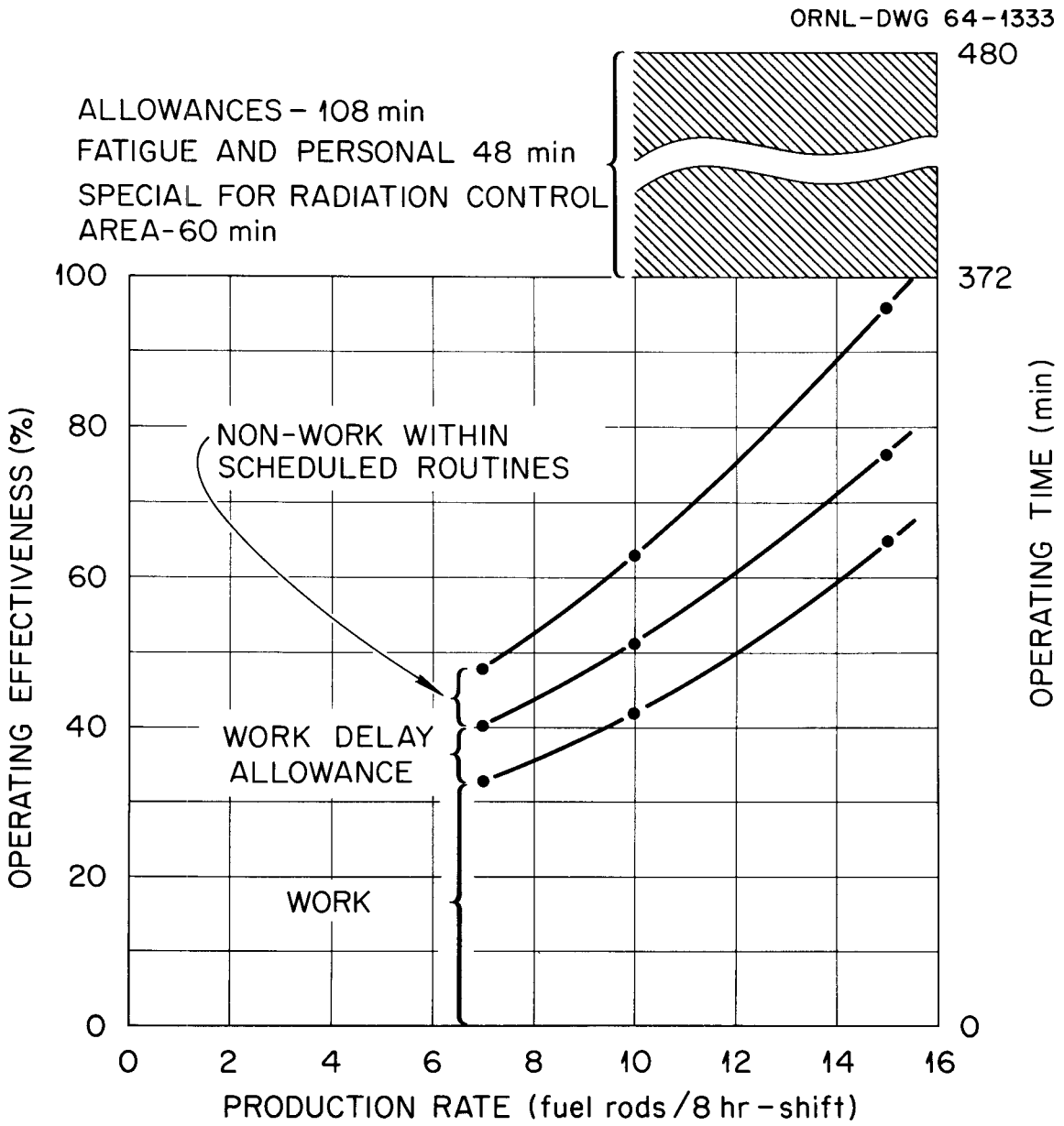

Fig. 1.4. Operating Effectiveness of $(Th,^{233}U)O_2$ Fabrication Pilot Plant.

Table 1.10. Analysis of the Operating Logbook for Offstream Time. Causes and Effects

Rod numbers in cask	0 through 120				121 through 240				241 through 360				361 through 480				481 through 600				601 through 720				721 through 840				841 through 900				901 through 1100				
Processing Dates (Starting – Ending)	6/16/63		8/30/63		9/3/63		9/30/63		10/1/63		10/18/63		10/18/63		11/14/63		11/15/63		12/11/63		12/11/63		12/31/63		1/3/64		1/29/64		1/30/64		2/14/64		2/17/64		3/9/64		
Breakdowns:	Lost Work Time (Crew Workday for routines = 21.7 hours)																																				
		Hours				Hours				Hours				Hours				Hours				Hours				Hours				Hours				Hours			Total
	No.	Range	Total	Avg.	No.	Range	Total	Avg.	No.	Range	Total	Avg.	No.	Range	Total	Avg.	No.	Range	Total	Avg.	No.	Range	Total	Avg.	No.	Range	Total	Avg.	No.	Range	Total	Avg.	No.	Range	Total	Avg.	Hours
Ball Mill	14	0–24	136	10																									1	1–4	4	4					140
Rider Rod	7	2–4	26	4	1	4	4	4	2	6–8	14	7													1	2–4	4	4									48
Rod (dropped in cubicle)	2	2	4	2					2	4	8	4																									12
Compactor:																																					
Iris Valve																					1	4	4	4													4
Tooling	1	1	1	1																																	1
Air Line																	1	1	1	1																	1
Adaptor Nut	7	.5–32	36.5	5																	1	.2	.2	.2	4	0.5	2.0	0.5					6	0.5	3	0.5	41.7
Hold Down Bolts	5	1–6	11	2	1	24	24	24	4	2–15	35	9	1	3	3	3	1	1	1	1					3	1–6	8	2.7					3	1–3	5.5	1.8	87.5
Anvil	1	2	2	2	2	2–3	5	2.5																													7
Hold Down Flange																					1	1	1	1													1
Assembly	1	4	4	4	1	4	4	4					5	4	20	4	1	6	6	6					5	4	20	4	3	2	6	2	2	2–8	10	5	70
Linkage													1	24	24	24																					24
Crusher	1	6	6	6									2	4	8	4																					14
Welder:																																					
Welding	2	2–3	5	2.5													1	8	8	8					2	1	2	1	1	0.5	0.5	0.5	1	4	4	4	19.5
Bell Jar	2	1–8	9	4.5	1	8	8	8																													17
Blender					2	8–16	24	12					1	8	8	8																					32
Feeder Tube																					1	8	8	8													8
Classifier	1	4	4	4																																	4
Scales	2	4	8	4																																	8
Scanner Tube	2	2	4	2									1	9	9	9[1]																					13
End Powder Preparation Maintenance	1	6	6	6																																	6
No feed from third level	1	43.4	43.4	43.4																					6	4–8	48	8	1	8	8	8	2.5	8	20	8	119.4
Leak Detector													1	2	2	2	1	.2	.2	.2																	2.2
Fraction Jar																	1	3	3	3																	3
Wash Down	1	2	2	2	1	2	2	2	1	2	2	2	1	2	2	2	1	2	2	2	1	2	2	2	1	2	2	2	1	2	2	2	1	2	2	2	18
SUB-TOTAL	51	–43.2	307.9		9	2–24	71		9	2–15	59		12	2–24	76		7	.2–8	21.2		5	.2–8	15.2		22	0.5–8	86	22.2	8	0.5–8	20.5	16.5	14.5	0.5–8	44.5	21.3	701.3
Campaign			21.7				86.8				21.7				43.4				86.8				–				43.4				130.2				–		
TOTAL			329.6				157.8				80.7				119.4				108				15.2				129.4				150.7				44.5		
Lost Work Time Days	15.2 days				7.3 days				3.7 days				5.5 days				5.0 days				0.7 days				5.9 days				6.9 days				2.0 days			
[3]Rework Days; Rods reworked	10.2 days for 43 rods				0.7 days for 7 rods				0.1 days for 1 rod				1.6 days for 16 rods				0.8 days for 8 rods				0.3 days for 3 rods				0.9 days for 9 rods				0.3 days for 4 rods				0.6 days for 9 rods				14.9 for 91 r
[4]Cask Crew Days; [5]Effectiveness	28.6 days, 29%				12. days, 64%				9.7 days, 78%				12.4 days, 63%				11.7 days, 66%				12.5 days, 62%				12.1 days, 69%				4.8 days, 81%				15.4 days, 62%				119.2
[2]Cask Process Days; [6]Effectiveness	53 days, 16%				16 days, 51%				12.5 days, 62%				17.5 days, 48%				13.5 days, 58%				13.5 days, 58%				17 days, 49.1%				5.1 days, 76%				16 days, 60%				164.1
Cask Total Days	54 days				20 days				13.5 days				19.5 days				17.5 days				13.5 days				19 days				12 days				18 days				187
																													Calculated on 15 rods/day schedule								

[1]Replace scanner tube

[2]Cask Process Days = Cask Total Days – Campaign Days, e.g., 54–1 = 53, Cask Process Days.

[3]Rework Days = (Cask Total Days – Lost Work Time Days) × $\frac{\text{No. of reworks}}{120 + \text{No. of reworks}}$, e.g., (54–15.2) × $\frac{43}{120 + 43}$ = 10.2, Rework Days.

[4]Cask Crew Days = (Cask Total Days – Lost Work Time Days) × $\frac{120}{120 + \text{No. of reworks}}$, e.g., (54 – 15.2) × $\frac{120}{120 + 43}$ = 28.6, Cask Crew Days.

[5]Crew Effectiveness = $\frac{\text{Effective Cask Days at rod schedule}}{\text{Cask Crew Days}}$ × 100, e.g., $\frac{8.35}{28.6}$ (7-rod day) × 100 = 29%

[6]Process Effectiveness = $\frac{\text{Effective Cask Days at rod schedule}}{\text{Cask Process Days}}$ × 100, e.g., $\frac{8.35}{53}$ (7-rod day) × 100 = 16%

The total body exposures that were experienced during the operating period are presented in Table 1.11. These values show that, operating in the facility with this type and concentration of fuel, the total body dose was less than one-tenth of the maximum permissible dose for one year. The finger rings and accessory film packs showed similar results.

The end product of the Kilorod operation was the production of 1100 fuel rods containing approximately 880 kg of fuel. It was necessary to compact 1191 rods to obtain 1100 specification-grade rods; 7.6% of the total rod production was recycled from the gamma-scanning step. Both the hardware and the fuel were recovered and secured from a rod not meeting the density specifications. The recycle rate between the compaction and gamma-scanning steps during the early campaign was nearly 20% and ranged to a low of 1% in the later campaigns.

The sole criterion for recycling a compacted rod was excessive variation of the density within the rod as determined by the gamma scanner.

The maximum transferable contamination was specified at 2000 dis min^{-1} cm^{-2}. The rods were routinely cleaned to approximately 500 dis min^{-1} cm^{-2}.

No rod was recycled due to the weld leaking when tested in the helium leak detector nor due to excessive weld roll over. The single cause for recycling a rod was excessive variation of the density within the rod as determined by the gamma scanner.

The average density of the compacted rods was 8.97 g/cm^3. Since the theoretical particle density was 10 g/cm^3, the 1100 rods were compacted to 89.7% of the theoretical density.

Fabrication of ^{233}U-Bearing Fuel Rods for Irradiation Tests

The initial motivation for the Kilorod Facility was to fabricate ^{233}U-bearing fuel rods for criticality experiments at Brookhaven National Laboratory. The operation of the lightly shielded (4 1/4-in. armor plate) facility to produce the BNL criticality rods was successful. Even so, an evaluation of the semiremote fabrication techniques employed would not be complete without a demonstration of the performance of the

Table 1.11. Body Exposure Experienced During Kilorod Facility Operation Period

Operator	Exposure, millirems			
	Film Badge		Pocket Meter	
	Total	Average Weekly	Range of Daily Value	Maximum Weekly
		3rd Quarter, 1963		
B	150	12	0–20	40
L	230	18	0–60	60
S	310	24	0–25	55
W	170	13	0–30	50
		4th Quarter, 1963		
B	250	19	0–10	30
L	290	22	0–15	45
S	200	15	0–20	35
W	120	9	0–10	35
		1st Quarter, 1964		
B	350	27	0–30	55
L	270	21	0–30	75
S	220	17	0–30	60
W	160	12	0–15	30

fuels at power reactor operating conditions. (The expected service conditions in the BNL critical experiment do not constitute a sufficient test for the rods in that they will experience essentially no burnup with a maximum operating temperature of only 50°C.)

Currently, an irradiation test is under way at the ETR to evaluate the semiremotely fabricated ^{233}U-containing elements. The irradiation test is a continuation of the ORNL thorium irradiation program; but, the current test is the first using ^{233}U-containing fuel. A second objective of current irradiation test is to evaluate the effects of sorbed gases in the fuel material. One purpose of the irradiation experiment is to determine whether these have any adverse effect on the cladding or whether they limit fuel performance. The irradiation test conditions are given elsewhere.[13]

The irradiation samples, which were made in the Kilorod Facility, contain (Th–3 wt % $^{233}U)O_2$ fuel and are almost identical to the 18-in. rods fabricated for the BNL critical experiments. A detailed description of the fabrication procedures and results used in fabricating the irradiation samples can be reviewed in another document.[14] A brief summary of fabrication procedures and results follow.

Fabrication Procedures. In the fabrication of the irradiation samples, it was necessary to fabricate two sets of rods (groups 1 and 2) because the results of the autoclave test on the first set of samples (group 1) raised doubts of their integrity. The group 2 rods were subsequently fabricated and are currently being used in the irradiation experiments. The group 1 rods are being retained for possible later irradiation tests.

In order to evaluate the effects of absorbed gases on the irradiation performance of the fuel, one-half of the rods in each group were loaded with material that was refired just prior to loading; the others used

---

[13] "Effects of Irradiation on Thorium Oxide Fuels," p. 82, this report.

[14] J. D. Sease and A. R. Olsen, Fabrication Procedures and Preirradiation Data for (^{233}U-Th)O_2-Bearing Irradiation Rods, report in prepatation.

normally processed fuel. The only difference in the procedure for the ETR-II rods and that for the standard BNL production rods was the inclusion of radiographic and autoclave inspection steps. A flow diagram of the fabrication steps is shown in Fig. 1.5.

The material for the group 1 rods was taken from the last batch of material processed for the BNL commitment with no particular effort made to differentiate this material from the normal production operation. The material for group 2 consisted of a composite of archive samples collected from the crushed and ground material during the course of the BNL production operations. The batch quantities for the rods were weighed using 55% of −6 +16 mesh material and 45% fine fraction.

After weighing (and refiring when applicable), the batch for one rod loading was placed in a transfer bottle, hand blended in the bottle for approximately 5 min, and fed into the rod using a vibratory feeder. The vibratory compactor was started before feeding began, and the compaction continued after the feeding was completed. Compaction after completion of feeding was accomplished with a static load of 1.5 kg resting on top of the fuel column.

After compaction, the fuel bed height was measured; and the overall compaction density calculated using the bed height and nominal tube dimensions. The density uniformity was then determined, using the gamma scanner. Before scanning each rod, the gamma-scanner instruments were calibrated using a set of standards made of lead-tin alloys.

The corrosion resistance of the elements was determined using a 750°F, 1500 psig autoclave test. The rods were then rechecked for contamination and weighed with an accuracy of 0.1 mg.

After autoclaving, the diameters of the rods were measured to within ±0.0001 in. using micrometers. The bow was measured by suspending the rods at the extremities between two "V" blocks and measuring the total indicated readout with a dial indicator while rotating the rod.

Fabrication Results. The compaction results of the two groups of rods are shown in Table 1.12. The higher density of the group 2 rods can be attributed to the setup of the compaction unit. Difficulties with the pneumatic vibratory drive unit were experienced in fabrication of the last eight rods (B-6 through 12, and B-13). The added compaction

ORNL-DWG 66-2236

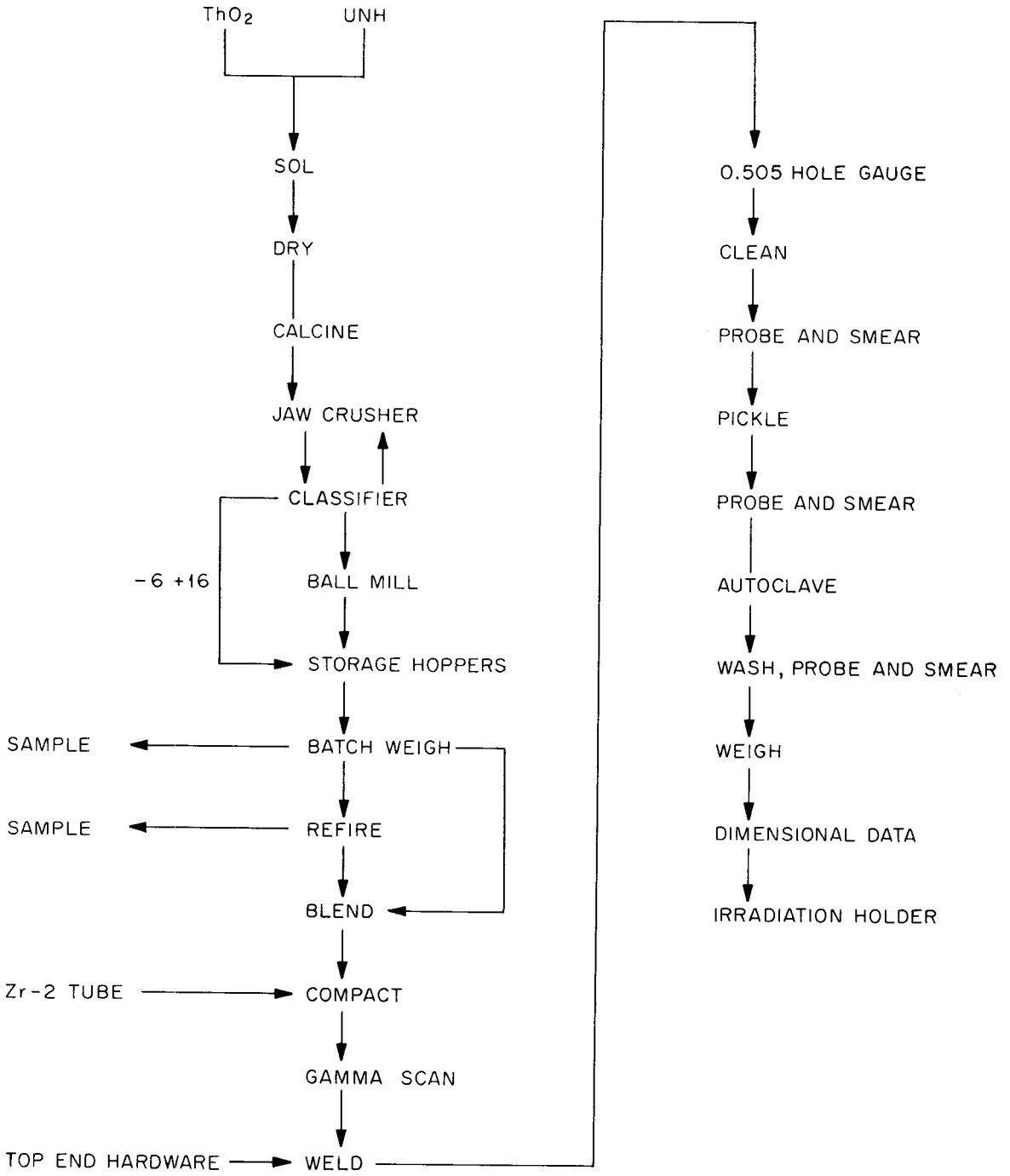

Fig. 1.5. Flow Diagram Used in the Fabrication of ETR-II Prototype Irradiation Fuel Rods.

Table 1.12. Compaction Data for ETR-II Prototype Fuel Rods

Rod Number	Group	Type Material	Feeding Time (min)	Total Compaction Time, min	Fuel Column (cm)	Weight of Fuel (g)	Compaction Density (% TD)[a]	Density Variation (%)[b]	Rods Used in Test 1
1H	1	Normal	4	10	37.98	312	88.1	4.5	
3H	1	Normal	4	10	38.10	313	87.7	5.0	
7H	1	Normal	3	10	36.51	294	85.5	2.5	
4H	1	Refired	4	10	36.93	306	88.6	2.0	
9H	1	Refired	3	9	38.10	306	85.7	2.5	
1B	2	Normal	3	7	36.20	313.5	92.4	2.0	
2B	2	Normal	2.75	7	35.56	305	91.5	1.5	x
3B	2	Normal	2	7	36.20	307	90.5	1.5	x
4B	2	Normal	3	7	35.88	310	92.2	1.5	
5B	2	Normal	3	7	36.83	312.5	90.6	2.0	x
13B	2	Normal	2	7	36.51	307.5	89.9	4.0	
7B	2	Refired	2	10	36.51	308.5	90.2	5.5	x
8B	2	Refired	2	12	36.20	304.5	89.8	4.0	x
9B	2	Refired	2	7	36.20	299	88.2	4.0	
10B	2	Refired	2	7	35.56	297.5	89.2	2.0	
11B	2	Refired	2	7	36.51	309	90.3	3.0	
12B	2	Refired	2	7	36.20	305	89.9	3.0	x

[a]Based on a theoretical density of 10.0 g/cm^3. The fuel volume was calculated using the nominal tube inside diameter of 0.430 in. The ±0.0015-in.-OD variation can account for ±0.5 variation in the theoretical density listed.

[b]Derived from gamma-scan traces, the listed valves are the total density variation from end to end of the fuel rod.

times of rods 7 and 8 were due to a faulty tube-to-vibrator coupling which resulted in a low density after the normal compaction time. The faulty coupling was replaced and additional compaction time was given to reach the equilibrium density.

The density variations also shown in Table 1.12 are quite good in comparison to previous experience. The reported density variation values were derived from comparison of gamma-scan traces of the rods with traces of standards, which were run with each rod to compensate for instrument drift. Poor tube coupling while compacting caused the larger density variations in rods 7B and 8B than in the other rods. Since the scans for these two rods showed deviations no greater than ±3%, the density variation in these rods are quite acceptable.

The results of contamination surveys of the rods are shown in Table 1.13. It was not difficult to remove transferable contamination from the rods; even so, the alpha probe reading after such cleaning, but before pickling, was extremely high. After pickling this value was reduced to a reasonable level, as shown in Table 1.13.

Kilorod Program Conclusions and Recommendations

The Kilorod Program was an unqualified success in that it met every program objective. The 10 kg/day design rate for the sol-gel operation was sustained, as scheduled, over long operating periods. The longest of these was 14 consecutive days in the November-December period. All sol-gel equipment except the calciner could produce at least double the production design rate. Rod-fabrication operations were similarly successful, with an average sustained production rate of 13 rods having been demonstrated over a period of 10 scheduled operating days. A maximum of 21 rods were fabricated in a single working day, once during the program. All chemical and fabrication specifications were met or exceeded.

From the Kilorod experience, the following conclusions are reached.

1. The sol-gel process for preparing a 3% UO_2–97% product is now a practical, working process, which, under operating conditions similar to those in the Kilorod program can be scaled up directly to any immediately foreseeable production rate.

Table 1.13. Health Physics Results of ETR-II Prototype Fuel Rods

Rod Number	Group	Type Material	Before Pickling		After Pickling and Autoclaving[a]			
					Smear[b]		Probe[c]	
			Smear[b] Alpha (dpm)	Probe[c] Alpha[d] (dpm)	Alpha (dpm)	Beta (dpm)	Alpha (dpm)	Beta-Gamma (mr/hr)
1H	1	Normal	90	~50,000	88	0	2090	80
3H	1	Normal	<30	~50,000	70	0	1020	85
7H	1	Normal	<30	~50,000	19	110	360	80
4H	1	Refire		~50,000	31	0	550	75
9H	1	Refire		~50,000	3	87	50	70
1B	2	Normal	<30	12,500	0	112	25	130
2B	2	Normal	<30	30,000	3	12	25	74
3B	2	Normal	<30	15,000	0	37	25	96
4B	2	Normal	<30	15,000	0	12	25	94
5B	2	Normal	<30	15,000	0	87	40	92
13B[e]	2	Normal	<30	5,000	30	0	2400	110
7B	2	Refire	<30	17,500	0	37	50	72
8B	2	Refire	<30	20,000	0	0	25	70
9B	2	Refire	<30	10,000	3	87	50	70
10B	2	Refire	36	12,500	18	12	25	76
11B	2	Refire	51	17,500	15	75	25	84
12B	2	Refire	72	27,500	0	12	25	85

[a]There was essentially no difference in the smear and probe readings after pickling and after autoclaving.

[b]Smear taken over entire rod surface of approximately 182 cm^2.

[c]Alpha probe taken with gas alpha proportional counter; beta-gamma probed with GM survey meter.

[d]The alpha probe readings for group 1 rods are order-of-magnitude readings. The actual reading for rod 9H was top, 250,000 dpm; middle, 4,000 dpm; and bottom, 150,000 dpm.

[e]Rod 13B was not pickled or autoclaved.

2. Likewise, a sol-gel, rod-fabrication combination is also a practical, working process that can be scaled up directly to any immediately foreseeable production rate.

3. Specifications requiring both high product purity and fuel element uniformity can be met routinely in a combined sol-gel, vibratory-compaction, fuel-rod-preparation plant.

4. Batch rejection and internal recycle of materials (as wastes) are almost nil in a sol-gel, vibratory-compaction operation as represented by the Kilorod installation.

5. Both sol-gel and rod-fabrication operations are amenable to rigid analytical control, as evidenced by the process control during this program.

6. Exposure of workers to radiation at the 38-ppm ^{232}U level was far below permissible limits.

7. Considerably higher ^{232}U concentrations can be handled safely in the present equipment by current operating procedures.

8. Loss of process materials in all operations can be held to extremely low if not insignificant values.

9. Aged ^{233}U (38 ppm ^{232}U) can be satisfactorily purified for use in the sol-gel process by a solvent extraction process based on extraction by di-*sec*-butylphenylphosphonate.

2. THORIUM-URANIUM FUEL CYCLE DEVELOPMENT FACILITY

Development of the thorium fuel cycle must eventually include an economic analysis based on experience with the various fuel-element reprocessing and fabrication techniques at pilot production levels. Since there appears to be an economic advantage in reducing the amount of decontamination in reprocessing and because of the buildup of radioactivity in ^{233}U fuels by the decay of ^{232}U, it is desirable to have a heavily shielded facility in which to develop and to study the economics of a variety of integrated fuel reprocessing schemes. The TUFCDF is being constructed to fulfill this need.

The facility has been sized to accommodate integrated recycle processes with equipment reduced in size from the anticipated production units so that a realistic and reliable basis for technical and economic analyses will exist. A conceptual design based on the size, shielding, containment, and developmental flexibility outlined in the criteria[1] was completed in July 1962. A report[2] on this design was presented in December 1962. Title I design was started in January 1963 and completed in December 1963, with very little change in the concept. Title II design was started in April 1964, and will be completed early in 1965. Construction is scheduled for completion in December 1966.

Building Design

TUFCDF will be constructed in the Melton Valley area near the Transuranium Processing Plant and High Flux Isotope Reactor (see Fig. 2.1).

---

[1]A. R. Irvine and A. L. Lotts, Criteria for the Design of the Thorium Fuel Cycle Development Facility, ORNL-TM-149 (March 1962).

[2]A. R. Irvine and A. L. Lotts, "The Thorium Fuel Cycle Development Facility Conceptual Design," pp. 330–50 in Proceedings of the Thorium Fuel Cycle Symposium, Gatlinburg, Tennessee, December 5–7, 1962, TID-7650, Bk 1 (July 1963).

ORNL PHOTO 64020 A

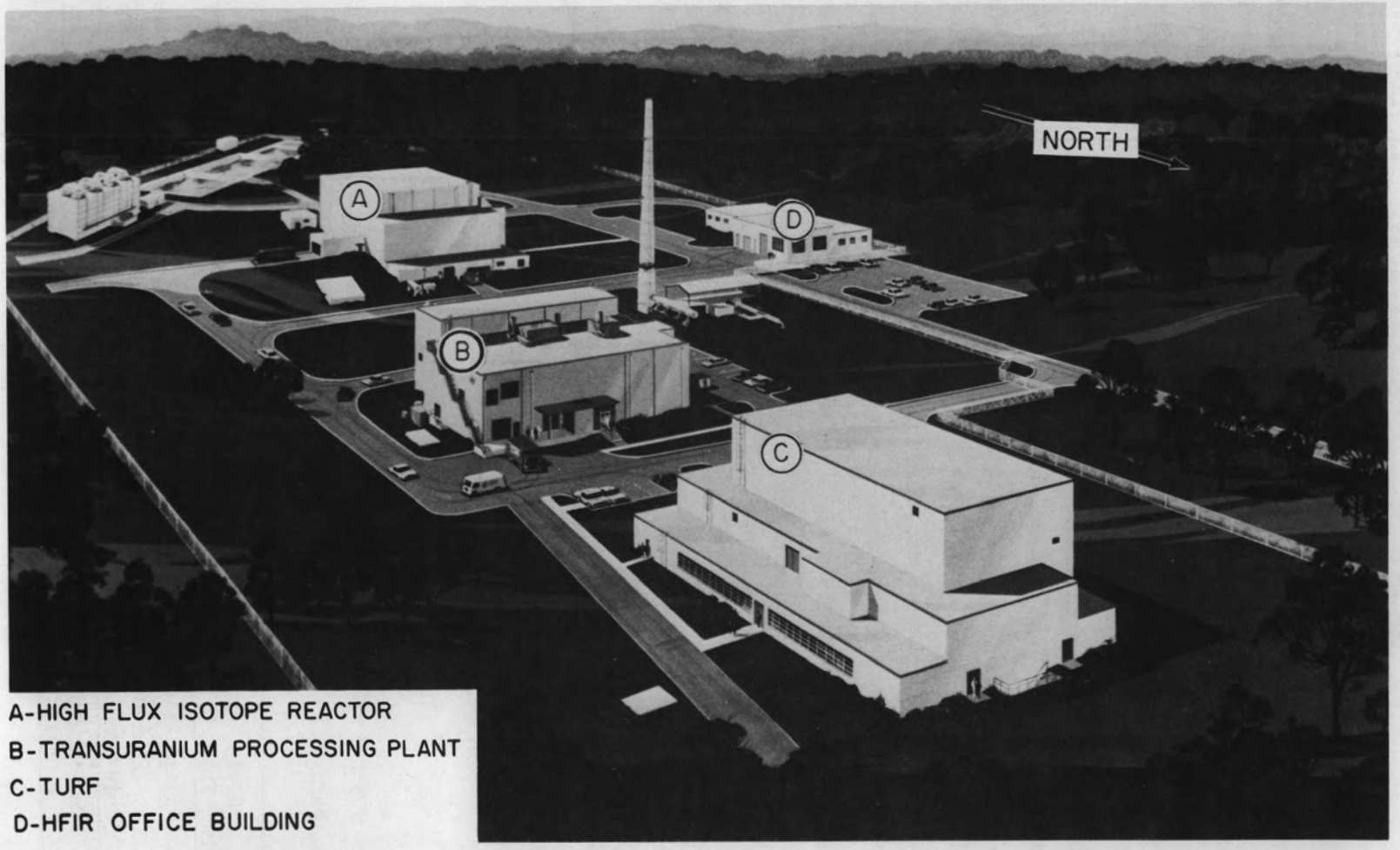

Fig. 2.1. Area Map Location of the Thorium-Uranium Fuel Cycle Development Facility.

It will be an irregularly shaped three-story building, approximately 162 ft long and 124 ft wide, with a partial basement. The plan of the first floor is shown in Fig. 2.2.

During the course of Title II design, few changes were made in the configuration and capabilities of the facility. The principal deviation concerned the increasing of the headroom in cells "C" (Mechanical Processing) and "D" (Contaminated Fabrication) to a total of 24 ft in order to provide for greater freedom in equipment design and increased operational capability. All other changes were of a minor nature and were made in the course of development of the details of design and did not affect the operational capability of the facility.

Preparation of Thoria-Base Solids

The equipment to be installed in the TUFCDF will, within reasonable limits, be small versions of the production-scale equipment it is anticipated will be built. All major operations will be demonstrated using prototype equipment, from which data relative to mechanical and metallurgical operability as well as to operating costs for a large plant may be based.

The process description presented here includes information obtained from development work and Pilot Plant demonstrations[3] of the sol-gel process developed at Oak Ridge National Laboratory.

A limited description of the processing equipment is presented as envisioned at the beginning of Title III design of the equipment.

Description of Sol-Gel Process

A description of the sol-gel process as adapted to the preparation of thoria-based oxides of urania and thoria in the TUFCDF is as follows: Thoria is dispersed in a nitrate medium containing uranyl nitrate.

---

[3]C. C. Haws, J. L. Matherne, F. W. Miles, and J. E. Van Cleve, Summary of the Kilorod Project — A Semiremote 10 kg/day Demonstration of $^{233}UO_2$-ThO_2 Fuel-Element Fabrication by the ORNL Sol-Gel Vibratory-Compaction Method, ORNL-3681 (September 1965).

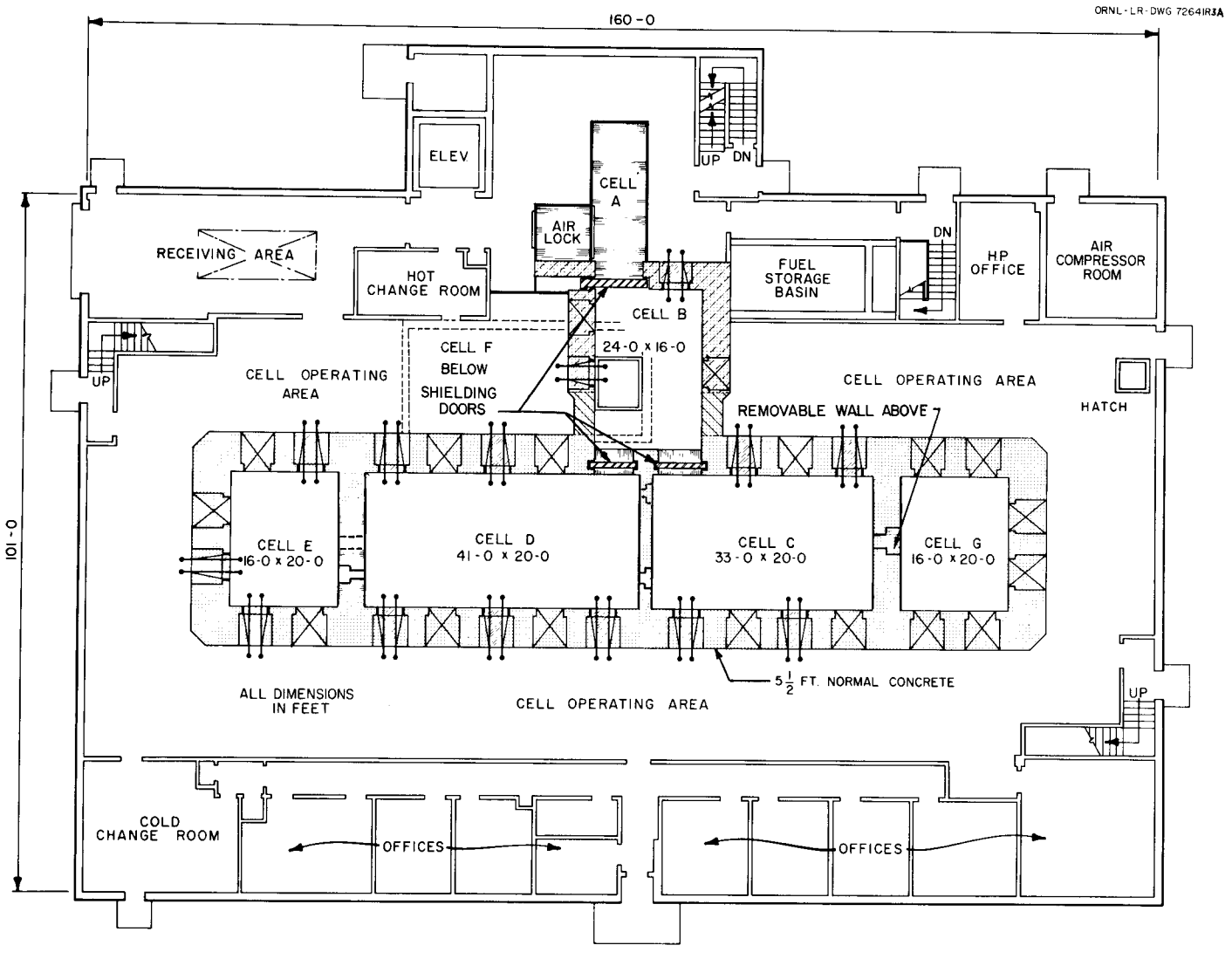

Fig. 2.2. First-Floor Plan of the Thorium-Uranium Fuel Cycle Development Facility.

Uranium is sorbed on the thoria surface, and the thorium-uranium sol is dried to produce a gel. This gel is calcined under controlled atmosphere at temperatures less than 1200°C to form dense (>99.5% of theoretical) homogeneous oxide particles suitable for vibratory compaction to dense beds of oxide (90 to 95% of particle density). The individual processing steps are discussed below.

Thoria suitable for dispersion to a stable sol is prepared from thorium nitrate by careful control of the initial heat-up rate, the denitration atmosphere, and the time of denitration.[4]

Steam-denitrated thoria is dispersed to a sol having a very large crystalline surface area, about 80 m^2/g of ThO_2, by the nitrate ion supplied, at least in part, by the uranyl nitrate solution. The following procedure is used to produce a sol having the desired properties. Thoria slurry containing 10 to 13 moles of ThO_2 per liter is added to an agitated solution of uranyl nitrate that contains the proper amount of nitrate ion for ThO_2 dispersion and hydrosol formation. The uranium content of the uranyl nitrate solution is chosen to give the desired uranium-to-thorium atom ratio and to produce a hydrosol containing 2 to 4 moles of total metal per liter of hydrosol.

The thoria-uranium nitrate solution is agitated thoroughly by pump-mixing and the resulting slurry is agitated an additional 1/2 hr at 80 to 90°C to effect complete dispersion and hydrosol formation.

The optimum amount of nitrate to achieve complete thoria dispersion is 0.077 mole of nitrate per mole of thoria. However, this nitrate-to-thoria ratio prevents complete uranium sorption on the thoria surface, and it is necessary to add to the dispersed hydrosol ammonium hydroxide in an amount equal to 0.017 mole per mole of thoria and to agitate for 1/2 hr after ammonia adjustment to assure complete sorption of the uranium on the thorium.

The nitrate-to-thorium mole ratio of 0.077 required for optimum dispersion of the hydrosol fixes an upper limit on the amount of uranium that may be added as stoichiometric uranyl nitrate solution. For

---

[4] O. C. Dean, A. T. Kleinsteuber, J. W. Snider, C. C. Haws, and P. A. Haas, Status and Progress Report for Thorium Fuel Cycle Development for Period Ending December 31, 1962, ORNL-3385, pp. 6, 8, and 9.

stoichiometric uranyl nitrate solution, the maximum obtainable uranium-to-thorium mole ratio is 0.0385; this ratio is reduced to 0.03 if the uranyl nitrate solution nitrate-to-uranium mole ratio is 2.56 (i.e., if nitric acid is present). The uranium content may be increased to about 0.10 mole uranium to thorium by the addition of more uranium as "ammonium diuranate." These nitrate requirements are based on the premise that the nitrogen-to-thorium ratio in the steam-denitrated thoria is less than 0.05 and preferably 0.03 mole of nitrogen per mole of thorium.

After uranium sorption is completed, the thorium-uranium hydrosol is evaporated to dryness in shallow pans. The initial liquid depth in the pans is adjusted to about 1 in. and drying conditions are selected to give varying size distribution of the dry gel. Sol drying times per batch of 1-in.-deep liquid may be varied between 3.5 and 48 hr to produce various size distributions of the dry gel.[5]

Sol drying temperatures have been varied from between 50 and 150°C in constant-temperature ovens, and between 80 and 135°C in larger batch units using conduction and convection heat transfer. Both radiant heat transfer and forced-convection heat transfer have been used successfully to dry sol. Present plans are to use radiant heat exchange to dry sol in the TUFCDF.

For the TUFCDF, sol drying by radiant heat transfer has been chosen. Here, a programmed evaporation and drying operation will be conducted on a semicontinuous basis. Metered batches of sol will be fed at fixed time intervals to the dryer trays. The trays of sol will be advanced to drying stations at five controlled temperature zones in the dryer. Temperatures at the five drying stations will be controlled to give the desired evaporation rates and drying rates as a batch of sol is converted to dry gel. When heated to 1150°C, dry gel containing 3 to 4 wt % volatiles will be discharged from the dryer.

The final step in the TUFCDF sol-gel processing schemes is the conversion of dry gel to oxides by calcination. Calcination of the dry gel in Ar–4% H_2 causes densification of the gel and converts the uranium and thorium to the respective tetravalent oxides in a uniform and

---

[5]"Particle Sizing," p. 57, this report.

homogeneous particle having essentially theoretical density. Densification is accomplished by heating the gel to 1150°C. Calcination of dry gel in the TUFCDF is conducted on a continuous basis in a vertical tube furnace.

Thoria and Uranyl Nitrate Feed Materials Properties

The properties of purified uranyl nitrate solution and of steam-denitrated thoria powder are tabulated below. These properties are among the essential ones for successful chemical and metallurgical performance of the sol-gel process.

Uranyl Nitrate Solution	Thoria Powder
NO_3^--to-U mole ratio: ≤ 2.4	Specific surface area: $>40\ m^2/g$
<100 parts Al^{+3} per million parts U	Nitrogen-to-thorium mole ratio: < 0.03
^{233}U: 100 to 150 g of U/liter	Those properties obtained by contacting preheated $Th(NO_3)_4$ crystals at 200°C, then steam contacting for 6 hr, during which time the temperature is raised from 200 to 475°C, with 3 hr of heating at ≥ 425°C.

Sol-Gel Process Equipment

Sol-gel process equipment and other supporting process equipment (except the uranium nitrate unloading station) that handles highly radioactive materials will be installed in the mechanical processing cell (Cell C) of the TUFCDF behind 5 1/2 ft of concrete shielding and operated and maintained remotely. This in-cell equipment train includes uranium nitrate storage, sampling, and metering equipment; sol blending, sampling and metering equipment; thorium oxide dispensing equipment; sol drying equipment; and gel calcination equipment with attendant oxide sampling and conveying units.

Out-of-cell equipment associated with the in-cell sol-gel equipment train, but located in unshielded areas, consists of miscellaneous reagent makeup and metering vessels. This out-of-cell equipment will be operated by direct contact methods as it presents no radiation hazard.

The in-cell thorium dispensing station consists of a dumping device for transferring thoria powder from the transfer container to a funnel located atop the sol blend tank. The thoria is wetted with demineralized water in the funnel and is allowed to flow by gravity into the blend tank and be mixed with the circulating uranyl nitrate solution by pump mixing. Weighed amounts of thoria powder (about 34 kg ThO_2) are supplied in transfer containers to the in-cell dispensing station.

The ^{233}U storage vessel will be an annular tank 42 in. in diameter with a solution capacity of 200 liters and a total volume of 250 liters, and it will be critically safe for concentrations up to 200 g/liter of ^{233}U. The vessel will be housed in a moveable frame along with a uranium sampler, a uranium transfer pump, and a uranium-metering and -transfer vessel.

The uranium transfer pump delivers uranyl nitrate solution from the storage vessel to the metering vessel. It is a TRU diaphragm pump[6] activated by alternate forces of vacuum and pressure to cause suction lift and pressure delivery of the pumped fluid. The pumped fluid is separated from the drive fluid by a flexible diaphragm. This pump has suction characteristics sufficient to lift the uranium solution above the storage tank level to the pump suction. Therefore, the pump is located at a fail-safe position atop the uranium storage vessel.

The uranium-metering and -transfer vessel is a 4-in.-ID cylindrical tank which delivers a fixed volume of solution to the sol-blend tank. This single vessel is equipped with a pneumatic level measuring system and a thermocouple for measuring temperature. Solution transfer from the uranium-metering vessel to the sol-blend tank is accomplished by

---

[6]T. S. Mackey, Development of an Air-Operated Metal Diaphragm Pump for the Transuranium Processing Facility, ORNL-TM-995 (December 1964).

pressurizing the metering vessel. The uranium metering system will be capable of metering and delivering to within 0.1% of a fixed volume.

The sol-blending and -dispensing system consists of a slab tank for blending, a sol recirculating pump, a sol heater, a sol metering-dispensing vessel and a sol sampler. The sol-blend tank is a 2-in.-thick slab tank about 6 ft wide and 6 ft high including the triangular shaped bottom section. The blend tank is equipped with pneumatic liquid-level sensing elements, thermocouples for temperature measurement, and water sprays in the top rectangular section. Appropriate openings are provided in the top of the blend tank for uranium and thorium oxide feed addition and openings for recirculating sol from the pump discharge and from the sol-metering vessel. A Durco Series U centrifugal pump with flooded suction and a mechanical seal (pressurized with external water) will recirculate about 30 gal./min of sol from the blend tank through an electrically heated heat exchanger back to the blend tank. With appropriate valve settings, the pump will deliver sol to the sol-metering tank. The sol pump and heat exchanger will be mechanically separable from the blend-tank network and may be removed individually using the cell crane system to the maintenance cells.

The sol-metering system will deliver a fixed volume of sol at regular time intervals to the sol dryer. Sol is metered in a 4-in.-diam tank and is discharged from the tank by pressurizing the tank. This tank is equipped with pneumatic liquid-level sensing tubes, thermocouples, a feed line, an air-blow line and overflow, and discharge lines. The sol-metering-vessel overflow outlet is located above the sol-blend tank to allow gravity flow of sol through the sol sampler back to the blend tank. Sol is forced from the metering vessel by air pressure sufficient to overcome a liquid seal in the discharge line to the sol dryer. Sol is sampled by an evacuated bottle-needle type sampler.

The sol dryer consists of six or seven flat trays that pass through controlled temperature zones in the dryer when the sol contained in the trays is volume reduced and dried to a gel prior to discharge from the dryer. Heat for the sol drying is supplied by radiating internal surfaces of the dryer, which are heated from electric heaters external to the tray enclosure. Radiating surfaces (150 to 500°C) and tray dwell

periods in a heated zone will be adjustable to give the desired sol drying rates. The sol dryer is designed to process 35 kg of thoria-urania gel per 24-hr day when a 2 M sol is fed to the dryer. The exact configuration of the dryer will be the result of detailed design by a private contractor.

Calcination of the dry gel to dense oxide fragments will be conducted in an electrically heated vertical tube shaft furnace. The furnace consists of a 3-in.-diam alumina tube through which heat is supplied to the gel as it flows by gravity through the heated zone of the tube. Calcined- and cooled-oxide fragment flow from the furnace is controlled by the rotation of a disk valve located at the bottom discharge opening of the alumina tube. The temperature profile in the furnace varies from 150°C at the top through an 1150°C zone in the mid-section to less than 100°C at the bottom discharge opening. At present the 1150°C temperature is obtained from 12 electrically heated glow-bars positioned perpendicular to the axis of the alumina tube and spanning 2 ft of the vertical tube. Thermal insulation and water-cooled external surfaces set the external dimension of the furnace at 2 × 2 × 5 ft high. An additional height of 4 to 5 ft is required to accommodate the solids sampling and exit flow control disk valve at the bottom of the furnace and the solids-level detection equipment atop the furnace.

Calcined solids are sampled continuously as they exit the furnace. A sample is taken of the oxide as it flows from the periphery of the disk valve and is further reduced in quantity by a standard Vezin sampler.

Oxide product discharge from the calcination furnace is collected in tared containers and transferred via the oxide product weighing station to a dumping station by use of a combination of mechanical conveyor and cell crane system. An exact description of the oxide handling equipment is not yet available. The oxide dumping station will deliver the material to the powder preparation equipment located in the adjacent cell of the facility.

The uranyl nitrate transfer hood is to be located outside the shielded processing cells. It will provide the necessary structure and

utilities to transfer radioactive solution from a shipping container to a storage vessel inside the shielded cells. This transfer hood will also be designed to provide for safe handling of heavy shipping containers including sampling, metering, and cast decontamination before and after solution transfer. Final design of the uranium transfer hood has not been started.

Oxide Fabrication Equipment

We are developing fabrication equipment to demonstrate, on a pilot plant scale in the TURF, the technical and economic feasibility of remote fabrication and assembly of rod-cluster fuel elements containing $(Th,^{233}U)O_2$. The method selected for fabrication of these elements is vibratory compaction of bulk oxide into stainless steel or Zircaloy-2 tubes and mechanical assembly of the compacted fuel rods into elements.

The major objective of the design of the oxide equipment is to be able to scale the process both technically and economically into a full production facility. The basic criterion for the equipment is that it be able to accommodate fuel rods 2 to 10 ft long and 1/4 to 3/4 in. in diameter.

However, the design of a large portion of the oxide fabrication equipment is greatly dependent upon the configuration of the particular element to be fabricated. In the absence of a firm commitment as to the fuel element to be fabricated and with the oxide equipment phase of the TURF projected on schedule, we reached a point that made further design unwise without a firm commitment to a particular element.

Currently, the design of the oxide phase of the TURF project is being brought to an orderly termination. Since the design status of the various pieces of equipment varies from complete final design to conceptual design, a concerted effort is being made to bring the design to a logical stopping point so that design can easily begin de novo. Even though we have decided to defer further design work, we are proceeding with the fabrication and mockup testing of two important equipment units so that we shall have a basis for assessment of the design philosophy used to date. These two units, the vibratory compactor

and its related fuel-blend transfer device, are two items that have given trouble during previous operations[7] and are absolutely essential to oxide fabrication process.

In the studies that follow we shall review the oxide fabrication process and discuss the design status of the equipment. Major emphasis will be placed on changes made during the year.

Basis for Process and Equipment Design

The proposed oxide fabrication procedure changed very little during the year;[8] the changes were those made for simplification of the powder preparation steps. A revised flow diagram is shown in Fig. 2.3.

The philosophy of the operation is to let each machine operate at its maximum capability and then to wait on the slower machine. Flexibility of the equipment in handling various geometries is achieved when possible by minor adjustment of components; however, the unit speed is not to be sacrificed for flexibility. By designing the separate equipment items to operate as fast as possible, we hope to gain unit operational data that can be directly applied to the design of future production facilities.

The design production rate of the process line was established at 40 fuel rods per 8-hr day based on a rod having dimensions of 0.452-in. OD, 0.412-in. ID and 63 1/2 in. long and the requirement of processing 35 kg of bulk oxide per day.

The oxide fabrication equipment will be located in two cells (Cells D and E) of the TURF. Fabrication operations involving direct contact with the fuel material or rods in the unsealed condition will be located in the contaminated fabrication cell (Cell D); the operations involving sealed and cleaned rods will be accomplished in the clean fabrication

---

[7] C. C. Haws, J. L. Matherne, F. W. Miles, and J. E. Van Cleve, Summary of the Kilorod Project — A Semiremote 10 kg/day Demonstration on $^{233}UO_2$-ThO_2 Fuel Element Fabrication by the ORNL Sol-Gel Vibratory-Compaction Method, ORNL-3681 (September 1965).

[8] R. G. Wymer and D. A. Douglas, Jr., Status and Progress Report for Thorium Fuel Cycle Development For Period Ending December 31, 1963, ORNL-3611, pp. 43–45.

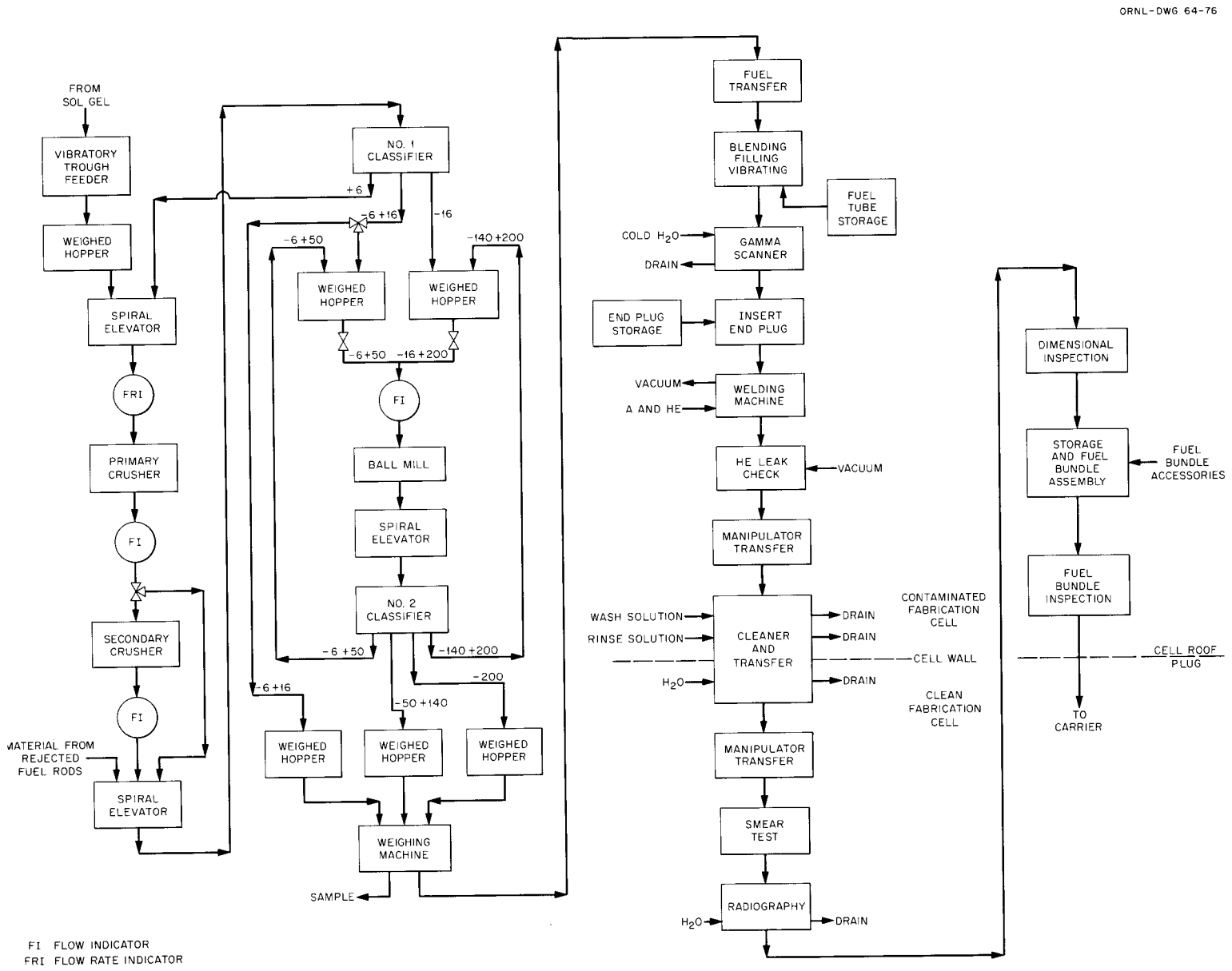

Fig. 2.3. Fabrication Flowsheet for Oxide Fuel Elements.

cell (Cell E). The two cells will be connected by a transfer device which incorporates a rod cleaning system. The proposed layout of the equipment in the two cells is shown in Fig. 2.4.

The maintenance concepts for the two cells are not the same because of the difference in degree of contamination that is expected in each of the cells. In the contaminated fabrication cell in which we expect a buildup of particulate contamination, we are designing the equipment so that it can be remotely installed and maintained by the cell crane and manipulation system. Also in this cell components that are subject to failure, such as motors and switches, are designed for remote removal without removing a complete assembly. In the clean fabrication cell, in which we expect little particulate contamination, we are planning to rely on contact maintenance techniques that require entry of the cell by personnel. The equipment for the clean fabrication cell will be designed to facilitate maintenance under such circumstances.

Automatic controls will be applied to each unit of equipment. The operation will be such that, after receiving a starting signal, each machine will automatically sequence through its cycle. To operate the process line, which contains a relatively large number of steps, a rate of 40 rods per day, it soon became evident that a special tube transfer machine would be essential to transfer rods between equipment units in each cell. The control of the tube transfer machines will be on a demand basis because of the wide differences in operating times of the process equipment. Initially, data would be collected manually; however, provision will be made for central data collection.

Equipment Design

The majority of the design activities during the year has been concentrated on the equipment for the contaminated fabrication cell. The clean cell fabrication equipment is almost completely dependent upon the configuration of the element to be fabricated; thus, we could not proceed with the design of this equipment. In the subsequent paragraphs, we shall discuss in detail the status of each unit of equipment. The equipment units are discussed as they appear in the process and are grouped by cell location.

ORNL-DWG 64-78R

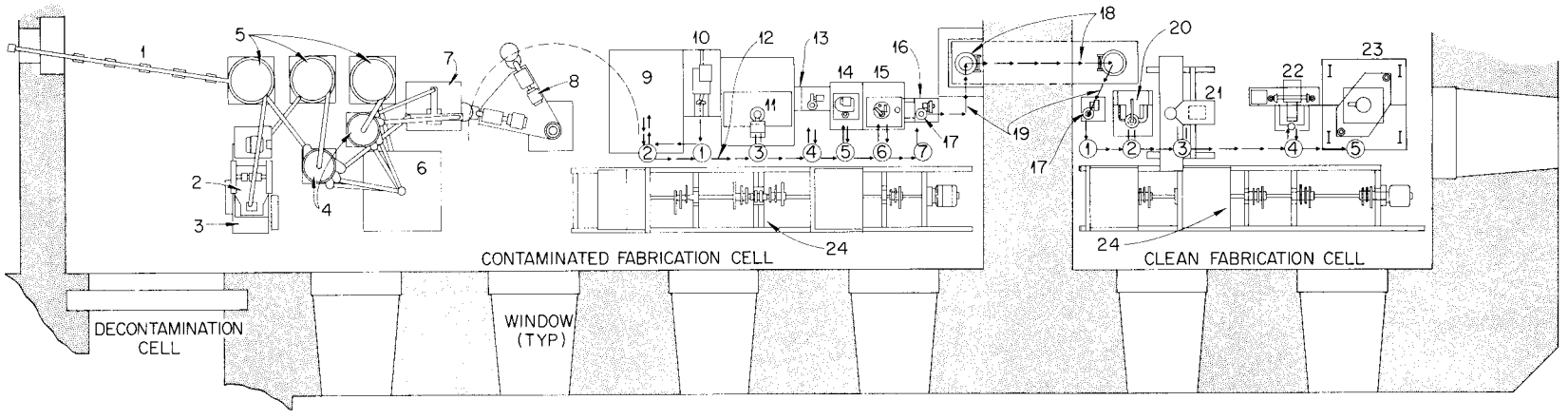

PLAN VIEW

① TRANSFER STOP POSITIONS
1. VIBRATORY TROUGH FEEDER
2. JAW CRUSHER
3. ROLL CRUSHER
4. CLASSIFIERS
5. VIBRATORY SPIRAL ELEVATORS
6. BALL MILL
7. WEIGHING MACHINE
8. FUEL TRANSFER MACHINE
9. VIBRATORY COMPACTOR
10. FUEL ROD MAGAZINE
11. GAMMA SCANNER
12. FUEL ROD FLOW
13. REJECT RACK
14. CAPPING MACHINE
15. WELDING MACHINE
16. INDEXING MACHINE
17. FUEL ROD BASKET
18. CLEANER TRANSFER MACHINE
19. TRANSFER IN FUEL ROD BASKET
20. LEAK CHECK MACHINE
21. WELD RADIOGRAPHY MACHINE
22. FUEL ROD DIMENSIONAL CHECK
23. FUEL ELEMENT ASSEMBLY AND INSPECTION MACHINE
24. FUEL ROD TRANSFER MACHINE

Fig. 2.4. Equipment Layout for Oxide Fabrication.

Powder Preparation. The bulk oxide will be processed in the powder preparation equipment into the proper particle-size distribution for vibratory compaction, and quantity for each rod loading will be obtained from the sized material. The powder preparation equipment has been designed to produce particle distributions consisting of three size fractions: 65% −6 +16 mesh; 15% −50 +140 mesh; and 25% −200 mesh material. This distribution represents what we consider the most complicated size distribution that we will be required to manufacture. The steps in powder preparation are presented in the first part of Fig. 2.3.

The crushing and grinding of the bulk oxide will be accomplished with two disk pulverizers. Although other processes were evaluated, it is our conclusion that two disk pulverizers operating at different settings can produce the desired particle breakup with very high throughput and good control.

The commercial disk pulverizers selected for use require only slight modification for better dust containment and a mechanism for remotely setting the distance between the grinding disks. Aluminum oxide grinding disks will be used to minimize contamination of the fuel material. Design modifications for the device have been completed. For classification, two commercial 18-in.-diam vibratory classifiers will be used. Only slight modification to reduce material holdup will be required for the standard units. Design modifications for the classifiers have not been completed. Weighed hoppers, which are located throughout the powder preparation system, serve to store oxide material, aid in inventory control, control feed rates, and act as valves to regulate material flow. Basically, each unit will consist of a hopper and a vibratory feeder suspended from a load-cell weighing device. Detailed design of the weighed hoppers has been completed.

The quantity of each of the size fractions required for one-rod loading will be dispensed with automatic batch-weighing equipment. Manufacturers have been contacted and a preliminary purchase specification for the equipment has been completed.

The powder conveyance system will consist of pipes for downward vertical material movement, simple commercial vibratory conveyors for

horizontal movement, and a commercial vibratory spiral elevator for upward movement. All equipment will be modified to afford maximum dust confinement. Preliminary design of the conveyors has been completed.

Fuel Transfer Unit. The fuel transfer unit accepts one fuel rod loading from the powder preparation equipment, blends it until homogeneous, and dispenses it to the vibratory compaction fill mechanism. It consists of a stainless steel blending vessel, which is opened and closed by a valve, a rotating mechanism for the blending can, and a support system which elevates and positions the can for filling and dispensing. Final design of this device is complete.

Vibratory Compactor. The function of the vibratory compactor is to fill and compact two fuel tubes, independently, after receiving the empty tube from the tube transfer machine and the fuel from the fuel transfer unit. During the fill-compact cycle, it is required that the fuel be completely contained and that any interruption of the fuel flow during the filling cycle be detected. After completion of the compaction cycle, the measurement of the fuel column height in the fuel tube is required. A pictorial representation of the compactor is shown in Fig. 2.5.

The compactor consists of two single rod units mounted on a common framework each of which operates independently. The unit has been designed on a component basis so that disabled components may be remotely removed for repair or replacement and remotely reinstalled. To accommodate rods of different heights, it will be necessary to change the height of the vibratory base; rods of different diameters are accommodated by a changing of components in the chuck and fill-receiving mechanism.

Detailed design of the vibratory compactor has been completed and the unit is now being fabricated.

Fuel Rod Check Weigher. The fuel rod check weigher that will determine the net weight of each loaded fuel rod will serve to determine the precise quantity of fuel loaded into each fuel rod and will also serve as a check on the fuel preparation weighing machine. The device will consist of a tube receiver-elevator and a weighing head. The

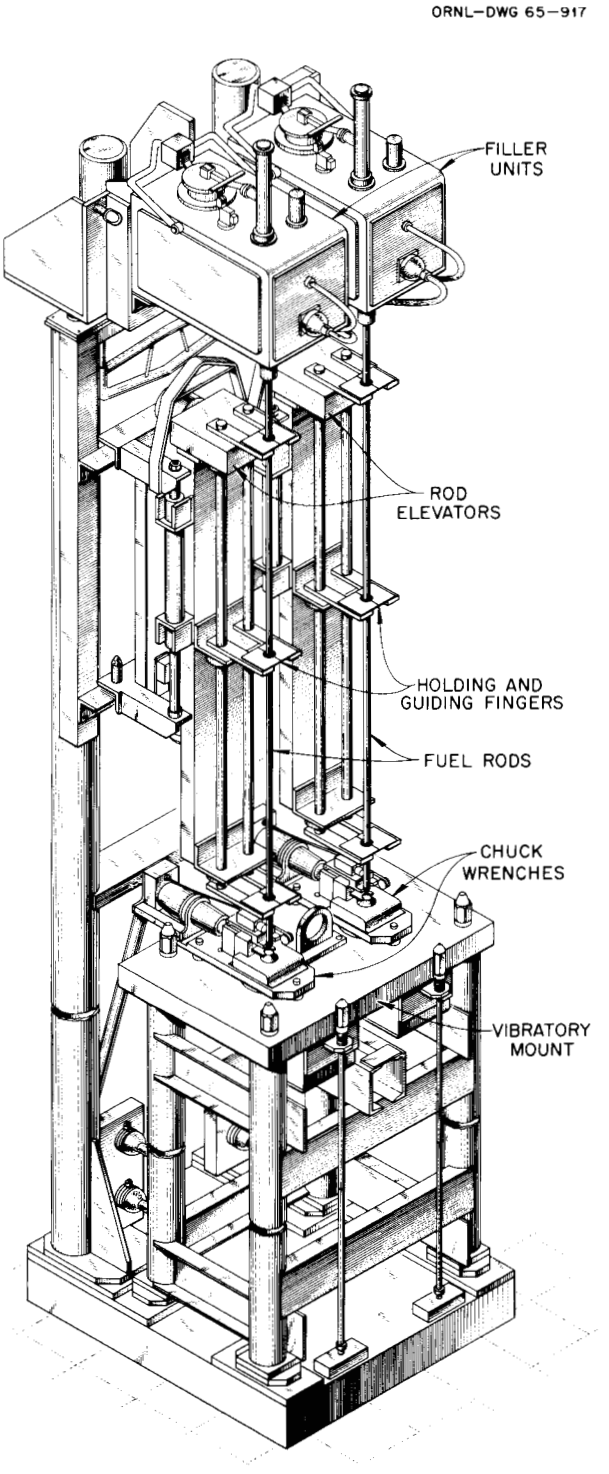

Fig. 2.5. Vibratory Compactor for Remote Fabrication.

tube receiver-elevator will serve to receive the rod from the tube transfer machine and place the rod in the chuck of the weighing head. The weighing head will consist of a commercial weighing device adapted for remote readout and handling of fuel rods. Fuel rod configuration changes are accommodated by changing chuck fingers and tube receiver-elevator grippers. Preliminary design and purchase specifications are complete.

Fuel Tube Magazine. The fuel tube magazine temporarily stores new fuel tubes for use in the process. It is to be loaded in the gloved maintenance area and unloaded by the tube transfer machine. It consists of a rotary magazine, indexing unit, and support stand. Final design drawings for this machine are available. For rod geometry changes, the only adjustments required is that for repositioning of the plate on which the tubes rest. Maintenance will be accomplished by removal of subassemblies to the gloved maintenance area.

Density Scanner. The function of the density scanner is to determine axial density variations within filled rods by measuring the attenuation of a collimated gamma beam through each rod perpendicular to its centerline. In order to meet the required overall throughput of the process line, it was necessary to design a device for scanning two rods simultaneously.

In the density scanner, the rod is fed vertically through a stationary collimated gamma beam. Although the displacement of the fuel rods vertically interferes periodically with the manipulation and bridge crane systems, we believe it to be a better solution than moving the very large and heavy shield for the detection system. The available space does not allow horizontal scanning. A large amount of shielding will be required around the detection crystal to reduce the in-cell background signal.

Design of the gamma-scanner assembly has been completed; however, detailing of the various parts has not been started.

Capping Machine. The capping machine inserts the top end cap into the fuel tube, charges the tube with helium, and cleans the weld surfaces. It consists of a cap pressing device, cap fueling device, an evacuation

and gas charging system, a tube receiver and elevator, and a rotary brush cleaner. Preliminary assembly drawings have been completed which indicate that the more difficult problems, such as sensing the cap position with respect to the tube end, cap feeding, and vacuum sealing, appear to have been solved. In keeping with the general control philosophy, it is expected that once started the machine will function automatically throughout its entire operational cycle. For purposes of maintenance, process operations, and tooling modifications, major components such as the press assembly, valving, cap magazine, cleaning mechanism, and seals are removable to the gloved maintenance area. Fuel rod size changes can be accommodated by changing cap grids in the feed magazine, by adjusting and retooling the rod elevating mechanism, and by interchanging diameter-dependent seals and collets. At present, sufficient information is available to permit the preparation of detailed fabrication drawings.

Welding Machine. The upper end-cap closure weld is made by an automatic gas-tungsten arc welder. Five assembly drawings that depict the machine configurations are complete. Major problems, such as establishing the critical electrode to tube end distance, provision of shielding gas and adequate cooling, and capability for the remote interchange of electrodes, have been solved. A special electrode holder and gas cap are mounted on an automatic weld positioning manipulator. The tube is positioned in an automatic chucking collet, which also serves as a chill block. Each of the aforementioned devices are integrated with a programable welder which controls shielding gas flow, arc parameters, and collet rotational speed.

Visual monitoring of operating parameters is inadequate. Therefore, all parameters are monitored by electromechanical means. When the operational cycle begins, all operations are sequenced automatically. Remote maintenance will be accomplished by removal of major subassemblies to the gloved maintenance area. Modifications required by a change in fuel rod configuration include adjustment of the rod elevator, interchange of collets and gas cap, and adjustment of position sensing devices. Initially, the welding head is set up to make an edge weld;

however, in the event it becomes necessary to make tangential welds, a welding head and electrode holder having a different configuration must be installed. Sufficient information is available to make detailed fabrication drawings.

Leak Check Unit. Closure welds are inspected for leaks by means of a helium leak detection system. The system consists of tube receiver-elevator, inspection head, and mass spectrometer-type helium leak detector. Preliminary assembly drawings showing the frame, inspection head, piping, and control systems have been prepared. Also, preliminary specifications for the leak detector are available. Provisions have been made to sense gross leaks prior to bringing the mass spectrometer detection system into the pumping circuit, thus avoiding helium contamination of the detector.

The helium leak detector will be located in the cell operating area; therefore, its maintenance will be by contact means. Remote maintenance will be accomplished by removing the inspection head and tube receiver to the gloved maintenance area. Interchange of filters will be done with the electromechanical manipulator. Once begun, all functions in the operational cycle will be sequenced automatically. Fuel rod configuration changes can be accommodated by adjusting the tube receiver-elevator and by interchanging the seal in the inspection head. All major problems have been solved and sufficient information exists to complete detailed fabrication drawings.

Fuel Rod Basket and Indexer. The fuel rod basket temporarily stores and transfers completed fuel rods. The device consists of a ten-position magazine into which fuel rods are placed by the tube-transfer machine and in which they are held by spring clips. Each basket mounts on an indexing device. The baskets must work with the tube transfer machine, ultrasonic cleaner, and alpha monitor.

Remote maintenance is performed by removing the indexing subassembly and baskets to the gloved maintenance area. Changes in rod configurations can be accommodated by replacing an extension spacer on the indexing base and by changing basket size. Preliminary assembly drawings are complete and sufficient information exists to prepare final fabrication drawings.

Cleaner Transfer Unit. Fuel rods are ultrasonically cleaned and transferred from the contaminated fabrication cell to the clean fabrication cell in the cleaner transfer machine. It is located in a cavity in the shielding wall separating the two cells. An enclosure, which surrounds the machine and closes the cavity, serves as an air lock between the cells.

The machine consists of a cleaning tank mounted on a traversing mechanism that moves it between parts in each cell. Power for the ultrasonic transducers and cleaning solutions are supplied from sources external to the cell.

Final design drawings of the mechanical components are complete; however, as yet, they are not approved for fabrication. Specifications for the ultrasonic cleaning system are currently in a preliminary stage. Preliminary design of cleaning solution piping and tankage is complete.

Maintenance will be accomplished by contact methods from the clean fabrication cell. Capability for processing various rod configurations is obtained by changing the fuel rod baskets.

Alpha Monitor. The alpha monitor inspects cleaned fuel rods for alpha contamination. From Kilorod experience,[9] it was determined that fuel rods that smeared clean gave high readings when directly probed.

Because of this fact and other information concerning the difficulty of in-cell mechanical smearing and counting, work began on a method for direct alpha monitoring of fuel rods in a high gamma background. As yet, results of this investigation are inconclusive; but from cursory experiments the method appears feasible. Features of this concept include direct alpha monitoring of rods and end caps, handling rods while in the cleaning basket thus minimizing transfer of contamination to the clean fabrication cell prior to monitoring, and rapid monitoring and disposition of rods.

---

[9] J. D. Sease and A. R. Olsen, Fabrication Procedure and Preirradiation Data for (^{233}U-Th)O_2-Bearing Irradiation Rods, (to be published).

Weld Radiography. End-cap welds are inspected for porosity, voids, and extraneous inclusions by means of an x-ray sensitive television system. To date, no drawings other than conceptual cell layouts have been made for this device. We cursorily examined one manufacturer's system and concluded that development is required if we are to obtain a satisfactory device. The usefulness of such a system appears to be limited to cladding thickness less than 0.030 in. and to edge type end-cap weld designs. It is further limited by its requirement for manual evaluation of good or bad welds. For greater cladding thickness and/or butt-welded end-cap designs, other inspection methods might be more suitable.

Dimensional Inspection Device. The dimensional inspection device to determine the dimensions of each rod to ensure that the rods can be readily placed in a prepared fuel element grid system will be used. The device will measure the rod diameters and bow. The rod bow measurement is intended primarily to detect sharp bends or kinks in the rods as this is the type of bow that will prevent inserting a rod in the grid basket.

The concept that is being pursued consists of a rod receiver and a series of opposing air gages that will be positioned along the length of the rod when a rod is inserted into the device. The rod receiver will rotate the rod between the air gages. The differential diameter readings will be an indication of bow. To date, no drawings have been prepared.

Fuel Element Assembly and Inspection Device. This machine loads completed fuel rods into preassembled mechanical grids, installs the top element end fitting, and inspects the bundle for assembly damage and compliance with overall dimensional specifications. Conceptually, such a device would consist of a rod storage system which makes use of the rod transfer baskets; a mechanical system for withdrawing, positioning, and inserting fuel rods; an end fitting installation system making use of a welded or swaged closure; and an inspection system. Rod-to-rod spacing inspection would most probably make use of gaged air probes which, when inserted into the rod bundles and traversed between grids, would readout dimensional information. External dimensional inspection

would most probably be by means of mechanical gages. The actual configuration of such a device is highly dependent upon the reference fuel element. Therefore, drawings other than conceptual have not been prepared.

Tube Transfer Machine. A tube transfer machine will be used in each cell to move fuel rods from station to station along the process line. The two transfer machines will be very similar except for the length of travel. The transfer machines will consist of two hands which alternately pick up a completed rod from the process station and deposit a new rod in its place as the machine travels down the process line. The machines will be sequenced on a demand of the process equipment controllers with the sequence paths of the tube transfer machine controlled by a logic system. Currently, a preliminary specification for a contaminated fabrication cell tube transfer machine has been prepared.

Summary of State of Oxide Fabrication Equipment

The effort during the past year provided equipment designs ranging from conceptual to approved for fabrication. Work was completed on schedule until the latter part of the year when this phase of the project was deferred. We firmly believe that most design problems have been solved and that those which remain appear to be within the scope of current technology.

3. PROCESS DEVELOPMENT AND EVALUATION

The scope of the Thorium-Utilization Program includes improvement and extension of sol-gel process flowsheets for thorium and thorium-uranium oxide and carbide production. It also includes development of remote Th-^{233}U fuel fabrication techniques and the preparation, irradiation testing, and evaluation of mixed thorium and uranium oxides and carbides, and of thorium alloys. In this section the results of the work in the above areas will be presented.

Extensions of the Sol-Gel Process

Particle Sizing

Several alternative methods were tested for obtaining the particle-size distributions needed for efficient vibratory compaction of sol-gel oxides. The original method of crushing, grinding, and sieving, as used in the Kilorod process and for other studies, can give any size distribution necessary and by use of blending can give 100% yields of size distributions that can be vibrated to high densities. The principal reason for considering alternative methods was to attempt to simplify the process; a secondary reason was to avoid the possibility of high gas-release rates from the fine fraction.

In order to permit efficient vibratory compaction and to produce acceptable fuel elements, the sizing procedure must satisfy four requirements:

1. The maximum particle diameter must be limited to that acceptable for the cladding dimensions; a particle diameter of one-fourth the cladding inside diameter might be a reasonable limit, although larger ratios have been used.

---

[1]C. C. Haws, J. L. Matherne, F. W. Miles, and J. E. Van Cleve, Summary of the Kilorod Project — A Semiremote 10 kg/day Demonstration of $^{233}UO_2$-ThO_2 Fuel-Element Fabrication by the ORNL Sol-Gel Vibratory-Compaction Method, ORNL-3681 (September 1965).

2. The correct fractions of coarse and fine material must be prepared. This is not a stringent requirement, since many mixtures can give good results; 60 wt % coarse, 15 wt % medium, and 25 wt % fine for a ternary mixture or 60 wt % coarse and 40 wt % fine for a binary mixture are typical mixtures used successfully.

3. The distribution of sizes within the fractions must allow efficient vibratory compaction. About 25 wt % of fine material is needed to fill the spaces between the coarse particles and these fine particles should be present as brood size distribution of −140 or −200 mesh material for the usual cladding dimensions.

4. The method must not introduce impurities, result in porous particles or particles of poor shapes for compaction, or otherwise result in unacceptable characteristics.

The methods that were considered as alternatives to the sizing by crushing, grinding, and sieving were:

1. Control of drying rates and of sol depths in the pans used in the drying oven in order to control gel fracturing so that the dried fragments spontaneously assume the proper size.
2. Formation of oxide microspheres by the procedures described elsewhere.[2] Either a mixture of large and small microspheres could be used, or small (< 100 μ) microspheres could be used as the fine fraction, with regular tray-dried sol-gel fragments as the coarse material.
3. Formation of rounded gel fragments and chunks by dripping sol into a boiling solvent to combine dispersion into small drops and rapid drying in one step.
4. Quenching of dried or partially calcined gel fragments to promote fracturing.
5. Ball-milling the dried gel instead of crushing and ball-milling the calcined oxide.

---

[2] "Formation of Microspheres from Oxide and Oxide-Carbon Sols," p. 64 , this chapter.

The results for the five methods will be discussed separately. In summary, the first, third, or fourth methods could not alone meet the four requirements listed. The first and fourth methods were capable of limiting the maximum size and of giving acceptable distributions of coarse fractions but only gave small amounts of −140 mesh material. The third method gave 5 to 10% of open porosity in the −40 mesh material and thus gave vibrated bulk densities which were about 3% lower than those obtained when regular sol-gel material was used as the fine fraction. The second method can give high-density oxide microspheres of controlled diameters less than 1000 μ, but preparation of −140 mesh material has been limited to hundred-gram quantities. This product should be good as the fine fraction; this will be confirmed after larger samples are prepared. However, the microsphere preparation involves several steps including use of an organic solvent and may not be a simplification for the preparation of fine fractions. The fifth method in combination with the first method can meet all four requirements. However, the process simplification which results from ball-milling the friable gel as compared to ball-milling the hard calcined oxide is not great, and the presence of fine fractions can cause difficulties during the calcination. This combination of the fifth and first methods was considered for the TUFCDF. The TUFCDF will probably be designed to use the first method to eliminate the need for crushing and then use the original process steps of ball-milling and sieving the calcined oxides to produce the fine fraction.

Controlled Drying Conditions to Promote Fracturing. The drying rate, the final drying temperature, the sol depth in the tray, and the sol composition were tested as variables for controlling the particle-size distribution. The particle-size distribution was primarily a function of the sol drying rate. Sols dried at a fast rate produced oxide particles with only 1 to 3 wt % of +4 mesh material while slow drying yielded 22 to 50 wt % of +4 mesh material. The yields of good −140 mesh particles were small for all values tested for all variables. In the TUFCDF the fast drying rates will be used to eliminate the need

for crushing to obtain the necessary coarse fraction size distribution. The conditions proposed for the design of the dryer from the results of experimental studies are:

1. An initial fast drying rate to remove about 60% of the water from the sol in about 2 hr. For the test dryer, this rate was obtained with an aluminum radiant panel at about 440°C and about 1.3 scfm of air passing over the 0.42-ft^2 tray.
2. Completion of drying in about three additional hours. For the test dryer, this rate was obtained with about 290°C radiant panel temperature and 1.3 scfm of air.

Samples prepared with several combinations of drying conditions were submitted for vibratory compaction tests. The vibratory compaction densities were considered satisfactory. Metallographic cross sections of the particles show them to be made of dense material with perhaps a very slight increase in porosity for the highest drying rate tested. The recommended drying cycle would permit average drying rates equivalent to 0.16 kg ThO_2 hr^{-1} ft^{-2}, or about five times the average rate in the Kilorod facility.

Microspheres as Sized Oxide Particles. When uniform spheres are poured into a container, they will usually assume a packing with a void volume fraction of 0.38 or a solids fraction of 0.62. A process for preparing theoretically dense spheres of thoria was developed and is described in detail.[2] When narrow size fractions of these spheres are poured into a cylinder which is tapped lightly on a solid surface, the bulk densities are 6.1 to 6.2 g/cm^3 which is 0.61 or 0.62 of the theoretical density of ThO_2. These spheres will be tested for compaction by vibration with −140 mesh or smaller microspheres as the fine fraction and with large spheres or regular sol-gel particles as the coarse fraction. Even if the spheres give good results, the preparation of spheres may not be a simplified process as compared to the preparation of fine fractions by grinding.

The packing of thoria microspheres for two widely different diameters was tested using −325 mesh (< 44 μ) as the fine fraction and −30 +40 mesh (420 to 590 μ) as the coarse fraction. The tap densities

of these materials in a cylinder were 6.3 g/cm^3 for the −325 mesh, 6.2 g/cm^3 for the −30 +40 mesh, and 8.2 g/cm^3 for a 28 wt % fine fraction–72 wt % coarse fraction mixture. These values are those expected for tap densities of single fractions, and high for a two-fraction mixture, but of course do not necessarily prove that vibratory compaction of spherical particles will give as high packed density as that obtained with crushed and ball-milled particles. If the fine fractions filled the channels between the coarse particles as effectively as they fill the cylinder by themselves, the density would be 8.6 g/cm^3.

The −325 mesh thoria spheres were made in a stirred baffled beaker at a mixer speed of 1500 rpm. A 2.5 M thoria sol was dispersed in the organic drying medium which consisted of 2 ethyl-1-hexanol with 0.4 vol % Ethomeen S-15. Less than 4 wt % of the thoria spheres were larger than 325 mesh after calcining at 1150°C. The −30 +40 mesh thoria spheres were prepared in the fluidized column using the same organic drying medium.

Dispersion and Drying in Boiling Solvent. Sol-gel products with size distributions that appeared promising for the fine fractions for vibratory compaction were prepared by dripping sol into a flask of 2-ethyl-1-hexanol–water boiling at 160 to 170°C. Rounded gel fragments and chunks were produced which were essentially all −40 mesh. With either thoria or thoria-urania sol and 1 vol % Span-80 in the 2-ethyl-1-hexanol, the products were over 20 wt % −325 mesh and about 50 wt % −140 mesh. The thoria-urania product prepared without adding Span-80 was 30 wt % −325 mesh and 70 wt % −140 mesh. When the boiling solution was kept at 135°C, the thoria-urania product was only 20 wt % −140 mesh, was porous, and had a low tap density.

Evaluation of the sol-gel oxides prepared by this method indicates that they are not suitable for use as the fine fraction in vibratory compaction because of open porosity. Although it was found that the size distributions of the particles were appropriate for the fine fraction of a two-fraction vibratory compaction mixture and that the pycnometric densities were 98.0 to 98.6% of theoretical, the vibrated bulk densities were decreased about 3% when these particles were substituted

for the regular sol-gel particles of about the same size distribution. Examination of cross sections of the particles disclosed open porosities of about 5 to 10 vol %. This explains the 3% decrease in packed density, since the mixture was 40 to 45 wt % of these fine fractions, and the remainder was regular sol-gel coarse particles.

Quenching to Promote Fracturing. In this approach, fragmentation of the gels by quenching in air or water after drying or firing to various temperatures was studied. Gels heated to 700°C and air quenched gave a particle size range suitable for the large fraction used in vibratory compaction and about half the medium fraction. Water quenching 700°C-fired gels led to a uniform medium fraction. It did not appear possible to obtain the fine fraction by this procedure.

Drying the gel to 150°C and then sprinkling with water gave about 90 wt % −4 to +20 mesh and 10 wt % −20 mesh product. Two 500-g batches containing fired mixtures of fractured gel plus 20 to 40% ball-milled gel were vibrated to bulk densities of 89% of the theoretical density.

In general, it appears that these quenching methods require extra process steps and have no advantages when compared to the control of drying rates and drying conditions.

Ball-Milling of Gel Before Calcination. This method can be used to produce the fine and medium fractions with the size distributions required for vibratory compaction. The size reduction is accomplished by removing small particles from the corners or surfaces of larger particles. Thus, grossly oversize particles are reduced in size only slowly and usually only one coarse particle is produced from one particle of oversize starting material. Therefore, ball-milling of the gel by itself is an inefficient method for limiting the maximum particle size, but it can be combined with use of controlled drying conditions to efficiently satisfy the four requirements listed.

Sizing of dried gels by ball-milling before calcination was tested using thoria-urania and pure thoria sols; calcined products were prepared with compositions, drying conditions, and ball-milling conditions as the variables. The fractions of products in various size ranges can be controlled by controlling the ball-milling conditions and can be

reproduced to ±10% of the amount in a fraction. Little effect on the size distributions of the ball-milled products was produced by drying times in excess of 24 hr, going to sol depths of 3/4 to 1 1/4 in. in the drying trays, or heating to 135 or 150°C after drying was completed at 90°C.

The ratios of U, NO_3^-, or NH_3 to thoria in the sols before drying affected the size distribution produced. A final drying temperature of 150°C gave about half as much +6 material and significantly more of both the −6 +16 and −16 fractions in the ball-milled product than the 90 or 135°C drying temperatures. The product obtained using a fast drying rate and two ball-milling conditions was all −4 mesh and had the size distributions shown in Table 3.1. This material with a uranium-to-(Th + U) mole ratio of 0.049 appeared to be tougher and required more intensive ball-milling than previously tested material with ratios of 0.03 or zero. It appears that the ball-milling should be done with a few large balls for a short time to favor the cracking of +6 material and the production of −16 +200 mesh material.

Table 3.1. Postcalcination Size Distributions of Materials Sized by Ball-Milling Gel[a]

Ball-Milling Conditions[b]		Calcined Oxide Size Distribution (wt %)					
Weight of Gel (g)	Time (min)	+16	−16 +20	−20 +100	−100 +140	−140 +200	−200
1203	20	42	13	28	3.4	2.1	11
786	30	14	12	46	7.3	4.3	16

[a]Sol: 2 M (Th + U); uranium-to-(Th + U) ratio of 0.049. Drying conditions: 3/4-in. sol depth and average drying rates of 0.21 kg $(Th + U)O_2$ hr^{-1} ft^{-2}.

[b]200 g of 1-in.-diam balls.

Formation of Microspheres from Oxide and Oxide-Carbon Sols

During the period covered by this report sol-gel development activity was concentrated on preparation of spherical particles or microspheres of thorium-uranium oxides and dicarbides. High-density, high-strength microspheres have excellent characteristics for use in dispersion fuels or with pyrolytic-carbon coatings. Such particles of 200 to 400-μ diameter are the preferred configuration of fuel particles for several gas-cooled reactors.

The sol-gel process for preparation of microspheres is very similar to the original sol-gel preparation of oxide fragments for vibratory compaction. The principal difference is that removal of water and gelation are accomplished by dispersing the sol as drops in an organic solvent that extracts water. The procedures for sol preparation were given in previous fuel cycle status reports.[3,4] Future studies will emphasize the engineering scaleup of the process for forming microspheres. A facility was designed and is being installed for this scaleup work. The design capacity of the facility is 10 kg ThO_2/day. Further scaleup will require tests of larger columns, development of high-capacity dispersers and evaluation of the solvent recycle system for long-term use.

Process Description. The process for conversion of sol into calcined microspheres involves six process steps:

1. dispersion of sol into drops of carefully controlled size,
2. suspension of the sol droplets in solvent and the concomitant extraction of water,
3. separation of gel microspheres from the solvent,
4. recovery of solvent for reuse,
5. drying of gel microspheres,
6. calcination and sintering of dried gel microspheres.

---

[3]D. E. Ferguson, Status and Progress Report for Thorium Fuel Cycle Development for Period Ending December 31, 1962, ORNL-3385, pp. 20–30.

[4]R. G. Wymer and D. A. Douglas, Status and Progress Report for Thorium Fuel Cycle Development for Period Ending December 31, 1963, ORNL-3611, pp. 51–59.

Each drop of sol from the dispersion contains the amount of thorium that will be in a microsphere. Any drops that contain too much or too little thorium will form oversize or undersize spheres that will be waste or will have to be recycled.

In the second step, the extraction of water causes gelation and thus converts the drop of sol into a solid gel sphere. This is the key process step. The slow extraction of water is essential to obtaining a microsphere with a high density and high strength. If the water is extracted too rapidly, the drop breaks into fragments or forms a hollow particle. Interfacial tension holds the drop in a spherical shape. This limits the maximum microsphere size, since gravitational and fluid drag forces will distort large drops.

Most of the process development work has been on the first two process steps. The calcination and sintering were done using the procedures and equipment that had been used for the original sol-gel process development studies.

Equipment. Most of the development studies were in a continuously operating system in which the first four process steps were accomplished (Fig. 3.1). This system will be described briefly as a whole; the important individual parts of the system will be discussed separately in subsequent sections. The sol is dispersed into drops which are released into the enlarged top of a tapered column. These drops are fluidized by a recirculated upflowing stream of the organic solvent. As the water is extracted and the sol drops shrink and gel into solid microspheres, the settling velocity increases. The column configuration and the flow rates are selected to permit the small gelled particles to drop out continuously while the larger sol drops are added to the top of the column. Separation of the gel spheres from the organic solvent is completed by discharging the product collector onto a fritted-glass filter and draining the solvent off through the fritted glass. The bed of gel spheres are dried by heating the bed and passing heated gases or superheated steam up through the fritted glass. Calcination and sintering to give the final, high-density, high-strength product is done in controlled atmosphere and controlled-temperature-program furnaces with final

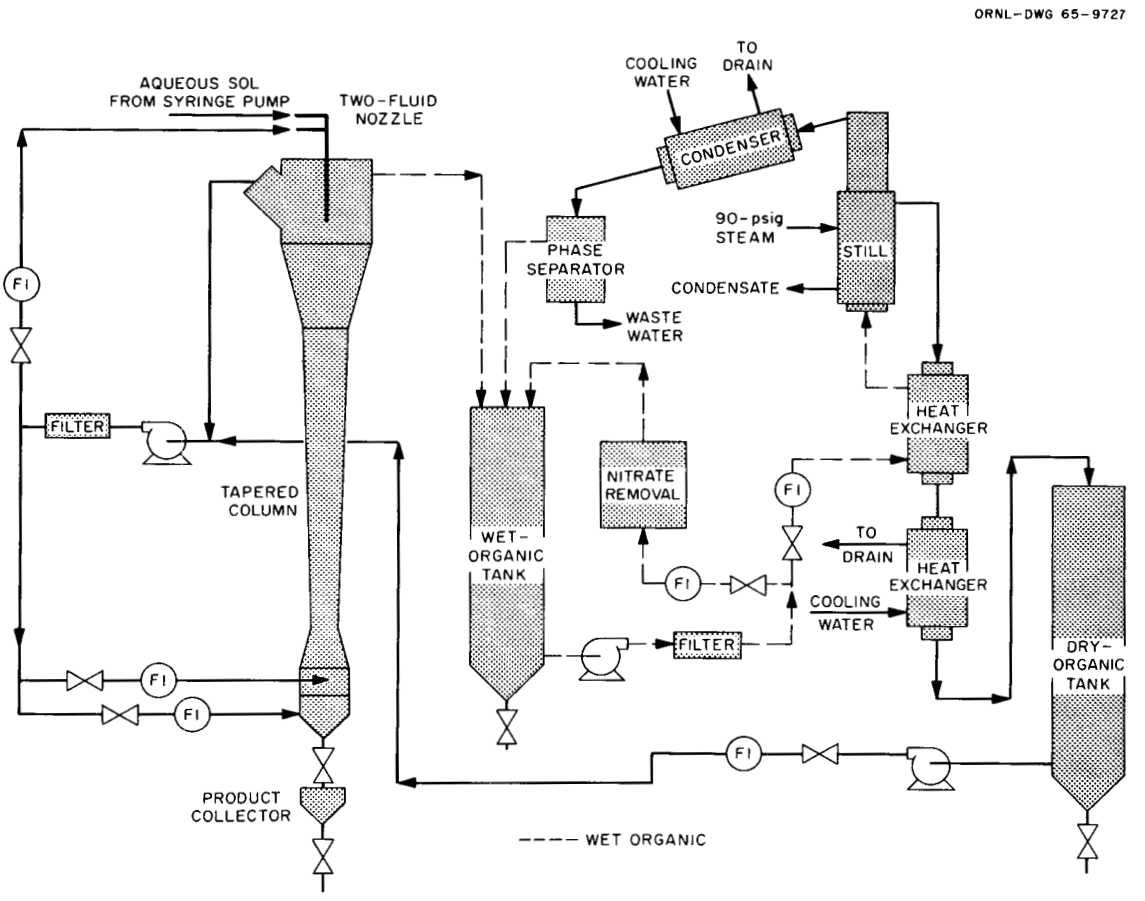

Fig. 3.1. Gel Microsphere Formation Column and Solvent Recovery System.

temperatures of 1150°C for oxide microspheres and 1800°C for dicarbide microspheres. Fresh or purified solvent is continuously added to the column and displaces a stream of "spent" solvent to a recovery system. Water is removed from the spent solvent by distillation. Other treatments may be necessary to remove impurities that accumulate as solvent degradation products or which are extracted from the sol.

Other types of equipment have been used for the same process steps. The column has been operated batchwise without removal of product or recovery of solvent. Agitation in baffled vessels has been used for dispersion and suspension of the sol drops when microspheres of less than 100 μ in diameter were prepared.

Dispersion of Sols. The microsphere preparation process requires the dispersion of sols into uniform drops of mean diameters which can be controlled between 100 and 2000 μ. The sol flow rates for the process development studies were 1 to 5 cm^3/min, but scaleup by a factor of 100 will be necessary. The need for sol-drop uniformity to minimize the amount of waste or recycle material was previously mentioned. Uniform sol drops are also necessary to the continuous operation of the microsphere column. Oversize drops would fall out immediately without drying and thus ruin part of the product. Undersize drops would not settle fast enough to fall out and would thus accumulate in the column.

Sol droplets of controlled diameters were initially formed in the tapered column system by discharging the sol through a small orifice. In order to eliminate the undesirably small orifice sizes required for free-fall drop formation, a two-fluid nozzle is being used to form the droplets (Fig. 3.2). The sol is introduced in the center of a flowing

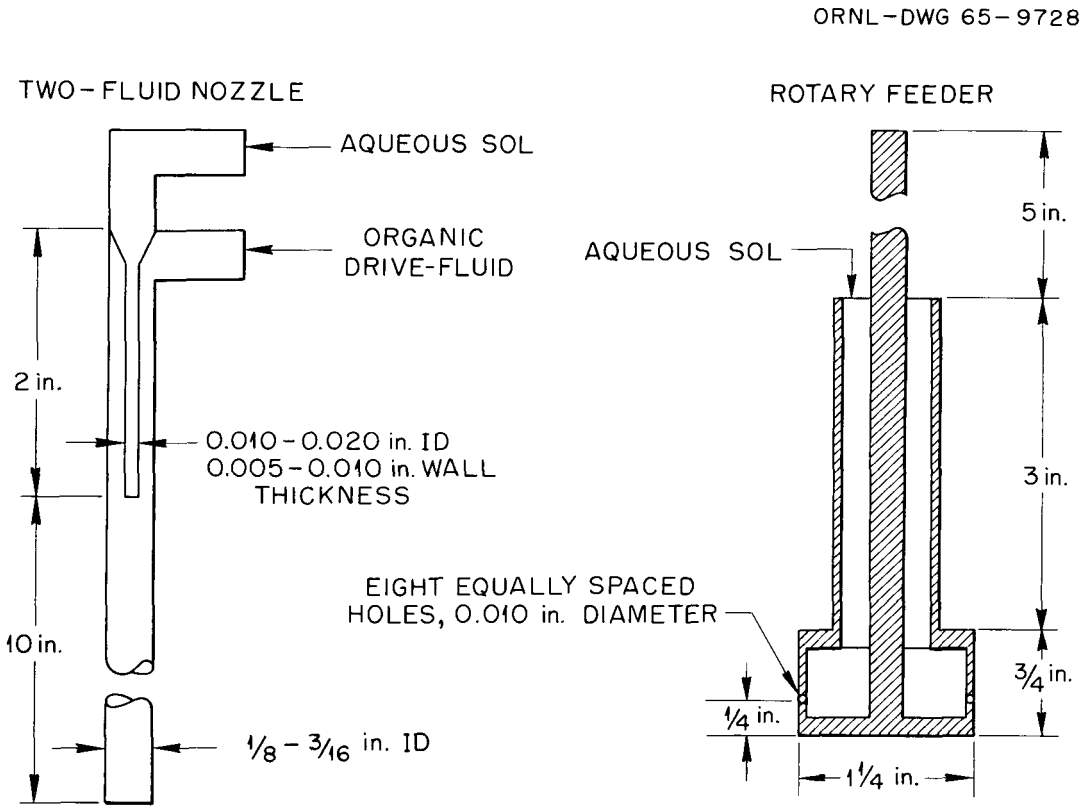

Fig. 3.2. Devices Used in Forming Sol Droplets.

organic stream which acts as the drive fluid. The continuous sol flow is accelerated to the drive-fluid velocity and then breaks up by a varicose mechanism to give sol droplets with a diameter which is 2 to 2.5 times greater than the minimum sol stream diameter. A nozzle length of 10 in. has been used to assure droplet formation before discharge into the tapered column. The breakup of a 3-M thoria sol in a glass two-fluid nozzle was photographed (Fig. 3.3). The organic solvent flow rate was adjusted to form the same size droplets in each case. About 1/8-in. length of the sol entry tube is visible at the extreme left of the figure. From this photograph it is evident that sol drops are being formed in a relatively short distance; the photograph also indicates the presence of some "satellite" droplets which are undesirable. The variables controlling drop formation can be related by the following equation:

$$D = k\sqrt{\frac{4f}{\pi V_{max}}} \quad , \tag{1}$$

where

D = sol droplet diameter, cm,

f = sol flow rate, cm^3/min,

V_{max} = maximum drive-fluid velocity, cm/min, and

k = constant for a particular system, usually 2.0 to 2.5.

Theoretically, the sol-droplet diameter should be independent of the sol-entry tube diameter. In order to form uniformly sized droplets with a two-fluid nozzle, the drive-fluid flow must be laminar, and therefore the sol should be injected in such a manner as to minimize disturbances. Using two nozzles simultaneously, a 3.1-M thoria gel was fed through each of the two nozzles at a rate of 2.5 cm^3/min for 4 hr. With a value of 2.4 for the constant, k, in Eq. (1), the drive-fluid flow rate was set to produce spheres with a calcined diameter of 230 μ. About 950 g of thoria spheres were formed with the following size distribution after calcination to 1150°C: 3.9 wt % > 250 μ, 72.3 wt % 210 to 250 μ, 13.5 wt % 150 to 210 μ, and 10.3 wt % < 150 μ.

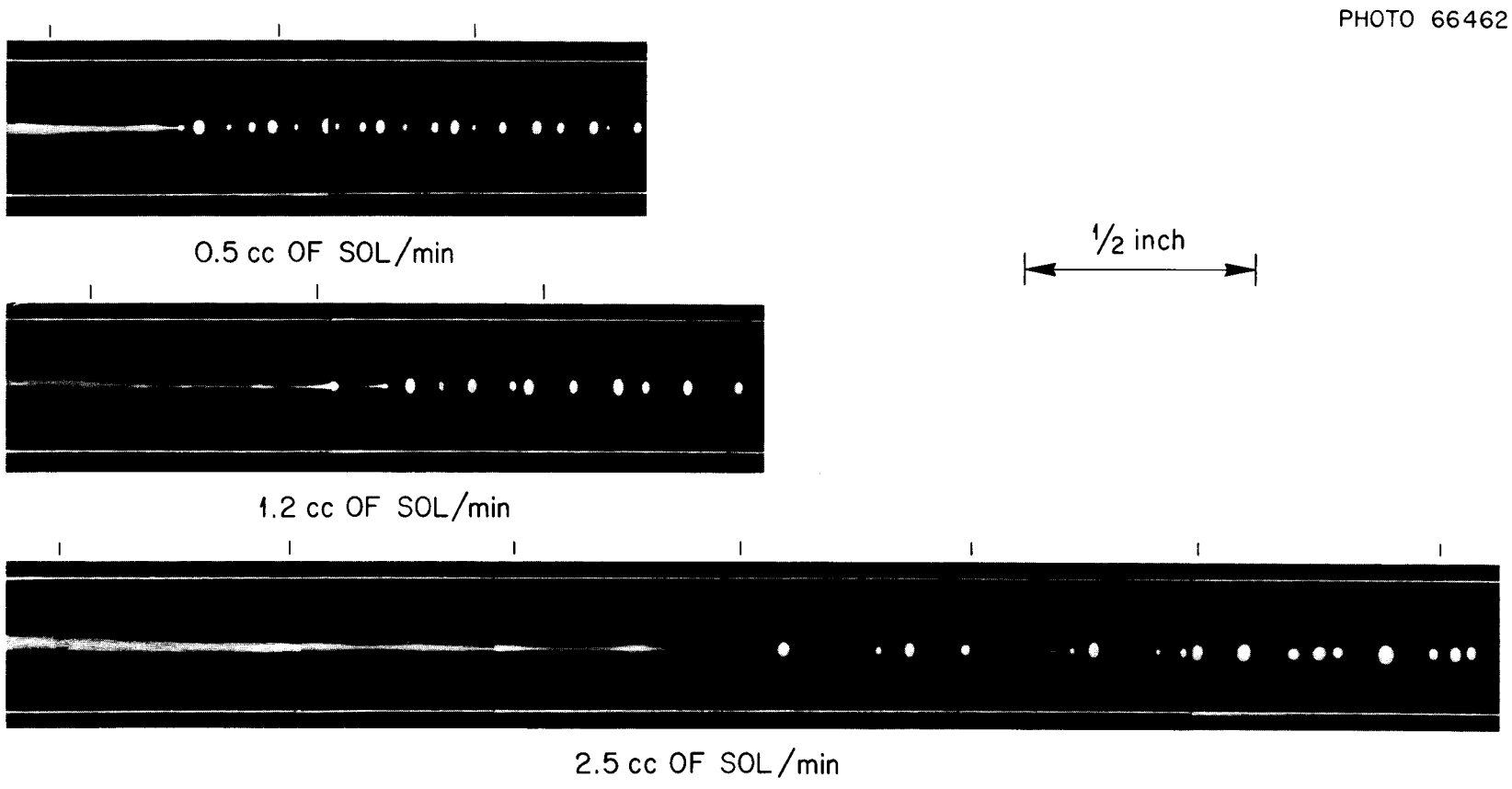

Fig. 3.3. Breakup of a 3-M Thoria Sol into Droplets.

Sol droplets in the desired size range were obtained with several rotary sol dispersers similar to the one shown in Fig. 3.2. A typical rotary disperser has eight holes, 10 mils in diameter, equally spaced at one elevation around a 1 1/4-in.-diam cylindrical surface. Initially the rotary disperser was run in air so that the droplet size could be controlled by the hole size and the centrifugal force of the forming droplet. This method of operation was unsatisfactory, because the sol drops were shattered into smaller droplets on entering the organic liquid. Encouraging results were obtained by running the disperser below the organic liquid level. This mode of operation allows the shear forces in the organic liquid to have a significant part in controlling the sol droplet size; the effect of shear may be varied by altering the geometry of the rotary disperser. The preliminary investigations indicate that the plugging of holes is not a problem, and that the droplet size is relatively independent of sol feed rate which has been varied from 5 to 15 cm^3/min. The major advantage of a rotary feeder compared to a two-fluid nozzle is its adaptability to scaleup or increased sol flow rates. Also, the sol flow to the rotary feeder does not need to be as steady and even as the flow to the two-fluid nozzle, which requires continuous, nonpulsating and accurately metered flows of both sol and organic. Using the rotary feeder illustrated in Fig. 3.2, about 195 g of thoria spheres were formed with the following size distribution after calcination at 1150°C: 6.2 wt % > 300 μ, 30.0 wt % 250 to 300 μ, 52.2 wt % 210 to 250 μ, 7.7 wt % 150 to 210 μ, and 3.9 wt % < 150 μ. For this run the sol feed rate was 5 cm^3/min and the rotation speed was 460 rpm.

Solvents and Surfactants. Several organic solvents were tried in tapered column systems to obtain a suitable water removal medium. In general, the long-chained alcohols are the most satisfactory solvents for forming spherical gelled particles. The alcohols 2-ethyl-1-hexanol and 2-methyl-1-pentanol were superior to the others tried. The halogenated solvents were avoided because of the health hazard and possible halogen contamination of the product. Essentially all of the engineering scale-up

studies have been done with 2-ethyl-1-hexanol. Considering its many excellent properties for this use, we are unlikely to find any other solvent which is significantly better.

A surfactant must be dissolved in the organic solvent to prevent coalescence of the sol drops with each other, coalescence of the sol drops on the column walls, or clustering together of partially dried drops. Surfactants also lower the interfacial tension between the sol and the solvent; the interfacial tension must be high enough to keep the drops spherical. A surfactant concentration of 0.1 to 0.5 vol % in the organic liquid seems to be sufficient. While many surfactants can be used, the column studies have been principally with three surfactants which were the most effective of the several types tested. Ethomeen S-15 and Amine O were successful in forming thoria spheres in all sizes, whereas, Span-80 can only be used for thoria sols in the size range of 100 to 300 μ. For a thoria–8 wt % urania sol, Ethomeen S-15 proved to be unsatisfactory, and Span-80 worked for sizes up to 1000 μ. Paraplex G-62 is a usable surfactant for thoria spheres in the size range of 500 to 1000 μ; however, for smaller spheroids, the partially gelled particles deposit on the tapered glass column. In general, the type of surfactant required is not highly predictable for a new sol and a specified particle size range, and trial tests are desirable for each new set of conditions.

Product Characteristics. Examples of the different sizes of thoria spheres that have been formed in 2-ethyl-1-hexanol and calcined at 1150°C are shown in Fig. 3.4. The first sample was formed in an agitated beaker at a stirrer speed of 1200 rpm. All of the particles are less than 40 μ in diameter, and a high percentage of the spheroids are less than 10 μ. The next three samples were formed in the tapered column system. The magnification of the picture of sample 1 is eight times that of the other three pictures. The average diameters of these last three samples are 250, 500, and 750 μ, respectively.

PHOTO 67081

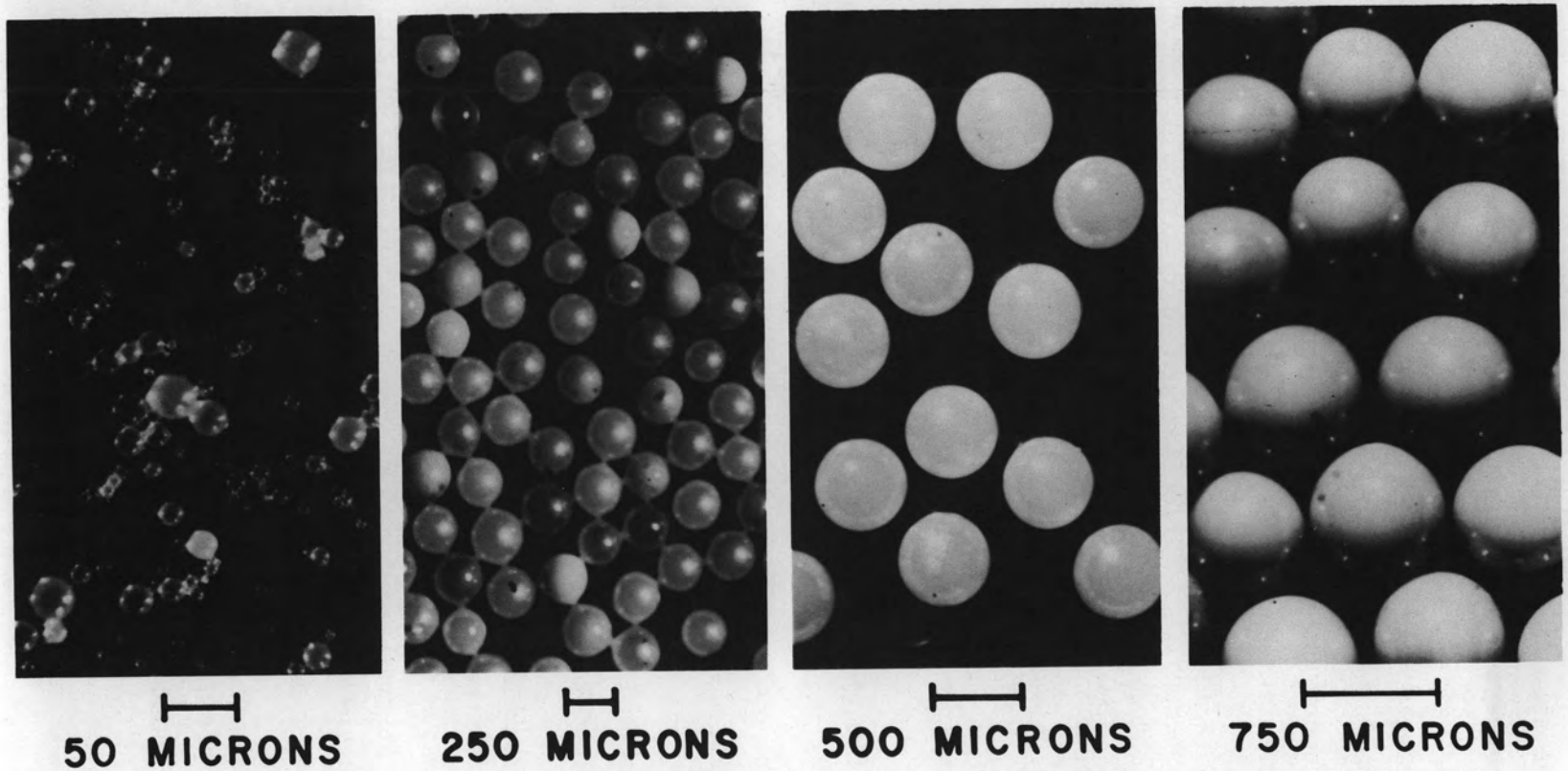

Fig. 3.4. Thoria Spheres Calcined at 1150°C.

Thoria gel and calcined spheres formed in the tapered column system are shown in Fig. 3.5. The gelled spheres are 1000 to 1050 μ in diameter and the calcined spheres are 700 to 750 μ. Thus, linear shrinkage in going from the gel to the calcined state is about 30%.

Figure 3.6 is a cross-sectioned view of the thoria gel and calcined spheres shown in Fig. 3.5. The cross section of gelled spheres indicates an outer layer of thoria, 100 to 150 μ thick, which appears to be harder and more dense than the core region. After calcination at 1150°C, the interior of the thoria spheres appears to be homogeneous with no evidence of porosity.

Gelled and calcined spheres of thoria–8 wt % urania (highly enriched) are shown in Fig. 3.7. The gel spheres are 350 to 400 μ and the calcined spheres are 250 to 300 μ. About 2200 g of these spheres were prepared in the tapered column for irradiation testing. The physical properties of the calcined spheres are: particle density, 99.4% of theoretical; krypton surface area, 0.003 m^2/g (which is less than two times the geometric surface area); and particle crushing strength (av of 25 particles), greater than 5.7 kg each.

By combining the product from several runs in the tapered column system, 19,400 g of thoria microspheres were made available for evaluation tests, pyrolytic-carbon-coating studies, and other uses. After calcining at 1150°C and screening, the size distribution of these combined preparations was:

Weight, g	Size Range, μ
990	150 to 210
12,850	210 to 250
3,400	250 to 297
1,130	297 to 420
1,050	420 to 500

About 65% of these oxide microspheres were prepared during a 95-hr continuous run.

Column Development. The column accomplishes the suspension of the drops during extraction of water and the continuous separation of gel microspheres from the sol drops. Also, the dispersion of the sol into

PHOTO 67082

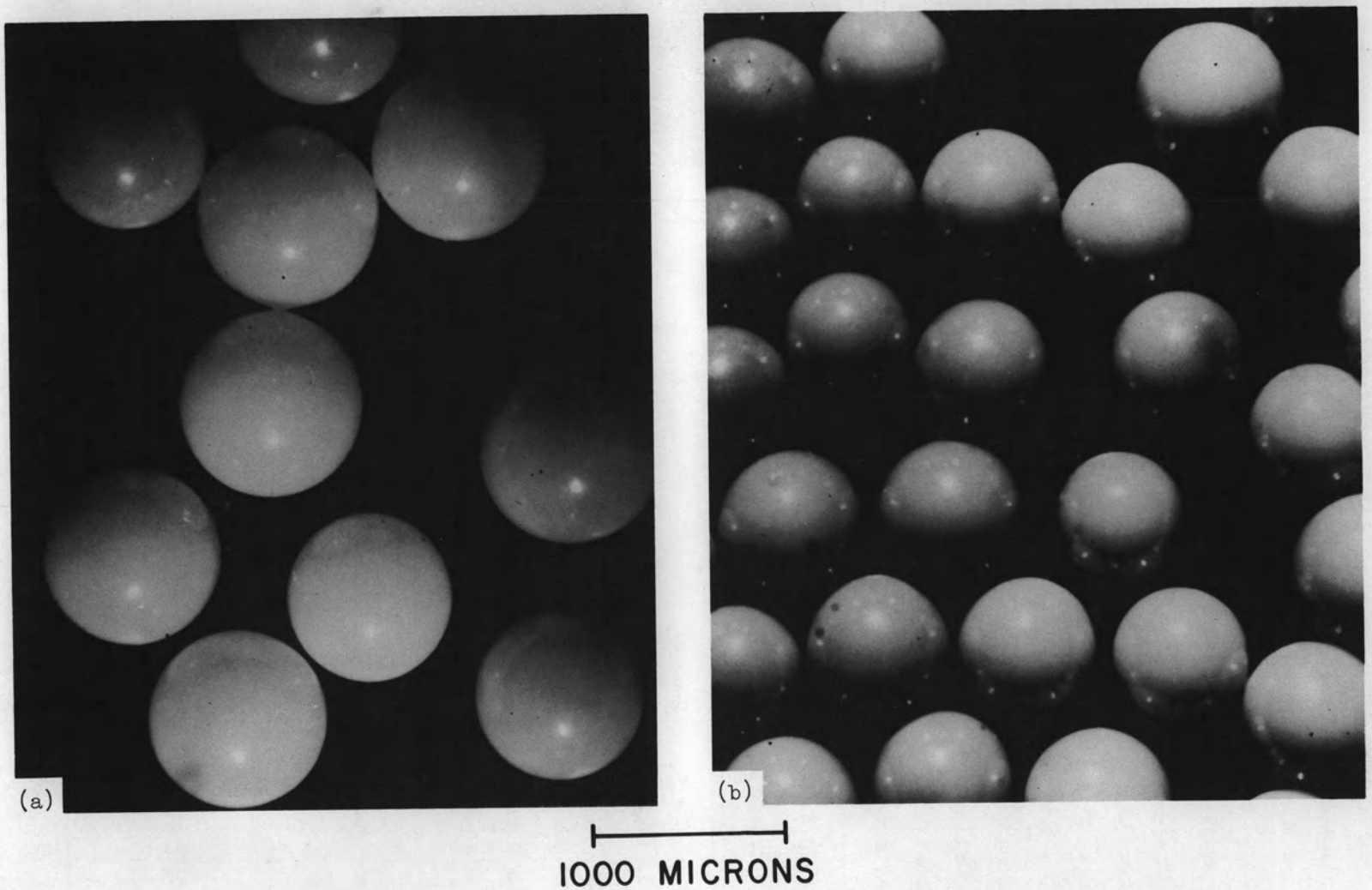

Fig. 3.5. Thoria Gel and Calcined Spheres Formed in the Tapered Column System. (a) Thoria Gel Spheres Dried at 100°C. (b) Thoria Spheres Calcined at 1150°C.

PHOTO 67085

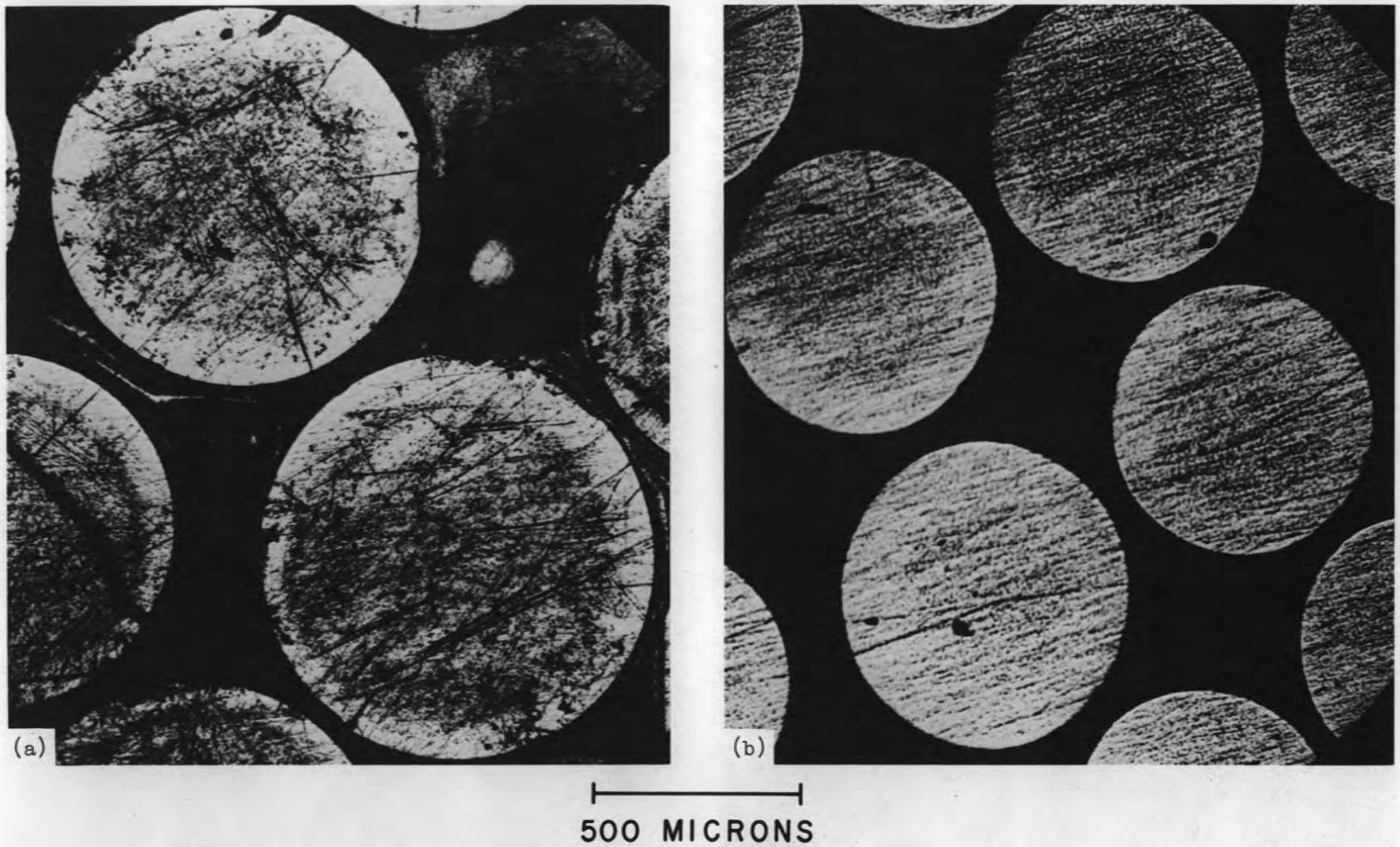

Fig. 3.6. Cross Section of (a) Thoria Gel Spheres and (b) Calcined Thoria Spheres.

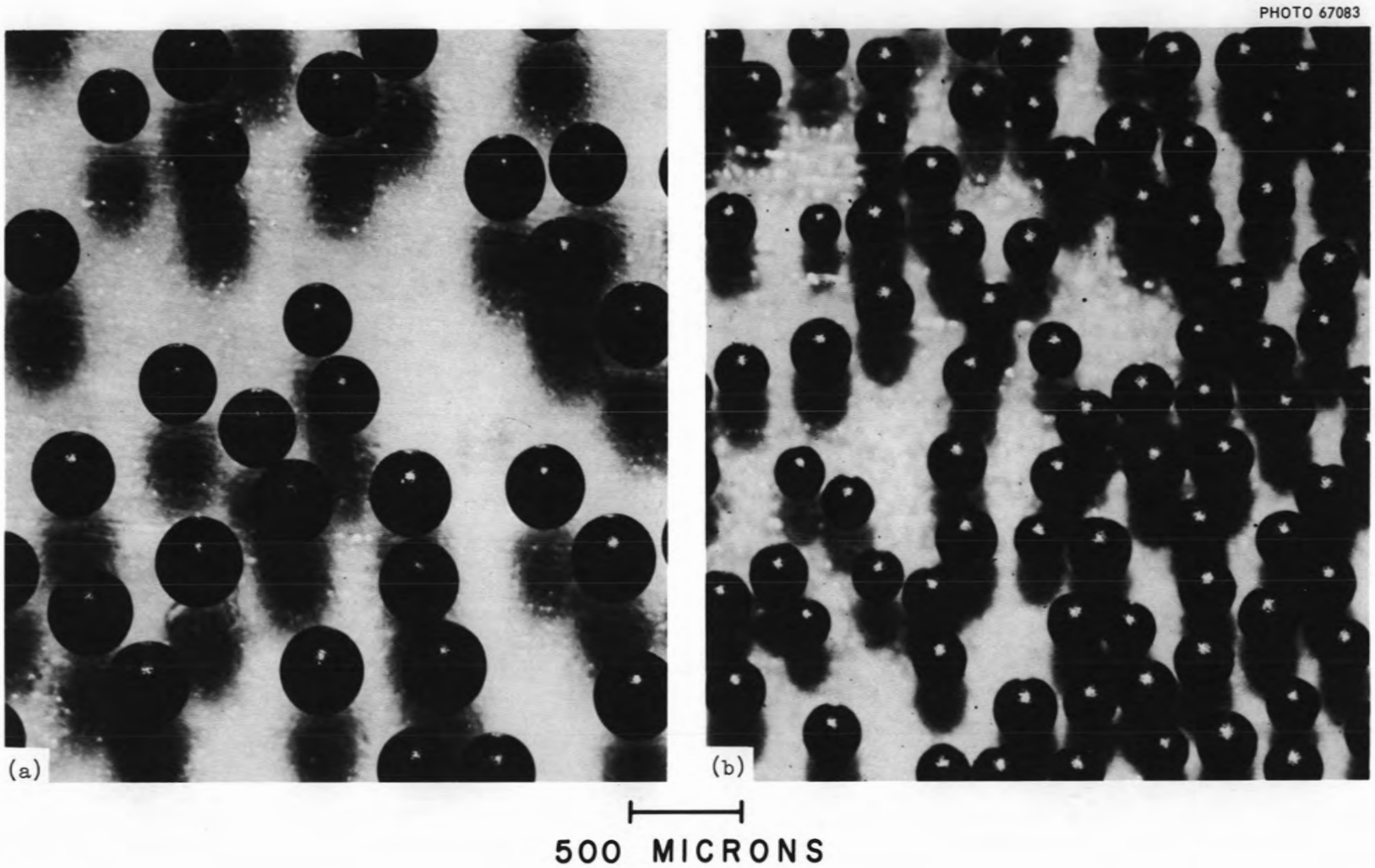

Fig. 3.7. Spheres of Thoria–8 wt % Urania (Highly Enriched). (a) Gelled. (b) Calcined.

drops is carried out in the enlarged top section of the column. For a given column and sol drop size, the upward flow of the organic solvent is selected to suspend the freshly formed drop of sol in the upper half of the column. As the water is extracted and the drop gels and densifies, the settling velocity with respect to the sol increases. The column configuration is selected to permit the drop to progress down the column as its settling velocity increases. Finally, the gel microsphere falls through the point of maximum fluidizing velocity and settles into a product collector.

The tapered glass columns were the most successful of several column configurations tested. Continuous addition of sol drops and removal of gel microspheres was possible for columns of up to 1/2-in.-minimum inside diameter by simply using smooth, gradual tapers and axial upflow of solvent. The axial upflow of the solvent is laminar and has the well-known parabolic velocity distribution across the column cross section.

When the tapered columns are scaled up to larger than 1/2-in. minimum inside diameter, the suspension of the sol drops and gel spheres becomes very unsatisfactory in several ways. The parabolic velocity distribution of the solvent results in a high net upward velocity of drops at the center and a high net downward velocity at the wall. These net flows result in axial mixing of the particles. In small diameter columns, these axial mixing patterns or cells have short unit lengths and the axial mixing is tolerable. As the column diameter is increased, the mixing extends throughout the bed thus bringing undried sol drops to the bottom of the bed. The nonuniform upflow at the minimum inside diameter cross section permits particles to drop out even though their settling velocity is lower than the average solvent velocity at this point. In the larger columns, drops fall preferentially in the region of low solvent velocity near the column wall. In the smaller columns, the sol drops are on the order of one-tenth the minimum column radius and cannot be exposed to as low an "average" velocity since they subtend a greater fraction of the parabolic velocity profile. The other nonuniformity was a time variation. Any increase in the particle

population one side of the column would increase the average density on that side. This would tend to decrease the upflow on that side. Thus, a uniform population of particles was unstable and a small accumulation of particles would lead to an increase in number until the relatively dense accumulation was dropped through one side of the cross section of minimum inside diameter.

These problems with maintaining fluidization in the larger columns were eliminated by introducing a solvent stream tangentially at the bottom of the column below the point of minimum diameter. This tangential stream produces a swirl which extends with decreasing intensity from one to three feet up the column. The mixing by the swirl prevents the accumulation of particles on one side of the column. The centrifugal forces produce an axial flow away from the tangential inlet point at the wall and toward the tangential inlet point at the center. By controlling a tangential flow and axial flow separately, the velocity profile across a diameter can be flattened or the upflow at the center may even be a minimum with a maximum between the center and the wall. The flattening of the velocity profile by the swirl reduced the amount of axial mixing so that the wet sol drops remained in the upper half of the column.

Most of the development studies were in a column of 2-in. minimum inside diameter (Fig. 3.8). A definite separation of the sol drops and the gelled particles was observed in this column (Fig. 3.9). The time required for gelation is on the order of 5 to 20 min depending on the initial sol molarity and the initial drop size.

Solvent Recycle. The solvent displaced from the microsphere-forming column to a "wet" solvent tank is purified by distillation to remove water and undergoes other treatments, if necessary, before it enters a "dry" solvent tank for recycle to the column. The water content of 2-ethyl-1-hexanol is efficiently reduced by a simple, single-stage distillation. The boiling point of the solvent changes rapidly with water content from 183°C for water-free solvent to 150°C for 0.4% H_2O, and 98°C for the azetrope when an aqueous phase is present.

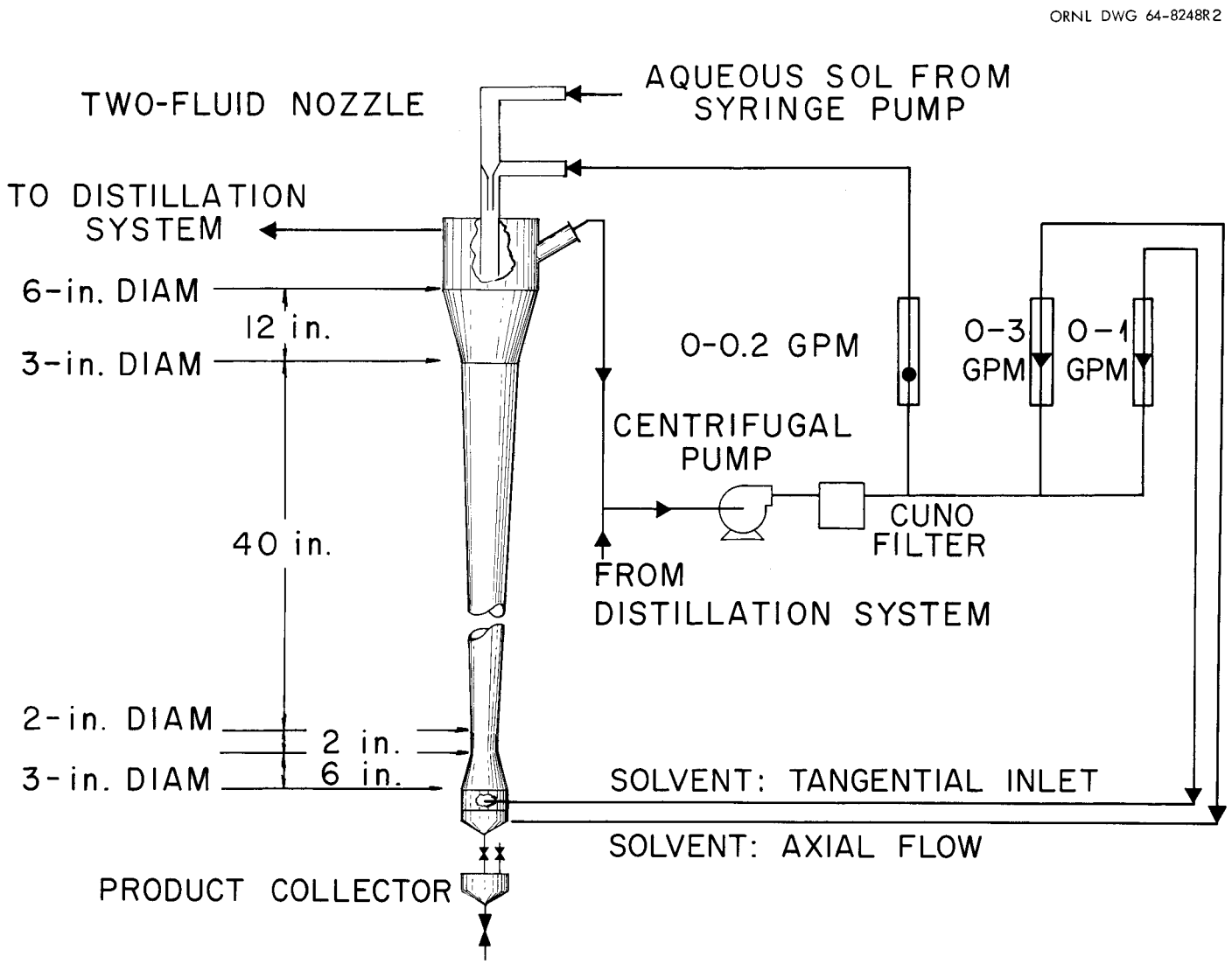

Fig. 3.8. Microsphere Column Configuration.

PHOTO 66616

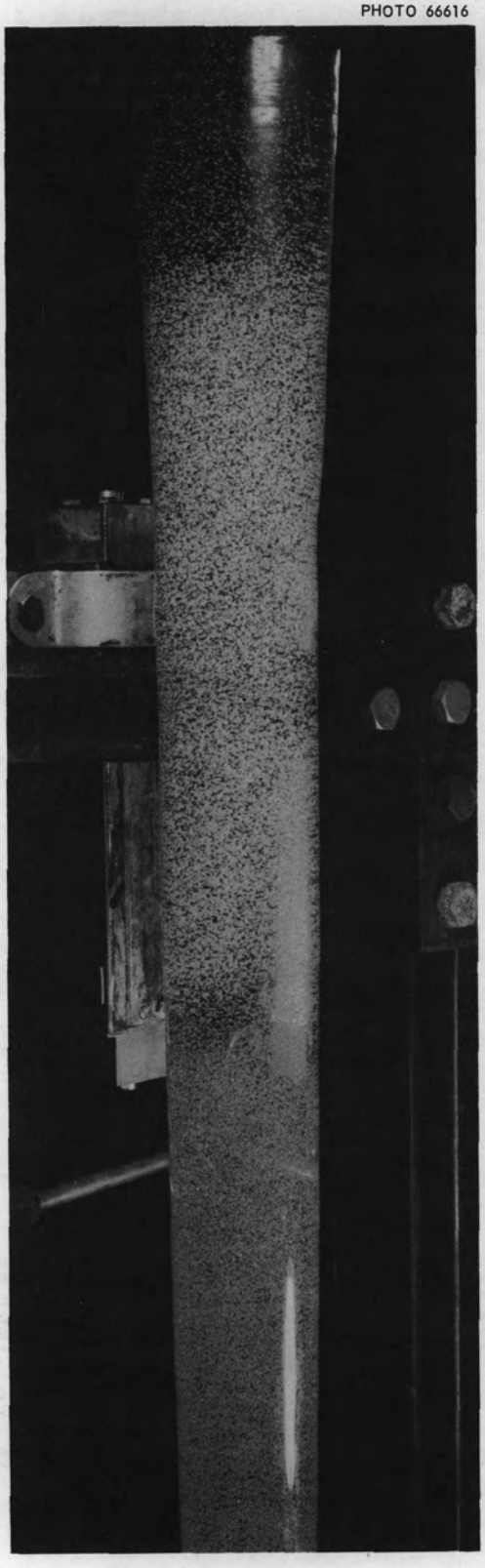

Fig. 3.9. The Upper Section of the Tapered Glass Column.

The mutual solubilities at room temperature are 2.55 wt % for water in 2-ethyl-1-hexanol and 0.1 wt % for 2-ethyl-1-hexanol in water. The operating conditions are usually selected to give 0.5 to 1.0 wt % H_2O in the solvent. Thus, the solvent processed in the recovery system is 100 to 1000 times the weight of the thorium plus uranium in the microsphere product.

A steam-heated still with 90 psig steam, heat exchangers, and a phase separator as shown in Fig. 3.1 is very simple and efficient in operation. Only a small fraction of the liquid is vaporized. Most of the heat load is sensible heat and a good heat exchanger minimizes the heating and cooling load. As water and 2-ethyl-1-hexanol are vaporized, the water content of the liquid decreases until the boiling point approaches the condensation temperature of 90 psig steam (165°C). Thus, the amount of boilup is automatically controlled without the need for any measurement or control devices. After the vapors are condensed, the aqueous and organic phases separate by gravity and are discharged through jacklegs. This single-stage distillation with separation of the the condensed liquids requires less heat than using reflux in a multiple stage column.

Gradual color changes of the solvent indicate the accumulation of surfactant or solvent degradation products. When amine-type surfactants are used, nitrate is extracted from the sol and appears to cause clustering problems for some sol compositions. The accumulation of these impurities has not caused any apparent deleterious effects for the longest runs which were made with pure thoria sols. If these impurities do limit the recycle of solvent, the costs of solvent treatment vs replacement will have to be considered.

The use of an ion exchange resin to remove nitrate illustrates the possibilities of unanticipated effects from impurities. Since nitrate was accumulating in the 2-ethyl-1-hexanol, the solvent was passed through Dowex 1-X8 resin in the hydroxide form to remove the nitrate. The thoria microsphere products had relatively low strengths and had particle densities of 8 to 9 g/cm^3 when the ion exchange resin was used as compared to > 9.8 g/cm^3 when the resin was not used.

Later tests showed that the accumulation of nitrate did not seem to affect the formation of pure thoria microspheres so use of the resin column was discontinued.

Effects of Irradiation on Thorium Oxide Fuels

While developing processes for preparing nuclear fuels and fabricating the fuel elements, it is essential to conduct a continuing program for testing the effects of radiation. In the thorium fuel cycle work, irradiation testing has been done on fuels packed into tubes by vibratory compaction and on pellets.

Evaluation of powder-compacted sol-gel and arc-fused oxide fuels under irradiation has continued. Table 3.2 presents the current program by capsule groupings and purpose. Table 3.3 includes a description of all the fuel rods that have been or are being irradiated while Tables 3.4 and 3.5 present the irradiation conditions and major postirradiation findings on the capsules examined to date.

Previous reports[5,6] have discussed some of the earlier observations in this program. For clarity, additional observations and those made on fuel rods examined during the past year will be presented in groups for greater clarity.

MTR-I and NRX-III

The initial evaluation of the chemically produced sol-gel powders and a comparison of such variables as fuel composition, bulk density, fuel rod geometry, and burnup is essentially complete. A peak linear heat rating of 507 w/cm (calculated maximum instantaneous) in a fuel rod

---

[5]D. E. Ferguson, Status and Progress Report for Thorium Fuel Cycle Development for Period Ending December 31, 1962, ORNL-3385, pp. 102–128.

[6]R. G. Wymer and D. A. Douglas, Status and Progress Report for Thorium Fuel Cycle Development for Period Ending December 31, 1963, ORNL-3611, pp. 81–112.

Table 3.2. Summary of Thorium Fuel Cycle Program Irradiations of Powder-Packed Capsules (Rods) of Type 304 Stainless Steel[a]

Designation	Number of Rods	Type of Oxide	Density (% theoretical)	Fuel Rod Dimensions (in.)			Linear Heat Rating (Btu hr^{-1} ft^{-1})	Peak Burnup (Mwd/tonne metal)	Status	Objective
				Length	OD	Wall				
MTR-I	7	Arc-fused Sol-Gel E	86 to 87	11	0.312	0.025	40,000	15,000 to 100,000	2 examined; 4 being examined; 1 in-reactor	Provide base-line data to use in comparing sol-gel and arc-fused oxide
MTR-II	2	Sol-Gel S	88 to 89	22	0.312	0.025	62,000	100,000	In-reactor	Obtain higher heat rating by increasing enrichment
MTR-III	6	Sol-Gel 35	86 to 89	12	0.438	0.025	85,000	100,000	In-reactor	Compare oxide calcining atmospheres and higher heat ratings obtained by increasing diameter
ETR-I	4	Sol-Gel 35	86 to 89	12	0.438	0.025	>100,000	22,000	Being examined	Same as for MTR-III
NRX-I	8	Sol-Gel A and B	86 to 87	11	0.312	0.025	17,000	16,000	Examined	Provide base-line data
NRX-II	4	Sol-Gel C Arc-fused	83 to 86	22	0.312	0.025	22,000	5,000	Examined	Study effect of increased length
NRX-III	6	Sol-Gel S	88 to 89	39	0.312	0.025	28,000	23,000	Being examined	Study effect of increased length
NRX-III	3	Sol-Gel ThO_2-PuO_2	74 to 76[b]	11	0.312	0.025	27,000	22,000	Being examined	Study ThO_2-PuO_2 oxide and lower packed density
ORR Loop	3	Sol-Gel 26	84 to 85	22	0.460	0.015	52,000	2,100	Examined	Study in pressurized water at 260°C and 1750 psi.
ORR Poolside	2	Sol-Gel D	85	7	0.625	0.020	35,000	5,000	Examined	Measure effective thermal conductivity using a central thermocouple in NaK at 315 psi, 540 and 705°C
ETR-II	6	BNL-Sol-Gel	90	19	0.499	0.035	~65,000	30,000 to 100,000	In-reactor	Study effects of remote fabrication and oxide recalcining
ETR-III	7	Sol-Gel ThO_2	88	19	0.499	0.035	~80,000	10,000 to 70,000	Being prepared	Study ThO_2 blanket material with gradually increasing heat rating and provide high Pa low fission-gas-product material for chemical processing

[a]Except ETR-II, ETR-III and two of the three ORR loop specimens were Zircaloy clad.

[b]Tamp packed.

Table 3.3. Description of Irradiation-Test Fuel Rods in the Evaluation Program of ThO_2-UO_2 Vibratorily Compacted Fuels

Group	Number	Fuel Rod Identification	Type of Oxide	Total[a] Uranium (wt %)	Cladding	Oxide Particle Size	Vibrated Density (% theoretical)[b]	Fuel Rod Dimension, cm		
								Length	OD	Wall
MTR-I	43-59	U-1	Arc fused	3.96	304 SS	(c)	85.7	28.70	0.797	0.0635
	43-60	U-2	Arc fused	3.96	304 SS	(c)	85.6	28.70	0.797	0.0635
	43-61	U-3	Arc fused	3.96	304 SS	(c)	85.5	28.70	0.797	0.0635
	43-62	U-5	Sol-gel E	3.96	304 SS	(c)	87.0	28.70	0.797	0.0635
	43-63	Z-5	Sol-gel E	3.96	304 SS	(c)	86.2	28.70	0.797	0.0635
	43-64	Z-7	Sol-gel E	3.96	304 SS	(c)	86.2	28.70	0.797	0.0635
	43-65	Z-8	Sol-gel E	3.96	304 SS	(c)	85.5	28.70	0.797	0.0635
MTR-II	43-75	E-6	Sol-gel S	5.0	304 SS	(d)	87.5	57.25	0.797	0.0635
	43-76	E-8	Sol-gel S	5.0	304 SS	(d)	87.9	57.25	0.797	0.0635
MTR-III	43-77	14	Sol-gel 35-1	5.02	304 SS	(e)	87.3	30.48	1.111	0.0635
	43-78	17	Sol-gel 35-1	5.02	304 SS	(e)	87.7	30.48	1.111	0.0635
	43-77	9	Sol-gel 35-2	5.02	304 SS	(e)	88.1	30.48	1.111	0.0635
	43-79	11	Sol-gel 35-2	5.02	304 SS	(e)	87.7	30.48	1.111	0.0635
	43-78	5	Sol-gel 35-3	5.02	304 SS	(e)	86.4	30.48	1.111	0.0635
	43-79	7	Sol-gel 35-3	5.02	304 SS	(e)	86.0	30.48	1.111	0.0635
ETR-I	43-80	18	Sol-gel 35-1	5.02	304 SS	(e)	88.1	30.48	1.111	0.0635
	43-80	10	Sol-gel 35-2	5.02	304 SS	(e)	89.4	30.48	1.111	0.0635
	43-81	8	Sol-gel 35-3	5.02	304 SS	(e)	85.1	30.48	1.111	0.0635
	43-81	20	Sol-gel 35-1	5.02	304 SS	(f)	88.3	30.48	1.111	0.0635
ETR-II	43-83	2B	Sol-gel Pr	2.77% ^{233}U	Zircaloy-2	(g)	91.5	48.26	1.267	0.0889
	43-85	3B	Sol-gel Pr	2.77% ^{233}U	Zircaloy-2	(g)	90.5	48.26	1.267	0.0889
	43-87	5B	Sol-gel Pr	2.77% ^{233}U	Zircaloy-2	(g)	90.6	48.26	1.267	0.0889
	43-84	7B	Sol-gel Re	2.77% ^{233}U	Zircaloy-2	(g)	90.2	48.26	1.267	0.0889
	43-86	8B	Sol-gel Re	2.77% ^{233}U	Zircaloy-2	(g)	89.8	48.26	1.267	0.0889
	43-88	12B	Sol-gel Re	2.77% ^{233}U	Zircaloy-2	(g)	89.9	48.26	1.267	0.0889
NRX-I	Holder No. 3	X-1	Sol-gel A	4.31	304 SS	(h)	85.7	26.67	0.797	0.0635
		X-2 (Z-1)	Sol-gel A	4.31	304 SS	(h)	84.7	26.67	0.797	0.0635
		X-8	Sol-gel A	4.31	304 SS	(h)	84.7	28.57	0.797	0.0635
		0-3	Sol-gel B	4.39	304 SS	(h)	85.7	26.67	0.797	0.0635
		0-4	Sol-gel B	4.39	304 SS	(h)	85.7	26.67	0.797	0.0635
		0-5	Sol-gel B	4.39	304 SS	(h)	84.7	28.19	0.797	0.0635
		0-6	Sol-gel B	4.39	304 SS	(h)	85.7	26.67	0.797	0.0635
		H-3	Sol-gel B	4.39	304 SS	(h)	85.7	26.67	0.797	0.0635
NRX-II	Holder No. 5	A-1	Arc fused	3.96	304 SS	(h)	85.5	57.15	0.797	0.0635
		A-2	Arc fused	3.96	304 SS	(h)	85.7	57.15	0.797	0.0635
		C-3	Sol-gel C	4.01	304 SS	(h)	83.3	57.15	0.797	0.0635
		C-4	Sol-gel C	4.01	304 SS	(h)	82.6	57.15	0.797	0.0635

Table 3.3. (Continued)

Group	Number	Fuel Rod Identification	Type of Oxide	Total[a] Uranium (wt %)	Cladding	Oxide Particle Size	Vibrated Density (% theoretical)	Fuel Rod Dimensions, cm		
								Length	OD	Wall
NRX-III	Holder No. 4	S1	Sol-gel S	5.00	304 SS	(i)	88.2	99.06	0.797	0.0635
		S2	Sol-gel S	5.00	304 SS	(i)	88.2	99.06	0.797	0.0635
		S4	Sol-gel S	5.00	304 SS	(i)	88.3	99.06	0.797	0.0635
		S5	Sol-gel S	5.00	304 SS	(i)	87.7	99.06	0.797	0.0635
		S7	Sol-gel S	5.00	304 SS	(i)	87.7	99.06	0.797	0.0635
		S8	Sol-gel S	5.00	304 SS	(i)	88.3	99.06	0.797	0.0635
		P-4	Sol gel	4.12% Pu	304 SS	(h)	75.3	28.57	0.797	0.0635
		P-5	Sol gel	4.12% Pu	304 SS	(h)	75.7	28.57	0.797	0.0635
		P-6	Sol gel	4.12% Pu	304 SS	(h)	74.0	28.57	0.797	0.0635
ORR	Loop	L1A	Sol-gel 26	5.35	304 SS	(j)	85.2	54.61	1.168	0.0381
		L1B	Sol-gel 26	5.35	Zircaloy-2	(j)	84.1	54.61	1.168	0.0381
		L1C	Sol-gel 26	5.31	Zircaloy-2	(j)	84.1	54.61	1.168	0.0381
ORR	Poolside	03-5	Sol-gel D	2.50	304H SS	(c)	84.8	17.80	1.587	0.0508
		03-6	Sol-gel D	2.50	304H SS	(c)	85.5	17.78	1.587	0.0508
MTR	43-39	712	Pressed and sintered	3.92	304 SS	Pellets	93	11.43	0.795	0.0635
	43-40	729	Pressed and sintered	3.92	304 SS	Pellets	93	11.43	0.795	0.0635
	43-41	730	Pressed and sintered	3.92	304 SS	Pellets	93	11.43	0.795	0.0635
	43-44	645	Pressed and sintered	3.92	304 SS	Pellets	93	11.43	0.795	0.0635

[a]Enriched in ^{235}U to 93%.

[b]Based upon a calculated density depending on composition (approximately 10.04 g/cm^3).

[c]Distribution A: 60 wt % −10 +16 mesh; 15 wt % −70 +140 mesh; 25 wt % −200 mesh.

[d]Distribution B: 55 wt % −10 +16 mesh; 5 wt % −16 +20 mesh; 10 wt % −70 +100 mesh; 10 wt % −100 +140 mesh; 20 wt % −325 mesh.

[e]Distribution C: 60 wt % −8 +16 mesh; 15 wt % −70 +100 mesh; 25 wt % −200 mesh.

[f]Distribution D: 70 wt % −8 +16 mesh; 30 wt % −200 mesh.

[g]Distribution E: remote fabrication distribution with two fractions (a) screen 55 wt % all −6 +16 mesh; (b) ball mill 45 wt % spread approximately − 30% +16 mesh; 8% −16 +50 mesh; 9% −50 +140 mesh; 6% −140 +200 mesh; balance −200 mesh.

[h]Distribution F: 60 wt % −10 +16 mesh; 15 wt % −70 +100 mesh; 25 wt % −200 mesh.

[i]Distribution G: 40 wt % −10 +16 mesh; 20 wt % −16 +20 mesh; 10 wt % −70 +100 mesh; 10 wt % −100 +140 mesh; 20 wt % −325 mesh.

[j]Distribution H: 60 wt % −6 +16 mesh; 25 wt % −50 +140 mesh; 15 wt % −200 mesh.

Table 3.4. Irradiation History of Examined Fuel Rods

Experiment		Fuel Rod Identification	Cladding Temperature (°C)	Average External Pressure (psia)	Exposure Time Reactor Full Power Days	Peak Linear Heat Rating		Peak Cladding Heat Flux		Maximum[a] Burnup	
Group	Number					Time Average (w/cm)	Maximum Instantaneous (w/cm)	Time Average (w/cm²)	Maximum Instantaneous (w/cm²)	(Mwd/tonne U+Th)	(fissions/cm³)
											$\times 10^{20}$
MTR-I		U-1	100	40	110.2	299	362	120	145	12,300	2.50
		U-2	100	40	376.2	297	388	119	155	42,100	8.56
		U-3[b]	100	40	707.5	267	419	107	168	71,000	14.43
		Z-5	100	40	110.2	341	426	137	172	14,000	2.87
		Z-7	100	40	375.2	286	347	114	138	40,200	8.23
		Z-8[b]	100	40	691.1	311	507	124	202	81,000	16.46
ETR-I		18[b]	100	180	140.5	870	1050	304	367	20,400	4.26
		10[b]	100	180	140.5	865	1044	302	365	20,000	4.28
		8[b]	100	180	140.5	914	1103	319	385	22,000	4.46
		20[b]	100	180	140.5	(c)	(c)	(c)	(c)	(c)	(c)
NRX-I		X-1	100	130	311.9	116	138	46	55	13,500	2.73
		X-8	100	130	311.9	141	168	57	67	16,360	3.29
		O-3	100	130	311.9	135	162	55	65	15,690	3.20
		O-5	100	130	311.9	125	148	50	60	14,450	2.91
		H-3	100	130	311.9	86	102	35	41	10,500	2.11
NRX-II		A-1	100	130	64.2	132	138	53	55	3,170	0.64
		A-2	100	130	64.2	178	188	72	75	4,310	0.88
		C-3	100	130	64.2	200	211	80	85	4,960	0.98
		C-4	100	130	64.2	166	175	67	70	4,160	0.81
NRX-III		S-1	100	130	278.7					(d)	
		S-2	100	130	278.7	237	292	95	117	23,950	5.02
		S-4	100	130	278.7					(d)	
		S-5	100	130	278.7					(d)	
		S-7	100	130	278.7					(d)	
		S-8	100	130	278.7	234	288	93	114	23,700	4.97
		P-4	100	130	278.7	245	321	98	128	29,100	5.22
		P-5	100	130	278.7					(d)	
		P-6	100	130	278.7	219	287	87	114	26,400	4.65
ORR	Loop	L1A	260	1750	29.6	381	389	104	106	1,600	0.34
		L1B	260	1750	29.6	499	509	136	139	2,100	0.45
		L1C	260	1750	29.6	410	418	112	114	1,730	0.38
ORR	Poolside	03-5	705	315	215.2	304	337	61	68	5,220	1.13
		03-6	540	315	215.2	275	297	55	60	4,040	0.88
MTR	43-39	712	100	40	905	420	652	168	261	119,400	26.41
	43-40	729	100	40	660	461		185		96,000	24.6
	43-41	730	100	40	497	270		108		37,000	10.8
ETR	43-44	645	100	180	406	394		158		50,000	12.8

[a]Based on 200 Mev per fission.

[b]Values based upon preliminary burnup analysis, therefore subject to change.

[c]Not available at this time.

[d]Not measured.

Table 3.5. Postirradiation Observations and Calculations

Experiment	Fuel Rod Identification	$\int_{T_o}^{T_c} k d\theta$ Time Average (w/cm)	$\int_{T_o}^{T_c} k d\theta$ Maximum Instantaneous (w/cm)	^{85}Kr Release (%)	Dimensional Changes Average (mm)	Dimensional Changes Maximum (mm)	Radial Extent of Microstructural Changes Void (cm)	Radial Extent of Microstructural Changes Columnar Grain Growth (cm)	Radial Extent of Microstructural Changes Equiaxed Grains (cm)	Various Changes[a] $\int_{T_o}^{T_v} k d\theta$ (w/cm)	Various Changes[a] $\int_{T_o}^{T_{cg}} k d\theta$ (w/cm)	Various Changes[a] $\int_{T_o}^{T_{eg}} k d\theta$ (w/cm)
MTR-I	U-1	33.8	39.8	2.4	+0.025	+0.025						
	U-2	33.7	41.9	7.2	0.000	−0.051			(c)			
	U-3[b]	31.6	44.7	6.4	+0.005	+0.013			(c)			
	Z-5	37.8	44.4	0.5	+0.025	+0.075						
	Z-7	32.8	38.4	13.2	−0.025	−0.037			(c)			
	Z-8[b]	34.6	52.7	17.0	+0.015	+0.058			0.1			31.5
ETR-I	18[b]	82.3	99.4	23.0	+0.025	+0.051	0.076	0.340	0.346	(d)	(d)	(d)
	10[b]	82.2	99.2	27.8	+0.037	+0.056	0.04	0.394	0.415	(d)	(d)	(d)
	8[b]	86.2	104	35.9	+0.027	+0.041	0.109	0.383	0.396	(d)	(d)	(d)
	20				+0.025	+0.051						
NRX-I	X-1	16.5	18.5	2.2	+0.025	+0.051						
	X-8	18.8	21.3	2.8	+0.025	+0.051						
	O-3	18.1	20.6	3.6	+0.025	+0.051						
	O-5	17.3	19.4	2.9	+0.025	+0.051						
	H-3	13.8	15.2	1.6	+0.025	+0.025						
NRX-II	A-1	18.0	18.6	3.5	−0.025	−0.076						
	A-2	22.0	23.1	3.3	0.000	+0.025						
	C-3	24.1	25.2	4.0	0.000	+0.102						
	C-4	21.0	21.3	Sample lost	+0.025	+0.102						
NRX-III	S-2	28.4	33.4	2.5	0.000	+0.025						
	S-8	28.2	32.4	0.9	0.000	+0.025						
	P-4	28.0	35.4	3.2	0.000	+0.025						
	P-6	25.6	32.2	0.5	+0.025	+0.051						
ORR Loop	L1A	46.5	47.4	2.3	+0.025	+0.102			0.311			31.2
	L1B	57.0	58.1	Failure	0.000	+0.229		0.152	0.406		54.2	35.4
	L1C	49.6	50.6	3.9	0.000	+0.102			0.330			38.2
ORR Poolside	03-5	54.5	60.5	18.3	−0.025	−0.229			0.660			35.5
	06-5	46.7	50.4	Gas lost	0.000	+0.051			(c)			(c)
MTR	712[b]	44.8	65.4	22.8								
	729	48.2		12.4								
	730	31.5		(e)								
ETR	645	42.6		(e)								

[a]Time average value.

[b]Based upon preliminary burnup data, therefore subject to change.

[c]Sintering boundary not delineated.

[d]Not calculated pending confirmation of the burnup analysis.

[e]Gas samples diluted with air in sampling and partially lost.

with a maximum burnup of 16.46×10^{20} fissions/cm^3 (81,000 Mwd/tonne Th + U) has been achieved in this series. A single rod is still under irradiation and has achieved a burnup in excess of 100,000 Mwd/tonne of thorium plus uranium.

NRX ThO_2-UO_2. — One of the parameters under consideration in the early scouting type irradiations was that of fuel geometry. In order to test long rods of vibratorily compacted sol-gel material, six stainless steel clad fuel rods 99 cm long (39 in.) were irradiated in the NRX at a moderate cladding heat flux of approximately 100 w/cm^2 to a burnup of 5×10^{20} fissions/cm^3 (23,900 Mwd/tonne Th + U). The rods were spirally wrapped with a wire to assure adequate coolant distribution in the reactor. Postirradiation examinations on all six rods indicated essentially no dimensional changes. Two of these rods, S-2 and S-8, were punctured for fission-gas sampling and subsequently sectioned for metallographic examinations and burnup analyses. As can be seen from the data in Tables 3.4 and 3.5, the fission-gas release was less than 3% of that formed, based upon ^{85}Kr analyses. The very low release from capsule S-8 is in part due to the very slow diffusion of free gas through this length of fuel. Two punctures were made on each rod, one at each end. Each rod was first punctured at the plenum end and allowed to come to equilibrium. A gas sample was obtained, the rod was removed from the puncture apparatus, the first puncture was sealed, and a second puncture was made on the opposite end. In the case of S-2, approximately 95% of the gas was collected with the first puncture. In the case of S-8, however, only 10% of the gas was obtained from the plenum and the total quantity collected was only about one-third of the quantity from S-2. The fact that fission gas was collected from both ends of both rods and that the second puncture had very little air indicated the diffusion rate was very slow. In an effort to see if a complete gas block existed in S-8 after the second sample was taken, the first hole was unplugged. After 16 hr, the gas sampling system pressure had risen only to 88 torr.

Since the system leak rates are not well enough known, a quantitative evaluation is impossible but qualitatively it appears that an essentially impermeable region existed somewhere in the unsintered fuel column.

Metallographic examination of the fuel indicated there was essentially no change in structure, although there had been some agglomeration of porosity in the central region of the fuel as can be seen in Figs. 3.10 and 3.11.

From these findings and those previously reported for NRX Groups I and II, it is apparent that there is no effect of length on the performance of vibratorily compacted sol-gel ThO_2-UO_2 fuel rods in lengths up to 99 cm irradiated under conditions comparable, with the exception of the low surface temperatures, to current power reactor fuel rod exposures.

NRX ThO_2-PuO_2. — As part of the original program, sol-gel ThO_2 was blended with PuO_2 as a potential crossed progeny fuel. Since remote vibratory compaction equipment was not available and because the effect of lower packed density is also of interest these rods were loaded by tamp-packing 28.5-cm-long stainless steel tubes to a density of 75% of theoretical. Three such rods were irradiated in the NRX reactor at a calculated maximum instantaneous peak linear heat rating of 321 w/cm to 5.22×10^{20} fissions/cm^3.

Postirradiation dimensions indicated no significant swelling on any of the three rods. Two of these were subjected to a detailed examination. Fission-gas release rates were 3.2 and 0.5% of the amount formed, comparable to the UO_2-ThO_2 rods exposed at the same time.

Preirradiation metallography has not been performed pending completion of the necessary plutonium handling facilities but the microstructures of the two irradiated rods appear to be significantly different. Since both specimens reacted vigorously to the attempted hot etching, only the as-polished structures were examined. Comparative radial composites are shown in Fig. 3.12. From an examination of these, it is apparent that the center of the higher heat rated rod P-4 shows

PHOTO 69437

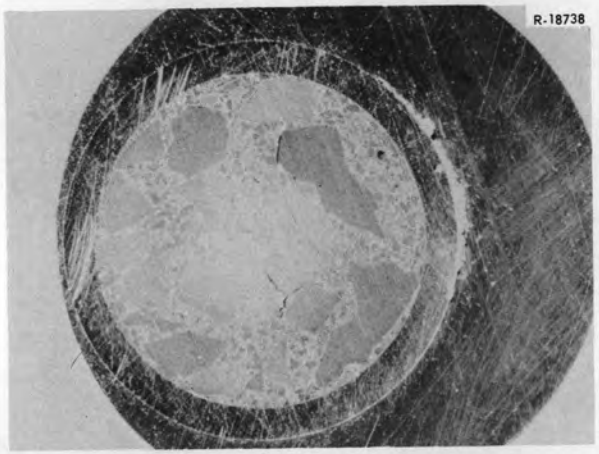

TRANSVERSE SECTION OF FUEL ROD 10X

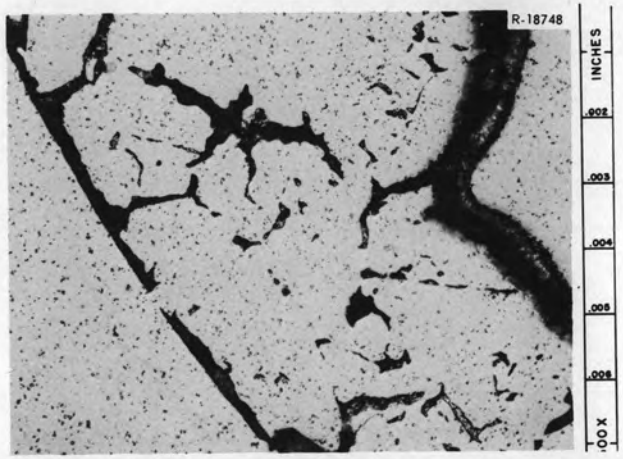

FUEL CENTER COLD ETCHED 500X

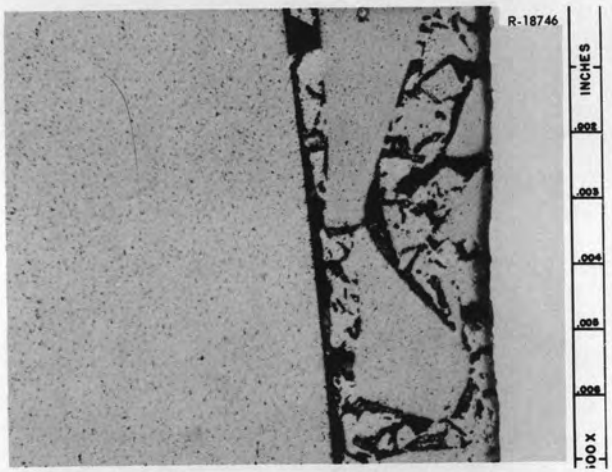

FUEL-CLAD INTERFACE COLD ETCHED 500X

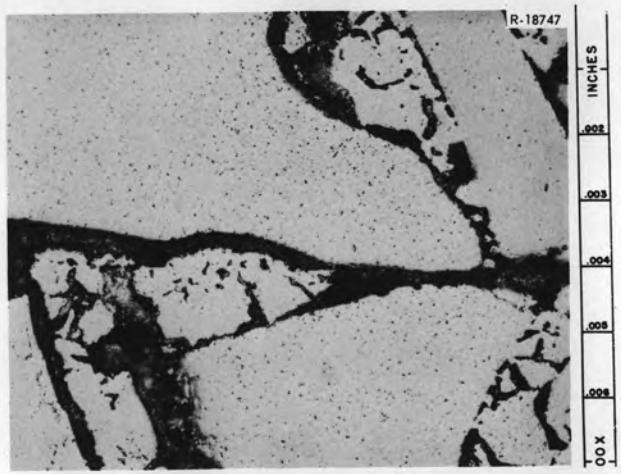

FUEL MID-RADIUS COLD ETCHED 500X

Fig. 3.10. Fuel Rod S-2 Vibratorily Compacted Sol-Gel ThO_2-UO_2 Irradiated to 5.02×10^{20} fissions/cm^3 at a Linear Heat Rating of 237 w/cm.

PHOTO 69438

TRANSVERSE SECTION OF FUEL ROD 10X

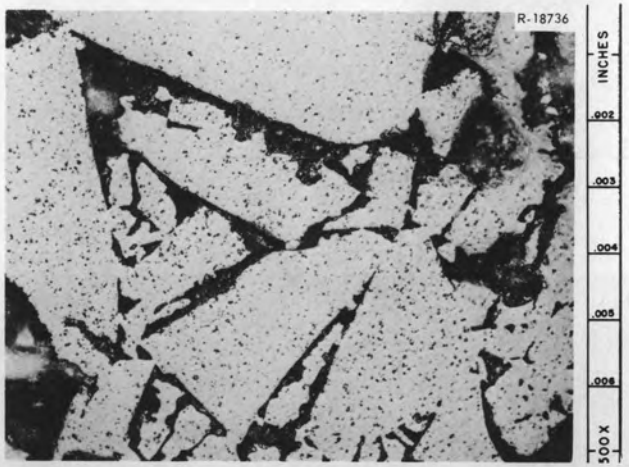

FUEL CENTER COLD ETCHED 500X

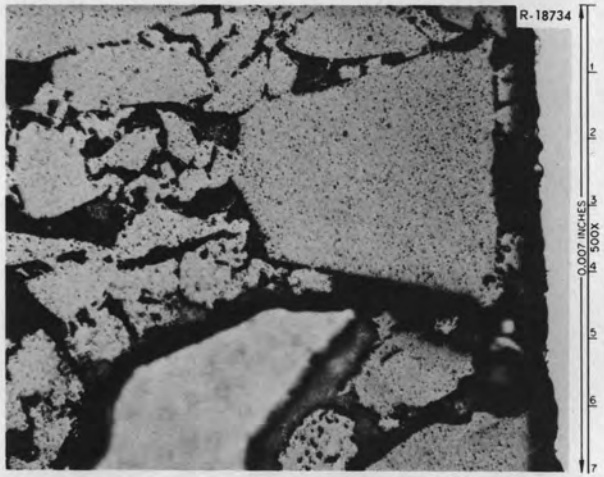

FUEL-CLAD INTERFACE COLD ETCHED 500X

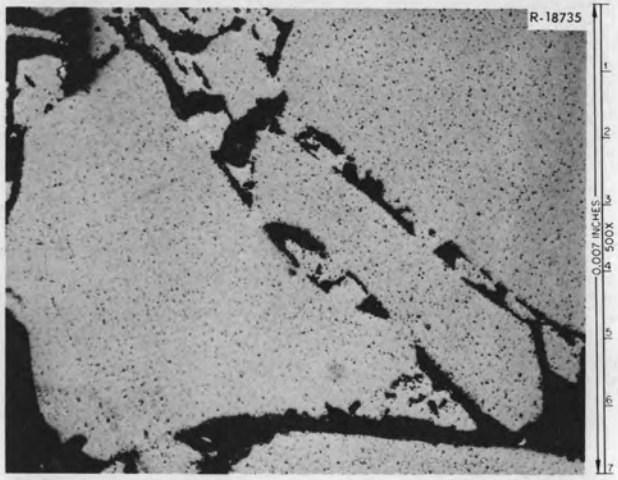

FUEL MID-RADIUS COLD ETCHED 500X

Fig. 3.11. Fuel Rod S-8 Vibratorily Compacted Sol-Gel ThO_2-UO_2 Irradiated to 4.97×10^{20} fissions/cm^3 at a Linear Heat Rating of 234 w/cm.

PHOTO 69434

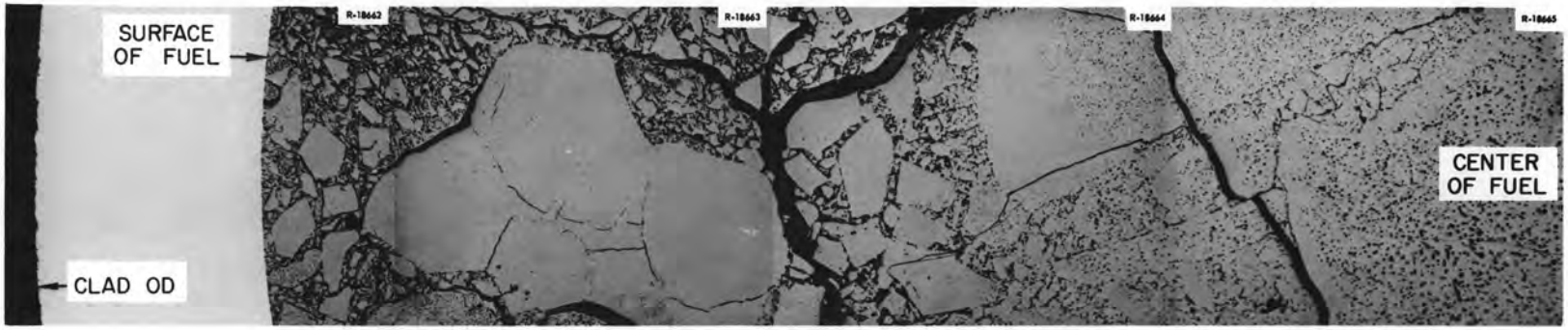

P-4 IRRADIATED (5.2×10^{20} fissions/cm^3) 100 X

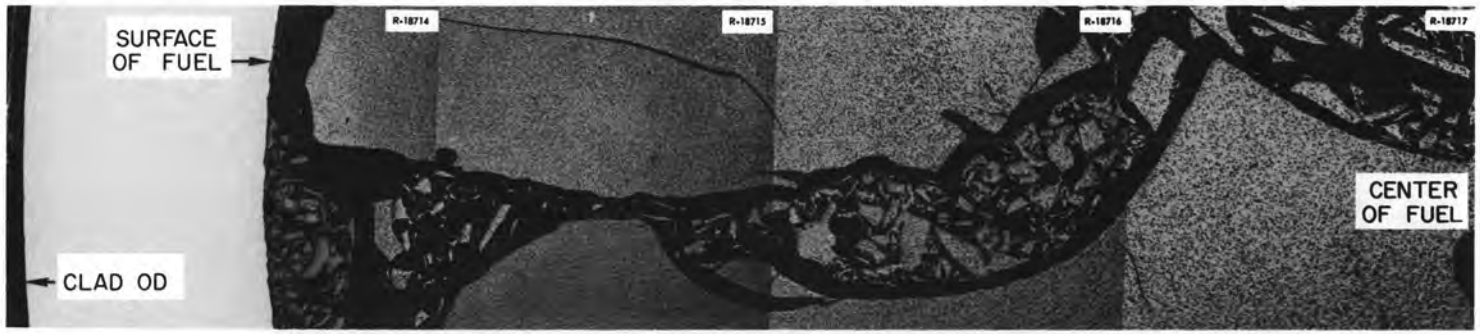

P-6 IRRADIATED (4.65×10^{20} fissions cm^3) 100 X

Fig. 3.12. Composite Photomicrographs Showing Typical Transverse Sections of Irradiated Tamp-Packed Sol-Gel ThO_2–5.2% PuO_2. Radial area from center to clad surface. 100X.

evidence of rather large porosity with spherical white metallic-appearing particles in the voids and dispersed throughout the matrix. This can be seen clearly in Fig. 3.13a which is an enlarged view of the central region. The remainder of the specimen is made up of void-free fuel fragments surrounded by mounting material, the grey phase shown in Fig. 3.13b. Fuel rod P-6, on the other hand, operated with a calculated maximum instantaneous $\int_{T_o}^{T_c} k d\theta$ of 32.2 w/cm and shows a more or less uniform distribution of fine porosity from the surface to the center with gradually increasing pore size near the center. Figure 3.14a and b show typical central and clad surface areas at higher magnification. There is no apparent interparticle phase in this sample although the central region does show a large number of fine white metallic-appearing particles. Polishing of this sample was very difficult as the low packed density particles tended to pull out in the process and the mounting plastic intrusion into the powder compact was not as complete as with capsule P-4.

Further attempts to obtain a better polished surface and additional comparisons of microstructures will be made as soon as facilities are available for the examination of the unirradiated fuel and the development of metallographic technique. Autoradiographs will also be obtained in an effort to identify possible fuel and fission-product concentrations.

Although the available data are not conclusive, the differences in microstructure and fission-gas-release rates between the two fuel rods may be explained on the basis of operating temperatures. Although there is no microscopic evidence of interparticle sintering in either case, the calculated maximum instantaneous $\int k d\theta$ for P-4 based upon the time averaged $\int k d\theta$ and fuel depletion calculations is 35.4 w/cm, the average value for sintering of ThO_2-UO_2 fuel as determined by the loop and poolside experiments. Since the actual instantaneous heat ratings could easily be ±10% from the calculated values, the difference between the two fuel rods could be as much as 10 w/cm. Such a difference would account for the lower degree of densification in P-6. The lower gas release is probably the result of two phenomena: first a slower diffusion to the interparticle voids at the lower operating temperature and secondly the previously mentioned very slow diffusion of free gas through unsintered powder compacts.

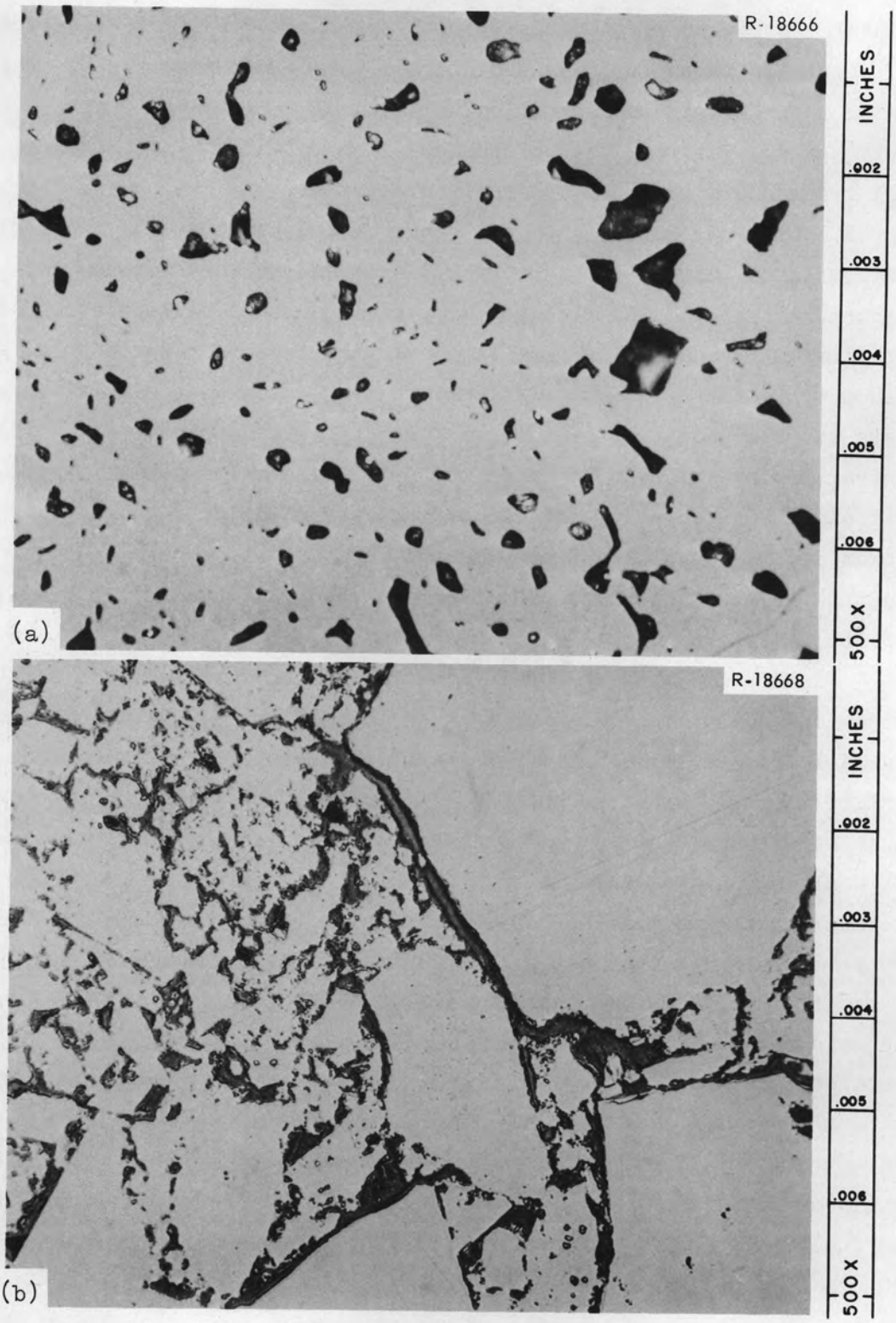

Fig. 3.13. Fuel Rod P-4 (ThO_2–5.2% PuO_2) Irradiated to 5.22×10^{20} fissions/cm^3. (a) Typical fuel center area transverse section. (b) Typical fuel area at clad-fuel interface transverse section.

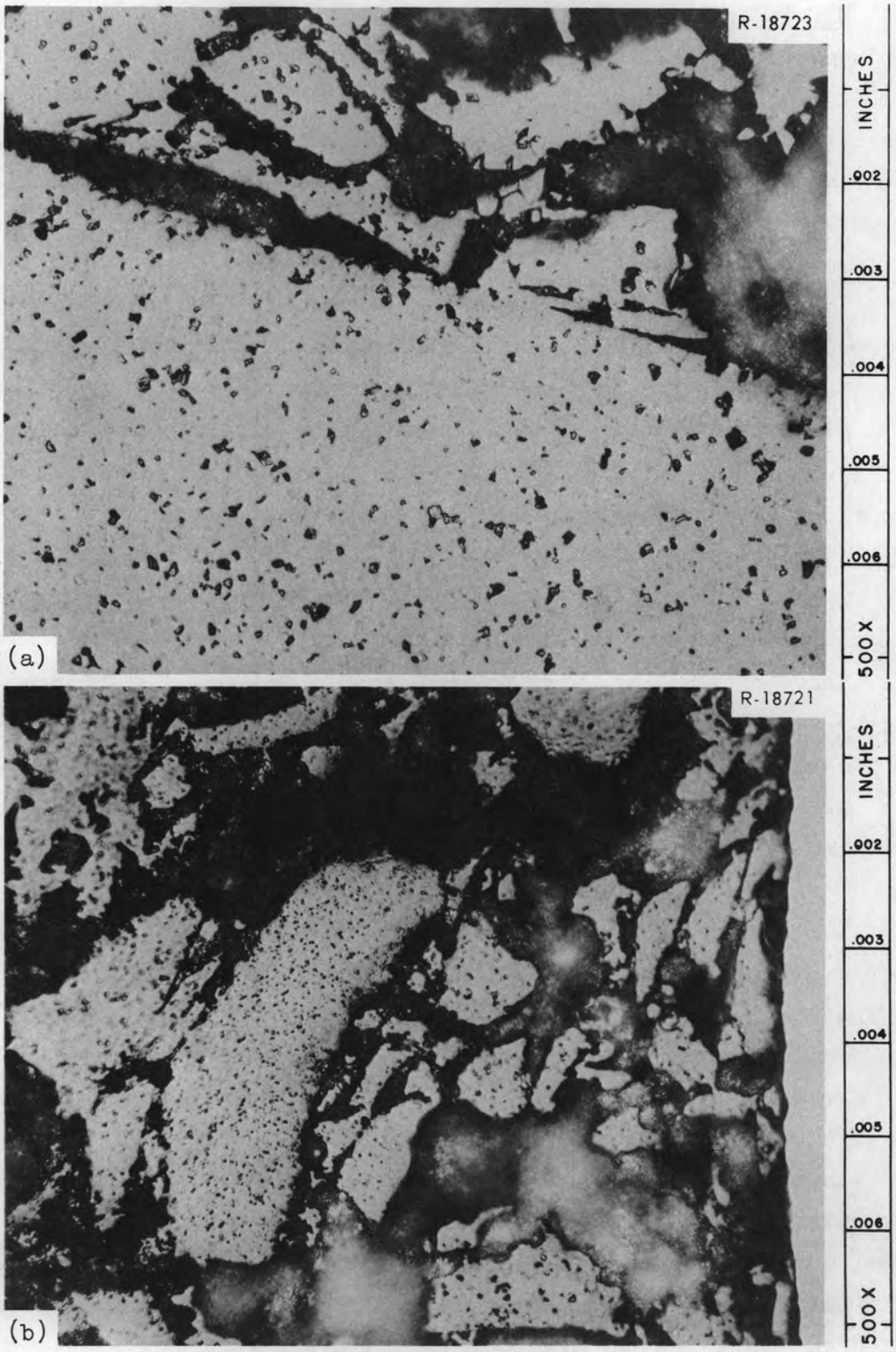

Fig. 3.14. Fuel Rod P-6 (ThO_2–5.2% PuO_2) Irradiated to 4.65×10^{20} fissions/cm^3. (a) Typical fuel center area transverse section. (b) Typical fuel area at clad-fuel interface transverse section.

MTR ThO_2-UO_2. — The MTR Group I rods contained either sol-gel or arc-fused fuel particles and were planned to compare the two types of fuel at moderate heat ratings with increasing incremental fuel burnup levels. During the past year, two additional rods of each type have been removed from the reactor for examination. Significant irradiation parameters are presented in Tables 3.4 and 3.5 together with some of the postirradiation findings.

These tests represent the highest burnup levels yet achieved with the powder compacted ThO_2-UO_2 fuels and permit a study of the effects of time and total fissions on such things as fission-gas release and grain growth. Although every effort was made to attain similar exposure conditions in the test reactor, over the two-year exposure period there were minor differences that make an exact comparison of one sol-gel rod with another and with its arc-fused counterpart impossible.

The fuel, regardless of its production technique, has shown excellent characteristics. Postirradiation dimensional analysis has shown no evidence of swelling. The percentage of fission-gas release did increase with burnup; however, there are insufficient data to define any precise relationship between release and burnup or heat rating. There only appears to be a general increase in release percentages with exposure time in these experiments where the time-averaged $\int_{T_o}^{T_c} k d\theta$ was less than 40 w/cm.

The time dependence of sintering, or more specifically equiaxed grain growth, is much more readily discernible in these experiments. Figures 3.15 and 3.16 are composite radial micrographs of the arc-fused powder compacts at various levels of exposure while Figs. 3.17 and 3.18 are similar composites of the sol-gel compacts. With both materials, the effects of prolonged exposure on microstructure are apparent.

In the case of the arc-fused material, the cracks in the original fragments were initially accentuated in the midradius region while there appeared to be an agglomeration of porosity at the fuel center (U-1). With continued irradiation (or time at temperature) the cracks apparently healed and there was the development of a grain structure within the individual fragments while the central porosity increased (U-2). Still

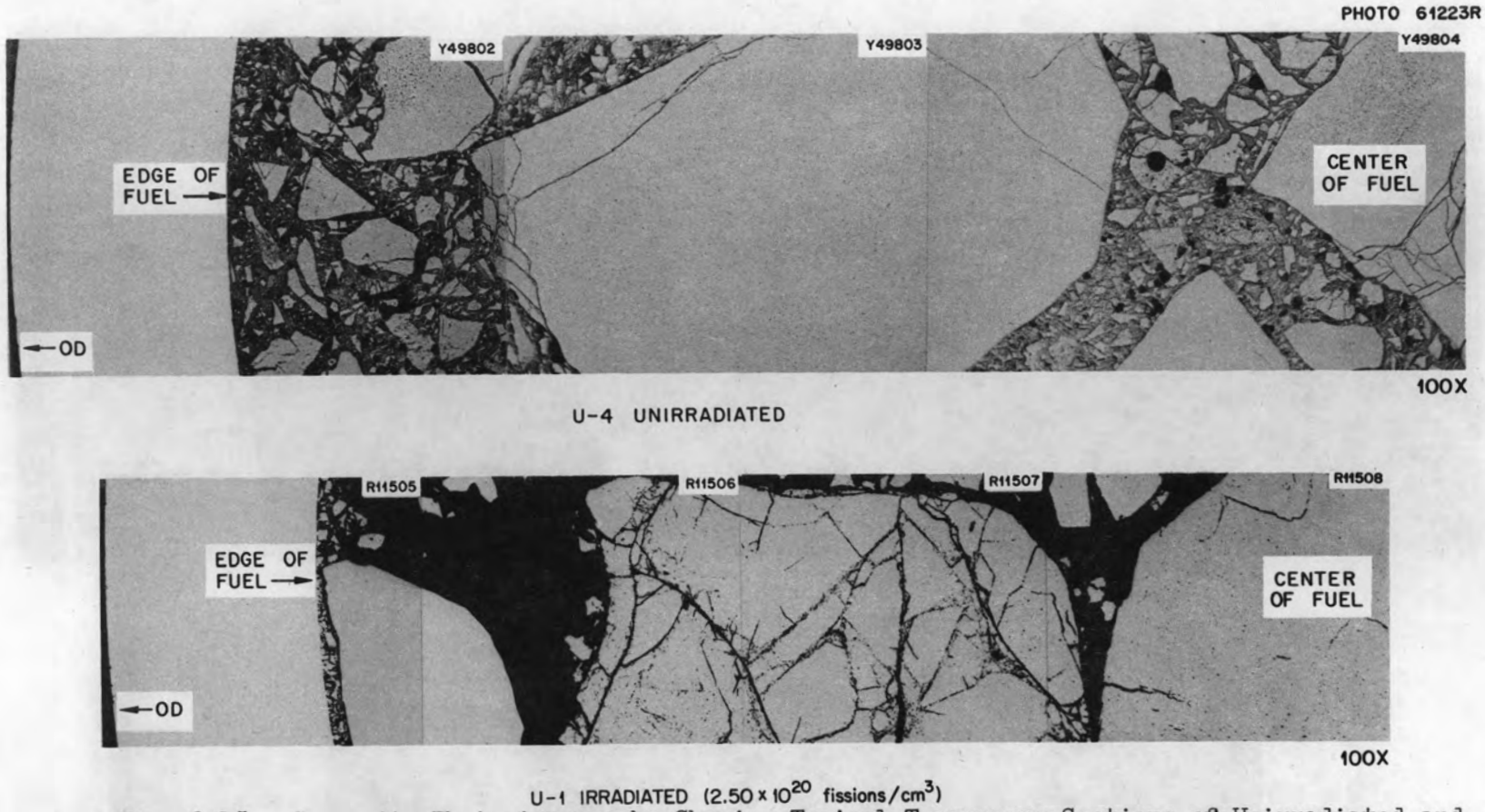

Fig. 3.15. Composite Photomicrographs Showing Typical Transverse Sections of Unirradiated and Irradiated Vibratorily Compacted Arc-Fused ThO_2–4.5% UO_2. Radial area from the outside edge to the center of the fuel. As polished.

PHOTO 69435

U-2 IRRADIATED (8.56×10^{20} fissions/cm^3) 100X

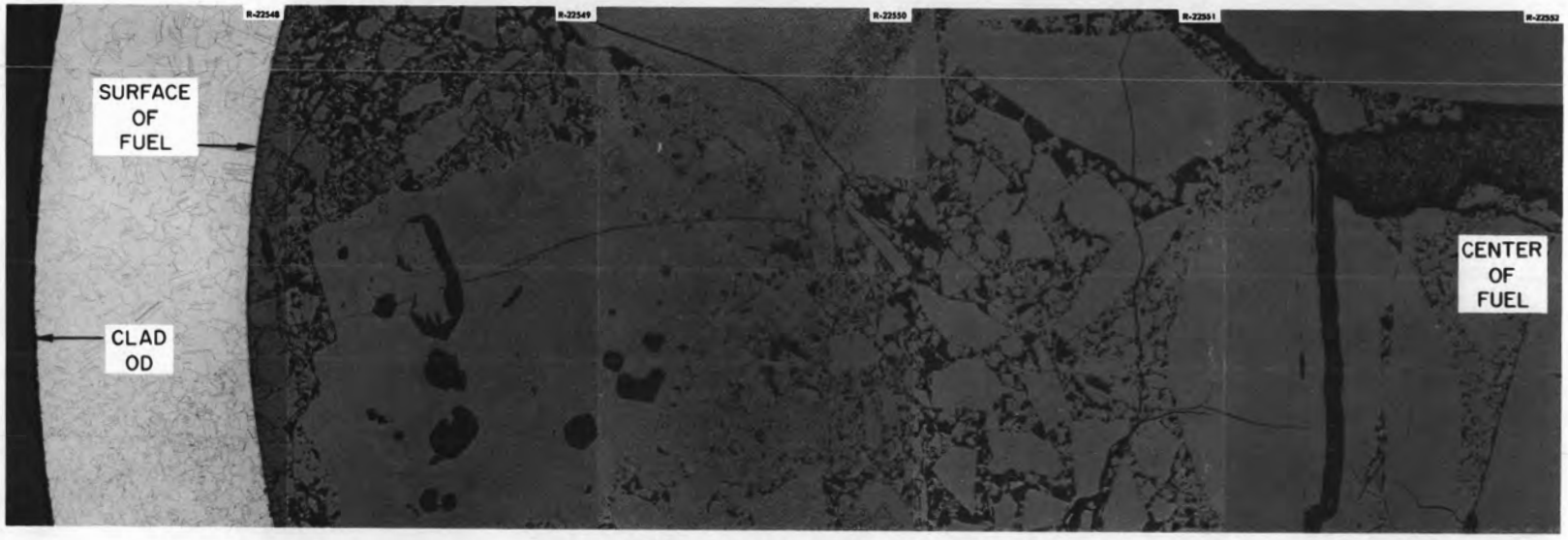

U-3 IRRADIATED (14.43×10^{20} fissions/cm^3) 100X

Fig. 3.16. Composite Photomicrograph Showing Typical Transverse Sections of Irradiated Vibratorily Compacted Arc-Fused ThO_2–4.5% UO_2. Radial area from the outside edge to the center of the fuel. As polished.

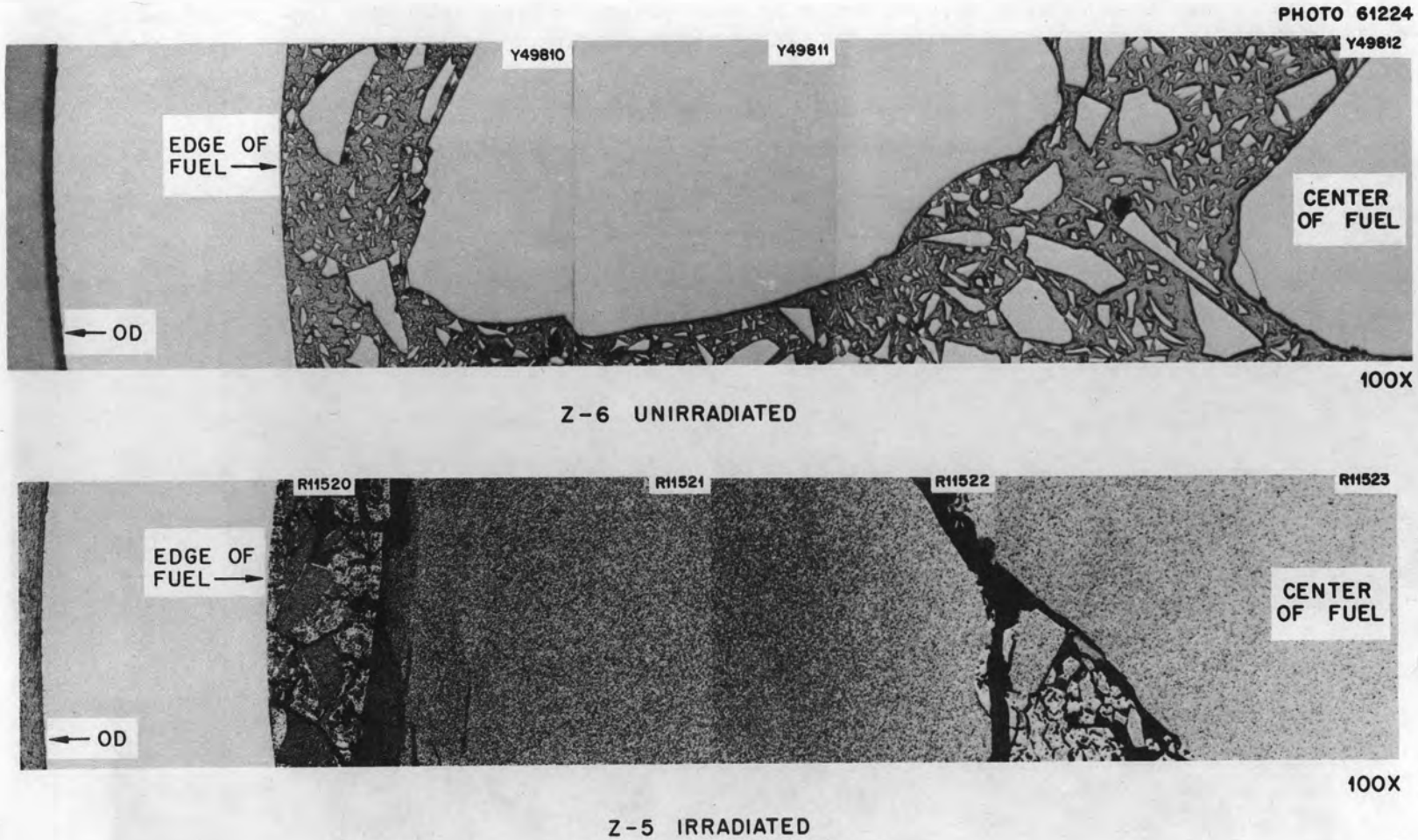

Fig. 3.17. Composite Photomicrographs Showing Typical Transverse Sections of Unirradiated and Irradiated Vibratorily Compacted Sol-Gel E ThO_2–4.5% UO_2. Radial area from the outside edge to the center of the fuel. As polished.

PHOTO 69433

Z-7 IRRADIATED (8.23×10^{20} fissions/cm^3) 100X

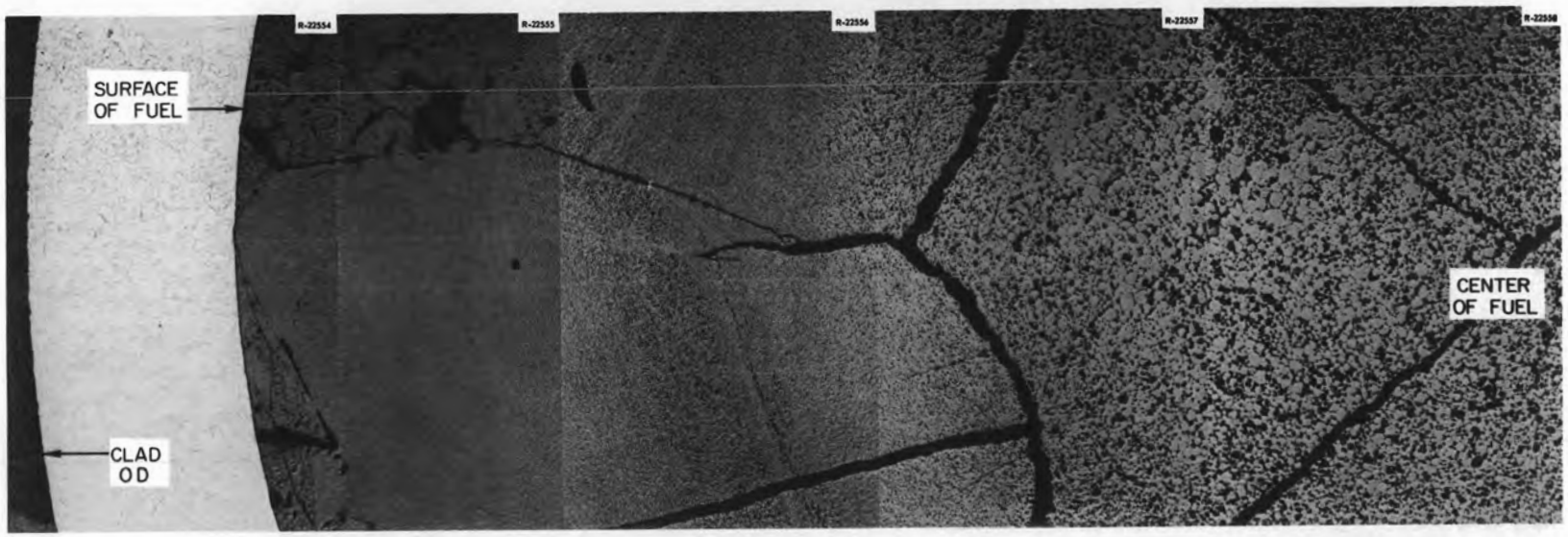

Z-8 IRRADIATED (16.46×10^{20} fissions/cm^3) 100X

Fig. 3.18. Composite Photomicrographs Showing Typical Transverse Sections of Irradiated Vibratorily Compacted Sol-Gel E ThO_2–4.5% UO_2. Radial area from the outside edge of cladding to center of the fuel. As polished.

fuel and some interparticle sintering while the outer two-thirds of the fuel has developed a finely dispersed porosity with a band of somewhat larger pores at the dividing line between the two structures.

The sol-gel fuel shows a similar microstructural evolution. The fuel fragments in the unirradiated material were crack free but did contain uniformly distributed microporosity. On irradiation, this porosity appears to agglomerate and accentuate the fine particle size of the original material (Z-5). Continued irradiation develops a distinct grain structure in the central regions with equiaxed grains some 6 to 8 μ in size, separated from the balance of the fuel by a circumferentially oriented crack. Within this central region, there is evidence of interparticle bonding. The distributed pores throughout the fuel appear to have increased in size (Z-7). After still more irradiation, the development of equiaxed grains in the central region is very distinct with maximum grain sizes reaching 60 μ in diameter. The circumferential crack still separates this area from the remainder of the fuel but there appears to be some interfragment growth in the outer two-thirds and as with the arc-fused material a band of moderately large pores is found in this area.

With both fuels after irradiation, there is a second shiny white metallic appearing phase developed in the central regions. Initially, this appears to be closely associated with porosity[7] but at exposures of approximately 8×10^{20} fissions/cm^3 or 375 reactor full-power days, this phase appears to be randomly distributed throughout the matrix as can be seen in Figs. 3.19a and b. The detailed metallography at higher magnification on the longer exposures has not been completed. A third light-grey phase was also found in some of the specimens located in discrete limited areas scattered throughout the fuel. Although this has not been definitely identified, the appearance and the location, with small fuel fragments, indicate that it is probably aluminum silicate contamination from the ball-milling operation.

---

[7]R. G. Wymer and D. A. Douglas, Status and Progress Report for Thorium Fuel Cycle Development for Period Ending December 31, 1963, ORNL-3611, pp. 81–112.

PHOTO 69432

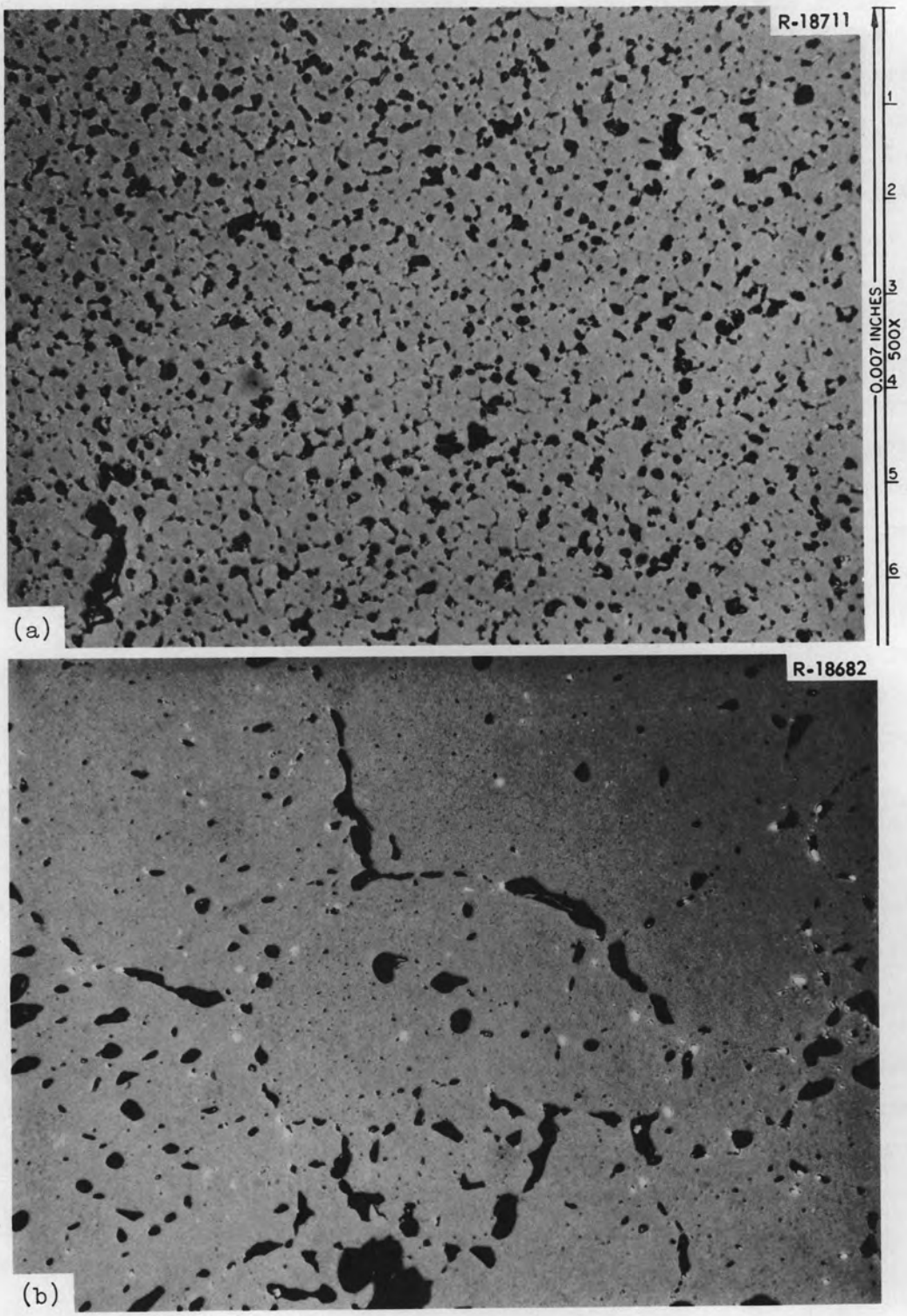

Fig. 3.19. Typical Central Regions of Irradiated Vibratorily Compacted ThO_2-UO_2 Fuels. (a) Sol-gel E after 8.23×10^{20} fissions/cm^3. (b) Arc-fused after 8.56×10^{20} fissions/cm^3. As polished.

The detailed metallography has not been completed on the highest burnup samples, and a satisfactory etchant is still being sought. Nevertheless, certain tentative conclusions can be drawn from the available data. (1) At the moderate linear heat ratings of this series, up to 500 w/cm, there are no abrupt or unusual microstructural changes at burnups to at least 80,000 Mwd/tonne of thorium plus uranium. (2) The development of diffusion-controlled phenomena such as pore migration, sintering, and grain growth is time dependent under essentially constant heat flux conditions. (3) There is no apparent difference in the behavior of sol-gel and arc-fused ThO_2-UO_2 fuels.

During the next year, one last fuel rod in this group containing sol-gel material will be discharged and examined after a burnup of over 100,000 Mwd/tonne of thorium plus uranium, and the detailed microstructures of the rods currently under examination will be completed, including autoradiography, x-ray diffraction analysis, and fission-product radial migration patterns.

ETR-I

The results of previously reported experiments have indicated that vibratorily compacted sol-gel ThO_2-UO_2 material is a satisfactory power reactor fuel. This has been confirmed by the attainment of even higher burnup levels reported here. However, the full utilization of this material requires an investigation of the maximum performance characteristics and an understanding of the effect of process variables on these characteristics. In an effort to do this experiment groups MTR-II, MTR-III, and ETR-I were prepared and inserted in the reactor.

The ETR-I group of four fuel rods was subjected to the highest flux with the expectation of producing central melting. A common sol-gel ThO_2–5.7% UO_2 preparation was calcined in three different atmospheres, air, Ar–4% H_2, and nitrogen, to produce sol-gel batches 35-1, 35-2, and 35-3, respectively. The available properties on this material are listed in Table 3.6 together with the properties of other fuels used in prior irradiations. The rods were exposed in the ETR to a maximum unperturbed thermal flux of 1.5×10^{14} for 140.5 reactor full-power days (accumulated unperturbed 1.8×10^{21} neutrons/cm^2).

Table 3.6. Summary of Properties of Uranium-Thorium Oxides Used in Fabrication of Irradiation Specimens

	Sol-Gel A	Sol-Gel B	Sol-Gel C[a]	Sol-Gel D[a]	Sol-Gel E[a]	Arc Fused	Sol-Gel S	Sol-Gel Batch 26	Sol-Gel Batch 35-1	Sol-Gel Batch 35-2	Sol-Gel Batch 35-3
Total uranium, wt %	4.31	4.39	4.01	2.50	4.0	3.96	5.21	5.35	5.13	5.12	5.05
Uranium enrichment, %	93	93	93	93	93	93	93	93	93	93	93
Carbon, ppm	110	100	60	40	130	120	80	40	173	47	59
Nitrogen, ppm	22	21	55	29	31	1130	30	13			
Iron, ppm	100	50	265	140	160	130	300	215			
Silicon, ppm	600	500	<20	<10	<10	20	20	<25			
BET surface area (N_2), m^2/g	0.20	0.26	0.03	0.008	0.011	0.11	0.17	0.047	0.196	0.213	0.241
Oxygen-to-uranium ratio	2.0	2.0	2.03	2.02	2.02	2.01	2.01	2.02	2.40	2.03	2.16
Volatile matter released in vacuum at 1200°C, cm^3/g	0.125	0.151	0.055	0.012	0.027	0.24	0.284	0.206	0.354	0.101	0.025
Lattice parameter, A	5.591	5.592	5.593		5.593	5.594	5.594				
Crystalline size, A	2400	1700	2200				1800				
Particle density,[b] g/cm^3	9.94	9.92	9.76	9.97	9.92	10.11	10.0	9.98	10.00	9.91	9.97
Packed density,[c] g/cm^3	8.69	8.69	8.36	8.74	8.74	8.6	8.8	8.50	9.00	8.95	8.90

[a]Cooled in pure argon after calcination in hydrogen.

[b]Toluene intrusion, pycnometric method. Theoretical density: 10.04 g/cm^3.

[c]NAVCO air vibrator, 1/25-in. piston; 5/16-in.- OD × 11-in. stainless steel tube.

Postirradiation examination of these fuel rods is currently in progress. To date, the dimensional analyses have shown no indications of swelling or bowing. Fission-gas samples have been obtained from three of the rods and gross gamma scans on all four. Based on the gamma scans which showed no anomalies, and the structures found, three rods have been sectioned and are currently being prepared for metallographic examination. Figures 3.20, 3.21, and 3.22 show the gross gamma scans and the comparative section locations. Figures 3.23, 3.24, and 3.25 show the resulting as-cut structures at the various section locations.

From these sections, it is apparent that the linear heat ratings were sufficient to develop a central void in all three of the rods. The levels of the gamma scans and the results of the preliminary burnup analysis reported in Table 3.4 indicate that there was a difference in fission rate and consequently in linear heat rating. The numbers reported are subject to revision, however, since an unexpected precipitation phenomenon in the analytical solutions caused erratic and unreliable analyses. Additional samples have been obtained and a revised procedure will be used to obtain more reliable results.

The extent of the central voids appears to match the indicated heat ratings, but the lack of any anomalies in the gamma scans and the appearance of the sections seem to indicate that the anticipated condition of central melting was not achieved although columnar grain growth is significant. Columnar grain growth has been shown to occur without melting in UO_2 (Ref 8) and in ThO_2-UO_2 in the ORR loop experiment L1B (Ref 9), but the probability of the effective thermal conductivity of the as-packed oxides being high enough to permit this in these experiments at full power was unlikely. Examination of the reactor startup on the first cycle of exposure of these rods shows that for the first 9 1/2 hr of exposure the reactor was never over 50% of full power. Since this

---

[8] J. R. MacEwan and V. B. Lawson, J. Am. Ceram. Soc. 45(1), 42 (1962).

[9] R. G. Wymer and D. A. Douglas, Status and Progress Report for Thorium Fuel Cycle Development for Period Ending December 31, 1963, ORNL-3611, pp. 81–112.

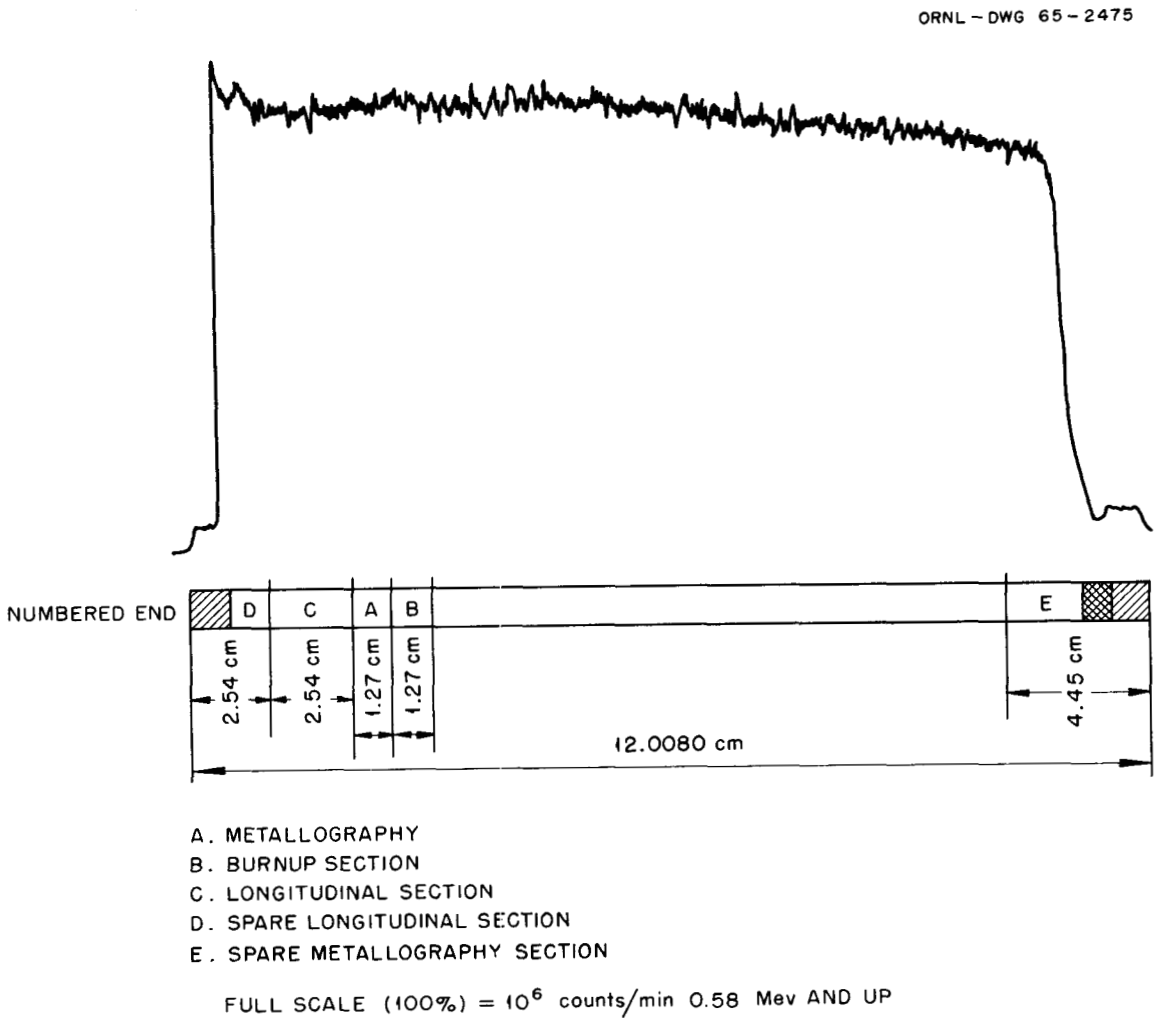

Fig. 3.20. ETR Group I, Capsule 18, Gross Gamma Scan and Sectioning Pattern.

ORNL-DWG 65-2472

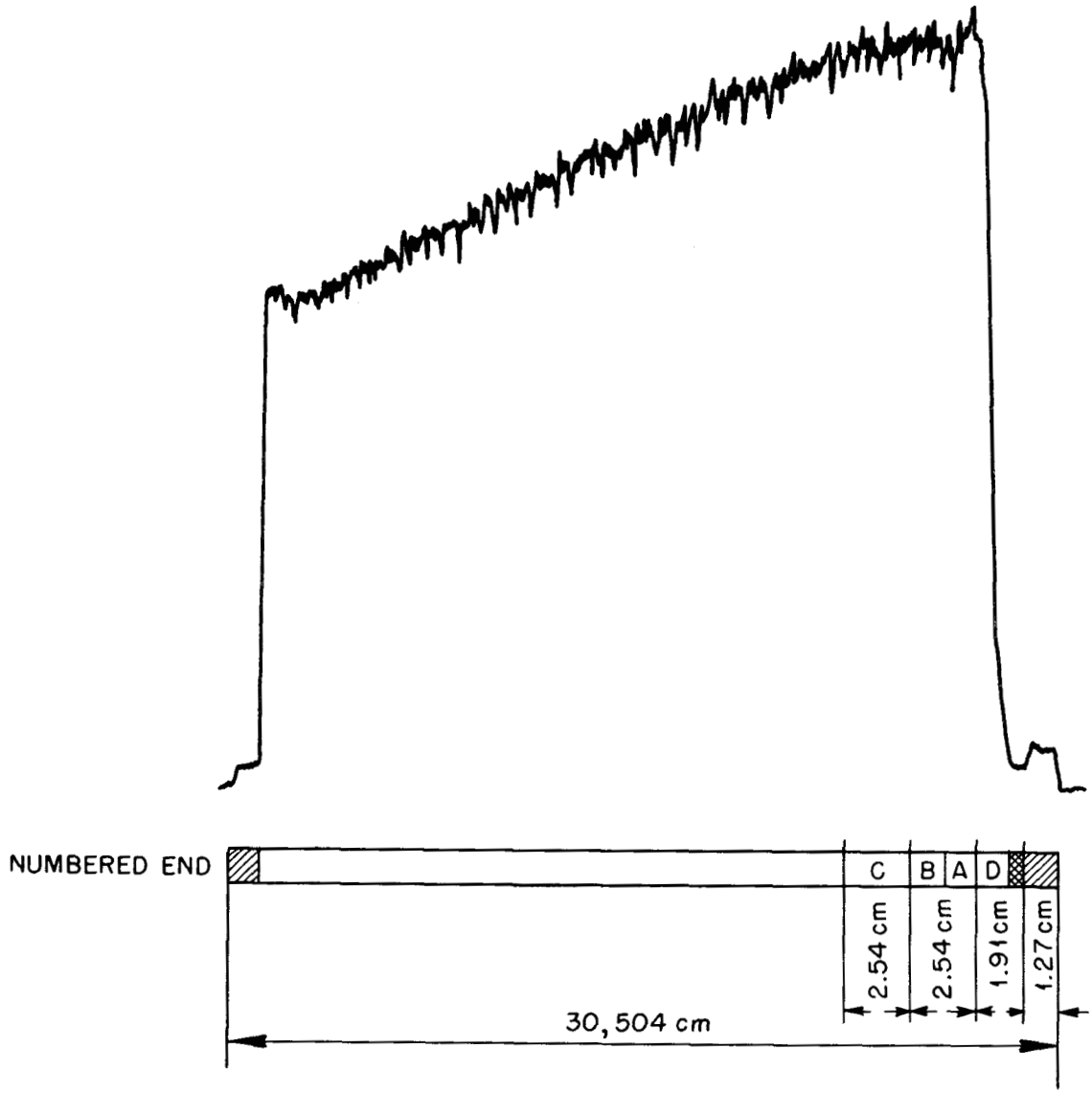

A. METALLOGRAPHY SECTION
B. BURNUP SECTION
C. LONGITUDINAL SECTION
D. SPARE

FULL SCALE (100%) = 500,000 counts/min 0.58 Mev AND UP

Fig. 3.21. ETR Group I, Capsule 10, Gross Gamma Scan and Sectioning Pattern.

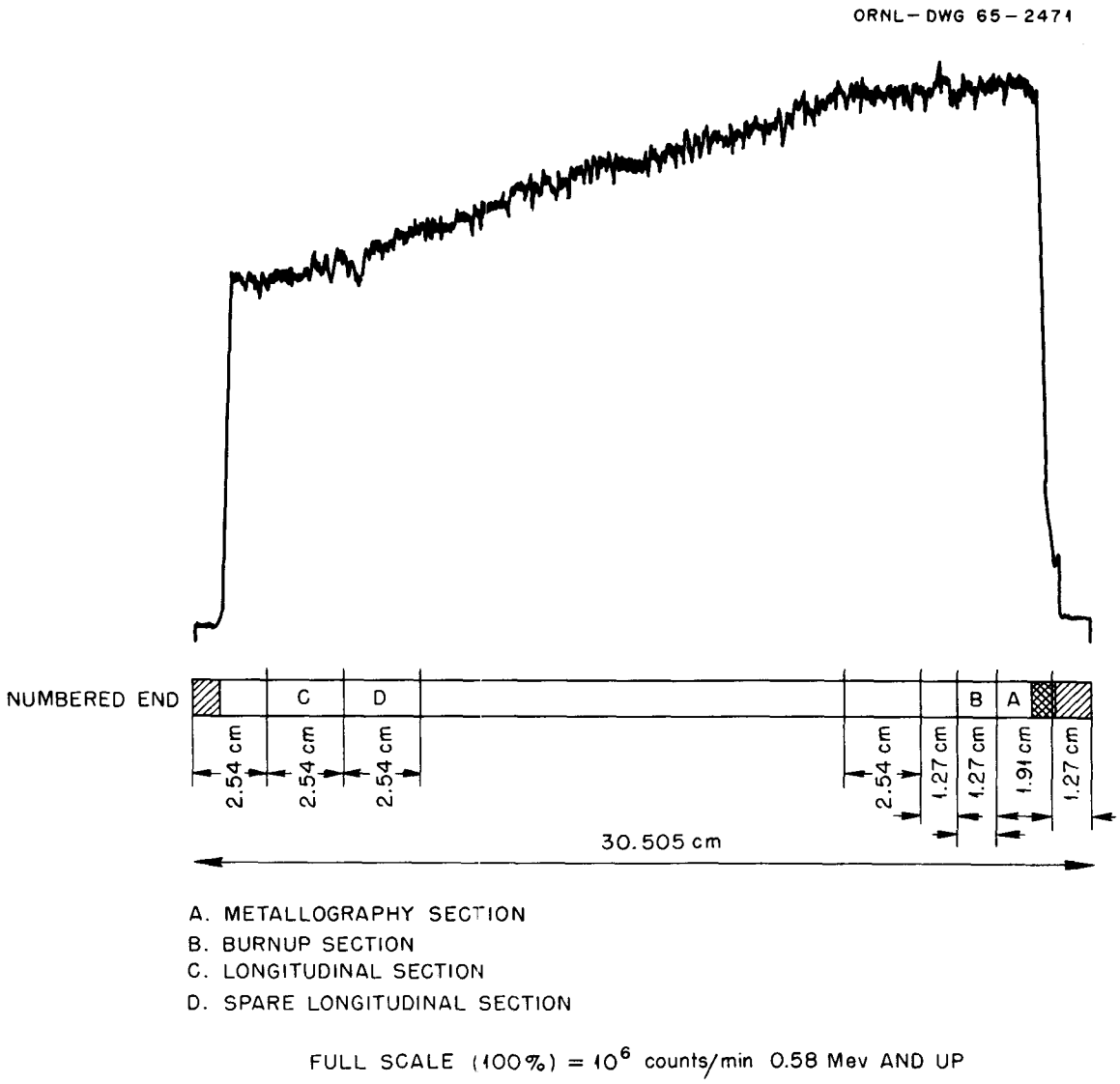

Fig. 3.22. ETR Group I, Capsule 8, Gross Gamma Scan and Sectioning Pattern.

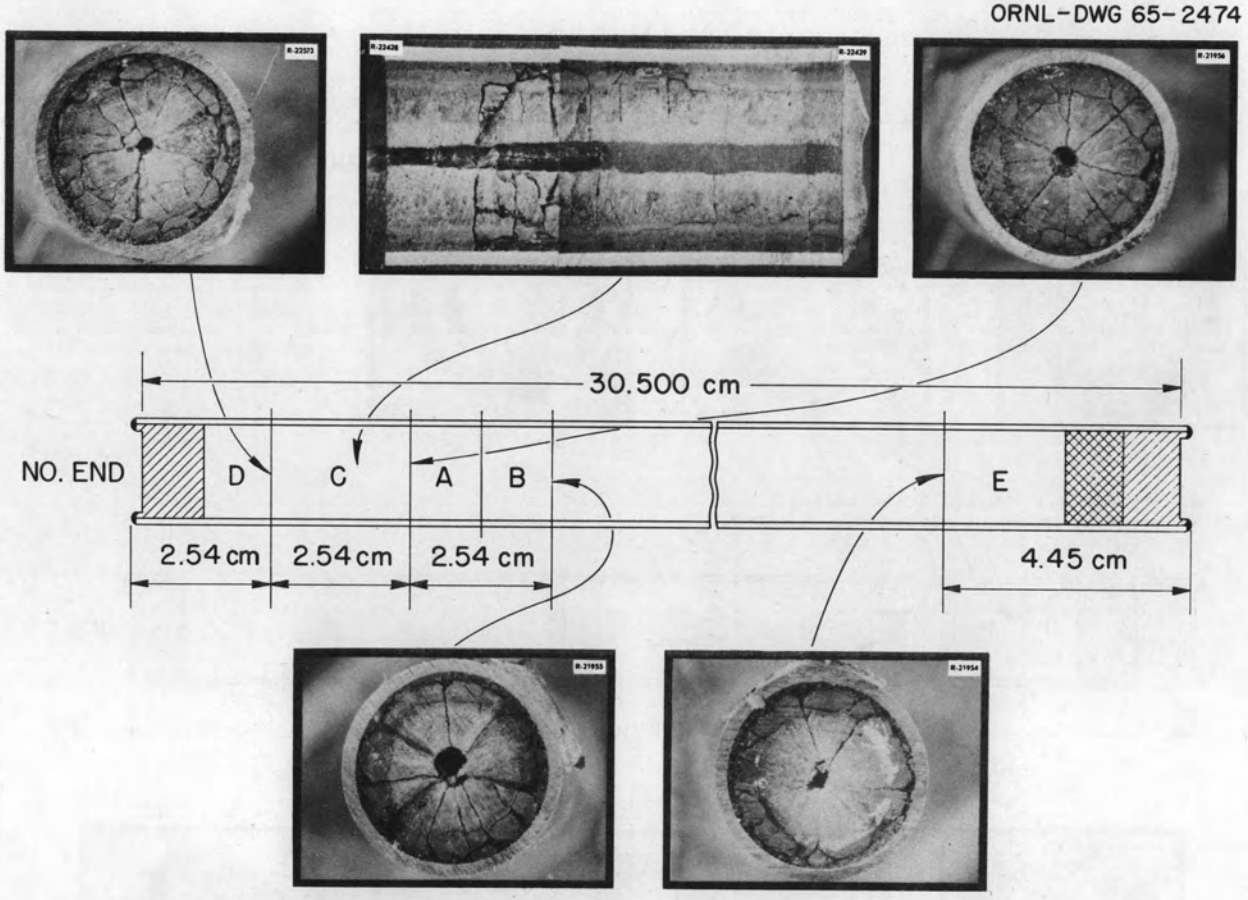

A. METALLOGRAPHY SECTION
B. BURNUP SECTION
C. LONGITUDINAL SECTION
D. SPARE LONGITUDINAL SECTION

Fig. 3.23. ETR Group I, Capsule 18, Macroscopic Views of Selected Specimen Locations, as Cut.

ORNL-DWG 65-2473

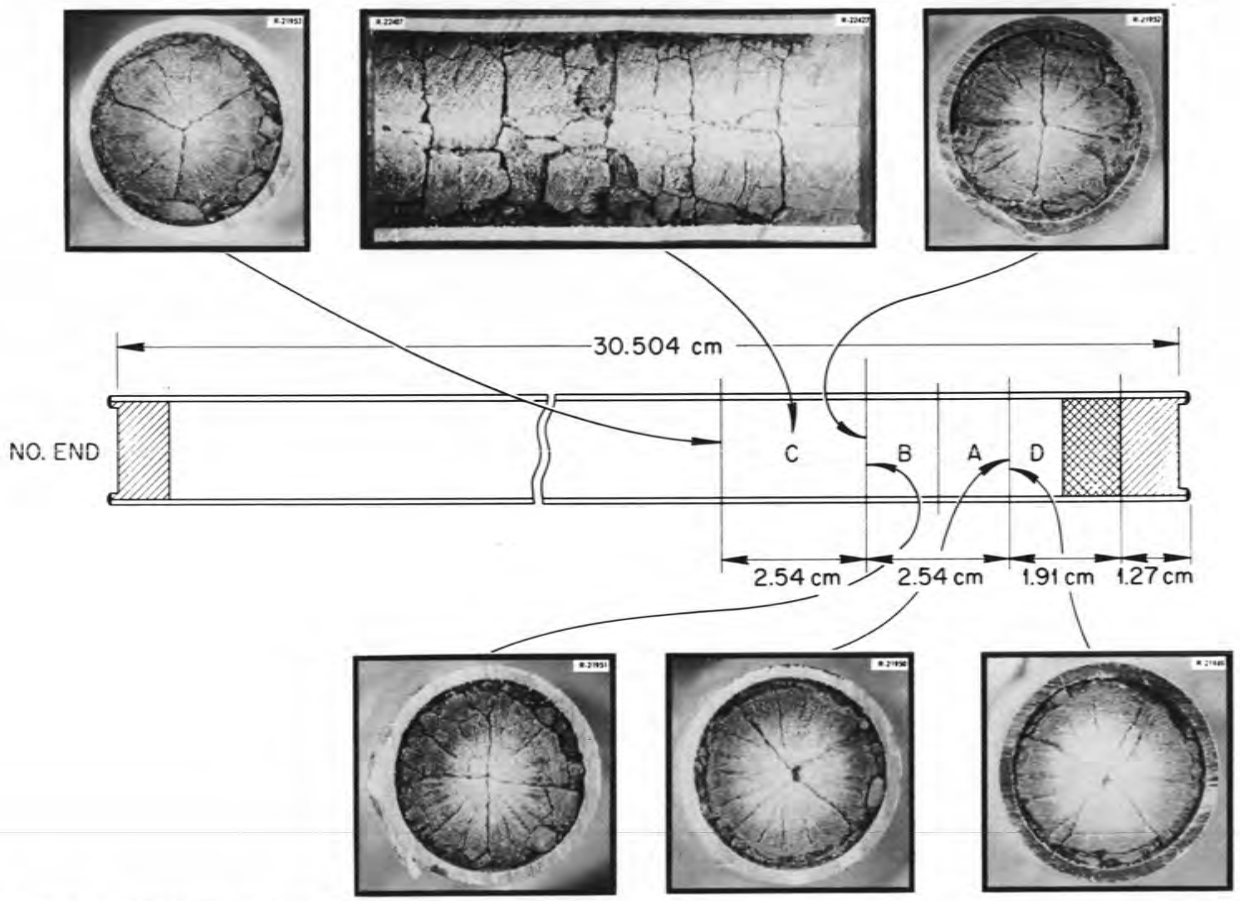

A. METALLOGRAPHY SECTION
B. BURNUP SECTION
C. LONGITUDINAL SECTION
D. SPARE

Fig. 3.24. ETR Group I, Capsule 10, Macroscopic Views of Selected Section Locations, as Cut.

ORNL-DWG 65-2470

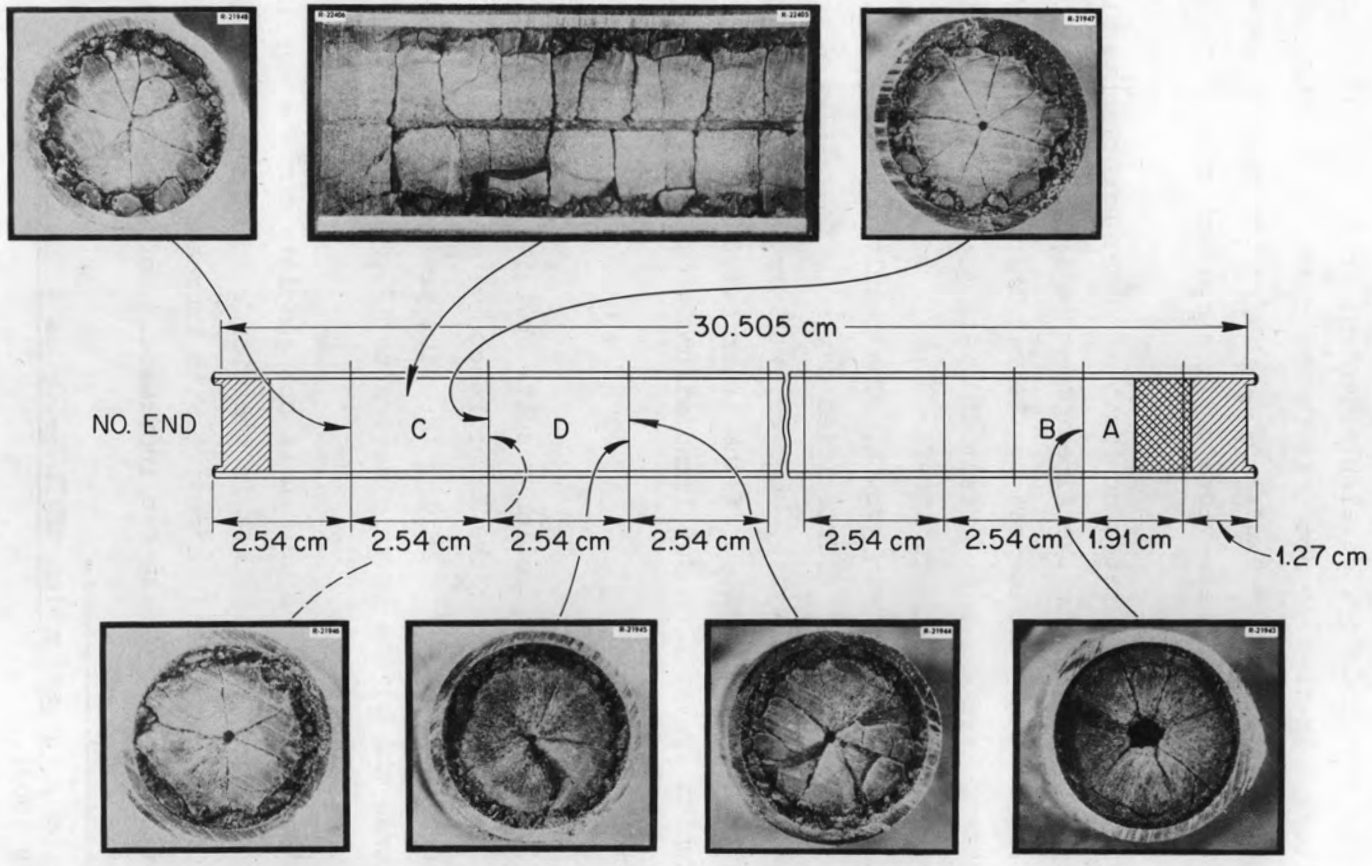

A. METALLOGRAPHY SECTION
B. BURNUP SECTION
C. LONGITUDINAL SECTION
D. SPARE LONGITUDINAL SECTION

Fig. 3.25. ETR Group I, Capsule 8, Macroscopic Views of Selected Section Locations, as Cut.

would have produced an $\int k d\theta$ very close to the 54 w/cm defined by experiment L1B for columnar grain growth it is entirely possible that during this time sufficient sintering and grain growth occurred to raise the effective thermal conductivity, develop a central void, and eliminate any actual melting. Whether or not this is the case, it is apparent that at a linear heat rating in excess of 1000 w/cm the maximum performance characteristics of these vibratorily compacted sol-gel fuels have not been reached.

The fission-gas-release rates contrary to other experiments appear to be inversely proportional to the linear heat rating. Probably the release rates are strongly influenced by the calcining atmosphere. Other experiments[10] have shown an effect on grain growth in short-time irradiations of hydrogen-fired and air-fired pellets, with the air-fired material showing more grain growth. The results of rod 20 which have been delayed by equipment difficulties may help to resolve this in the near future. A final analysis, however, will require the detailed evaluation of these rods and those of the lower rated rods in the MTR-III group which are still under irradiation.

Pellet Fuel

The postirradiation examination results on three pelletized ThO_2–4.45% UO_2 irradiated under the Power Reactor Fuel Reprocessing Program have been reported.[9,11] During the past year, a fourth specimen, which extends the burnup in this series to 120,000 Mwd/tonne thorium plus uranium, became available.

The examination of this specimen is not complete but the available data indicate no significant changes in behavior even at this high level of exposure (26.41×10^{20} fissions/cm^3). With increasing exposure the percentage of fission-gas release has increased. Unfortunately, the gas

---

[10] S.V.K. Rao, Investigation of ThO_2-UO_2 as a Nuclear Fuel, AECL-1785 (July 1963).

[11] S. A. Rabin, J. W. Ullman, E. L. Long, Jr., M. F. Osborne, and A. E. Goldman, Irradiation Behavior of High Burnup ThO_2–4.45% UO_2 Fuel Rods, ORNL-3837 (October 1965).

samples from the low burnup specimens in this series were lost in sampling. This, coupled with the varying heat ratings with burnup, prevent evaluation of any possible lattice saturation phenomenon. The increase in release between capsules 729 and 712 is probably the result of the extended exposure time, 905 reactor full-power days instead of 660, and the resultant greater diffusion.

The gamma scan of this capsule was somewhat unique in that there were two distinct peaks near one end located at what would have been the centers of two of the original pellets. This scan, together with the sectioning pattern, is shown in Fig. 3.26. In an effort to determine the source of these peaks, various locations along the capsule were examined with a multichannel analyzer. The cobalt 1.17 and 1.33 Mev gammas from the stainless steel cladding indicated no difference in the neutron dose from end to end. The ^{134}Cs and ^{137}Cs peaks at 0.6 and 0.8 Mev were found to be the predominant energies in the peak regions and at the pellet end plug interfaces. The migration of this volatile fission product to the cooler end regions has been seen before but the peaking in the centers of the original pellets was unexpected. Based upon the counting rates, the concentrations at the cooled ends were 120 and 145% of the uniformly distributed concentration while the two peaks reached approximately 155%. In an effort to identify any macrostructural defects which might be the cause of this intrapellet peaking, the area of the anomalies was sectioned longitudinally. A view of this section, together with the various transverse sections, is shown in Fig. 3.27. There is no apparent difference in the macrostructure at the regions of high cesium concentration. The fuel was severely fragmented as it was in the other specimens in this group. This fragmentation is such that the original pellet interfaces cannot be clearly delineated at this magnification. It is interesting to note that, although there is a large number of longitudinal and transverse cracks, along with the radially oriented cracks, every transverse section shows a circumferentially oriented crack or cracks similar to those developed in the powder-compacted rods at the higher exposure levels. As a result of this circumferential crack, a roughly cored geometry develops.

ORNL-DWG 65-2477

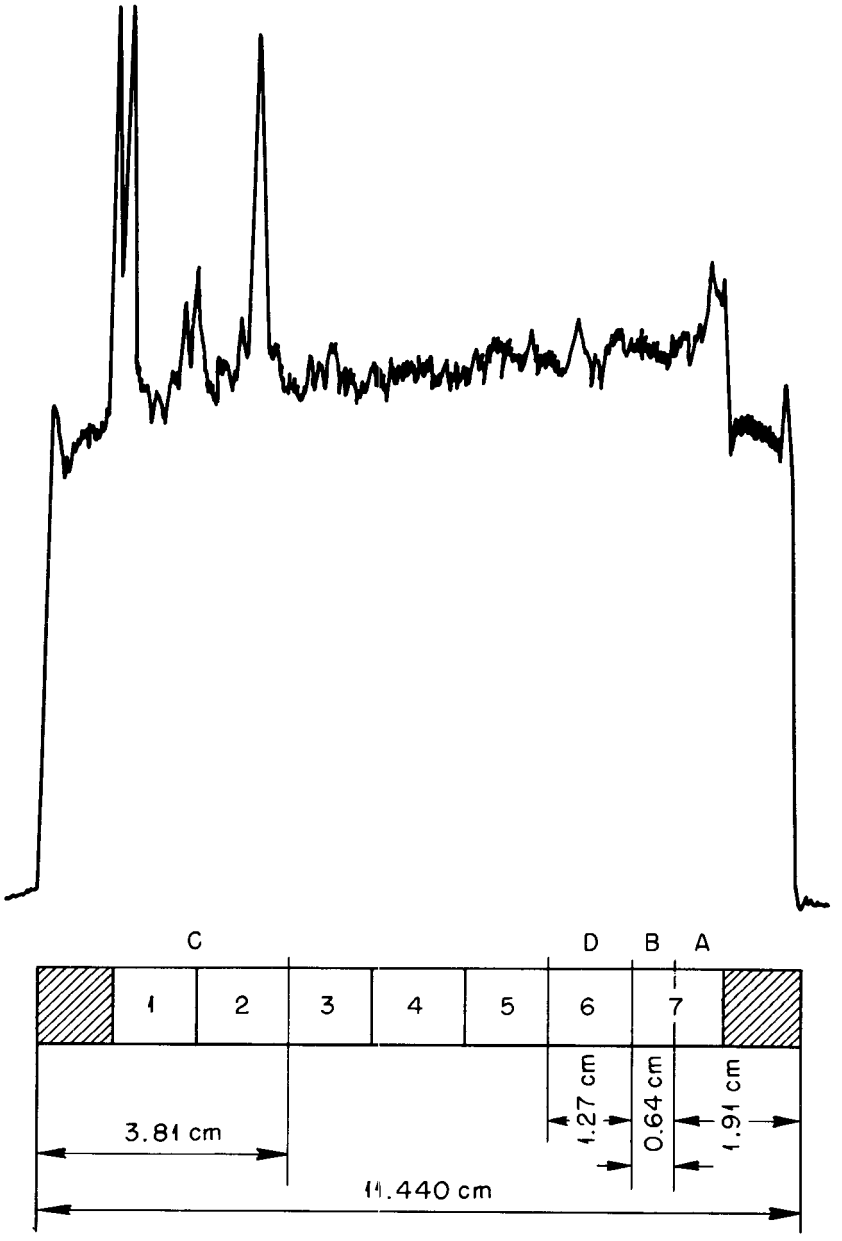

A. METALLOGRAPHY SECTION
B. BURNUP SECTION
C. LONGITUDINAL SECTION
D. NEUTRON ACTIVATION SECTION

FULL SCALE (100%) = 200,000 counts/min 0.58 Mev AND UP

Fig. 3.26. Gross Gamma Scan and Sectioning Pattern of Pellet Rod 712.

ORNL-DWG 65-2476

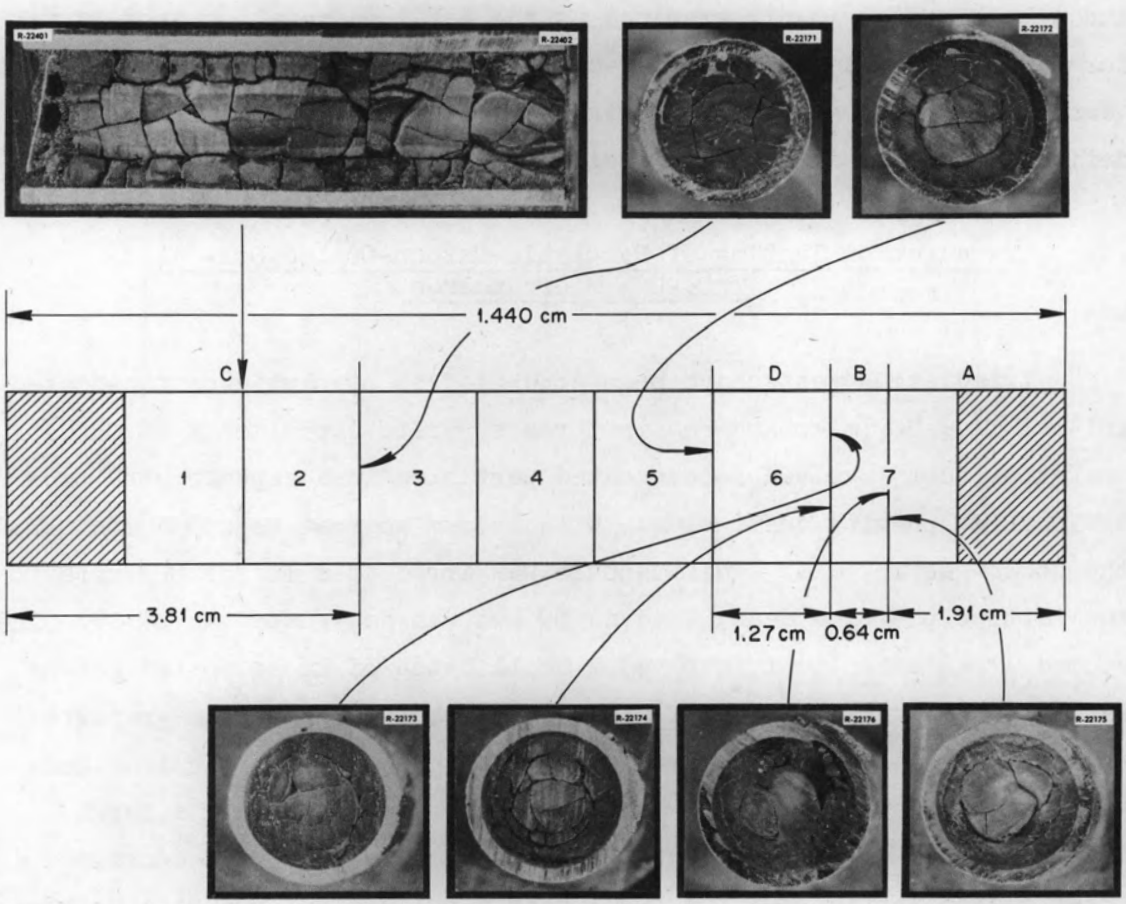

A. METALLOGRAPHY SECTION
B. BURNUP SECTION
C. LONGITUDINAL SECTION
D. NEUTRON ACTIVATION SPECIMEN

Fig. 3.27. Macroscopic Views of Selected Section Locations of Pellet Rod 712, as Cut.

Although precise limits of these circumferential cracks developed by thermal cycling cannot be defined, the average diameter of this core is such that the calculated $\int k d\theta$ at the crack is approximately 31 w/cm or roughly the limit of equiaxed grain growth defined by the powder compacted fuel tests. This is similar to the observations on UO_2 (Ref 12) and will be more closely examined as the detailed metallography is performed. At the same time, autoradiographs will be obtained and a microgamma scan across a transverse diameter will be obtained in an effort to define the extent and type of radial fission-product migration.

Irradiation Testing of Pyrolytic-Carbon-Coated Sol-Gel ThO_2-UO_2 Microspheres

Irradiation tests have been conducted on pyrolytic-carbon-coated sol-gel ThO_2-UO_2 microspheres in three separate experiments at ORNL. One experiment involved loose coated particles in a capsule with provisions for purging continuously with helium so that we could monitor the noble-gas release. This capsule was irradiated in the ORR core in the lattice position designated as B9 and was designated as B9-19. The second irradiation test involved a small batch of loose coated sol-gel particles contained in one of nineteen holes in a 6-cm-diam graphite sphere. This element was irradiated in an ORR poolside facility and was not purged with helium. The third experiment involved a large batch of mixed sol-gel ThO_2-UO_2 and sol-gel ThO_2 particles contained as loose coated particles in an annulus of a cylindrical graphite holder. These particles were vented to the helium coolant and the noble-gas release was monitored by a periodic sampling of the loop.

Details of the irradiation facilities are given elsewhere.[13] The facilities were developed as a part of the Advanced Gas-Cooled Reactor

---

[12] J. Belle (ed.), Uranium Dioxide: Properties and Nuclear Applications, p. 635, USAEC, Naval Reactors, Division of Reactor Development, Washington, D. C. (1961).

[13] D. B. Trauger, Some Major Fuel Irradiation Test Facilities at the Oak Ridge National Laboratory, ORNL-3574 (April 1964).

Fuel Development Program at ORNL, and details of the precursor experiments to those involving the coated sol-gel particles may be found in the GCR Semiannual Progress Reports. Results of the experiments on the sol-gel particles are given below.

Experiment B9-19

Capsule B9-19 contained ThO_2–8 wt % UO_2 particles with duplex pyrolytic-carbon coatings (lot OR-206). Characteristics of the coated particles are given in Table 3.7 together with a description of the other batches of sol-gel coated particles to be discussed. These particles were irradiated in the graphite holder shown in Fig. 3.28. Irradiation conditions and average fission-gas release rates are shown in Table 3.8.

Table 3.7. Properties of Coated Sol-Gel Microspheres

	Coated Particle Designation		
	OR-205	OR-206	OR-182L
Fuel Material	ThO_2	$(U,Th)O_2$	$(U,Th)O_2$
Uranium content, wt %	0.0	3.1	3.31
Uranium enrichment, at. %		93	93
Thorium content, wt %	33.8	36.8	39.8
Thorium-to-uranium ratio	∞	12	12
Average Core Diameter, μ	243	206	206
Type of Coating	Duplex	Duplex	Duplex
Average Coating Thickness, μ	128	100	96
Particle Density,[a] g/cm^3	2.87	2.94	1.71

[a]Measured with helium pycnometer.

ORNL-DWG 57280R4

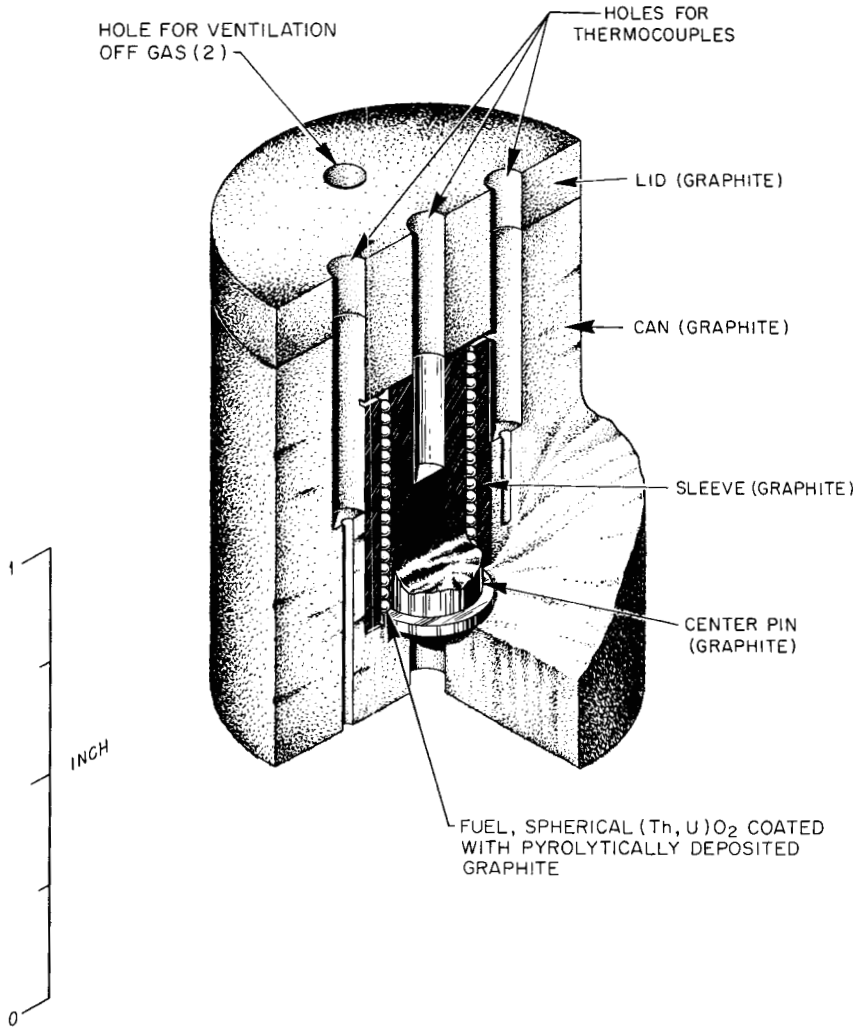

Fig. 3.28. Graphite Holder Containing Unsupported Pyrolytic-Carbon-Coated Particles.

Table 3.8. Fission-Gas Release from Coated Sol-Gel Microspheres in Capsule B9-19

Batch Number	Number of Particles	Burnup (at. % heavy metal)	Irradiation Temperature (°C)	Average Fractional Fission-Gas Release Rate ($\times 10^{-6}$)				
				^{85m}Kr	^{87}Kr	^{88}Kr	^{133}Xe	^{135}Xe
OR-206	6640	0.65	1200	3.1	1.7	2.3	2.0	0.8

Postirradiation examination of the particles showed no failed coatings, but some cracking of the inner coating layer as shown in Fig. 3.29. Damage to the inner coatings of pyrolytic carbon is frequently observed with UC_2 cores so that the damage is probably due to fission-recoil effects. The most significant thing is that the sol-gel material is still in the form of the oxide and that no marked fuel-coating interactions occurred. It is hypothesized that the CO formed by the reaction

$$(Th,U)O_2 + 4C \rightarrow (Th,U)C_2 + 2CO$$

is retained by the pyrolytic-carbon coating so that thermodynamic equilibrium is maintained. This result is important in coated particle economics because it obviates the need for the conversion of the oxide to the carbide before the coatings are applied.

AVR Capsule 01-8

An AVR irradiation capsule contains two 6-cm-diam fueled graphite spheres in a static (sealed) compartment and one in a sweep compartment with provisions for a helium purge. A schematic diagram of an AVR capsule is shown in Fig. 3.30. One of the objectives of capsule 01-8 was to check out the concept of a fueled graphite sphere containing loose coated particles within an array of machined holes. Because of a lack of information on coated particles with sol-gel oxide cores, we decided to fuel one of the nineteen holes of the element in the top static position (designated ORNL-VS2-2) with batch OR-182L, which was described in Table 3.7. A photograph and radiograph of the sphere are shown in Fig. 3.31. The plug marked with the "X" contained the sol-gel particles.

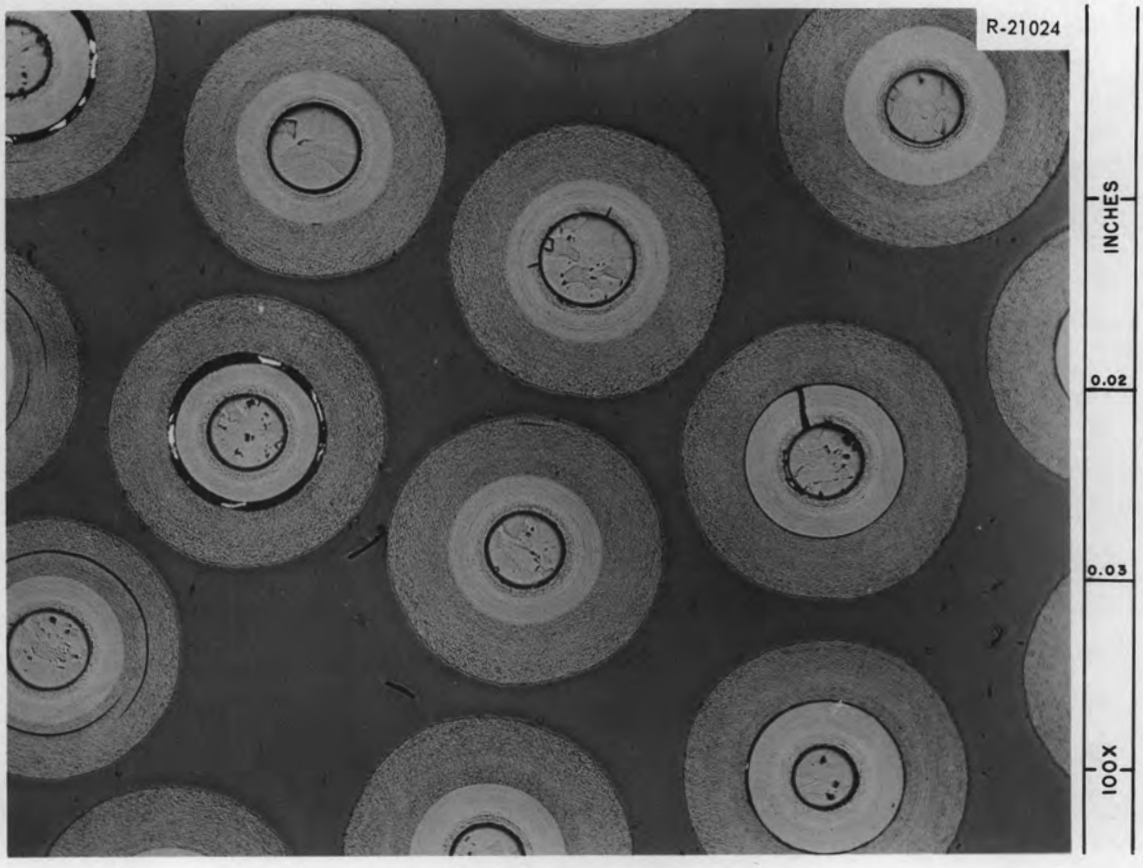

Fig. 3.29. Appearance of Typical Coated Particles After Irradiation in Capsule B9-19. As polished.

Operating conditions for sphere ORNL-VS2-2 are given in Table 3.9. The burnup of the sol-gel fuel was small because of the low flux in the poolside position. Since the sol-gel particles were contained within the inner row of particles, the average temperature of the sol-gel particles would be expected to be near that of the center of the fuel element. Thus irradiation conditions were not too different from Capsule B9-19.

Table 3.9. Operating Conditions for Sphere ORNL-VS2-2 Containing Pyrolytic-Carbon-Coated Sol-Gel Oxide Particles

Capsule	Position	Days at Full Power	Average Temperature (°C)		Burnup of Sol-Gel Particles (at. % heavy metal)
			Surface	Center	
01-8	Top static	42.5	744	1133	0.034

ORNL-DWG 63-3061

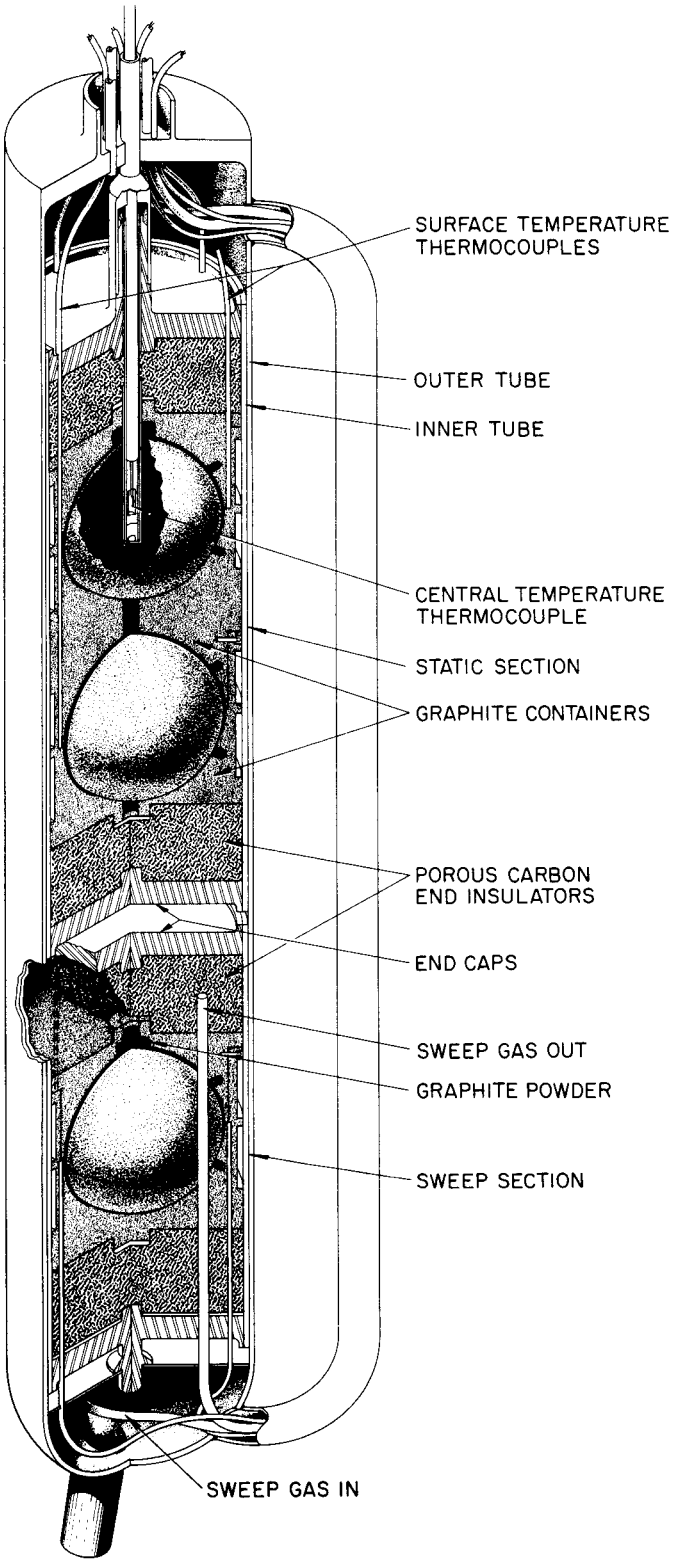

Fig. 3.30. Schematic Diagram of an AVR Capsule Design.

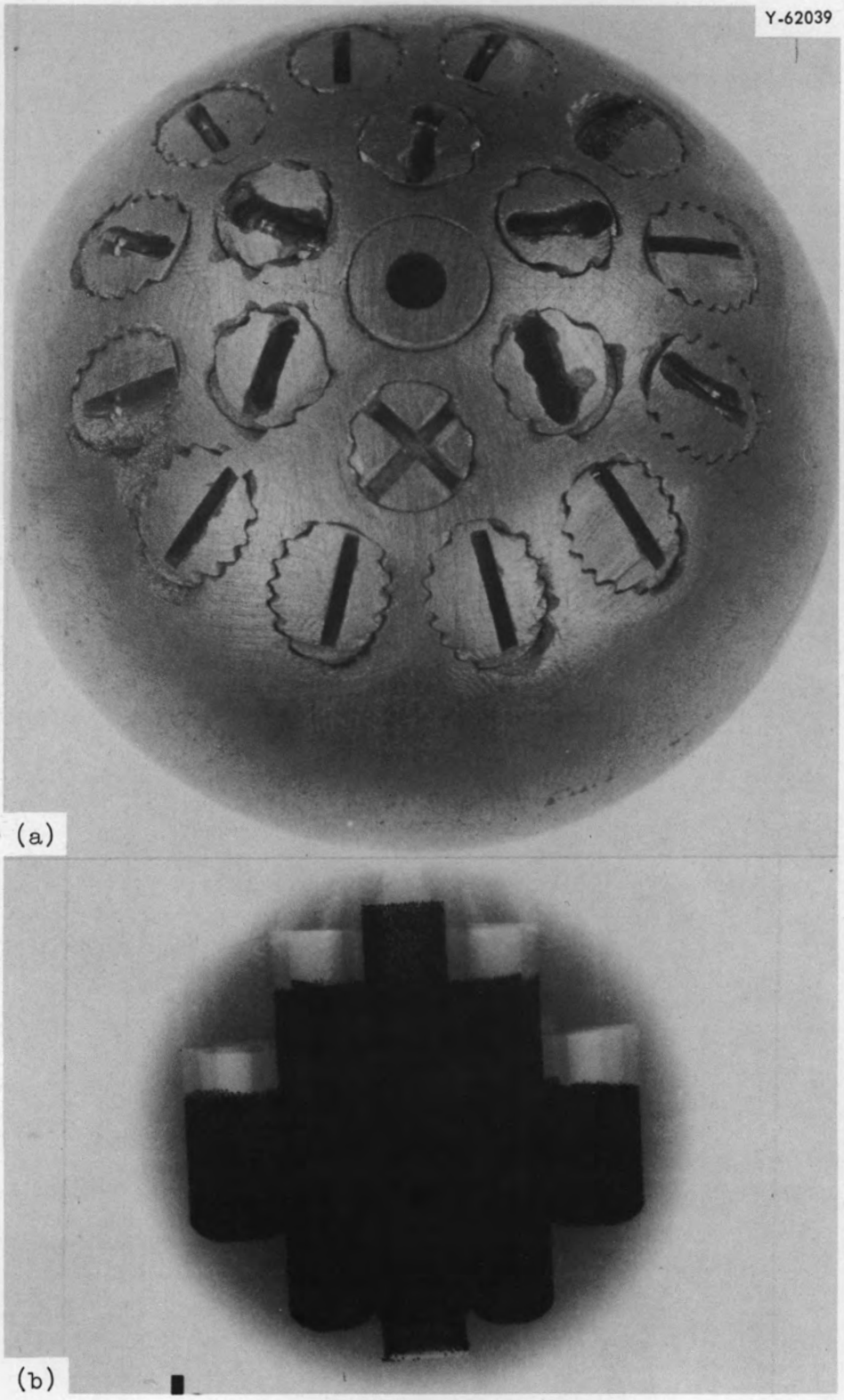

Fig. 3.31. (a) Photograph and (b) Radiograph of ORNL-VS2-2 Multi-hole Sphere (Not to Scale).

Examination of the particles from batch OR-182L after irradiation revealed no extensive interactions between the oxide cores and the carbon coatings; however, a phase, metallic in appearance, was observed and is shown in Fig. 3.32. The phase, which has not yet been identified, was also found in delaminations in the pyrolytic-carbon coatings. In short, there was excellent agreement between this experiment and B9-19.

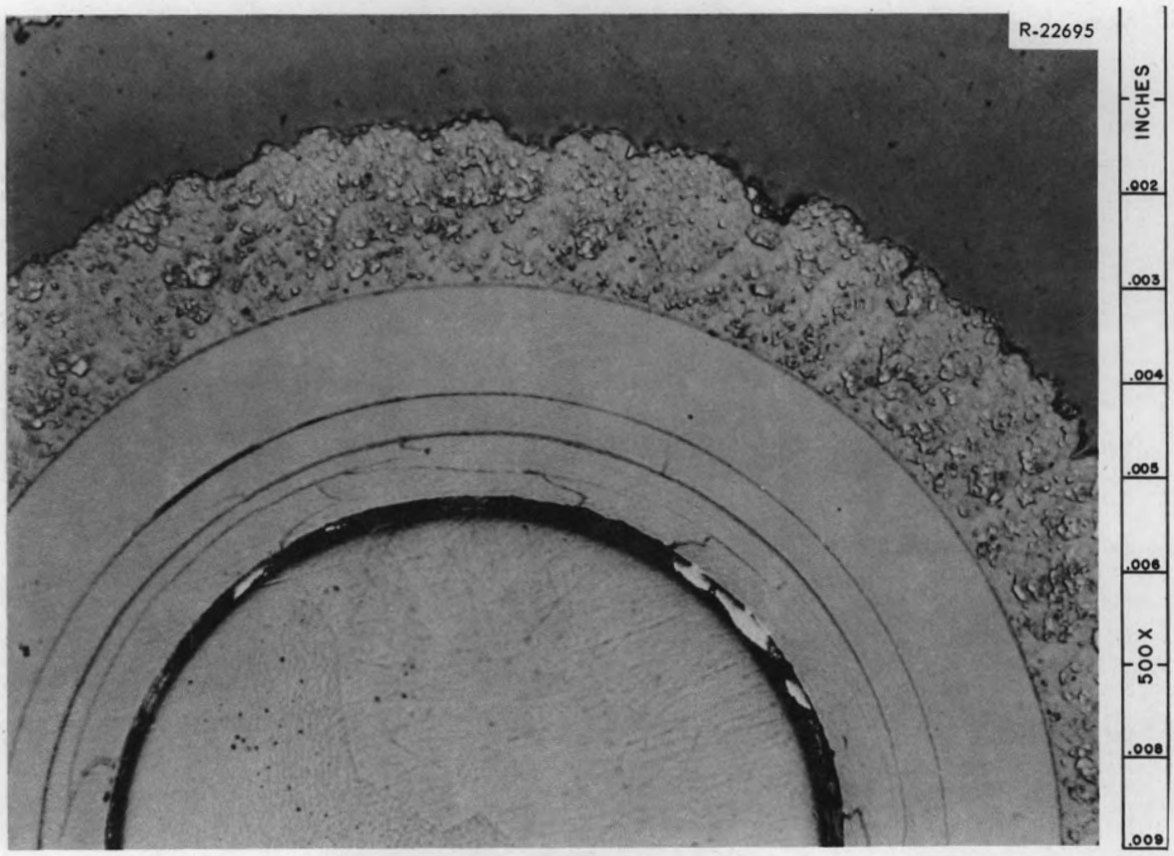

Fig. 3.32. As-Polished Microstructure of Sol-Gel ThO_2-UO_2 with a Duplex Pyrolytic-Carbon Coating After Irradiation in Capsule 01-8. Note metallic particles at the fuel-coating interface.

ORR Loop 1, Element 14

ORR loop 1 is a helium-cooled loop designed for irradiating gas-cooled fuel elements or capsules. A test assembly containing coated particles and designated test 14 was prepared recently for loop 1 and is now being irradiated. The test assembly consists of two compartments, each containing a mixture of loose pyrolytic-carbon-coated ThO_2 and $(Th,U)O_2$ particles (lots OR-205 and OR-206) in ATJ graphite holders. The particle cores were fabricated by the sol-gel process at ORNL. The particles are described in Table 3.7. About 53.4 g of $(Th,U)O_2$ particles were blended with 10.6 g of ThO_2 particles to form the mixture.

The graphite holders are positioned one on top of the other, as shown in Fig. 3.33. The loose coated particles in the top compartment are contained within an annulus formed by a graphite tube and rod. The bottom compartment consists of a solid graphite rod with five holes located symmetrically around the axis to contain loose particles. The bottom compartment is clad with stainless steel tubing and is sealed. The top compartment is clad with stainless steel tubing but is vented to the loop through a porous nickel plug. Thermocouples are provided to measure the central and surface temperatures of the upper graphite container. The lower compartment is uninstrumented because of its low heat-generation rate.

In addition to coated particles, the top compartment contains five BeO pellets in contact with graphite. These pellets are located inside the central graphite rod and were included to check the compatibility of BeO and graphite under simulated service conditions.

Irradiation of experimental fuel assembly No. 14 is continuing. Burnup of the sol-gel prepared $(Th,U)O_2$ coated particles, contained in the vented portion of this assembly, after completion of three ORR cycles is estimated to be 2.0 wt % heavy metal (33% ^{235}U consumption including absorption and fission in ^{235}U).

The central temperature of the assembly is being maintained at 1370°C, with a mixture of approximately 13% Ne in helium as loop coolant. Equilibrium levels of the noble-gas fission products in the loop gas under these operating conditions indicate R/B values of approximately

ORNL-DWG 64-7809R

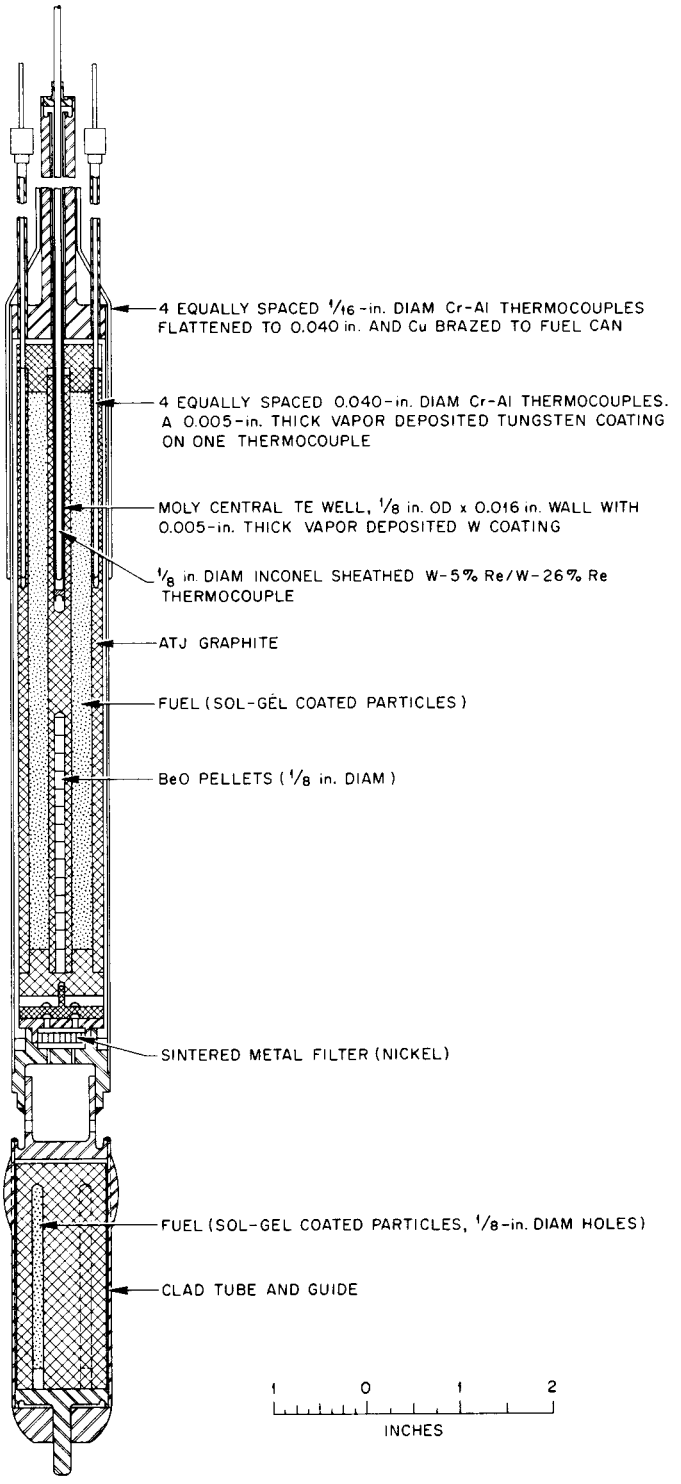

Fig. 3.33. Oak Ridge Research Reactor Loop No. 1.

1.9×10^{-5} for ^{85m}Kr, 1.0×10^{-5} for ^{87}Kr, 2.5×10^{-5} for ^{88}Kr, 1.5×10^{-5} for ^{135}Xe, and 1.4×10^{-5} for ^{133}Xe. Irradiation of this assembly will continue for one more ORR cycle.

The low levels of fission-gas activity in the loop indicate that the particle coatings are still intact even though the burnup and integrated fast dose are considerably higher than in the previously described tests.

It may be concluded that sol-gel derived oxide microspheres with pyrolytic-carbon coatings show promise for use as a fuel in high-temperature, gas-cooled reactor applications. Burnups of the order of 2 at. % heavy metal have been achieved at temperatures near 1400°C without excessive fission-gas release.

Vibratory Compaction Studies

Experimental studies of vibration energy characteristics required for obtaining high bulk densities are essentially complete. Although analyses of these experiments are in progress, some general conclusions are apparent. The most important factor that contributes to a high bulk density of powder-packed fuels is a relatively high radial acceleration level of the tube wall. In addition, the tube must vibrate in a longitudinal mode at a relatively high acceleration level. In this respect, the electrodynamic shaker cannot compare favorably with pneumatic vibrators. Contrary to previous ideas, compaction is not at all aided by the transmission of an extremely high acceleration pulse directly into the powders. Apparently, densification is achieved by a combination of the radial expansion and contraction of the tube wall and agitation of the powder by the longitudinal mode. The first provides a settling effect and the latter orients the particles into a good geometrical fit.

The energy transfer mechanics between the anvil, coupling, and tube were also studied. These studies led to improved design for

off-the-shelf pneumatic vibrators such as the Branford Vibrator Company's VIV and the NAVCO bin hopper type.

A final report covering these aspects, as well as others concerned with vibratory compaction, is being prepared.

Permeability of Vibratorily Compacted Fuels

Previous studies[14] of the mechanism of waterlogging failures in fuel elements were concerned primarily with permeability measurements of sol-gel oxide fuel elements. Extension of this work has resulted in a broadening of the experimental program with permeability of the fuel being only one of several variables considered.[15]

Waterlogging is the entrance of water through a cladding flaw into the available void space within a fuel element. The subsequent possibility of catastrophic failure of a fuel element depends on the stresses imposed on the cladding as the water is ejected upon increasing reactor power. These stresses are interrelated functions of: (1) the permeability of the fuel element, (2) the available void volume, (3) the geometry of the fuel element, and (4) the rate of temperature rise. All unbonded fuel elements are subject to waterlogging and it seems probable that any fully waterlogged element will fail upon a large power excursion from low power. Except for this condition, limitations on reactor startup procedures (based on the interrelations of the above variables) should greatly minimize the possibility of waterlogging failure.

During the past year experimental work to determine the interaction of these variables has been in progress.

---

[14]M. J. Kelly and J. C. Griess, Reactor Chemistry Div. Ann. Progr. Rept. Jan. 31, 1964, ORNL-3591, pp. 109–112.

[15]M. J. Kelly and J. C. Griess, An Analytical Approach to Waterlogging Failure, ORNL-3867 (to be published).

The permeability of pellet-loaded fuel rods is much greater than that of powder-packed rods because of the annular clearance between the fuel and the cladding. In powder-packed rods no annular clearance exists, and the permeability of the compact determines the overall permeability of the fuel element.

The permeability of the compacted fuel decreases inversely with the square of the surface area per unit volume and increases directly as the cube of the void percentage.[16] The associated proportionality constants have not been established for dense packings. Practical considerations dictate as small a void fraction as possible (8 to 12%); and, while the surface area could be controlled by elimination of very fine material, this is not economically attractive.

The range of permeability for compacts prepared for the Kilorod program is from 10^{-3} to 5×10^{-3} Darcy. Other compacts studied have permeabilities ranging from 10^{-4} to 1. Since extremely fine powders pack poorly, it is expected that practical fuel rods will have permeabilities above 10^{-3}. After the reactor has achieved its operating power level that permeability will be increased by consolidation of the fine powder fraction as a result of sintering.

In contrast to compacted fuels, sintered pellets normally have most of their porosity unavailable (i.e., closed pores). The available void space in a pellet rod is primarily the annular space between pellet and cladding plus any deliberately incorporated fission-gas gap. The available porosity within a powder-packed rod corresponds to the void volume since all of the void space is interconnected by finite passages. In either type of fuel, all of the free volume must be considered as available when considering waterlogging failure.

In general, fuel elements are long compared to their diameter. Tubular elements are most common, but other shapes are used. For waterlogging failure flow the full length of an element must be considered at the effective cross section of the fuel.

---

[16] F. C. Carman, Flow of Gases Through Porous Media, pp. 8–20, Butterworths, London, 1956.

Finally, the rate of temperature rise is the most important variable in waterlogging studies and may be controlled over a wide range during reactor startup. It is not measured directly but can be calculated with reasonable accuracy from the physical characteristics of the reactor assemblies and the rate of reactor power rise.

Theoretical Considerations

The properties of water are well-known. These, together with the description of the properties of fuel elements make it possible to construct a simplified model from which to calculate the effects of waterlogging.

Maximum internal pressure in an element is the sum of the pressure drop down the length of the element and the pressure drop across the cladding defect through which it is assumed that the water enters and must leave. This total pressure is created by flow from expansion upon increasing temperature plus the vapor pressure. Little work has been done on the defect pressure drop, and it will not be considered here.

The pressure drop down the length of the element depends on the flow caused by the expansion of liquid within the tube and may be described by:

$$\Delta P_{flow} = \left[\left(\frac{LV}{Ak} \right) \left(\frac{dT}{dt} \right) \left(\eta \frac{dV}{dT} \right) \right] \left(\text{a constant} \right) , \qquad (2)$$

where

V = the free volume in fuel element, ml

$\frac{dV}{dT}$ = the rate of volume change with temperature, $\frac{ml}{°K}$

η = the viscosity at T, centipoise

L = the length of fuel pack, cm

A = the cross-sectional area of fuel pack, cm^2

k = the permeability of fuel pack, Darcy

$\frac{dT}{dt}$ = the rate of temperature change with time, $\frac{°K}{sec}$.

The term $\left(\frac{LV}{Ak}\right)$ is a property of the mechanical system and $\left(\eta \frac{dV}{dT}\right)$ is a property of the fluid. The term $\frac{dT}{dt}$ is related to both terms.

Figure 3.34 is a plot of $\eta\frac{dV}{dT}$ vs T prepared using the expansion properties of water and the viscosity of liquid or vapor as required. If $\frac{dT}{dt}$ were constant, the model equation would be simple to use. However, the assembly has a specific heat of about 1 calorie per centimeter of length and when it is waterlogged, about 10% of this is due to water. Thus, the pressure rise is unduly weighted by the heat of vaporization of the water. This results in a change in $\frac{dT}{dt}$ that depresses the total pressure. The temperature at which this occurs is directly dependent on the pressure drop across the defect.

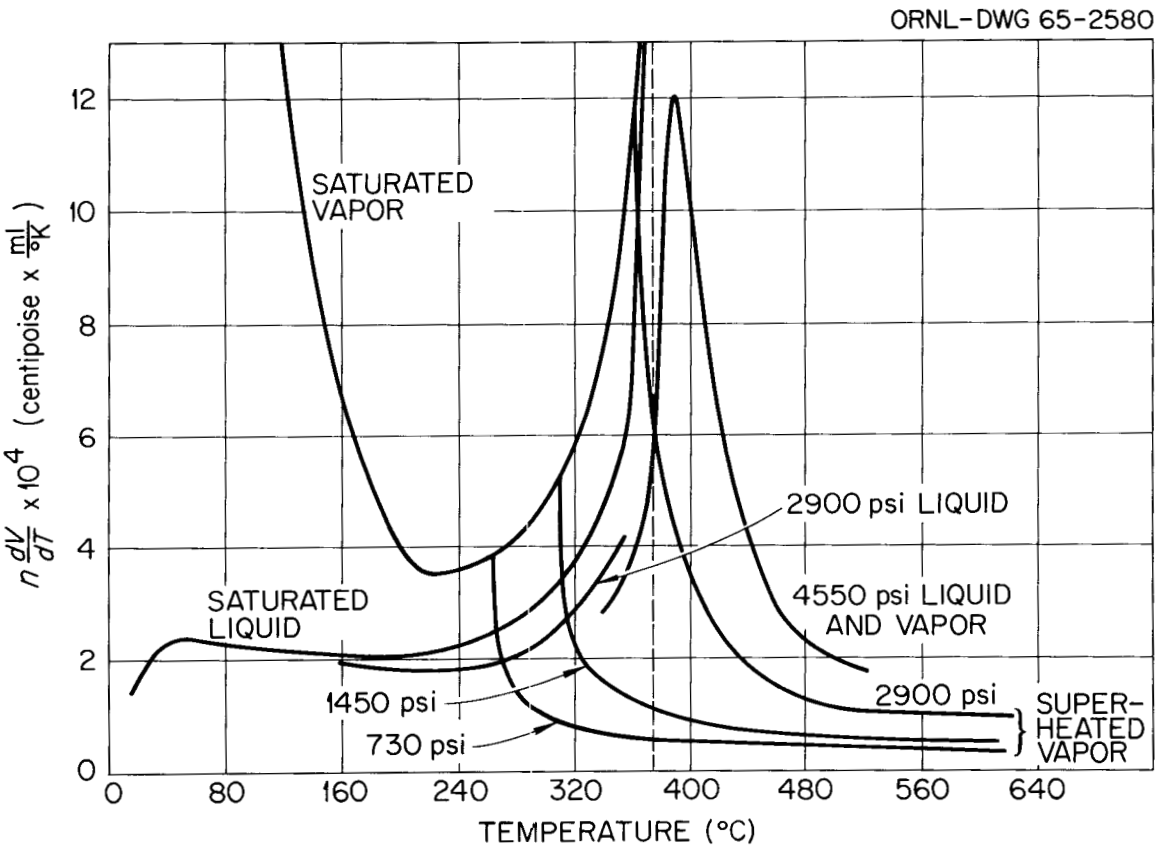

Fig. 3.34. Plot of the Product of the Rate of Thermal Expansion and Viscosity vs Temperature for Water, Liquid, and Vapor at Various Pressures.

Experimental Studies

The most practical method to simulate the stresses on a waterlogged fuel element during reactor startup is to completely fill the void space of a test element with water and then supply energy in a manner simulating that produced by fission. Electrical current passing through the cladding was used for this purpose. It is felt that the rate of expansion of the cladding being greater than that of the fuel does not compromise the results since flow down the element caused by fluid expansion provides the compressive force necessary to retain firm fuel packing. The source used to supply current to heat the cladding has been described elsewhere.[17]

The original test elements were rods formed from 1/4-in.-diam stainless steel pipe, schematically shown in Fig. 3.35 by filling with fuel of nominal "Kilorod" size distribution and density. Numerous tests from fully waterlogged conditions were made on two experimental assemblies. Test results showed that a much longer assembly was necessary to obtain data adequate for analytic extrapolation. A prototype "Kilorod" element was therefore obtained and installed in place of the shorter test pieces. This assembly has a packed fuel length of $\sim$ 105 cm and a cross-sectional area of 0.94 cm^2.

Results and Conclusions

A plot of data from a short test element is shown in Fig. 3.36. The time period associated with these experiments was such that the heating current was merely turned on at a previously chosen setting. Neither constant power nor a particular $\frac{dT}{dt}$ program could be obtained. Data from these experiments have been fitted to the following empirical equation for the pressure drop down the element:

$$\Delta P = \left(3.1 - 2.3 \times 10^{-3}\ T \frac{dT}{dt} \right) \frac{LV}{Ak} \times 10^{-4} \quad . \qquad (3)$$

---

[17] J. C. Griess et al., Effect of Heat Flux on the Corrosion of Aluminum by Water, ORNL-2939, p. 8 and 9 (1960).

ORNL-DWG 65-2581

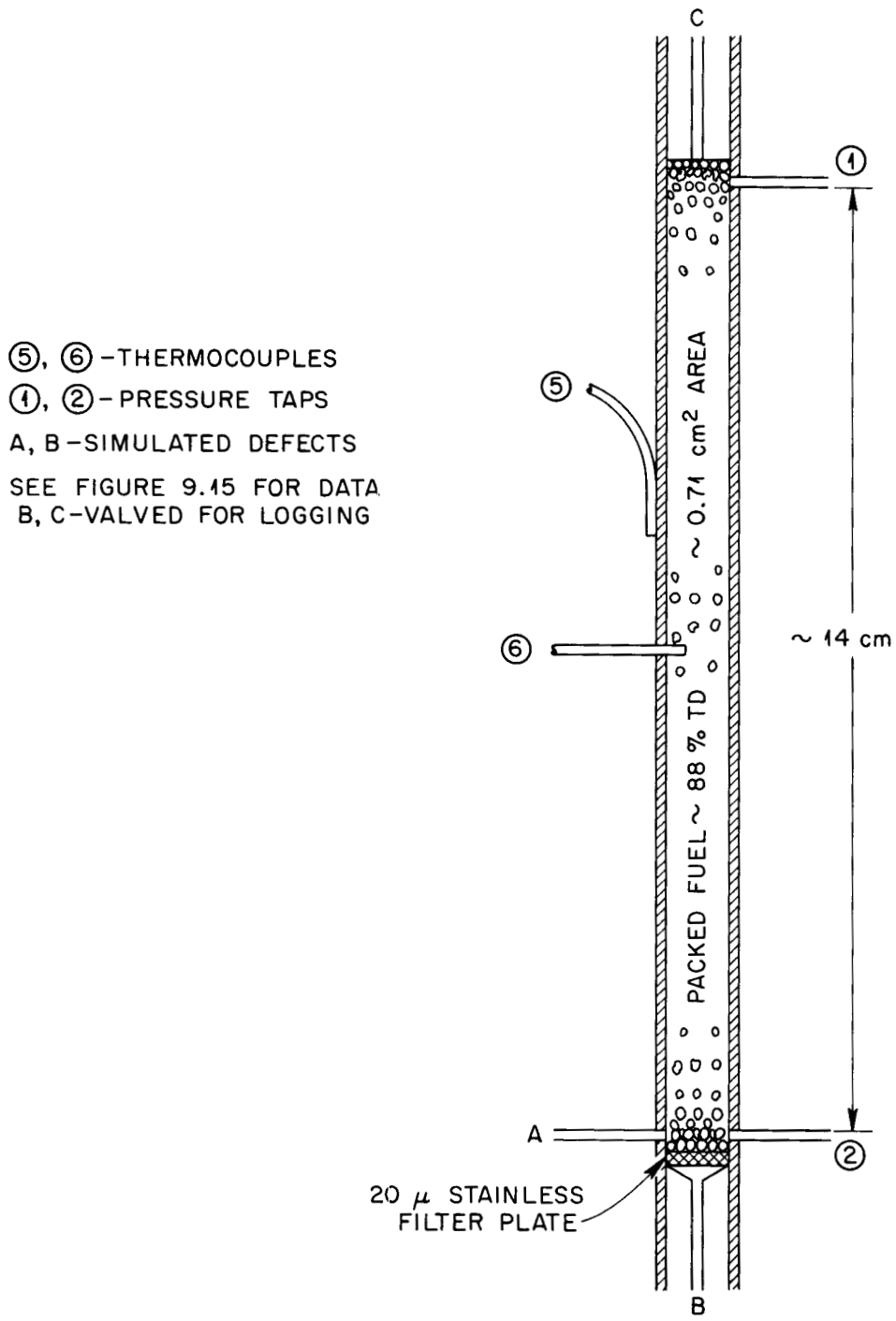

Fig. 3.35. Schematic of Test Element.

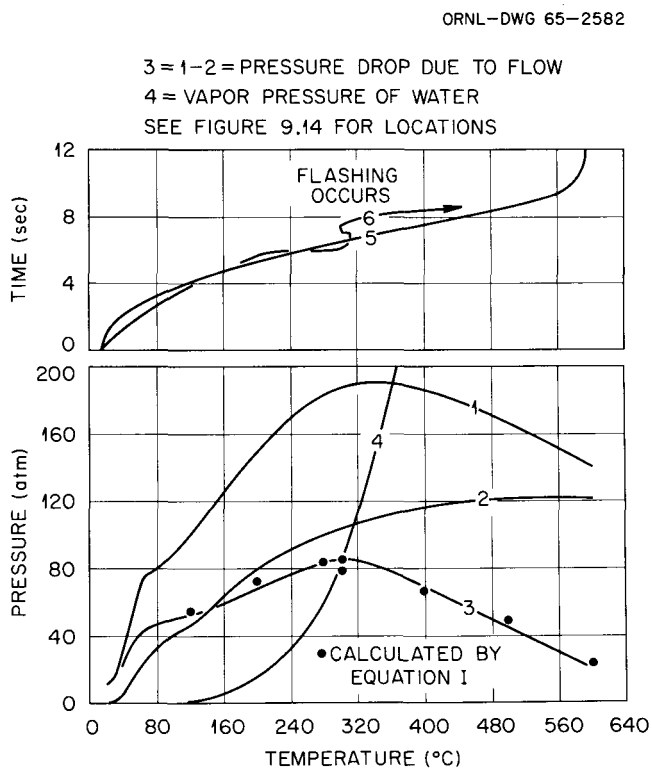

Fig. 3.36. Typical Test Data Obtained with a Short Test Element.

The experimental data can be fitted to our theoretical equation with gratifying precision up to the temperature at which "flashing" flow appears within the element if $\frac{dT}{dt}$ is obtained from wall temperature data. Flashing flow can only occur when the internal vapor pressure exceeds the pressure drop across the defect. Once this occurs, rapid loss of internal liquid occurs and a superheated vapor system is reached before the critical temperature. The extreme volume increase at the critical temperature is avoided and the maximum pressure occurs shortly after flashing starts.

In order to explain the observed experimental results after flashing occurs, the liquid water must be assumed to be entrained by the saturated steam and travel at steam velocity and viscosity. After expulsion of the entrained liquid, the superheated steam system can again be related to our theoretical equation with fair agreement.

The previously reported change[18] in effective permeability when changing from liquid water to gas as a test fluid was not observed when changing from liquid water to steam. Permeability measurements using steam (250 to 300°C) gave values identical with liquid water within the precision of the measurement for the test elements. Permeability measurements using nitrogen gas yielded values several times those of water as observed with previous samples. The postulated surface interaction with water apparently is equally effective with water vapor.

A few preliminary experiments with the "Kilorod" element at a constant power input appear to confirm our assumptions from short element data.

Present data indicate that an analytic interpretation of waterlogging stresses is feasible. The extension of such results to a general case, even if empirical, should supply guidelines for reactor operations and fuel element designers which will minimize the opportunity for waterlogging failure. The pressure effects at a defect assume greater importance now that a quantitative explanation involving internal steam formation and flashing flow has been invoked. An effort will be made to determine the effect of various defect parameters.

Sintering of Sol-Gel Oxides

Pellets of sol-gel ThO_2–3 wt % UO_2 were fabricated from powdered material in the dried-gel state to determine the effect of calcining temperature and gaseous environment and of sintering environment on the properties of the finished pellets.

Gel material that had been air dried at 80°C was micropulverized and screened to –200 mesh prior to calcination, pressing, and sintering. For one portion, all heat treatments were carried out in air while for the other they were carried out in hydrogen. Process variables for

---

[18]M. J. Kelly and J. C. Griess, Reactor Chemistry Div. Ann. Progr. Rept. Jan. 31, 1964, ORNL-3591, pp. 109–112.

each portion were as follows: powder calcination temperature (1 hr) – 400, 650, 750 (air only), and 900°C; isostatic cold pressure – 10,000, 22,500, and 35,000 psi. The pellets were lightly formed under uniaxial loading prior to isostatic pressing. The density after this operation was 3.8 g/cm^3 except for the material calcined at 900°C which required higher pressures (formed densities of 4.0 to 4.5 g/cm^3) to achieve sufficient green strength for handling purposes. All pellets were heated to 1000°C over a 36-hr period and finally sintered for 2 hr at 1450°C.

The conditions used and the results are shown in Table 3.10. A graphical representation of the effects of green density and calcining conditions is presented in Fig. 3.37. We observed that cracking of the pellets in the series treated in hydrogen occurred after slow heating to 1000°C. Also, for a comparable cold-pressed density, powders calcined in hydrogen sintered to a lower density than powders calcined in air at the same temperature. On the basis of these observations, calcination and sintering in air are to be preferred for the material and process conditions considered in this study.

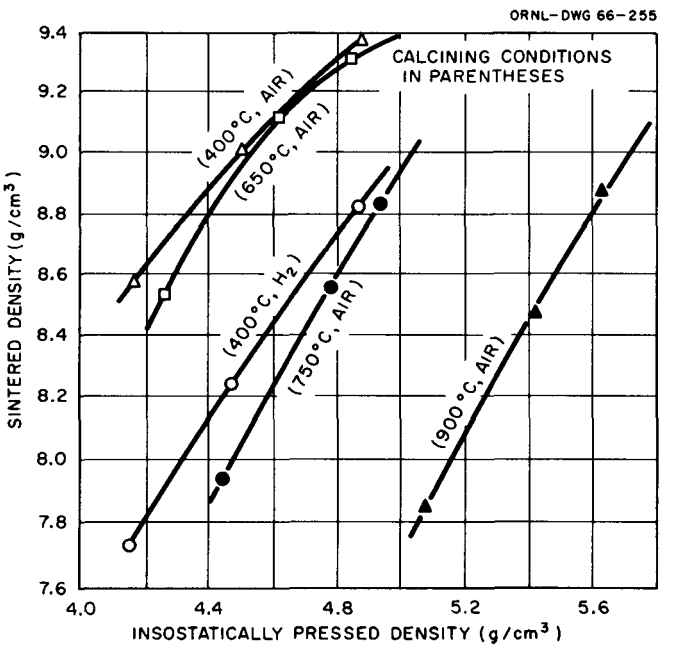

Fig. 3.37. Effect of Green Density and Calcining Conditions on the Sintering Characteristics of ThO_2–3 wt % UO_2 Powder Derived from the ORNL Sol-Gel Process.

Table 3.10. Results of Sintering Air-Dried, −200 Mesh Sol-Gel ThO_2–3 wt % UO_2 Powder for 2 hr at 1450°C

Calcining Temperature (°C)	Density after Uniaxial Forming[a] (g/cm^3)	Isostatic Pressure (psi)	Density after Isostatic Pressing[a] (g/cm^3)	Sintered Density[a,b] (g/cm^3)
		$\times 10^3$		
		Series Treated in Hydrogen		
400	3.76	10	4.15	7.72[c]
400	3.76	22.5	4.48	8.25[c]
400	3.75	35	4.83	8.82[c]
650	3.71	10	4.19	(d)
650	3.72	22.5	4.54	(d)
650	3.72	35	4.77	(d)
900	4.00	10	4.54	(d)
900	4.00	22.5	4.89	(d)
900	4.01	35	5.11	(d)
		Series Treated in Air		
400	3.77	10	4.16	8.58
400	3.73	22.5	4.49	9.11
400	3.73	35	4.79	9.39
650	3.75	10	4.26	8.54
650	3.73	22.5	4.62	9.12
650	3.73	35	4.84	9.31
750	3.78	10	4.44	7.92
750	3.78	22.5	4.80	8.57
750	3.78	35	4.95	8.84
900	4.50	10	5.09	7.87
900	4.58	22.5	5.42	8.48
900	4.58	35	5.63	8.89

[a]Each value is average obtained from two pellets.

[b]Sintering schedule: (1) heat slowly (36 hr) to 1000°C; (2) heat to 1450°C for 2 hr.

[c]Pellets cracked after slow heating to 1000°C but were sintered in hydrogen for 2 hr at 1450°C to obtain values listed.

[d]Pellets cracked after slow heating to 1000°C and were not sintered at 1450°C.

We found that calcining temperatures higher than 650°C render the powder less sinterable, although powder calcined at 900°C in air gave a sintered density of approximately 89% of theoretical after isostatic pressing to 35,000 psi. Pellets prepared from powder calcined at 400°C in air and pressed to 35,000 psi gave a sintered density of approximately 94% of theoretical.

Thorium Metal Fuels

A preliminary investigation of the dispersion strengthening characteristics of the Th-ThO_2 system has been completed and a report is being prepared. The following summarizes the findings of this work.

In a powder-metallurgy dispersion-strengthened alloy, the interparticle spacing of the dispersion phase is controlled by the particle size of the matrix powder used. If the interparticle spacing is to be sufficiently close to effect strengthening, a matrix powder of submicron particle size is needed. Two processes for producing thorium powder in the submicron size range were investigated: dry milling of thorium hydride and milling of thorium powder in the presence of surfactants. The latter process was abandoned due to severe reaction of the thorium with the organic surfactants.

Satisfactory dispersion structures were produced by milling a mixture of thorium hydride and ultrafine "Vitro" thoria. The milling reduced the particle size of thorium hydride and distributed the ThO_2 throughout the blend. After milling, the blend was consolidated by vacuum hot pressing (during which hydrogen was removed) followed by hot extrusion.

Thorium plus 10 vol % ThO_2 alloys produced by this process exhibited creep rates at 800°C less one-third those reported for the strongest arc-melted thorium alloy (Th + 5% U + 2% Zr). (Ref 19) Electron microscopy studies of the dispersion structure were conducted both from the

---

[19]R. H. Cole and L. E. Wilkinson, Development of High Strength Ternary and Quaternary Thorium-Uranium Base Alloys, ATL-A-128, p. 138 (November 1961).

strengthening aspect and for controlling fission-gas swelling through surface tension restraint.[20] Some clustering or "chaining" of the dispersoid particles was observed. This is possibly attributed to the "Vitro" thoria, which exhibited a similar "chaining" in the as-received condition.

This work was extended to combining solid solution and dispersion strengthening. Zirconium was selected as the solid solution additive on the basis of previous work.[21] Alloys of this type were found to be inferior to dispersion strengthened thorium. This effect is thought to be due to scavenging of the matrix in combination with coalescence of the dispersant. Since it is possible that uranium additions may behave in a similar manner, this phenomenon is being investigated further.

A study to determine the chemical compatibility of various uranium compounds as fissile constituents in a thorium matrix has been initiated. Earlier tests with UC, UO_2, and niobium- and graphite-coated UO_2 showed only graphite-coated UO_2 to resist reaction, and its compatibility was marginal.[22] Materials presently under examination are: sol-gel $(Th,U)O_2$, $(Th,U)C$, UB_2, UB_4, US, and UP. Two differentiations, 3:1 and 1:1, thorium to uranium were used in the oxide.

Recent investigation of SLIS-type[23] uranium-base alloys, produced by splat-cooling, points to an alternate method for introducing stable, ultrafine dispersions in fuels. In an effort to evaluate the applicability of this technique to thorium-base alloys, a contract for the production of several thorium-beryllium, SLIS-type alloys has been let to Nuclear Metals, Inc. These alloys will be evaluated with respect to elevated-temperature properties and amenability to fuel production.

---

[20] R. S. Barnes, A Theory of Swelling and Gas Release for Reactor Materials, AERE-R-4429 (October 1963).

[21] J. A. Burka and J. P. Hammond, Evaluation of Thorium-Base Alloys for High-Temperature Strength, ORNL-3771 (April 1965).

[22] J. A. Burka and J. P. Hammond, Metals and Ceramics Div. Ann. Progr. Rept. May 31, 1962, ORNL-3313, p. 98.

[23] A. R. Kaufmann and W. C. Muner, Development of Uranium-Base Alloys Strengthened by SLIS Technique, NMI-1262 (Dec. 2, 1964).

Fabrication and Economics of Fueled-Graphite Elements

Our evaluation of the economics of fabricating fueled-graphite elements containing particles coated with pyrolytic carbon has revealed the factors that contribute substantially to cost. In one study in which we assumed reasonable extensions of technology, we found that the coating operation accounted for 30% of the total cost (including fuel element hardware) in low capacity (~ 100 kg/day) plants and ranged to as much as 40% in high capacity (3000 kg/day) plants. Furthermore, the costs for coating did not decrease with increase in plant capacity at a rate comparable to other steps in the process.

These cost data confirmed quantitatively our intuitive impressions of the need for improvements in coating technology that would lead to additional economies. This requirement is especially true for remote applications, in which the cost of difficult operations is disproportionately exaggerated.

The conventional technology for preparation of spherical particles, whether oxide or carbide, results in high costs. Heretofore, the technology for making spherical carbide particles has consisted of various mechanical methods of consolidating combinations of UO_2, ThO_2, and carbon and then treating these at high temperature (2500°C) to complete the necessary reactions, to densify the material, and to complete spheroidization, all of which is a long and involved process. We thought that the process would be difficult and expensive to perform remotely and acknowledged a need for the development of a less complicated process for obtaining spherical particles of $(U,Th)O_2$ and $(U,Th)C_2$.

Accordingly, we have pressed development in three areas:

1. The preparation of spherical particles of $(U,Th)C_2$;
2. The direct conversion of $(U,Th)O_2$ microspheres to $(U,Th)C_2$; and
3. The coating of microspheres with pyrolytic carbon.

We have made theoretical calculations for and studied models of fluidized bed and rotary drum coaters in an attempt to optimize such systems; we have examined the feasibility of converting $(U,Th)O_2$ to $(U,Th)C_2$ without mixing carbon within the oxide particles and at lower

temperature than is used conventionally. Moreover, we have designed and started construction of a pilot line for demonstration of microsphere preparation and coating on a significant scale. All of this work is discussed in the sections which follow.

Fluidized-Bed Studies

Gas Flow Calculations for Fluidized-Bed Coating of Nuclear Fuel Particles. One of the main problems in designing apparatus for efficient coating of nuclear fuel particles is that the gas-flow requirements for fluidization and for coating are not well established. This is because the diameter and the density of the particles change during the coating process and because the temperature, density, and viscosity of the gases vary drastically inside the coating apparatus.

To study this problem, we calculated the theoretical flow requirements of the fluidizing gas and of the coating gas in nuclear fuel particle coating processes.

We have modified generally accepted gas-flow relations in fluidized beds[24,25] to include a number of assumptions applicable to nuclear fuel particles. This led to the following equation representing the minimum gas flow for fluidization:

$$G_{mf} = 5.53 \times 10^{-7} \frac{D^2}{\mu} (\rho_s - \rho_f)\rho_f \quad , \qquad (4)$$

where

G_{mf} = mass gas flow, g sec^{-1} cm^{-2},
D = particle diameter, μ,
μ = gas viscosity, centipoise,
ρ_s = overall density of the particles, g/cm^3,
ρ_f = density of the fluidizing gases, g/cm^3.

We used a computer program to calculate G_{mf} for values of the parameters usually encountered in the coating of nuclear fuel particles. Figure 3.38, which shows a typical set of curves for fluidization with

---

[24]F. A. Zenz and D. F. Othmer, Fluidization and Fluid Particle System, Reinhold, New York, 1960.

[25]M. Leva, Fluidization, McGraw-Hill, New York, 1959.

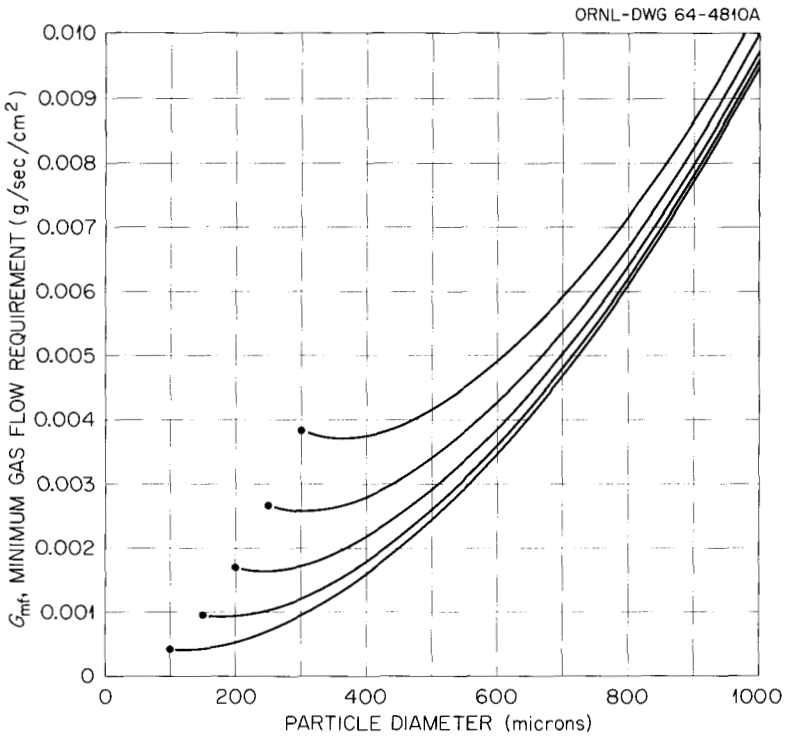

Fig. 3.38. Minimum Gas Flow for Fluidization G_{mf} with Helium at 20°C, 1 atm, Particle Density = 9.0 g/cm^3, and Coating Density = 2.0 g/cm^3.

helium at 20°C, indicates that G_{mf} goes through a minimum during the particle growth period. The mass gas flow decreases continuously with increasing temperatures as shown in Fig. 3.39. Finally a nomograph shown in Fig. 3.40 was established for quick calculation of G_{mf}.

When a constant stream of coating gas is blown through a given fluidized bed of particles, the mass rate of deposition is constant, for constant coating-gas decomposition efficiency. On the other hand, the linear growth rate of the coating (diameter increase) is constantly decreasing because of the increasing surface area of the particles.

Figure 3.41 is a typical set of curves representing the theoretical variation of particle diameters with time at constant coating-gas flow for an initial linear coating growth of 0.46 μ/min (particle diameter increase of 0.98 μ/min), an initial particle density of 9.0 g/cm^3, and a coating density of 2.0 g/cm^3. The curves flatten rapidly with time, especially for small particles, because of the constant volume of coating deposited on the ever-increasing surface of the particles. In the

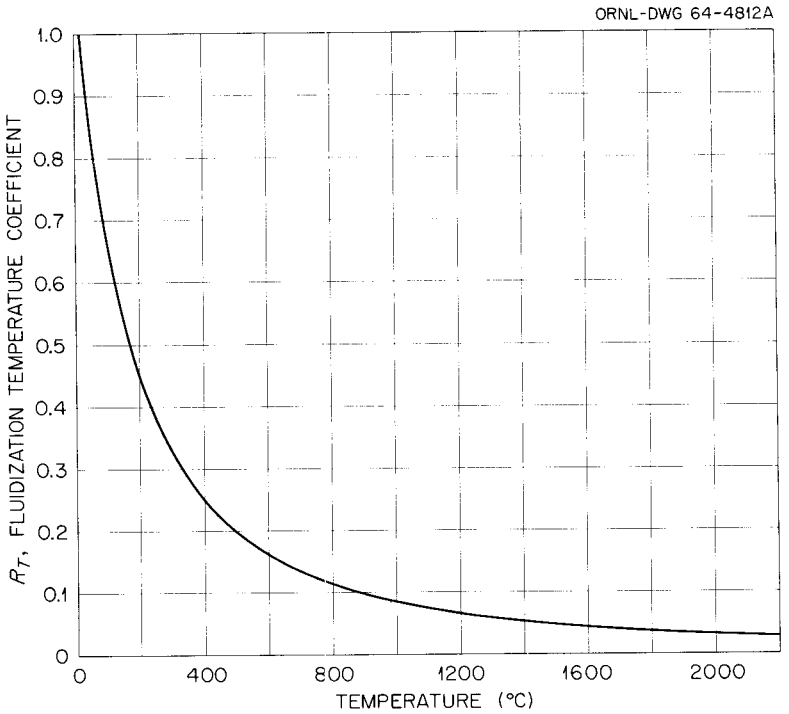

Fig. 3.39. Temperature Coefficient of G_{mf} for Helium at 1 atm Pressure.

example of Fig. 3.41, it would take 600 min to increase the diameter of particles from 150 to 350 μ. On the other hand, the coating time would be only 200 min for the same initial particle diameter and initial coating rate, if one could keep the linear growth of the coating constant by constantly increasing the flow of coating gas. This is represented by the tangent to the curve at the point corresponding to the 150-μ initial diameter.

In many coating processes, the flow rate of coating gas compatible with a certain type of coating is limited to a maximum value, and it is possible that this maximum value corresponds to a constant flow of coating gas per unit surface area of particles.[26] We have calculated

---

[26]R. L. Beatty, F. L. Carlsen, and J. L. Cook, "Pyrolytic Carbon Coatings on Ceramic Fuel Particles," paper presented at the American Nuclear Society Meeting, San Francisco, California, Nov. 30–Dec. 3, 1964, to be published.

ORNL-DWG 64-1536

NOMOGRAM OF EQUATIONS

$$G'_{mf} \cong 2 \times 10^{-3} \cdot \frac{D^2}{\mu} (\rho_s - \rho_f)\, \rho_f$$

$$G''_{mf} \cong 2\, G'_{mf}$$

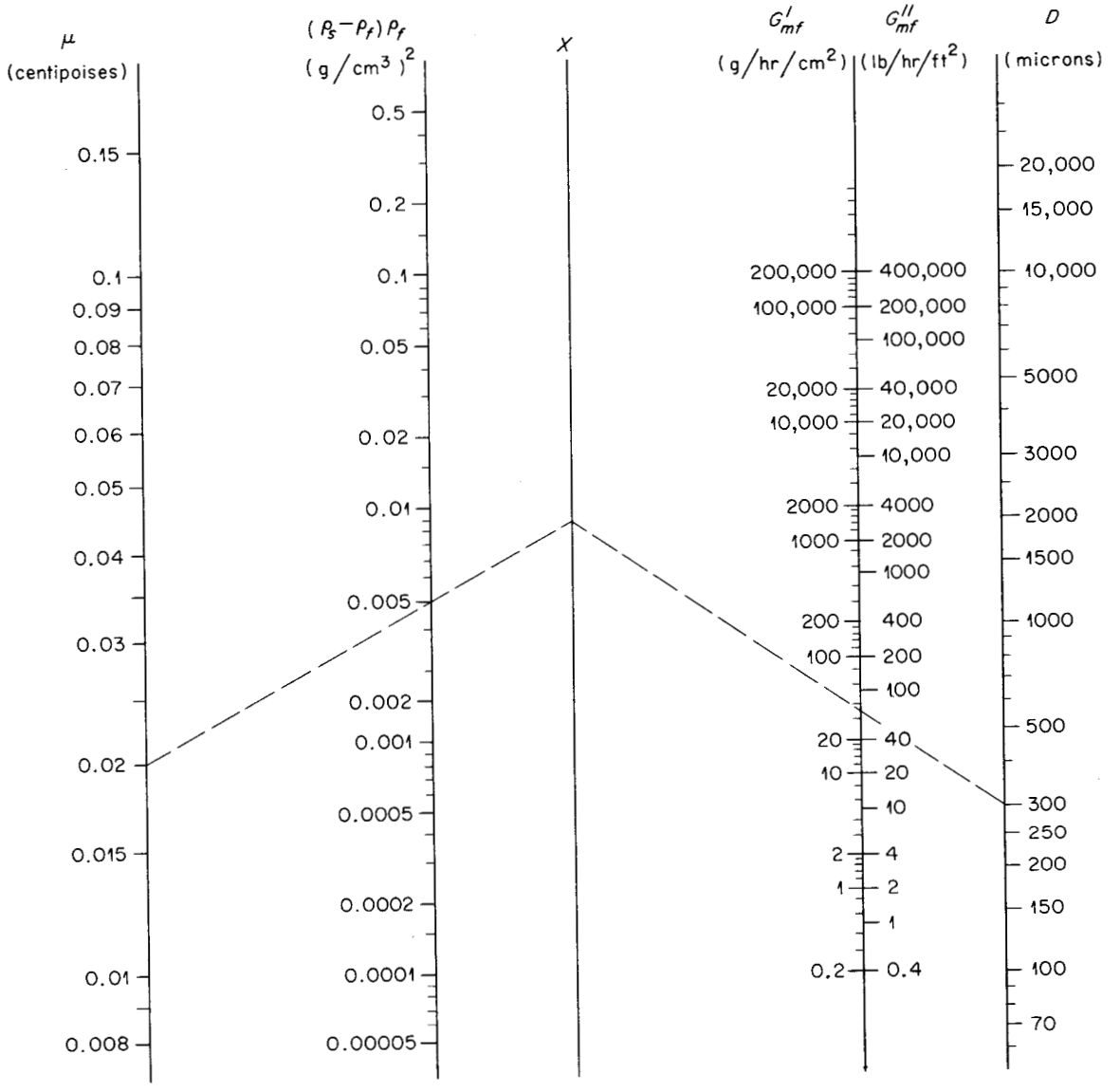

Fig. 3.40. Nomograph of Equations.

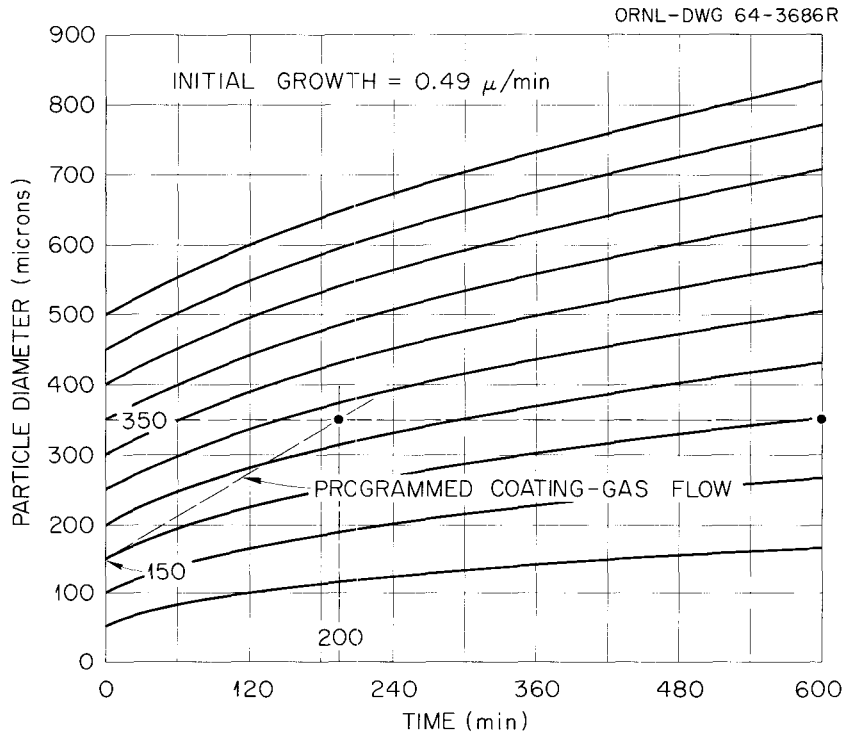

Fig. 3.41. Particle Growth at Constant Coating-Gas Flow. Core Density 9.0 g/cm^3 and Coating Density of 2.0 g/cm^3.

how the total flow of coating gas should theoretically be programmed to correspond to that constant value of flow per unit of surface area. The curves of Fig. 3.42 show the results for a constant particle-diameter growth rate of 0.98 μ min^{-1} g^{-1} for particle and coating densities of 9.0 and 2.0 g/cm^3, respectively. They indicate that the required variations of coating-gas flow are appreciable, especially for particles smaller than 200 μ in diameter.

In summary, our study shows that programming of the flow of fluidizing jar and of the coating gas should increase the efficiency of fluidized-bed coating processes.

Studies of Fluidized-Bed Models at Ambient Temperature. The design of most existing fluidized-bed coaters still departs very little from those used in initial research.[27] Consequently, deposition efficiencies

[27]J. M. Blocher, Jr., M. F. Browning, and J. H. Oxley, "Fluidized-Bed Processing of Particulate Nuclear Fuels," presented at the Symposium on Nuclear Experience with Fluidized Beds, Battelle Memorial Institute, 55th AIChE Meeting, May 17–20, 1964.

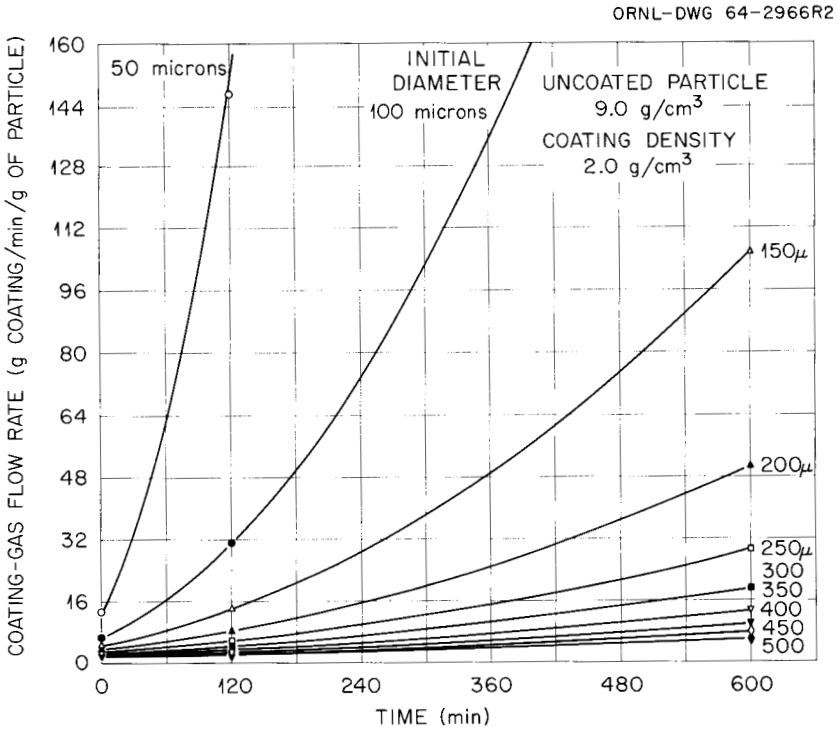

Fig. 3.42. Programming of Coating-Gas Flow for a Constant Particle Growth Rate of 0.98 μ/min.

are low, equipment capacities are small, and maintenance work is always appreciable. Accordingly, we studied the effect of column geometry on fluidized-bed characteristics to establish a basis for the design of improved fluidized-bed coaters. We used a slow-motion moving picture to observe particles fluidized by air in glass or plastic models at ambient temperature.

Figure 3.43 shows a typical apparatus used in this investigation. It consisted of a glass column placed above a metallic gas distributor. A simple connection allowed easy changes of these two parts. Air reached the various inlets of the gas distributor through the pipes shown at the bottom of the picture. In some instances, the conical part of the glass column was extended to a narrow apex, and a single tube was substituted for the multiple inlet nozzle.

We used mostly iron shot and glass beads in the experiments because they eliminated the contamination problem and because their densities of 7.8 g/cm^3 and 2.6 g/cm^3, respectively, were comparable to those of common

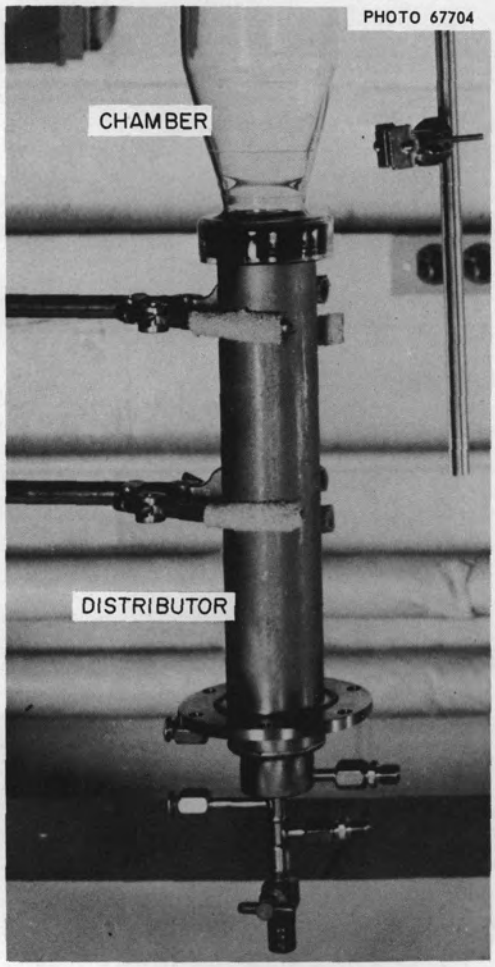

Fig. 3.43. Glass Column and Metallic Gas Distributor for Fluidization Studies.

nuclear fuel particles (frequently 8.5 g/cm^3 for uncoated particles and 3.2 g/cm^3 for coated particles). In each case, only the most spherical particles of commercial products were selected in order to ensure a geometry comparable to that of ORNL sol-gel nuclear fuel particles.[28] Generally, we used 250-μ-diam particles, but other sizes were investigated also.

---

[28]D. E. Ferguson, O. C. Dean, and D. A. Douglas, "The Sol-Gel Process for the Remote Preparation and Fabrication of Recycle Fuels," paper presented at the 3rd United Nations International Conference on the Peaceful Uses of Atomic Energy, Geneva, August 31–September 19, 1964, A-Conf-28-P-237.

Conically shaped columns with single-inlet gas nozzles have been widely used for coating nuclear fuel particles in fluidized bed.[29–31] We have built a large number of glass columns of this type and found that a 3-in.-diam cylindrical column connected to a small tubular gas inlet by a 30° contained-angle cone was particularly suitable for a study of the performance of this equipment. In such a column, we observed spouting beds with gas inlets smaller than 1/16 in. in diameter; that is, particles were rapidly entrained vertically in the central part of the bed and formed a small geyser above the surface of the bed. A major part of the bed had only a slow or erratic motion. On the other hand, when the diameter of the gas inlet was 3/8 in. or larger, particles had a tendency to fall through the gas distributor and considerable bubbling occurred in the bed. We have related this phenomenon to the velocity of entrainment of the particles and established equations to calculate that velocity for a large range of temperature and gas or particle characteristics.

A 3/16-in.-diam gas inlet tube gave best fluidization conditions with a flow of 10 to 40 liters/min air for 200 g of iron spheres and 5 to 15 liters/min air for 200 g of glass beads. In all cases bubbles formed at the neck of the conical part of the reactor, expanded while traveling upward, formed a temporary dome at the top of the bed and suddenly burst, leaving a thin vertical column of particles which collapsed immediately. This is shown in the sequence of photographs in Fig. 3.44. In no case was it possible to obtain a perfectly smooth and

---

[29] J. M. Blocher, Jr., M. F. Browning, A. C. Secrest, V. M. Secrest, J. H. Oxley, "Preparation of Ceramic-Coated Nuclear Fuel Particles," pp. 57–73 in Nuclear Reactor Chemistry Second Conference, Gatlinburg, October 10–12, 1961, TID-7622 (July 1962).

[30] W. D. Goeddel, Development and Utilization of Pyrolytic-Carbon-Coated Carbide Fuel for the High-Temperature Gas-Cooled Reactor, GA-4699 (November 1963).

[31] R. A. Huddle, J. R. Gough, and H. Beutler, "Coated-Particle Fuel for the Dragon Reactor Experiment," pp. 349–373 in Ceramic-Matrix Fuels Containing Coated Particles, Proceedings of a Symposium Held at Battelle Memorial Institute, November 5 and 6, 1962, TID-7654 (1963).

PHOTO 68017

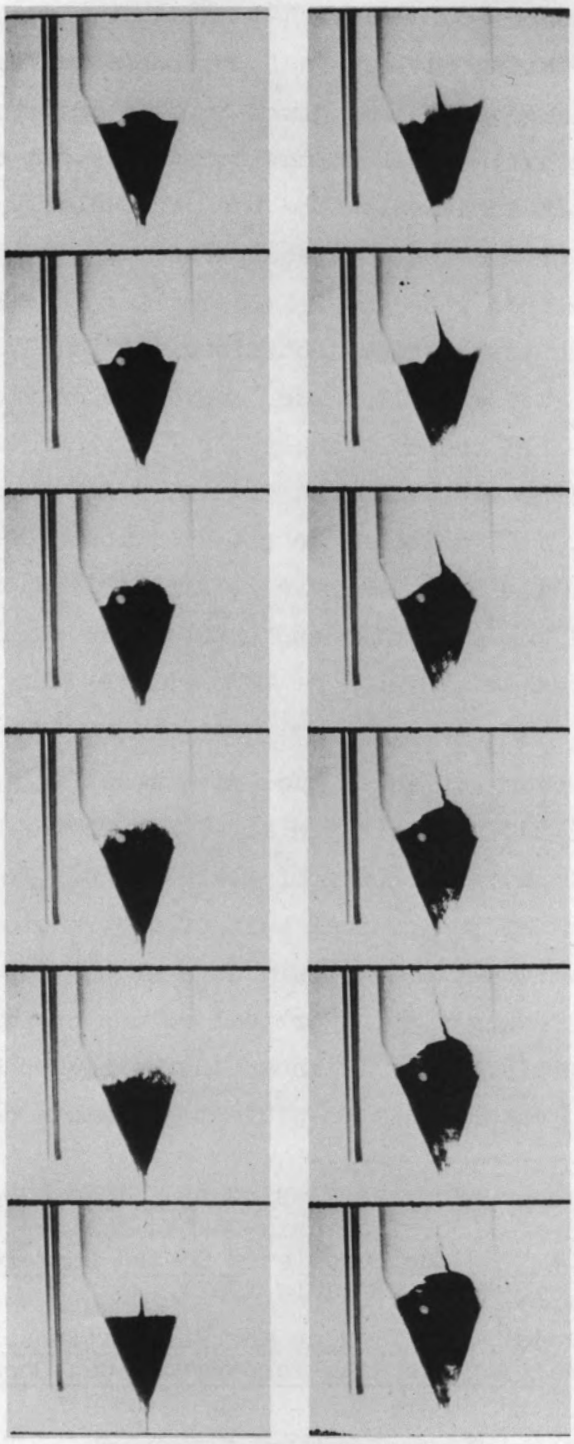

Fig. 3.44. Typical Fluidization Pattern with 300 g of 250-μ-Iron Spheres for 10 liters/min Air (Left) and 40 liters/min Air (Right).

uniform downward motion of the particles at the periphery of the 3-in.-diam reactor, especially when the change was larger than 200 g. Conditions deteriorated further when the diameter of the column was increased. Finally, the constant presence of a bubble at the bottom of the conical part of the vessel is probably another drawback of this type of equipment since it would cause a carbon deposit at that point on the wall of the coating furnaces.

We devoted the major part of our effort to multiple-orifice gas distributors since they appear more amenable to scaleup than the single-orifice nozzles.

Multiple-orifice inlets produced smaller bubbles than those of the single-orifice nozzles and therefore caused a better gas-solid contact. However, bubbles coalesced in the upper part of the bed.

We observed that the zone of fluidization was always limited approximately to the region starting at the gas distributor and expanding upward in a 30° cone. This can be seen in the sequences of views in Fig. 3.45. In all three cases the fluidized zone is below the large bubbles exploding at the surface of the bed. Since the rest of the bed was poorly agitated, if at all, it appears that a 30° cone shape of the bottom part of the column is quite desirable. This is in agreement with the observations of Takeda,[32] who also studied the effect of the cone angle in fluidization column.

We found that bubbles were the main factor in the gas-solids transfer processes that occurred in our fluidized beds. As previously indicated by P. N. Rowe,[33] bubbles are responsible for solids movement and cause rapid upward movement of particles immediately behind a rising bubble. In our columns, this resulted in a constant overall pattern of particle circulation with an upward flow in the center and a downward flow at the periphery of the chamber.

---

[32]K. Takeda, Chem. Eng. (Tokyo) 21(3), 124–29 (1957).

[33]P. N. Rowe, Chem. Eng. Progr. Symp. Ser. 58(38), 42–56 (1962).

PHOTO 68018

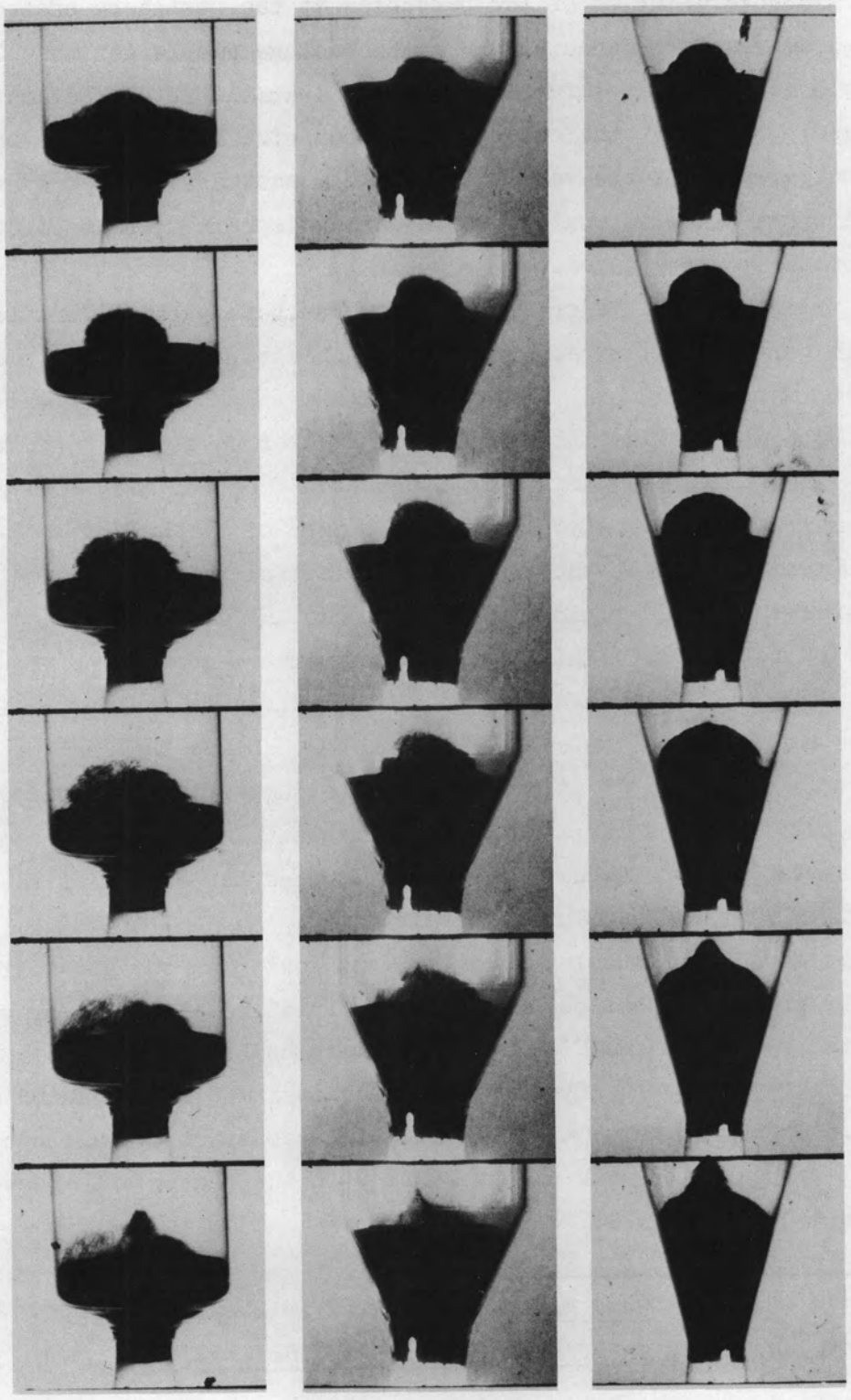

Fig. 3.45. Effect of the Column Cone Angle on Fluidization Characteristics – 120° (Left), 60° (Center), and 30° (Right).

Since in actual coating furnaces particles would be coated mostly at the lower part of the bed where the coating gas is introduced, the "cycling time" of the particles is an indication of the coating efficiency. We therefore studied that factor and more especially the "return time"; that is, the time required by the particles to travel from the top to the bottom of the chamber, and the "wall velocity"; that is, the downward velocity of the particles at the periphery.

We found that the "wall velocity" increases with increasing gas flow as shown in Fig. 3.46 and decreases with increasing bed charges. This means that fluidized-bed coating furnaces should be operated with large gas flows (with gas velocities close to the velocity of the particle entrainment) and with relatively low beds. A large bed height appears to be a detriment on two accounts: (1) it creates a long path for the return of the particles to the coating zone, and (2) it decreases the velocity of the particles along that path.

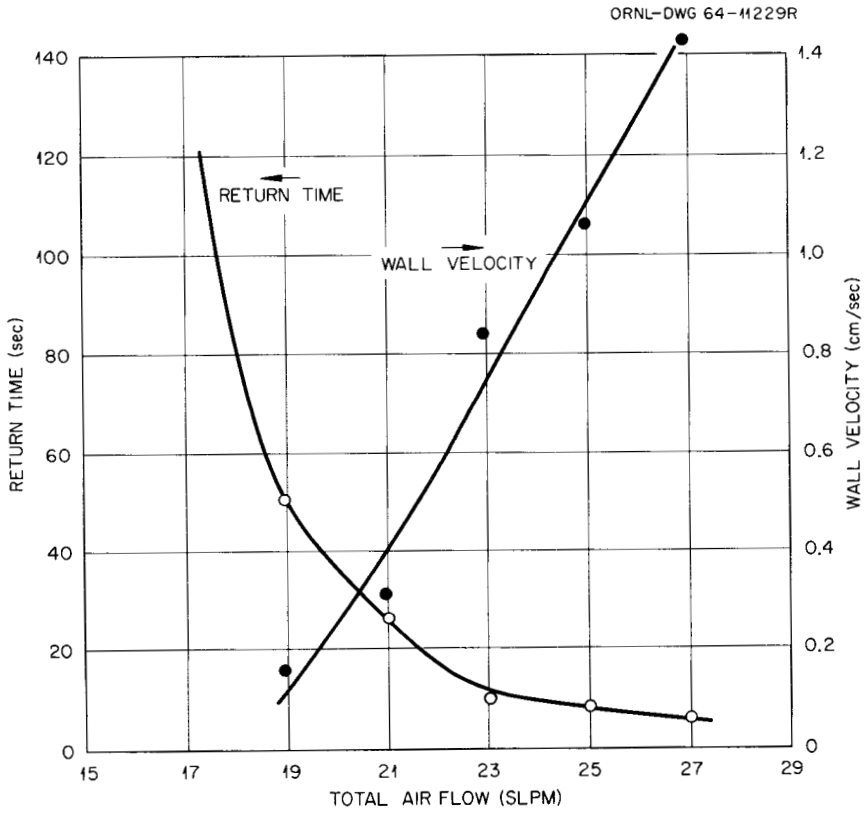

Fig. 3.46. "Wall Velocity" and "Return Time" of Particles for Various Gas Flows.

We found that a porous plate was a good gas distributor, causing little channeling. Unfortunately, this device does not lend itself easily to the exacting temperature control necessary to avoid a premature decomposition of the coating gas in fluidized-bed coating furnaces. At the same time, we observed that a multiple-orifice gas distributor, which can easily be cooled if necessary, caused little more channeling than a porous plate. However, our picture clearly demonstrated, as previously noted by Grohse,[34] that the bottom portion of a bed placed on a flat multiple-orifice plate was not expanded and hence not fluidized. Apparently, the air leaving the gas inlets did not flare out sufficiently fast and left many particles motionless between the holes. In actual fluidized-bed coating furnaces, this would affect the uniformity of the coating. We solved this problem by designing a plate in the form of a shallow cone. After many experiments, we gave the plate wall a slope slightly larger than the angle of slide of the particles to enable them to roll down toward the center of the plate. The effect of that slope on the "wall velocity," and hence on the "return time" of the particle, was quite dramatic as shown by Fig. 3.47. Proper design of the gas distributor should therefore lead to a much shorter cycling time of the particles and hence a much higher coating efficiency. Figure 3.48 shows a schematic cross section of the gas distributor that we were planning to use in our 5-in.-ID fluidized-bed coating furnace.

In summary, our observations of fluidized particles in glass models indicated that multiple-orifice gas distributors were preferable to single gas inlet nozzles for larger columns because they caused better gas-solid contact and a more uniform motion of the particles.

An angle of 30° between the walls of the lower part of the chamber appeared most satisfactory.

We also observed a general circular motion of the particles upward in the center and downward at the periphery of the columns. The "cycling time" of the particles could be shortened appreciably by designing a multiple orifice in the form of a shallow cone with a 120° contained

---

[34]E. W. Grohse, A.I.Ch.E. (Am. Inst. Chem. Engrs.) J. 1(3), pp. 358–65 (1965).

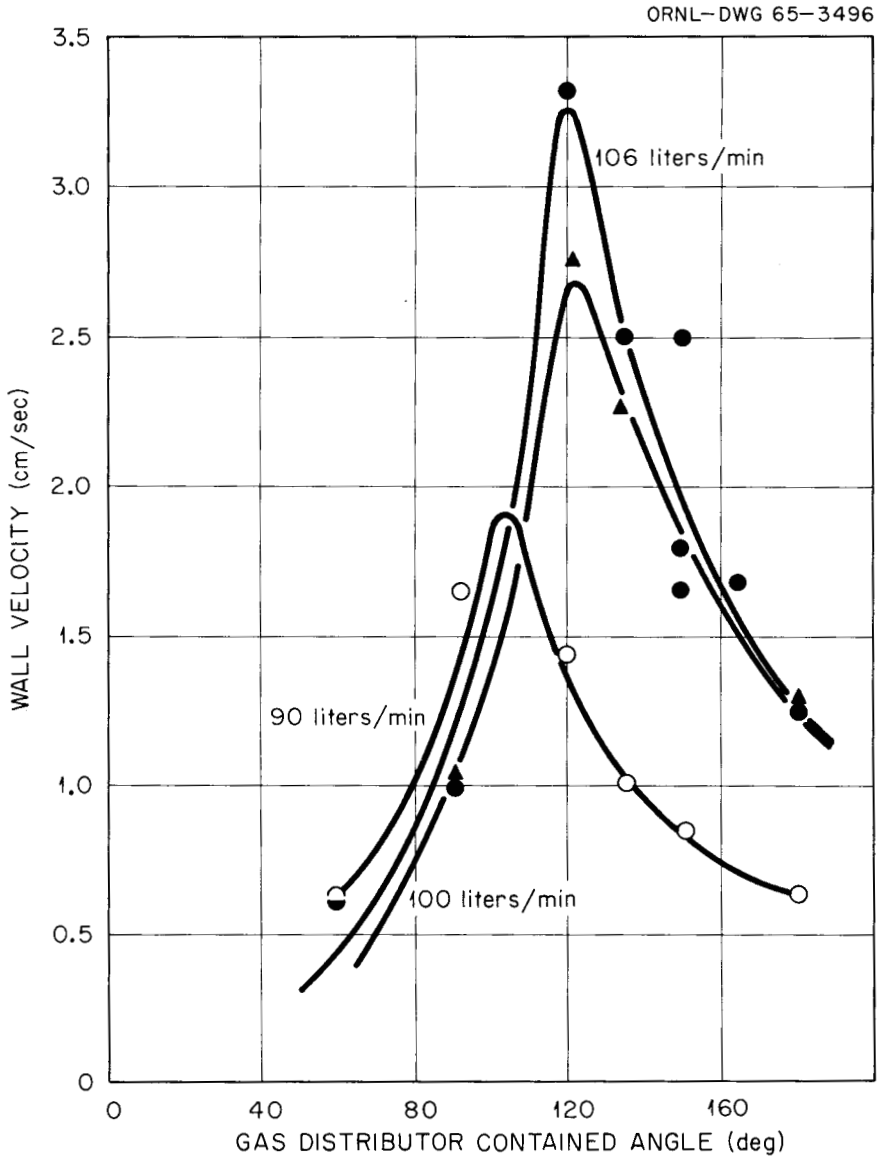

Fig. 3.47. Effect of the Gas Distributor Cone Angle on the Particle "Wall Velocity" in a Fluidized Bed.

angle. In actual coating furnaces, a shorter cycling would result in an increased coating efficiency since most of the coating appears only at the bottom of the column where the coating gas is introduced.

ORNL-DWG 64-11227

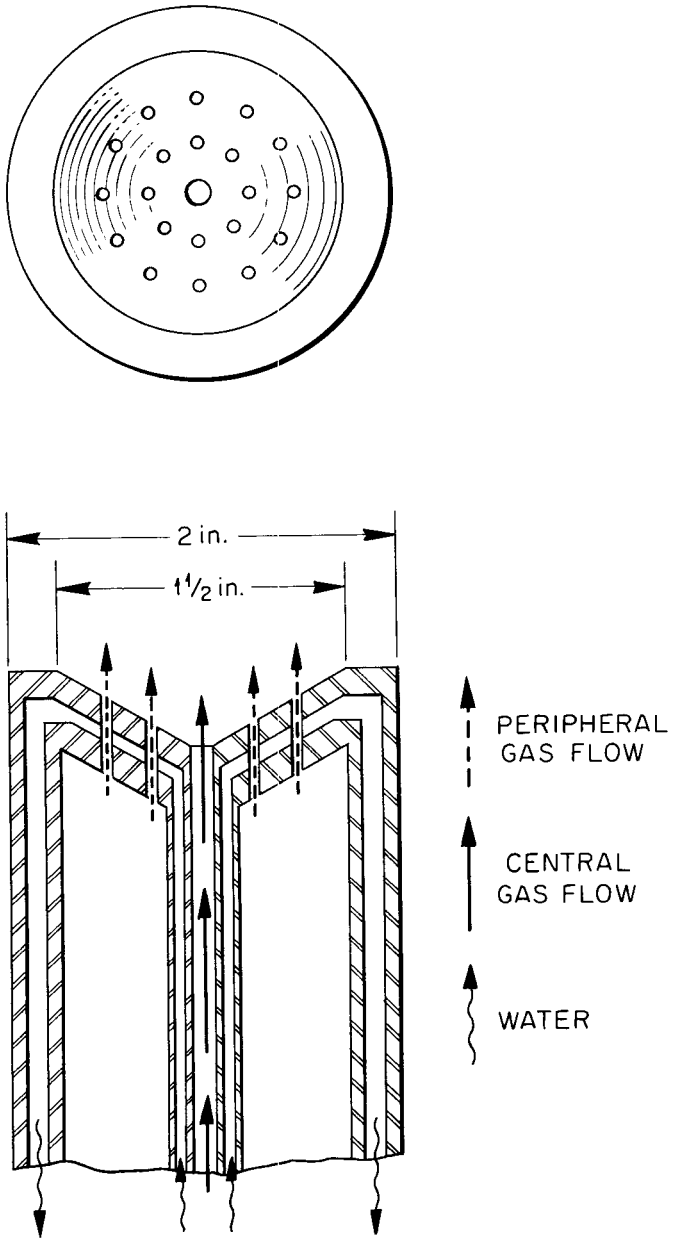

Fig. 3.48. Schematic Cross Section of Dual Gas Flow Distributor for Fluidized-Bed Coating of Nuclear Fuel Particles.

Rotating-Drum Studies

The rotating-drum coating process consists of blowing a coating gas over a charge of nuclear fuel particles placed in a heated cylindrical drum rotating around a horizontal axis.[35–39] Since the motion of particles is in this case independent of the gas flow, the process can, in theory, be more easily operated than fluidized-bed methods in which the gas flow has to be adjusted to control the coating conditions and particle motion simultaneously. Furthermore, the construction of rotating-drum coaters appears amenable to large-scale or remote operations since these drums are similar to rotating mixers which are widely used in industry.

On the other hand, the motion of particles in rotating-drum coaters has to be adjusted in a very precise manner to achieve uniform coating and to avoid the formation of irregular particle shapes or the agglomeration of particles. To study this factor, we have simulated the geometrical characteristics of high-temperature coaters in glass or plastic models and we have observed the motion of near-spherical nuclear fuel particles or of rheologically similar materials in those models. We have found that the angles of slide of these particles on smooth graphite, glass

---

[35]Coating Fuel Elements. Final Report for the Period November 15, 1958 Through November 14, 1959, NUMEC-NYO-2801.

[36]F. Benesovsky, "Development of Production Scale Procedures for Coating Fuel Particles," (Metallwerk Plansee Aktiengesellschaft, Reutte/Tyrol, Austria) Vienna International Atomic Agency, 1963, Preprint CN-16/1 (Conf-120-1) from Conference on Nuclear Materials Technology, Including Non-Metallic Fuel Elements, Prague, July 1963.

[37]M. P. Lepie, "Pyrographite Coating of Nuclear Fuel Particles," pp. 319–33 in Ceramic-Matrix Fuels Containing Coated Particles, Proceedings of a Symposium Held at Battelle Memorial Institute, November 5 and 6, 1962, TID-7654 (1963).

[38]J. M. Blocher, Jr., M. F. Browning, and J. H. Oxley, "Fluidized-Bed Processing of Particulate Fuels," paper presented at the American Institute of Chemical Engineers Meeting, May 17–20, 1964.

[39]H. G. Sowman, R. L. Surver, and J. R. Johnson, Nucl. Sci. Eng. 20, 231 (1964).

or steel are small. Consequently, their friction coefficients, that is, the tangents of the angles of slide, are small and consequently the particles have a tendency to slip on smooth rotating-drum walls or even to remain motionless.

We found that the slippage of particles on a slowly rotating, cylindrical wall or the absence of such slippage, could be related to the angle of slide and to the amount of charge in the drum. We prepared the following equation derived from a relation representing the slippage of belts on pulleys[40] to relate these variables:

$$\theta_m = \frac{0.693}{k} \tag{5}$$

where

θ_m = minimum subtended angle for complete entrainment of the charge (i.e., the angle subtending the arc of contact between charge and drum),

k = static friction coefficient (tangent of the angle of slide).

Figure 3.49 represents a curve of the data calculated by Eq. (5) and two experimental values. For nearly spherical particles and smooth-wall cylindrical drums, θ_m is frequently larger than 150°. This means that the depth of the bed must be larger than 75% of the drum radius; otherwise, particles will remain motionless in the rotating drums or will be entrained at less angular speed than that of the drum wall. Furthermore, the minimum angle for complete entrainment, θ_m, increases with increasing rotational speed as shown in Fig. 3.50.

The slippage of the charge in smooth drums may result in poor agitation of the charge and may cause agglomeration of the particles or their adherence to the wall in rotating-drum coating processes. The cure to this problem consists of increasing the initial loading of the drum but is limited by consideration of surface-to-volume ratios and by the considerable charge-volume increase during coating, which may lead to an overloaded drum.

---

[40] T. Baumeister and L. S. Marks, Mechanical Engineer's Handbook, pp. 3–50, McGraw-Hill, New York, 1958.

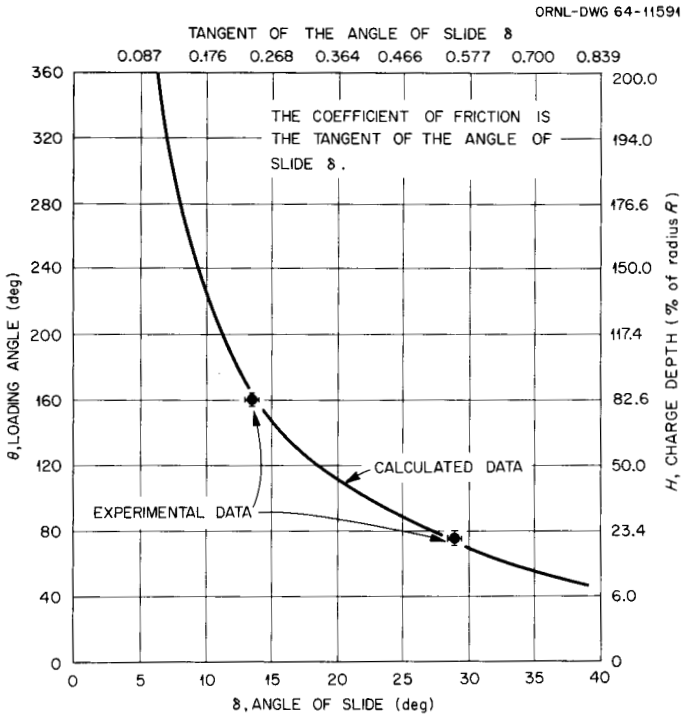

Fig. 3.49. Loading Necessary to Avoid Slippage of the Charge at Low Angular Speeds as a Function of Friction.

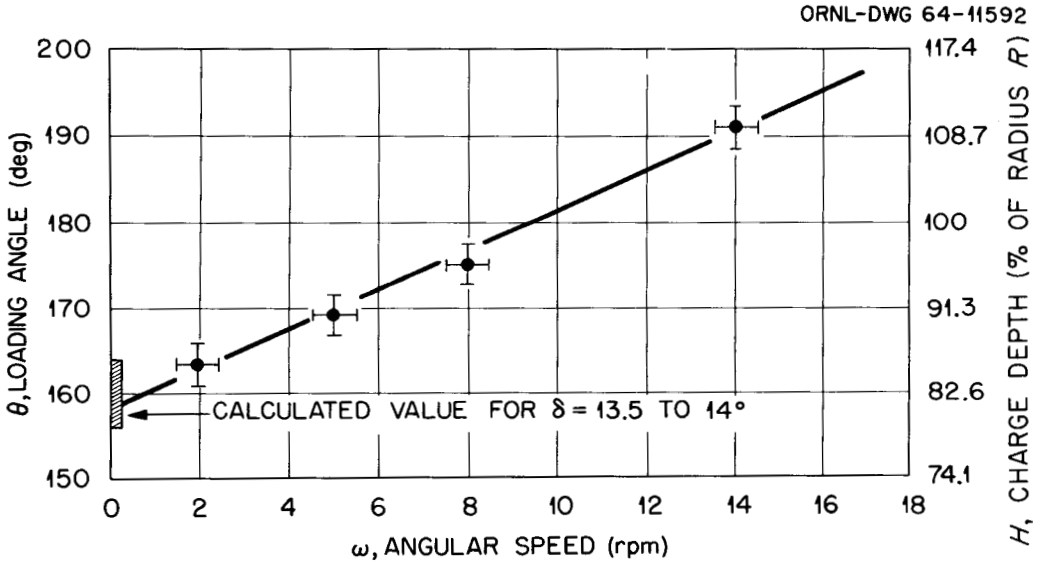

Fig. 3.50. Variation of the Loading Necessary to Avoid Slippage as a Function of the Angular Speed for a Given Material and Drum (Static Angle of Slide δ = 13.5 to 14°).

Our motion picture study in plastic models showed how the charge of the drum can remain motionless, be entrained at a lower angular speed, or be entrained at the same speed as the rotating drum. In the latter case, the bulk of the charge rotates as a unit, and only a thin layer of particles tumbles at the top of the bed, as shown in Fig. 3.51. This is similar to the motion of particles observed in some ball mills and rotary mixers.[41] The shape of the upper surface of the tumbling bed for various loading and rotation speeds is shown in Fig. 3.52. When there is no slippage of the charge in a rotating drum, the angular velocity of the rotating part of the bed is equal to that of the drum. On the other hand, the velocity of the particles in the tumbling layer of the charge is a more complicated function of the speed of rotation as shown in Fig. 3.53. The ratio of the time spent by the particles in the tumbling layer to the time spent in the rotating part of the bed for typical conditions is shown in Fig. 3.54. The curves show that particles

[41] K. W. Carley-Macauly and M. B. Donald, Chem. Eng. Sci. 19, 191 (1964).

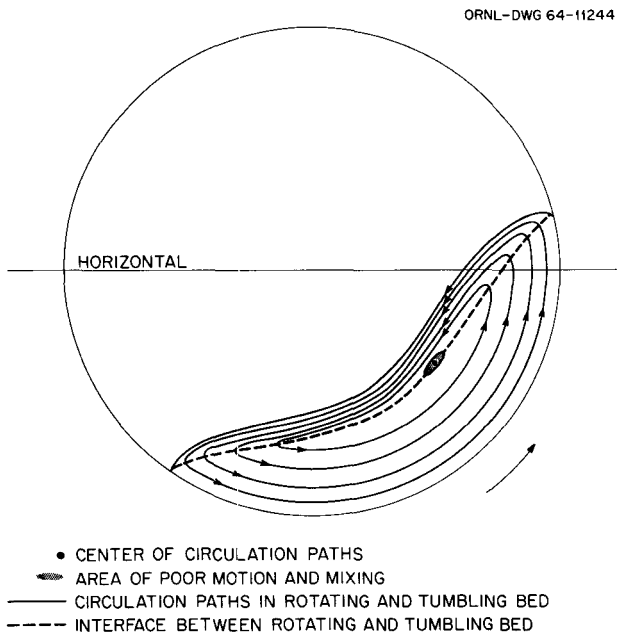

Fig. 3.51. Motion Path Pattern for a Radius of 8.5 cm, a Charge Depth of 40% of the Radius, and a Rotational Speed of 40 rpm.

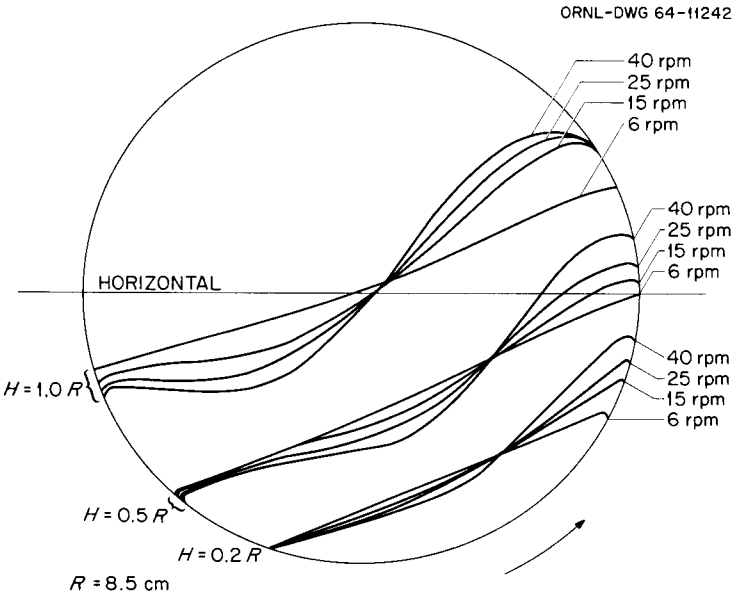

Fig. 3.52. Shape of the Upper Surface of the Tumbling Bed for Different Loadings at Different Rotational Speeds.

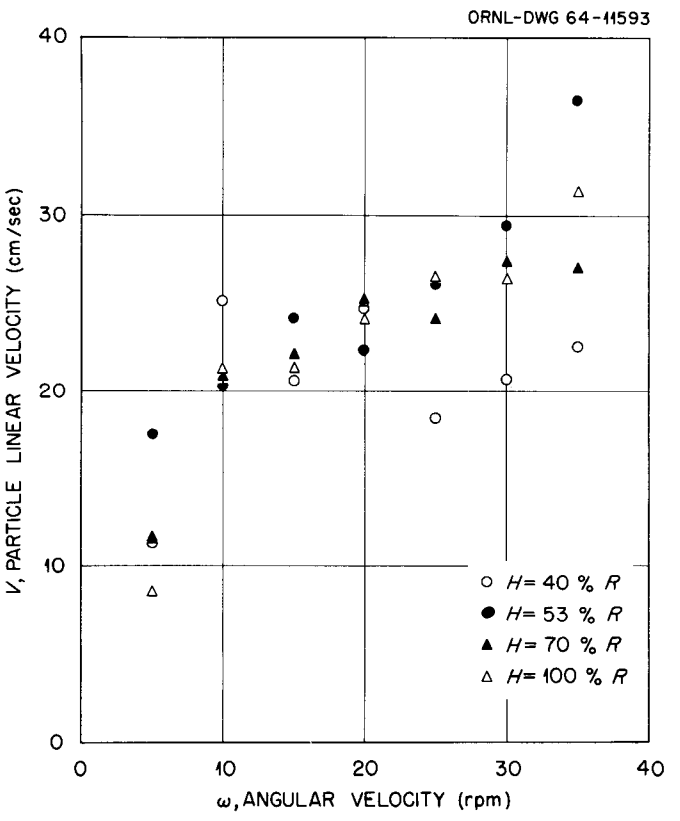

Fig. 3.53. Superficial Linear Velocity of Particles in the Tumbling Part of the Bed in a Rotating Drum.

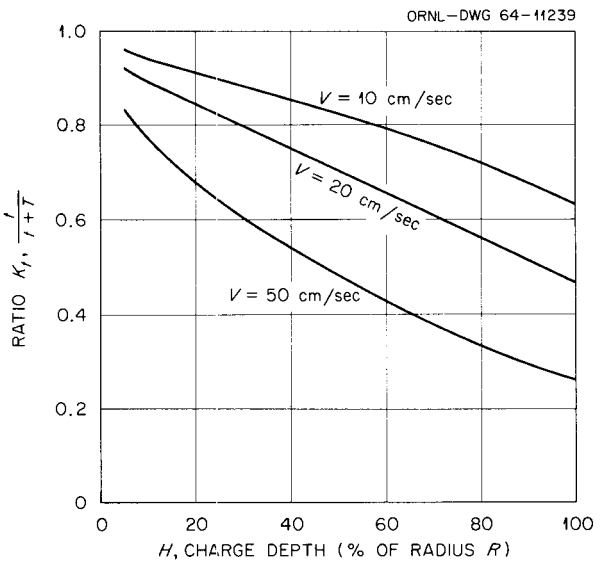

Fig. 3.54. Relative Time in Tumbling Layer for a Rotation Speed of 20 rpm and a Drum Radius of 10 cm.

frequently spend as much as 50% of their time in the rotating part of the bed where they are static relative to one another and to the wall. This value can be decreased by decreasing the amount of charge in the drum, but this may cause slippage as previously explained. A most probable consequence of this phenomenon is that the particles will often agglomerate or stick to the wall of the drum in coating processes, even when the charge does not slide on the rotating wall.

In conclusion, our investigation has shown that spherical or near-spherical nuclear fuel particles will not be properly agitated in horizontally rotating, smooth drums unless loading, rotational speed, and wall-surface characteristics are carefully selected. Furthermore, even when these variables are optimized, the particles remain motionless relative to one another and to the wall for an appreciable fraction of time. Thus, we conclude that smooth drums are unsuitable for coating. Therefore, we are investigating additional mechanical means for providing proper particle motions in rotating drums.

Experiments on Conversion of Sol-Gel Microspheres from ThO_2 to ThC_2

An experimental study was carried out to determine the feasibility of converting dense sol-gel oxide microspheres to dense carbide microspheres by methods adaptable to remote operations. This study was performed to provide information for the design and development of equipment that might be used in the proposed Thorium-Uranium Recycle Facility for refabrication of gas-cooled reactor fuels containing carbon-coated car carbide fuel particles.

The basic process investigated was that of heating the oxide particles in the presence of carbon and removing the reaction-product gases in a dynamic vacuum or in a flowing inert gas. The conditions and results of the experiments performed are listed in Table 3.11.

Initial feasibility was established when a dilute dispersion of fully dense ThO_2 particles in graphite flour (approx 9% ThO_2 by weight) was heated for 2 hr at 2200°C and 10^{-2} torr (experiment 1 in Table 3.11). Complete conversion to ThC_2 was observed in most particles, as shown in Fig. 3.55, although small spherical regions of unconverted ThO_2 were found near the center of some particles as shown in Fig. 3.56. The ThC_2 microstructures exhibit the typical banded ThC_2 structure resulting from the martensitic-type transformation of the face-centered-cubic to the body-centered-tetragonal structure at 1410°C during cooling.[42] It was encouraging to note that the particles retained their spherical shape and were apparently fully dense after the high-temperature conversion. The absence of pores suggests that the conversion mechanism involves bulk diffusion of oxygen ions radially through the carbide structure and that the formation of carbon monoxide gas occurs at the surface of the particle. Examination of the reaction interface in the partially converted material (see Fig. 3.56a) revealed that reaction occurred more rapidly at grain boundaries than within the grains themselves.

---

[42]N. A. Hill and O. B. Cavin, GCR Program Semiann. Progr. Rept. Sept. 30, 1964, ORNL-3731, pp. 34–37.

Table 3.11. Test Conditions and Results of Experiments on Conversion of 300- to 400-μ-diam Sol-Gel Microspheres from ThO_2 to ThC_2

Experiment Designation[a]	Carbon Source[b]	Carbon-to-Thoria Weight Ratio	Speed of Crucible Rotation (rpm)	Temperature (°C)	Time (hr)	Observations[c]
1	Graphite flour	10:1	0[d]	2200	2	Conversion incomplete in some particles
2	Graphite flour	1:1	0[d]	2200	2	Some reaction-bonding to crucible, severe agglomeration; conversion incomplete
3	Graphite crucible[e]	0	0	2200	2	All particles severely reaction-bonded to crucible
4	Graphite crucible	0	14	2000	2	Reaction-bonding to crucible, conversion incomplete
5	Graphite flour	1:1	14	2000	2	Reaction-bonding to crucible; conversion incomplete but better than for experiment 4
6	Graphite flour	1:1	44	2000	2	Conversion incomplete
7	Lampblack	1:1	44	2000	2	Conversion incomplete but better than for experiment 6
8	Lampblack	1:1	44	2300	1	Severe agglomeration and porosity
9	Lampblack	1:1	44	2200	2	Agglomeration
10	Lampblack	1:1	44	2200	1 1/2	Conversion incomplete
11	Lampblack	1:1	44	2100	5	Conversion incomplete in some particles
12	Lampblack	1:1	44	2150	5	Successful in all respects

[a]All experiments performed in flowing argon except 1, in which system was evacuated to 10^{-2} torr.

[b]Graphite flour: "NCC No. 38." Lampblack: "Thermax" pretreated at 2200°C for 2 hr at 10^{-5} torr.

[c]Only those observations that rendered experiment unsuccessful are listed.

[d]Experiment performed in stationary bed of particles dispersed in graphite flour.

[e]Layer of particles on bottom of graphite crucible; no graphite flour or lampblack.

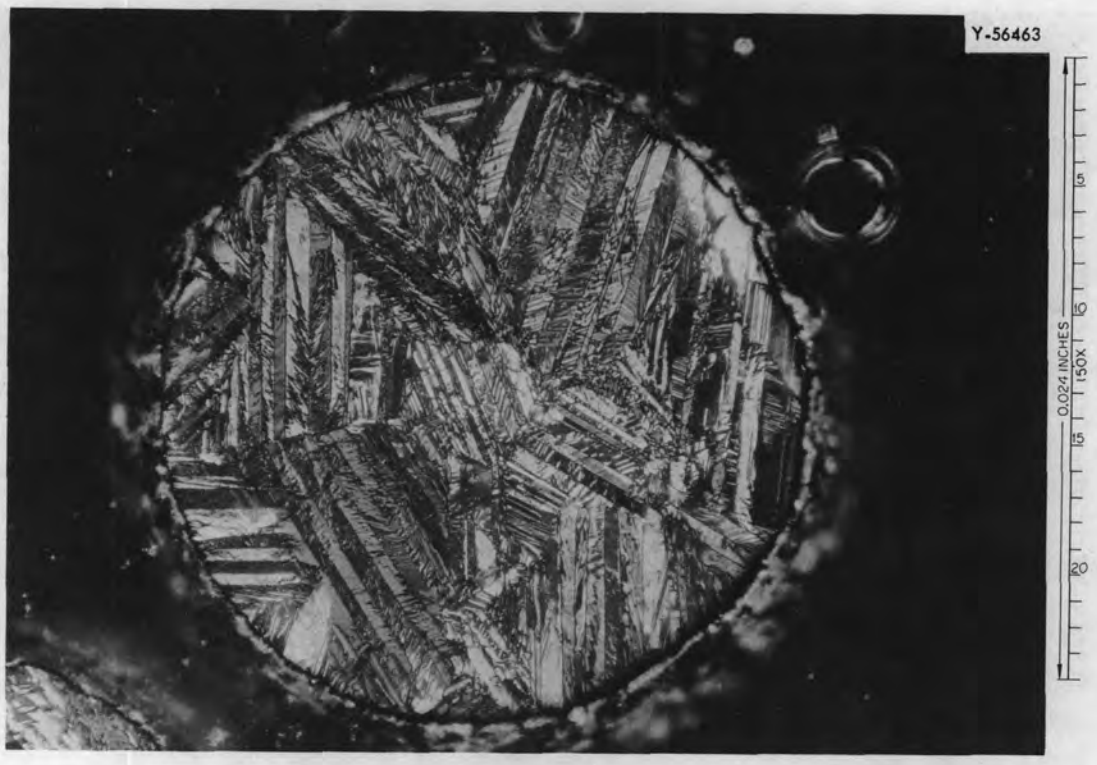

Fig. 3.55. Microstructure of ThC_2 Microsphere Derived from a Sol-Gel ThO_2 Microsphere by Heating at 2200°C for 2 hr at a Pressure of 10^{-2} torr in a Stationary Crucible with Graphite-to-ThO_2 Weight Ratio of 10:1. As polished. Polarized light.

The second experiment was performed with a tenfold reduction in graphite-to-ThO_2 weight ratio in flowing argon for 2 hr at 2200°C. The less-than-ideal distribution of this larger concentration of particles in the graphite flour led to severe agglomeration, due to sintering, and reaction-bonding of some particles to the crucible wall; conversion again was not complete in all particles. In the third test a single layer of particles was heated under similar conditions but in the absence of graphite flour. Conversion was complete in all cases but the particles were, of course, severely reaction-bonded to the crucible.

Subsequent experiments were aimed at optimizing the process with respect to time and temperature and simplicity of operation. A simple scaleup of the first experiment was considered to be undesirable because of the large proportion of graphite flour and the elaborate blending and loading techniques required to prevent particle agglomeration due to sintering and reaction-bonding of particles to the crucible. In addition, the use of large remote vacuum systems was to be avoided. To this end,

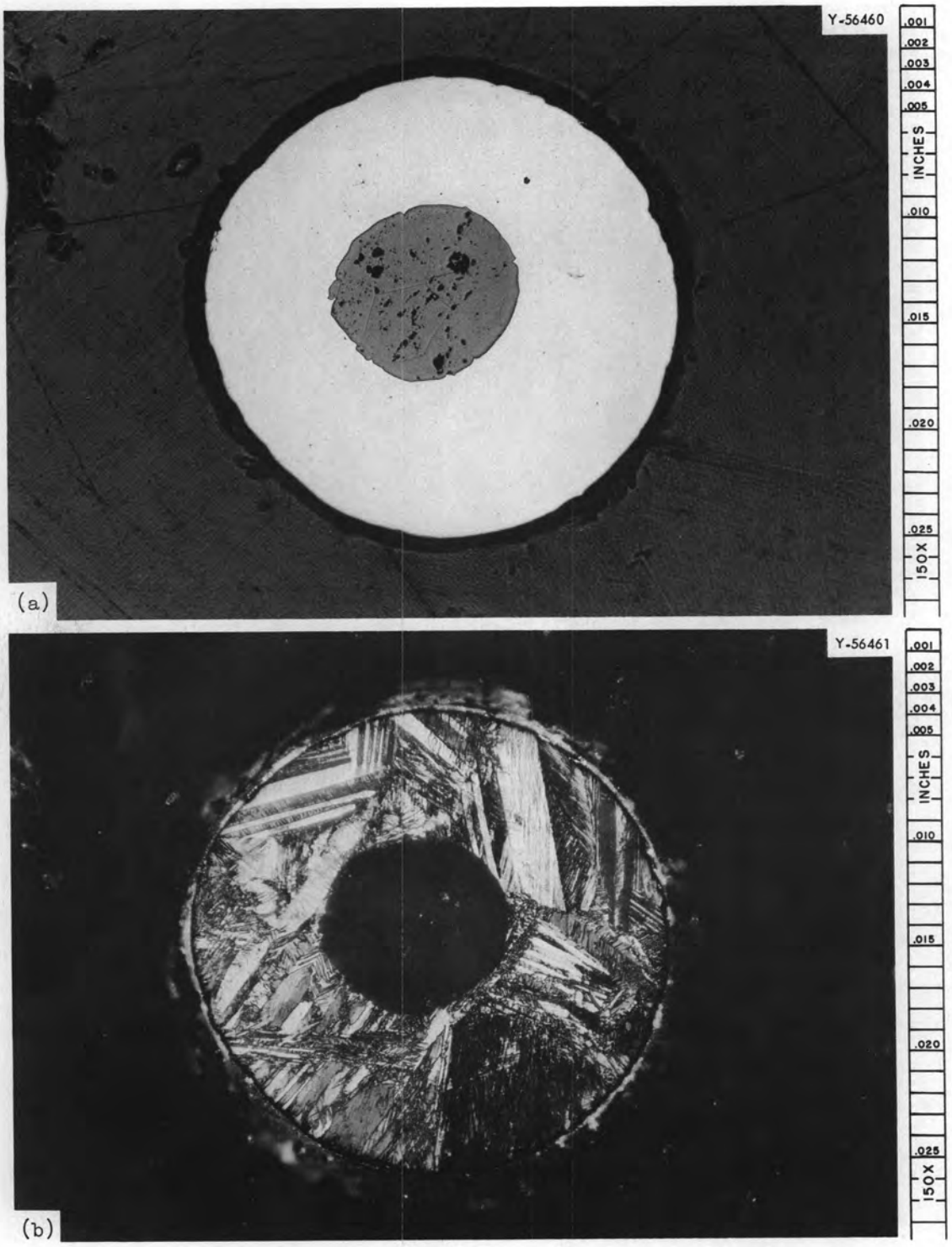

Fig. 3.56. Microstructure of Partially Converted ThC_2 Microsphere Derived from a Sol-Gel ThO_2 Microsphere by Heating at 2200°C for 2 hr at a Pressure of 10^{-2} torr in a Stationary Crucible with Graphite-to-ThO_2 Weight Ratio of 10:1. (a) Bright field. (b) Polarized light. As polished.

conversion experiments were performed in a cylindrical graphite crucible, 5 in. long and 1 3/4 in. in inside diameter, rotated horizontally about the cylindrical axis under flowing argon. Principal variables were temperature (2000 to 2300°C), time (1 to 6 hr), carbon source (graphite flour and lampblack), and rotation speed (14 and 44 rpm). Fully dense ThO_2 particles, 300 to 400 μ in diameter, and a fixed carbon-to-thoria weight ratio of 1:1 were employed.

It was ultimately determined that complete conversion in the absence of agglomeration or reaction-bonding to the crucible could be achieved reproducibly with lampblack in 5 hr at 2150°C at a rotation speed of 44 rpm. Shorter exposure times at 2150°C and comparable times at lower temperatures resulted in incomplete conversion at this rotation speed (see, for example Fig. 3.57); higher temperatures resulted in

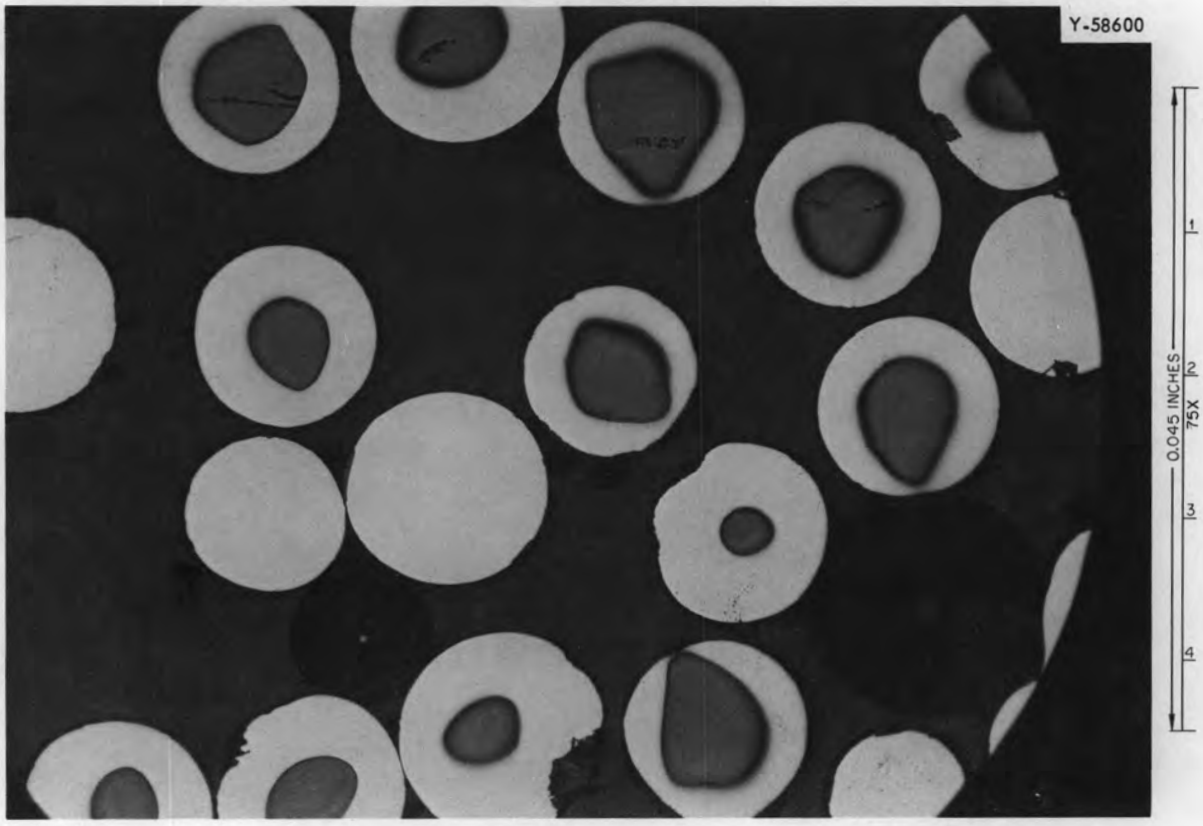

Fig. 3.57. Product of Process for Converting 300 to 400-μ Sol-Gel ThO_2 Microspheres to ThC_2 Showing Variations in Degree of Conversion after Heating with an Equal Weight of Lampblack at 2100°C for 5 hr in 1 atm Ar During Rotation at 44 rpm. (White phase is ThC_2 and dark phase is unconverted ThO_2.) As polished. Bright field.

more-or-less severe agglomeration after time periods sufficient to effect complete conversion (see Fig. 3.58). The higher rotation speed was selected early in the study when severe reaction-bonding to the crucible was observed at the lower speed after only 2 hr at 2000°C. Lampblack (Thermax) was selected as the carbon source because of its demonstrated higher reactivity relative to the graphite flour used (NCC No. 38).

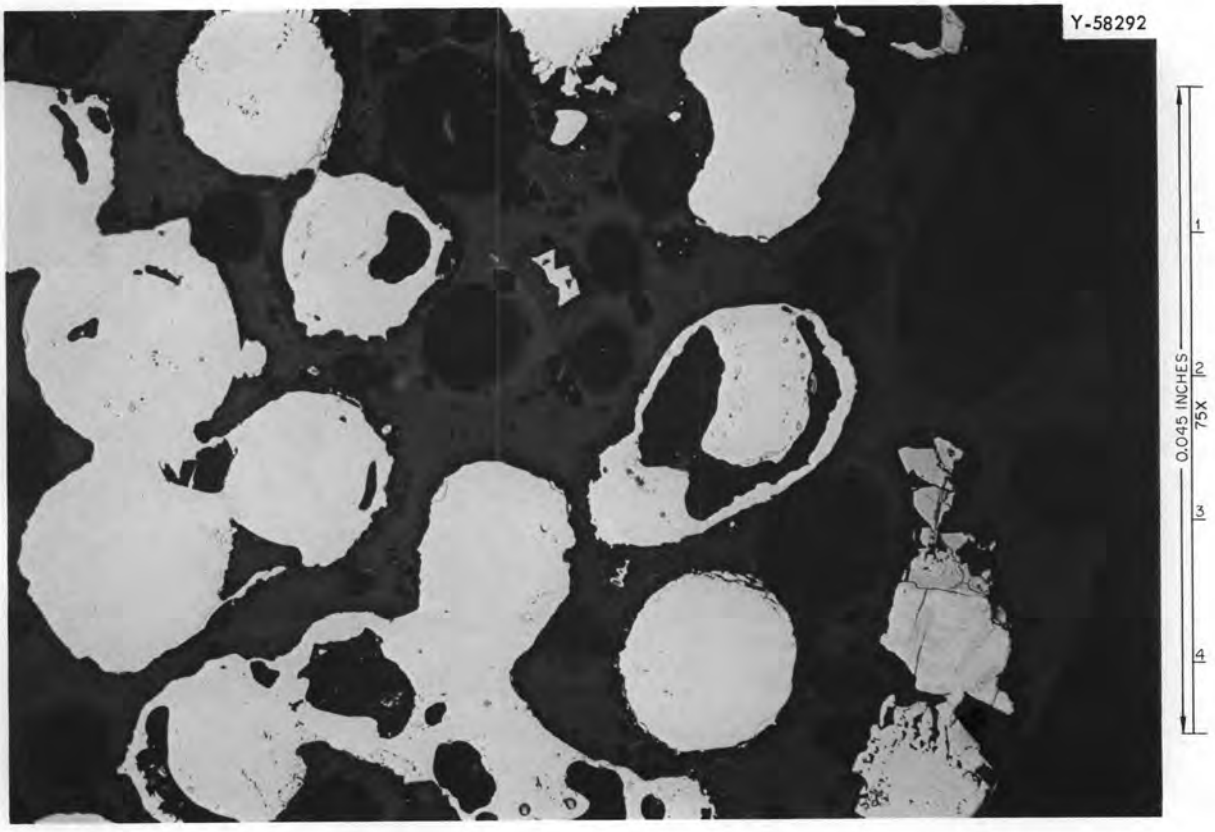

Fig. 3.58. Product of Heating Sol-Gel ThO_2 Microspheres, 300 to 400 μ in Diameter with an Equal Weight of Lampblack at 2300°C for 1 hr, in 1 atm Ar During Rotation at 44 rpm. (The white material is ThC_2 and the dark areas are holes.) Bright field. As polished.

Metallographic examination showed that the converted particles retained their sphericity and high density and x-ray diffraction analysis revealed the presence of only ThC_2. Photomicrographs of both the unconverted sol-gel oxide microspheres and the converted carbide particles are shown in Figs. 3.59 and 3.60. From 1 to 2% doublets of the type shown in Fig. 3.60 were observed. It should be noted that, while none appears in the field of Fig. 3.59, comparable proportions of doublets have been observed in sol-gel oxide microspheres. Based on a 3.8% change in theoretical density in converting ThO_2 (10.00 g/cm^3) to ThC_2 (9.62 g/cm^3), it was calculated that the volume increase was 0.76% and the diametral increase was 0.26%.

The results of preliminary experiments using conventionally prepared UO_2 particles, 150 to 250 μ in diameter, indicated that UO_2 particles may be converted to the carbide in the same manner as the ThO_2 particles. It was demonstrated, however, that temperatures lower than 2150°C will be required to prevent reaction-bonding to the crucible and particle agglomeration under the conditions used in the ThO_2 experiments described above.

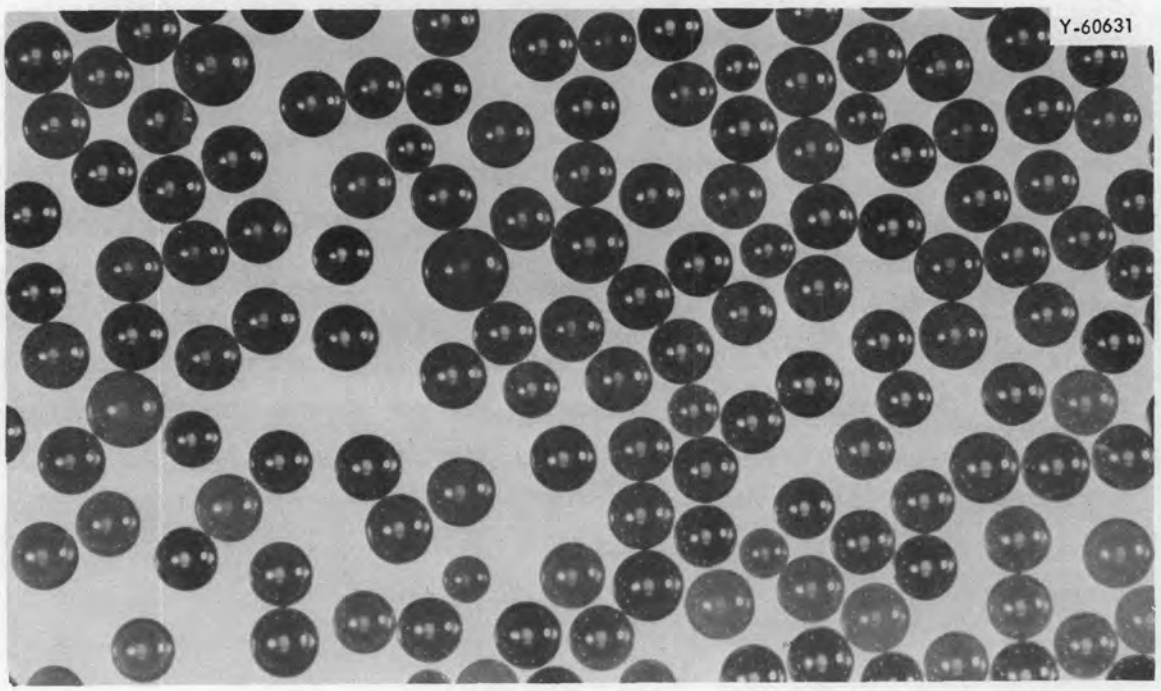

Fig. 3.59. Sol-Gel ThO_2 Microspheres 300 to 400 μ in Diameter, Before Heat Treatment for Conversion to the Dicarbide. 33X.

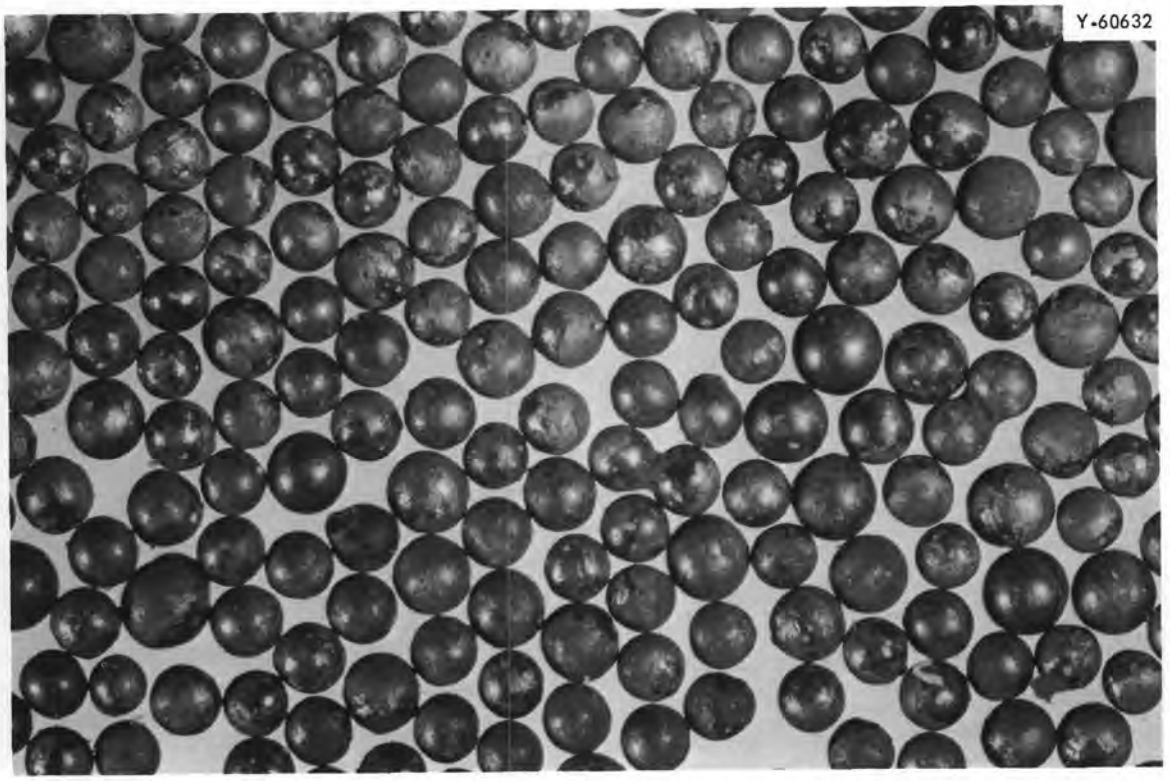

Fig. 3.60. Microspheres of ThC_2 Derived from 300- to 400-μ Sol-Gel ThO_2 Microspheres by Heating with an Equal Weight of Lampblack for 5 hr at 2150°C in atm Ar During Rotation at 44 rpm. (The dull surface appearance of the particles is caused by residual lampblack.) 33×.

Pilot-Scale Microsphere Fabrication Line

A pilot-scale microsphere fabrication line is now being installed in the Coated Particle Development Laboratory. During the past year, we have prepared the laboratory and designed the equipment that will be used.

The purpose of the laboratory is to develop coated particle processes and equipment suitable for scaled-up use in the Thorium Uranium Recycle Facility. Development work will include microsphere preparation, converting oxide particles to carbides, and coating of particles with pyrolytic carbon, all with natural thorium and uranium of various enrichments.

The laboratory is located on the second floor of Building 4508 of the Metals and Ceramics Division; it has been equipped with hood-type enclosures and an inert-atmosphere glove box for control of alpha contamination and air-reactive materials.

Work will consist of starting with prepared thorium-uranium sols, converting these sols into microspheres by the sol-gel microsphere process, and calcining them for densification, followed by coating with pyrolytic carbon in a fluidized-bed furnace by the cracking of gaseous hydrocarbons.

The general laboratory arrangement is shown in Fig. 3.61. The equipment for preparation of microspheres occupies the western half of Room 241. This equipment includes a sphere formation equipment enclosure which contains a microsphere-forming column, distillation system and associated equipment, a dryer and furnace enclosure which contains a dryer and calcining furnace, and alcohol storage tanks and associated instruments.

The equipment for pyrolytic-carbon coating of particles and the associated operations occupies the eastern half of Room 241 and includes a vacuum glove box which provides an inert-gas atmosphere for storage, weighing, blending, inspecting, and separating carbide microspheres, a particle-coating furnace enclosure which contains a resistance-heated furnace and fluidizing device, and an 8-ft fume hood for storage of particles before and after coating.

Services to the laboratory include two exhaust systems filtered by 99.95% efficient filters, one of which has a water scrubber prior to filtering. Piping services include argon, compressed air, methane, cold-process water, hot-process water, fire-protection water, natural gas, helium, and 125 psig steam. Adequate electrical services have been provided for envisioned future expansion.

Microsphere Preparation. The microsphere preparation portion of this process is shown in Fig. 3.62. Microspheres are formed by drying hydrosol droplets in 2-ethyl-1-hexanol. The hydrosol is introduced in the form of small droplets at the top of a column (3-in. microsphere-forming column) which has an upflow of an immiscible organic,

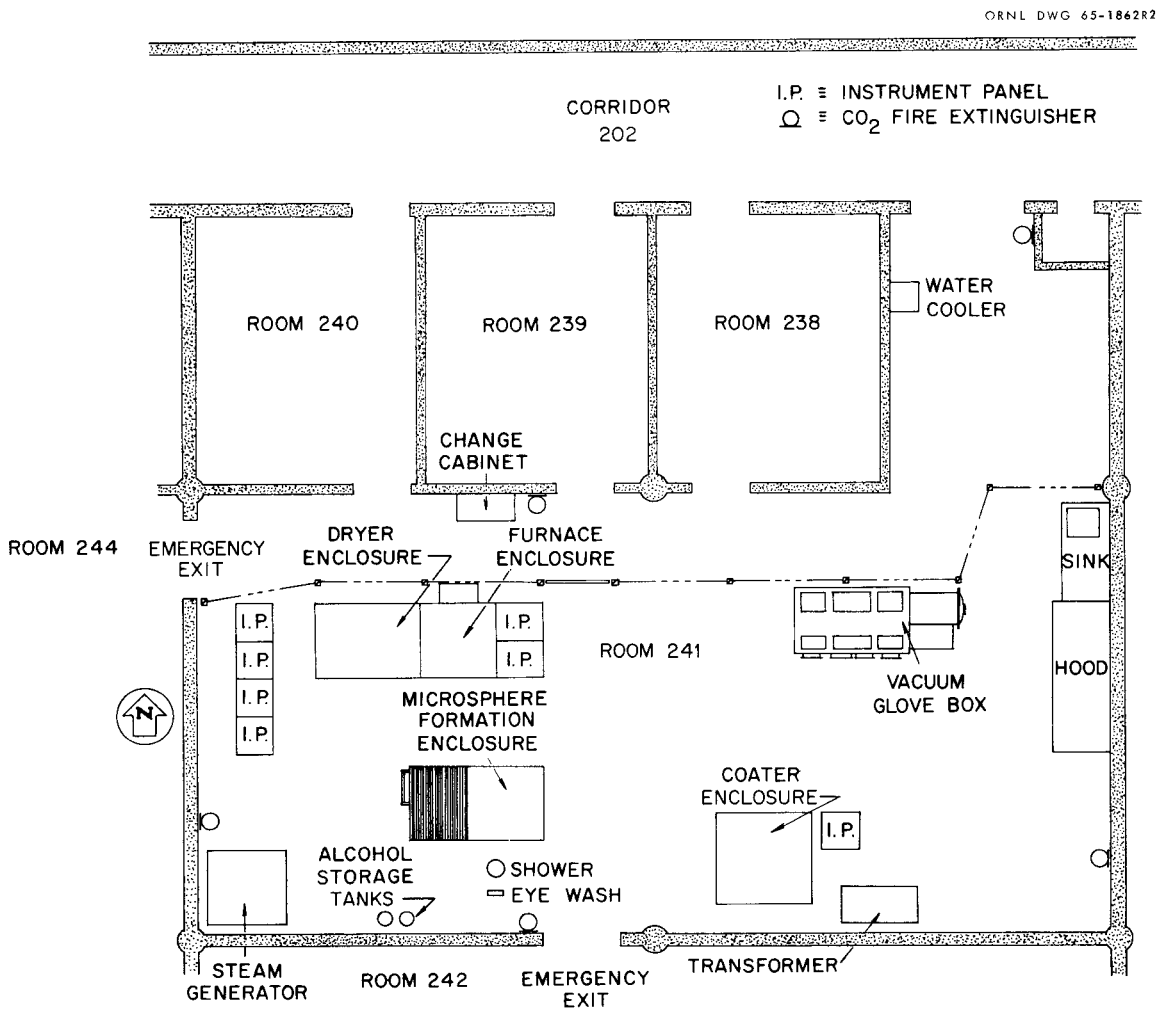

Fig. 3.61. Coated Particle Development Laboratory Equipment Layout.

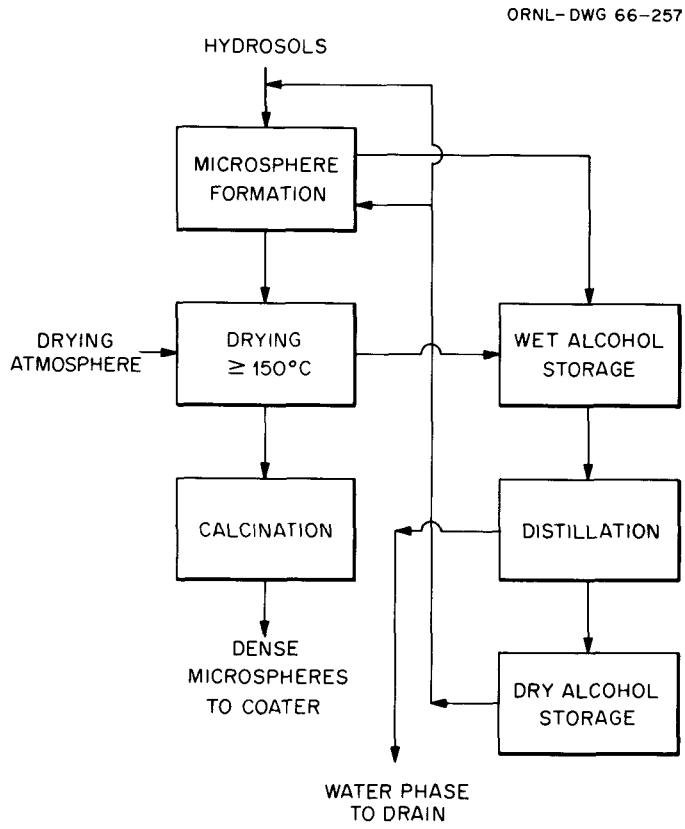

Fig. 3.62. Microsphere-Forming Flow Diagram.

2-ethyl-1-hexanol. The organic serves as a fluidizing medium and at the same time removes water from the droplets. As water is removed, the droplets become smaller and, consequently, require a higher fluidizing velocity which is accomplished with a tapered column.

The hydrosol droplets are formed by a two-fluid nozzle at the top of the column. This is accomplished by jetting the hydrosol into the center of a faster flowing stream of 2-ethyl-1-hexanol. In order to keep the hydrosol droplets from sticking to each other and wetting the column wall while water is being extracted, a surfactant is dissolved in the organic phase. The surfactants used include Ethomeen S-15 (a tertiary amine), Span-80 (Sorbitan mono-oleate) and Paraplex G-62 [a Rohm and Haas plasticizer used in poly(vinyl chloride) tubing]. These are used in quantities of less than 1/2 vol % alcohol.

As water is extracted from the hydrosol, the 2-ethyl-1-hexanol, which saturates at 2.6 wt % water, becomes saturated and its drying capacity decreases. Distillation of the 2-ethyl-1-hexanol removes the water. Therefore, a distillation system is operated during microsphere-forming column operation to keep the water content of the 2-ethyl-1-hexanol at a low value. The distillation system consists of a preheat section, a vaporization section, and a condenser. The condensate which contains from 50 to 75 vol % water is passed through a phase separator where the water-heavy phase (saturated with 0.1% 2-ethyl-1-hexanol) is sent to the drain and the 2-ethyl-1-hexanol phase is returned to the wet alcohol storage tank.

After column drying, the microspheres are strong enough to permit handling. The microspheres will be transferred by jetting them from the collection pot located at the bottom of the microsphere-forming column into the dryer. The dryer is a steam-heated vessel with a porous plate that retains the microspheres and allows the 2-ethyl-1-hexanol to drain from them. Following the draining step, argon is passed up through the porous plate to further dry the microspheres. The dried microspheres are then fired at approximately 1150°C for densification.

A box furnace is used to sinter the ThO_2 or ThO_2-UO_2 microspheres. This furnace has provisions for either air, argon, or Ar–4% H_2 (a non-explosive mixture) atmosphere control.

The oxide microsphere conversions to carbide and coating process are shown in Fig. 3.63. Microspheres are inspected for imperfections and for conformance to dimensional specifications. Next they are weighed into batches and one of two process options is selected. (The conversion of oxide to carbide will be done in another laboratory.) One route is directly from the weighing step to the coater. This means is used when one desires to coat oxide microspheres or carbide microspheres that have been prepared by the sol-gel process. The second route involves converting oxide microspheres to carbide microspheres by heating the material in a rotary conversion furnace with carbon flour. After conversion, the carbide microspheres are separated from the excess carbon

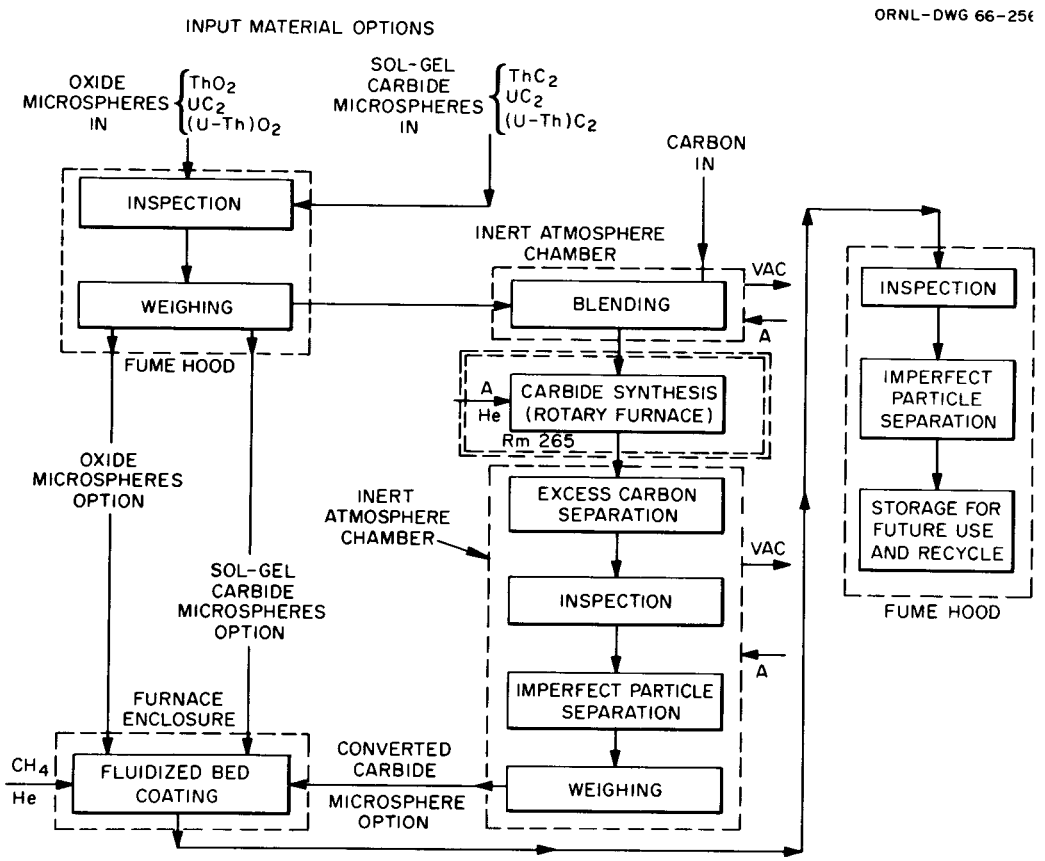

Fig. 3.63. Microsphere Coating Process Flow Diagram.

flour and inspected for size and imperfections. Material is separated and weighed preparatory to loading into the coater. The microspheres are thus coated with pyrolytic carbon. Once the coated particles are removed from the coating furnace, they are again inspected for imperfections and conformance to coating thickness specifications. At this point in the process, the coated particles are stored for future use or recycling.

The operation of this process will enable us to evaluate coating parameters, fluidized-bed nozzle configurations, process control techniques, and methods of inspection.

Objectives include finding means for increasing the throughput of particle coating devices, learning to make coated microspheres on a reproducible and controllable basis, and discovering equipment and operational problems which are important from the standpoint of future remote operations.

Design and installation of general laboratory services have been completed. Equipment enclosures currently are being fabricated and are to be delivered and installed in early 1965. The vacuum chamber and microsphere coating furnace have been delivered and are awaiting installation.

4. BASIC STUDIES

Preparation of Special Materials for Advanced Fuels

The primary objectives of this work are to obtain uniform gel spheres of thoria-carbon and thoria-urania-carbon which will calcine to dense, uniform microspheres of dicarbides. The objective of a dense dicarbide sphere has been reached only in a qualified sense. Dicarbide microspheres having a density of 80% of theoretical have been prepared, but higher densities appear difficult to attain by the present approach. This problem is one for further study. Encapsulation studies on sols were completed under a contract at Southwest Research Institute.

Control of Sol-Gel Particle Porosity

A small percentage of voidage in sol-gel particles may be desirable as traps for fission product and other gases. In addition, it may also be useful as "sinks" for relief of particle strains which may be generated by thermal and irradiation-induced stresses. The voidage should be mainly of the internal type and not surface-connected through open pores. It may be desirable that some open porosity be available to enhance acid dissolution rates of the high-fired material for reprocessing purposes.

Studies of particle porosity control have been of a scouting nature and much work remains to be done. Three methods of generating voidage in the particles have been scouted: (1) carbon is added to thoria sol, which upon drying and firing generates carbon dioxide which produces porosity, (2) thoria gel is fired at temperatures below that required for complete densification, and (3) high-fired thoria particles of appreciable and known porosity are suspended in sols prior to drying and calcination.

The first method appeared to be the most promising in the scouting tests. The third method failed because of sedimentation of the high-fired ThO_2 component from the sol. Although agitation was employed

during the early stages of evaporation of the sol, sedimentation could not be prevented.

In the method where carbon was added to a uranium-thorium oxide sol, the particles that resulted after drying and firing showed porosities that were consistent with the amount of carbon added (Table 4.1).

Table 4.1. Properties of Controlled-Porosity Uranium-Thorium Oxide

Carbon-to-Thorium Atom Ratio	Uranium Content (wt %)	Density, g/cm³			Open Porosity[c]	
		Mercury Displacement		Helium Displacement		
		Bulk[a]	Particle[b]		(vol %)	Average
0.0835	2.74	9.16	9.53	9.92	3.95	
0.0835	2.69	9.56	10.02		4.60	
0.0835	2.88	9.22	9.52	9.57	3.12	3.89
0.0417	2.75	9.75	9.86		1.15	
0.0417	2.71	9.59	9.76	9.77	1.71	1.43
0.0208	2.81	9.67	9.83	9.85	1.61	
0.0208	2.68	9.59	9.64	9.71	0.56	1.09

[a]By mercury at 1 atm; fills only voids and spaces between particles.

[b]By mercury at 545 atm; pores of diameter greater than 0.022 μ are filled.

[c]Calculated from difference between bulk and particle densities.

Although the products were colored from gray to black instead of the normal white, the carbon contents were less than 100 ppm. The open porosity indicates the extent to which acid is able to contact the oxide surface during dissolution, because the rate of dissolution is expected to be proportional to the porosity. The preparation in which the carbon-to-thorium ratio is 0.0417 would probably be the preferred one of the group tested, since it would be expected to pack to a density of 86% of theoretical and yet dissolve at a rate of 5 to 15 times that of the normally produced oxide.

When gels of $(Th,U)O_2$ were fired at temperaturs below the normal temperature of 1150°C which is required for maximum densification, porosity was introduced, although not in a uniform manner with respect to temperature (Table 4.2). The high surface area and moderately low porosity of 0.56 vol % for the 900°C preparation suggest that this material contains many pores whose diameters are less than 0.022 μ. A water adsorption test was applied to particles of −100 mesh. This test consists of determining the amount of water required to immobilize or "set" a sample of powder as determined by titration. Samples fired at 1000°C are probably the choice within this group since high liquid porosity and mercury porosity are obtained while still maintaining a reasonably high density.

Table 4.2. Effect of Firing Temperature on Physical Properties of Thorium Oxide

Firing Temperature (°C)	Particle Density, g/cm³				Porosity by Mercury Method[a]		Surface Area by Krypton
	H_2O	Toluene	Helium	Mercury	(vol %)	(cm³/g)	(m²/g)
1150	9.86	9.90	9.97	9.83	0.1	0.001	0.019
1000	9.78	9.78		10.1	3.8	0.038	0.007
900	9.38	9.66	9.48	8.5	0.56	0.006	7.1[b]

[a]Includes only pores having a diameter > 0.022 μ.

[b]By neon instead of krypton.

Preparation of Zirconia Sols

Various preparative methods are being investigated for the preparation of zirconia sols. Both reduction of zirconyl nitrate with formic acid and precipitation of hydrous zirconium oxide and redispersion in zirconyl nitrate solutions produced stable sols. In both cases, however, NO_3^--to-ZrO_2 mole ratios of unity or greater were required to form fluid, transparent sols. In general, such high ratios lead to undesirable amounts of gas release on firing and to incompatibility problems. Steam

hydrolysis of the nitrate and redispersion of the denitrated oxide was not very successful as a preparative method. Dehydration of the oxide at temperatures above 100°C is irreversible and temperatures considerably greater than 100°C are required for the denitration step. Precipitation of the hydrous oxide with ammonium hydroxide and subsequent repeptization with water or dilute nitric acid has been unsatisfactory; however, considerably more work needs to be performed before discarding this approach.

Stable zirconia sols were prepared by adding formic acid solution to aqueous solutions of zirconyl nitrate to reduce the nitrate ion. Stable sols are produced at NO_3^--to-ZrO_2 mole ratios of about unity. The sols were formed to gel microspheres in 2-ethyl-1-hexanol and then fired to oxide spheres having a density of 4.9 g/cm^3. In some of the preparations, the microspheres were cracked after firing. Zirconia sols from formate reduction are flocculated when added to thoria sols and appear to be negatively charged.

In the precipitation methods for preparing zirconia sols, ammonia is added to a 1 M zirconyl nitrate solution until a pH value of 2.1 is attained where hydrous oxide precipitate begins to appear, the mixture is digested at 100°C for 20 hr, and the precipitation is completed by dropwise addition of ammonia. The precipitated hydrous oxide is separated by filtration and washed with six separate volumes of water. The filter cake is then treated with additional zirconyl nitrate solution to peptize it to a sol. Mole ratios of NO_3^- to ZrO_2 of approximately 0.1 produced highly viscous opaque sols. Further addition of zirconyl nitrate solution produced a fluid, transparent sol at a NO_3^--to-ZrO_2 mole ratio of approximately 1. The specific conductances of the sols increased linearly with nitrate concentration. In sols where the NO_3^--to-ZrO_2 mole ratios were less than one, formate ion could be substituted for NO_3^- on an equivalent basis, with no apparent change in the stability of the sol.

It has not been possible thus far to apply the steam denitration technique to produce a dispersible zirconium oxide in the manner that has been demonstrated so successfully with thoria. Denitration at 350°C produced a zirconia product which had a crystallite size of about 130A and a surface area of 17.5 m^2/g (about 25% of the area calculated from the crystallite size). The zirconia could not be dispersed in water or

in dilute nitric acid. Treatment with HNO_3-HF solutions did not increase the specific surface area significantly. The difference between the geometric and measured surface area suggests aggregation of the crystallites.

Preparation of Thorium Nitride

The feasibility of preparing thorium nitride by an adaptation of the sol-gel process has been scouted and the possibilities look promising. The principle of the preparative method is converting carbon-containing thoria gels to thorium nitride by firing the gels to temperatures near 2000°C in nitrogen gas. It has been demonstrated by several workers that carbides are converted to nitrides when carbides are treated with nitrogen at elevated temperatures. The advantage of starting with a gel is that a single calcination step may yield the nitride from a readily obtainable oxide.

Thorium nitride microspheres were prepared in 10-g lots by firing thoria-carbon spheres in nitrogen at 1800 to 1850°C for 1 to 1.5 hr. When the temperature exceeded this range, the spheres sintered to each other. X-ray diffraction analyses showed the presence of ThN, Th_2N_3, and some thorium carbonitride. Carbon-to-thorium atomic ratios of 2 and 3.5 have been investigated. Much work remains to be done to define conditions whereby a pure nitride product is attained.

Sol Encapsulation Studies: Southwest Research Institute

This project was completed and reported.[1] The study had two objectives: (1) to use the encapsulation of sols in a shell of organic polymer as an initial step in the preparation of microspheres and (2) to prepare stable, low-viscosity dispersions of carbon blacks in water and in various sols.

---

[1]E. C. Martin, Encapsulation of Sols to Produce Rounded Particles, Final Summary Report, ORNL subcontract No. 2326, Southwest Research Institute, San Antonio, Texas (Oct. 21, 1964).

This investigation, conducted at the Southwest Research Institute, was mainly concerned with encapsulation of sols. It was thought that smooth gel microspheres could be obtained by encapsulating the sol in a shell of organic material and subsequently either allowing water to diffuse from the capsules or a gelling agent to diffuse into the capsules. These gels when dried and calcined would yield dense microspheres. The capsule would be destroyed by the high-temperature calcination to yield a uniform, smooth sphere. The possibility also existed that carbon could be incorporated in the capsule shell and upon calcination in an inert atmosphere, carbon-coated spheres would be produced.

Several polymer systems were investigated for the encapsulation of thoria sols or thoria-urania sols. Polymers with a high permeability for water were selected to evaluate the feasibility of gelling the sol by diffusion of water from the encapsulated sol through the polymer shell. In all instances, the polymer shells collapsed into misshapen "pods" when water diffused from the encapsulated sols. This behavior was thought to result from water diffusing from the capsules too rapidly, which created voids within the polymer shell. The polymers used for capsule coatings were not elastomers and thus did not contract as the sol volume was decreased by diffusion of water through the polymer shell. Suspending the capsules in liquids that swelled the polymer shell and also extracted water from the sol showed some promise. However, no completely satisfactory results were obtained. The capsules usually deformed in shape, and in some cases the sols crystallized. Polymers used in the encapsulation studies were: ethylene-vinyl acetate copolymers, methacrylates, cellulose acetate butyrates, ethyl cellulose, phenoxy resins, and poly(vinylpyrrolidone).

Ultrasonic dispersion and nonionic surfactants showed some promise as a means of preparing concentrated carbon sols (approx 8 M). Using Renex 30, a nonionic ether of poly(oxyethylene) and a branched alcohol manufactured by Atlas, an 8-M excelsior carbon dispersion was obtained. The concentration of the surfactant was 1.8 vol % based on the dispersion, and the Brookfield viscosity was 20 cps measured using a No. 1 spindle at rpm. Such dispersions were attainable both in water and in 2 M ThO_2–4% UO_2 sols. A 10 cps viscosity 8-M carbon sol in isopropyl

alcohol was obtained with poly(vinylpyrrolidone) as dispersing agent. Attempts to disperse carbon blacks in benzene, toluene, and cyclohexane were unsuccessful.

The preparative procedure for the carbon sols was to add the appropriate amount of carbon to 80 g of water and then begin ultrasonic agitation in a Bronson Sonifier. While dispersing the carbon with the Sonifier, the surfactant was added dropwise until a low-viscosity dispersion could be maintained. The dispersion was then diluted to 100 ml with water, placed in an ice bath and mixed with Sonifier for 1 hr. In several instances, it was necessary to add 2-ethyl-1-hexanol (1 drop per 100 ml of dispersion) in order to prevent foaming.

Fission-Gas Release from Thoria Fuels

The kinetics and mechanisms of fission-gas release from ceramic fuels have been investigated for many years. Several facets of this problem have not been resolved. One of these is the rapid release of fission gas from a fuel material as the temperature is increased. Since increasing the temperature of a material causes increased dislocation mobility, it is reasonable to expect that dislocations might be the means by which fission gases are swept from the lattice during a temperature increase. Experiments designed to test this hypothesis are being conducted. These are described in the last report and elsewhere.[2] We have established a qualitative similarity between the kinetics of creep in ThO_2 and ^{133}Xe release from ThO_2. There is a strong correspondence between the creep rate of ThO_2 bushings and the simultaneous ^{133}Xe release rate. We have also applied stress to thoria bushings by quenching in helium from 1400°C. After this treatment, which causes the quenching in of dislocations and thermally induced stresses, the burst release of fission gas observed upon heating to a given temperature is greatly increased. This fact also strongly indicates that dislocations play a large part in the "heating burst" release of fission gas from ceramic fuels.

---

[2]R. G. Wymer and D. A. Douglas, Jr., Status and Progress Report for Thorium Fuel Cycle Development for Period Ending December 31, 1963, ORNL-3611, pp. 152 and 153; and C. S. Morgan, R. B. Fitts, and J. L. Scott, J. Am. Ceram. Soc. 48(3), 166 (1965).

We are constructing a new compressive creep apparatus for use with this program. The new furnace consists of essentially a set of carbon dies in a vacuum system. The dies are induction-heated around the sample. The load is transmitted to the dies through a bellows. One of the principal difficulties with this system, as with any high-temperature creep furnace, is the measurement of sample temperature. The sample is located inside the 1600°C carbon dies, in a vacuum, inside the induction heating coil, and in the induction field. We feel that a thermocouple will be the best temperature-sensing device to use under these conditions.

Due to the small amount of available information on the use of thermocouples in induction fields at temperatures to 1600°C in vacuum and in the presence of carbon, we decided to test their response to these conditions. We are using a Brown recorder, Pt vs Pt–10% Rh thermocouples, and gold and nickel points for these thermocouples to test the effects of the induction field on temperature measurement. We have measured the gold and nickel melting points within ±2°C (the accuracy of reading the Brown chart). There seems to be no interference with the thermocouple readings by the 10-kc induction field. An 89-hr test of the Pt vs Pt–10% Rh thermocouple in a carbon block at 1380°C showed a relatively steady drift in the temperature indication from the thermocouple. After 89 hr, the thermocouple indicated 1265°C for the 1380°C carbon block. We plan to test W vs W–26% Rh thermocouples under these conditions. We also shall attempt to shield the Pt vs Pt–10% Rh thermocouple from the carbon.

We are using electron microscopy techniques as an aid in resolving the basic mechanisms of release of fission gas from ceramic fuels. We have chosen to perform the initial work on this phase of the investigation with urania samples rather than thoria. This is due to the ready availability of UO_2 single crystals, the greater amount of background information on fission-gas release from UO_2, and the similarity of fission-gas release behavior in the two materials. The following sample preparation technique has been developed for use by C. K. H. DuBose of

the Electron Microscopy Group of the Metals and Ceramics Division at ORNL. The 20-mil-thick UO_2 samples are first reduced to 1/8-in. squares with a wire saw. Silver is then vapor deposited on one side and the edges protected with lacquer. The central area of the sample, 1/16 in. across, is electropolished down to about 3 mils in thickness in a jet of electrolyte with a fairly high applied voltage (150 v). This area is then further thinned in another electrolyte at lower voltage. The last thinning is monitored by a photocell which stops the etching when the sample becomes transparent. Samples of single-crystal and sintered, compacted UO_2 are now being prepared for irradiation.

We have measured the release of fission gas by thoria, urania, uranium nitride, and V + 1 wt % U fuels during low-temperature (< 100°C) neutron activation. The results show that the fractional release of fission gas at low temperature and dose is a function only of the surface area of the sample. In other words, the low-temperature neutron activation test yields an accurate measurement of the surface area of a nuclear fuel sample. The relationship for fractional ^{133}Xe release (F) and the surface area (S) of a sample (cm^2/cm^3) is given by

$$\log F = -6.104 + 0.865 \log S.$$

The principal advantages of this technique are the small size of sample required (usually considerably smaller than for the standard BET test) and the fact that the measurement is made on the test sample itself rather than on a group of "similar" samples. The data are being analyzed in detail at present and a report will be prepared for publication.

Gas Evolution from Thoria-Urania Sol-Gel Material

Thoria–3% UO_2 sol-gel material prepared for use as a reactor fuel evolves small amounts of gases when heated. Development of excessive pressure of such gases in a sealed fuel element could result in rupture of the element; this possibility might be increased if reaction between evolved gas and metal were possible (e.g., zirconium alloy might form hydride with hydrogen). Studies have been initiated to better define the factors that affect both the nature and the amount of gas evolved from sol-gel material.

Sol-gel material prepared from ^{233}U is of primary interest for actual reactor fuel preparation. Uranium-233 is quite radioactive and requires remote handling. The first experiments have, therefore, been done with sol-gel preparations (designated H-II and SC) containing natural or depleted uranium, and representative of materials prepared in engineering-scale equipment. Experimental factors which have been controlled in the experiments to date include the nature of the sol-gel material under observation, the temperature of outgassing, the particle size of the material, and the atmosphere to which the material was exposed prior to the outgassing operation. Previous work had shown that the quantity of gas evolved during heating was dependent on the temperature; this factor was held constant at 1000°C in most experiments in order to permit exploration of the effect of other variables. The related factors of surface area and particle size were considered likely to be of primary importance in controlling gas evolution, and considerable attention was paid to the use of various sized fractions of ground and screened material. An attempt was made to prevent the inadvertent sorption of atmospheric CO_2 or H_2O on the freshly ground and sized material by performing grinding and sizing operations inside a plastic bag in an inert atmosphere. Brief exposure to air was permitted in most experiments during the weighing and loading of samples, and no controlled study has yet been made of the effect of this exposure.

The experimentally observed quantities of the study have been the total gas evolved, the composition of the evolved gas, the rates of gas evolution, and the ability of the material to sorb and desorb gases.

Effects of Particle Size on Gas Evolution

A strong effect of particle size on the total gas evolved at 1000°C from SC material was observed, as indicated by Fig. 4.1. The results are plotted on a scale of relative surface area, derived from the arithmetic average particle diameters with an assumed value of 1.0 for surface area of spherical particles of 1.0-mil diameter. The linearity of the relationship and the extrapolation to zero gas evolution at zero surface area suggests that the evolved gas (essentially all CO_2) was being

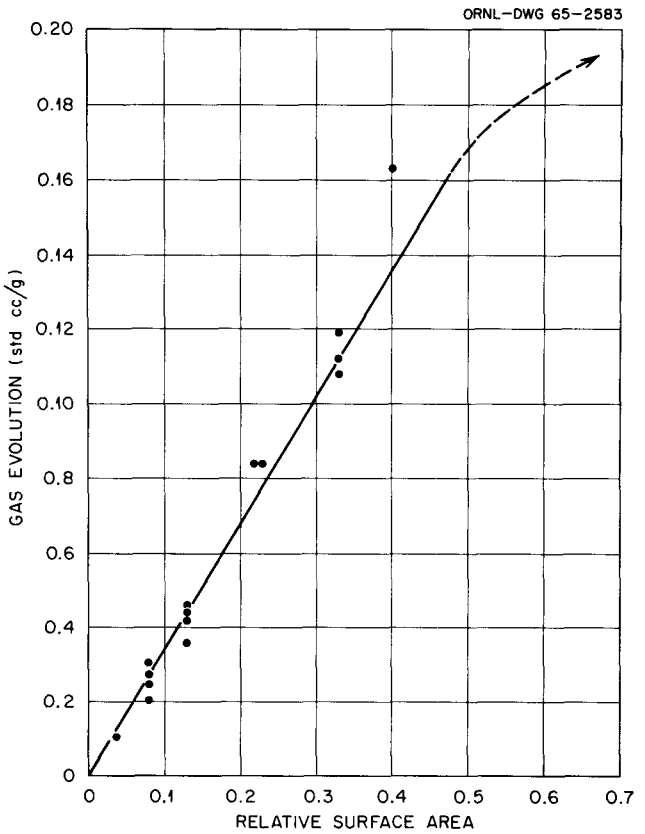

Fig. 4.1. Effect of Particle Size (Relative Surface Area) on Total Gas Evolution from SC Sol-Gel Material at 1000°C.

released only from the surface exposed by grinding and not from the interior of the particles. Such behavior is typical of chemisorbed material.

A strong effect of particle size was also found when the H-II material was tested at 1000°C. Eight times as much gas was released from −270 mesh material as from −20 +40 mesh material. The maximum volumes of gas obtained were as high as 1.0 std cm^3/g; this was six times as much as was released from the SC material. The composition of the gas was substantially different: CO and hydrogen were present as important constituents. Particle size was found to have an important effect on both the gas composition and the total volume of gas. Figure 4.2 shows the relationship between surface area (measured by the BET method) and the gas composition. Extrapolation of the relationship of Fig. 4.2 to the very low BET surface area of 0.1 m^2/g suggests

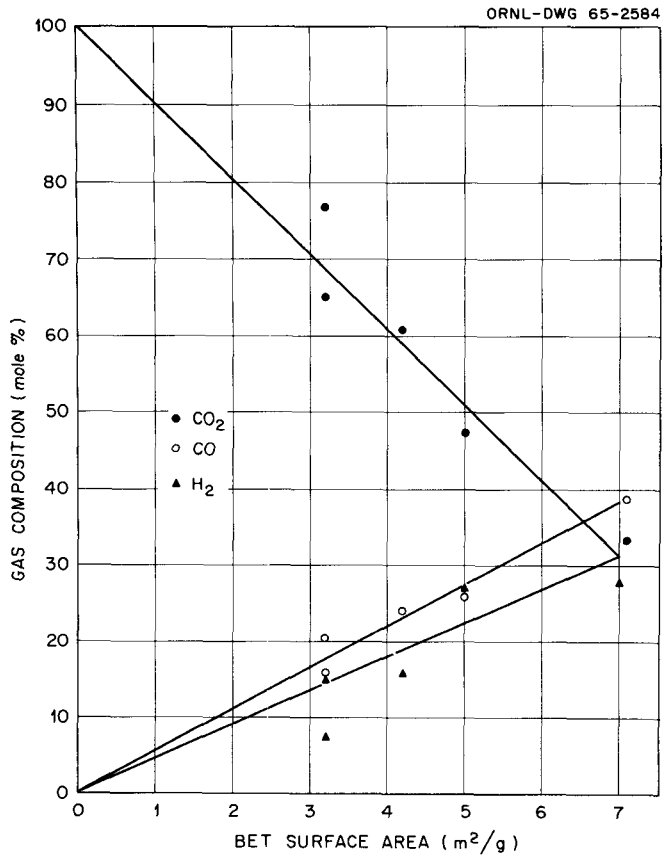

Fig. 4.2. Effect of BET Surface Area on Composition of Gas Evolved from H-II Sol-Gel Material at 1000°C.

that the gas evolved would be about 99% CO_2 – just what was observed in tests of the SC material that had such a low surface area.

Effect of Temperature on Gas Evolution

Measurements of the total gas evolved and the rate of the evolution were made on –270 mesh samples of the H-II material at temperatures of 1000 and 1200°C, and there was some evidence that at 1200°C an initially higher gas release was being followed by a slow removal or consumption process. It is possible that the surface of the sol-gel material at 1200°C was catalyzing the water-gas reaction,

$$H_2 + CO_2 \rightleftarrows CO + H_2O ,$$

for which the value of the equilibrium constant is around 2.7 at 1200°C. The analytical technique which was used in the experiments did not

provide values for water. As a consequence, the reaction of hydrogen and CO_2 to form CO and H_2O could have resulted in an apparent decrease in the total gas evolved.

Reversible Gas Sorption on Sol-Gel Material

In studies of particle size effects, the SC material had released a gas which was essentially pure CO_2. After these tests, some of the samples were exposed to air to determine whether CO_2 would be sorbed and, if so, to what extent. Reevacuation at 1000°C was used to remove any sorbed gas, and it was found that less than 10% of the original amount was evolved. This suggested that, for the SC material, the originally evolved CO_2 had been present in the original material as it was exposed by grinding and had not come from adventitious sorption from the air during a brief exposure during weighing. The small amount of gas involved made it inadvisable to perform further studies of reversible CO_2 sorption with this material.

A sample of −270 mesh H-II material was used for a series of studies of the reversible sorption and desorption of CO_2; the desorption was followed as a function of time at various temperatures, while the sorption was always achieved by exposing the sample to 1 atm of dry CO_2 and permitting it to cool to room temperature in this environment. The samples were then evacuated at room temperature before the test boat was inserted into the preestablished temperature region of the furnace. Figure 4.3 shows the results of successive tests at 250, 500, 750, and 1000°C. The desorption was quite rapid, and temperatures of 500°C or higher were apparently adequate to remove all the sorbed gas in these tests. The reversibility of the CO_2 sorption-desorption is illustrated by Fig. 4.4, showing how the pressure in the apparatus (originally evacuated at room temperature after exposing the sample to 1 atm CO_2) changed as the H-II sample was heated to 1000°C and then allowed to cool down. A similar reversibility was found for SC material, but the amounts of gas and pressures were negligible.

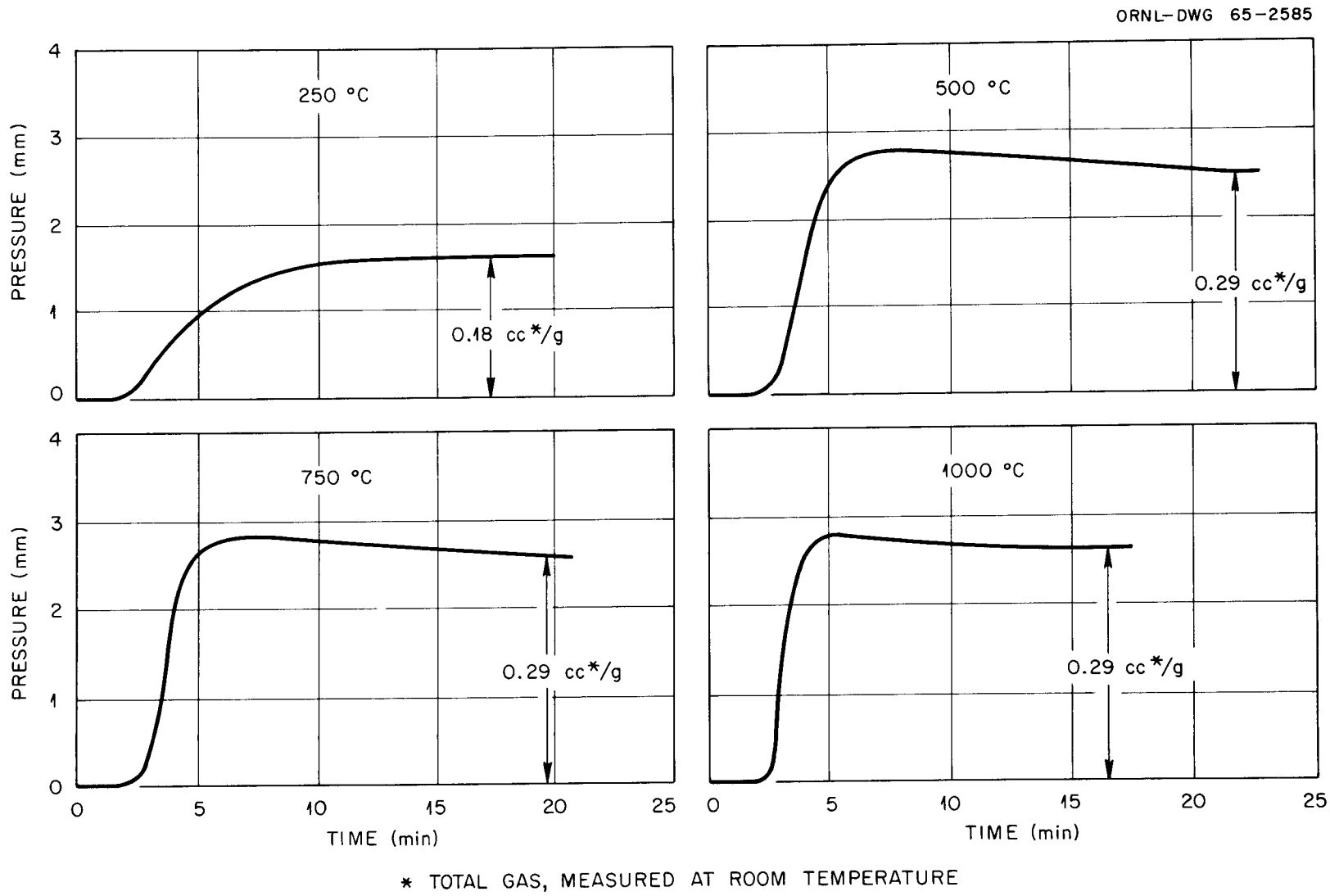

Fig. 4.3. Desorption of CO_2 from H-II Sol-Gel Material at Various Temperatures.

ORNL-DWG 65-2586

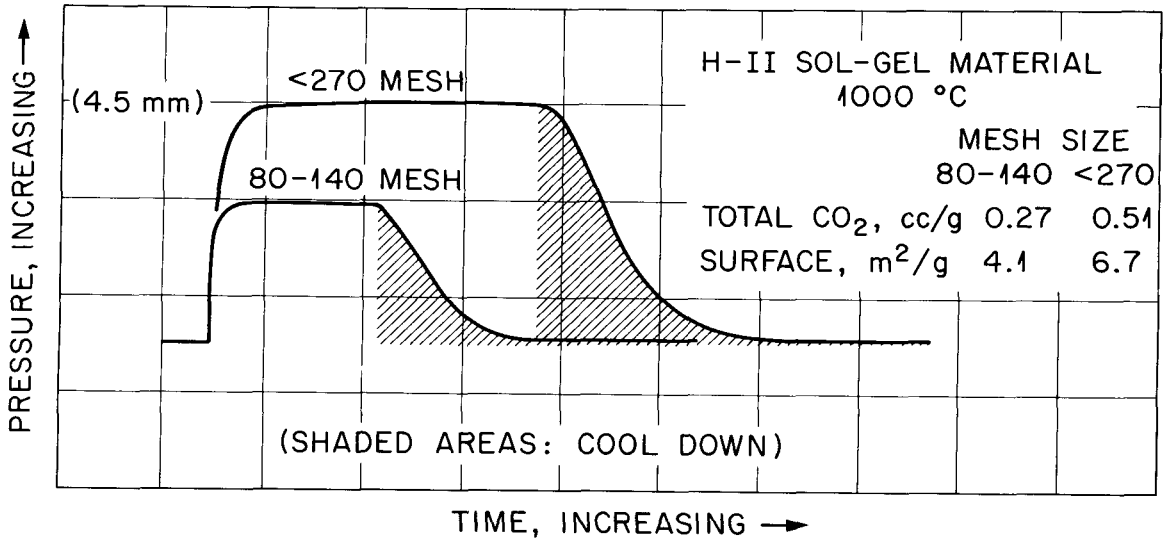

Fig. 4.4. Reversibility of CO_2 Desorption from H-II Sol-Gel Material at 1000°C.

Moisture Adsorption Characteristics of Sol-Gel Material

One of the problems associated with the use of ThO_2–3% UO_2 as a reactor fuel is related to its moisture adsorption characteristics. A more precise knowledge of this property would be useful in the specification of production standards. Moreover, the minimization of the moisture content of these gels would tend to reduce the "aqueous gas pressure" in the sealed fuel elements under actual reactor operating conditions. Finally, there is a suggestion that occluded water tends to react with some of the gases evolved from thoria prepared by the sol-gel process, with the subsequent reduction of the sol-gel surface area.

In view of the foregoing "aqueous gas pressure" problem it was considered advisable to initiate, along with our gas evolution studies, an auxiliary isopiestic study on the moisture characteristics of thorium sol-gel material, covering a diversity of experimental conditions such as are expected to occur in the preparation of this material. For this preliminary survey, three samples of H-II sol-gel material (mesh size $\leq$ 270) were equilibrated with water at varying vapor pressures as well as at different equilibrium temperatures, the latter ranging from 100°C to as high as 176°C. Table 4.3 summarizes the results of this

survey. Special features in the preparative history of the three samples are listed in the footnotes to the table.

Table 4.3. Percent of Water Retained by H-II Sol-Gel Thoria at Several Temperatures

Temperature (°C)	Equilibrium Vapor Pressure of Water (atm)	Percent of Water Retained at Equilibrium,[a] wt %		
		No. 39	No. 37	No. 38
100	1.0	8.16	4.22	4.08
145	4.0	8.02	5.43	5.33
176	9.0	9.39	5.32	5.32

[a]Sample No. 39, H-II, mesh size ≤ 270, heated to 1000°C.

Sample No. 37, H-II, mesh size ≤ 270, heated to 1200°C.

Sample No. 38, H-II, mesh size ≤ 270, heated to 1000°C but rapidly quenched by moving the boat to the cold zone of the furnace.

Discussion

The following statements summarize what has been learned so far about gas evolution and sorption from sol-gel thoria–3% urania by studies on two different samples of nonradioactive laboratory-prepared material.

1. There is a large difference in the gas-release behavior of obstensibly similar materials, suggesting that preparatory methods may ultimately be refined to provide material with more uniform properties.

2. The amount of gas evolved depends strongly on the exposed surface area of the material. It appears to be evolved from the material itself and not to be a consequence of sorption after grinding and sizing. The question has been raised, but not answered, whether use in a reactor will cause changes leading to the release of potentially available gas.

3. The composition of the gas evolved appears to depend significantly on the particle size (surface area exposed) of the material. It is possible that the surface of the material can catalyze the water-gas reaction at elevated temperatures.

4. Carbon dioxide is reversibly sorbed on the material but may be removed by treatment at temperatures as low as 500°C.

5. Isopiestic studies at temperatures of 100 to 176°C revealed that the amounts of water retained by the thorium sol-gel represented significant percentages of the total sample weights (as high as 9%). Raising the temperature did not decrease the ability of the gels to bind water (in contrast to the behavior of many solids). Gel that had been heated to 1200°C and then cooled slowly adsorbed less water in the isopiestic tests than gel that had been heated only to 1000°C, possibly because of a reduction in surface area as a consequence of sintering at 1200°C.

The gas evolution and sorption studies will be continued.

Separation of Protactinium from Irradiated Thorium Salts

Basis of Studies

A number of significant benefits may be derived from the prompt removal of ^{233}Pa from thorium irradiated in a nuclear reactor or blanket. If ^{233}Pa is permitted to reach appreciable concentrations, neutron capture with the production of nonfissionable ^{234}U can result in a reduction of the conversion factor and reactivity of the reactor system. Isotopic purity of the ^{233}U and its ultimate value are markedly reduced. Appreciable production of ^{232}U occurs by (n,2n) reactions on ^{233}Pa or ^{233}U, and high radiation levels from unstable high energy α-emitting daughters of ^{232}U lead to increased shielding requirements and to higher costs in the design of ^{233}U recovery facilities. Thus a process for prompt withdrawal of ^{233}Pa at reasonable levels from a reactor blanket could have important consequences in the economics of the thorium fuel cycle; a low steady-state protactinium level could be maintained in the reactor, and high purity ^{233}U could be produced.

In a series of experiments Malm and Fried[3,4] succeeded in demonstrating that a process based on the apparent volatility of protactinium chloride might be useful in the prompt removal of protactinium from irradiated thorium. It was claimed upon chlorination of irradiated thorium metal or oxide with $AlCl_3$ or with $AlCl_3$ and Cl_2, or upon direct reaction of irradiated $ThCl_4$ with $AlCl_3$, protactinium chloride might be distilled from the mixture at temperatures as low as 100°C. The latter process, which promised the highest yield of protactinium, was selected for further investigation.

Previously reported data[5] indicated the solubility of $ThCl_4$ in $AlCl_3$ to be low. Inference from the examination of the phase diagrams of analogs of thorium chloride with aluminum chloride suggested that the presence of a third component such as $ZrCl_4$ might enhance thorium solubility, and work on the relevant binary systems was initiated. Previous studies[5] had indicated little mutual solubility in the $ZrCl_4$-$ThCl_4$ system. Work on the $AlCl_3$-$ZrCl_4$ binary system is reported below.

$AlCl_3$-$ZrCl_4$ Phase Studies

The aluminum chloride-zirconium chloride system was studied throughout the range of composition using differential, thermal, and visual analysis. Figure 4.5 shows a preliminary solid-liquid binary phase diagram; concentrations shown assume monomeric $AlCl_3$. The open circles on the diagram represent information derived from differential thermal analysis experiments while the solid circles are data obtained by the direct viewing of melting in quartz capsules. Visual observations were necessary for the 10 to 25% $ZrCl_4$ region of the diagram due to the

---

[3]J. G. Malm and S. Fried, Chemistry Division Summary Report July–September, 1950, ANL-4545, Section C-1, p. 12.

[4]J. G. Malm and S. Fried, Separation of Protactinium from Contaminants, U. S. Patent 2,893,825, July 7, 1959.

[5]A. J. Shor and E. L. Compere, Reactor Chemistry Div. Ann. Progr. Rept. Jan. 31, 1964, ORNL-3591, pp. 56–58.

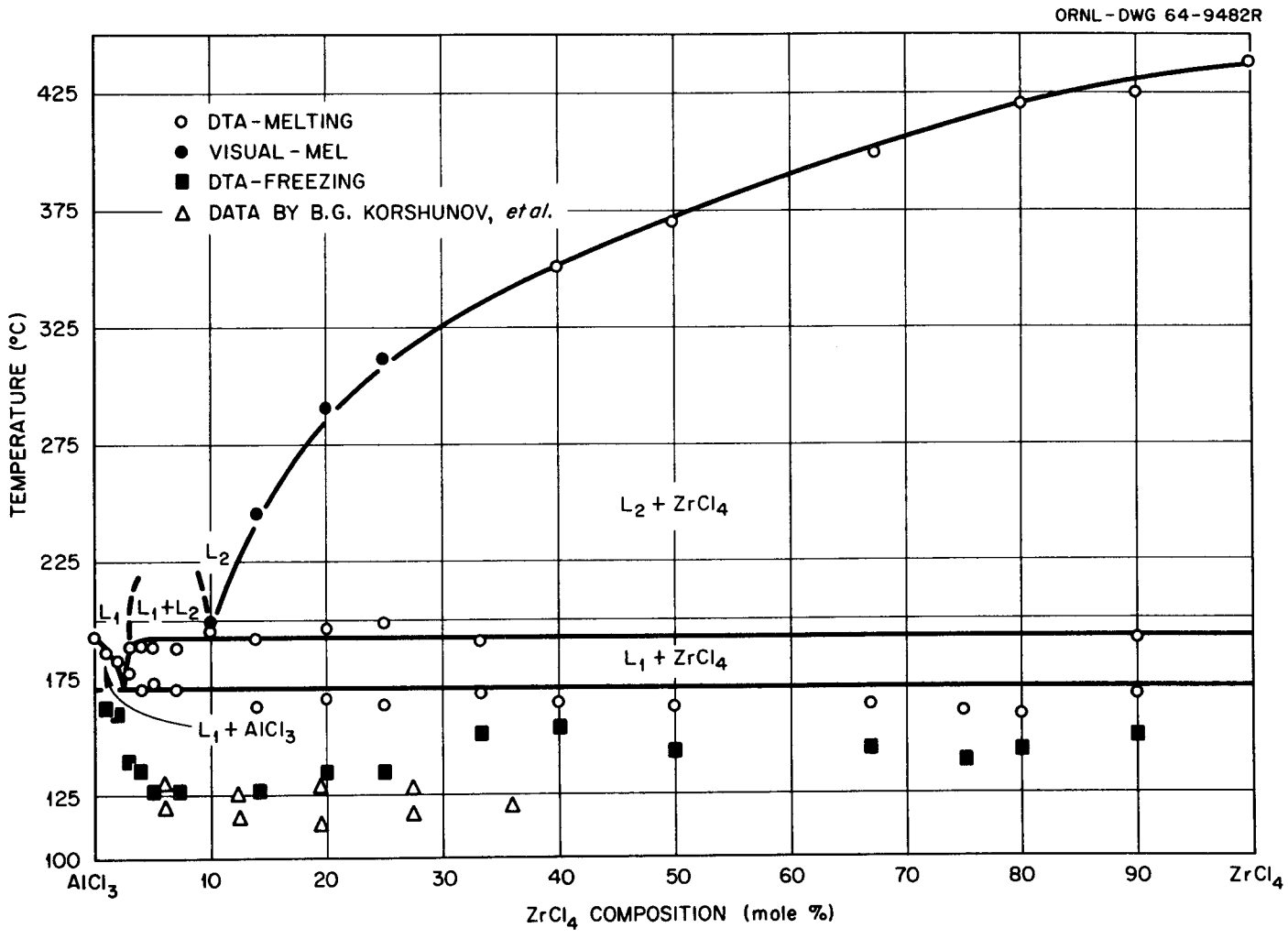

Fig. 4.5. Preliminary Phase Diagram, $AlCl_3$-$ZrCl_4$ System. Ref: B. G. Korshunov, A. M. Reznik, and I. S. Morozov, Tr. Mosk. Inst. Tonkoi Khim. Teknol. 7, 127 (1958).

steepness of the liquidus curve in this range. Direct visual observations of eutectic and monotectic temperatures on heating were obscure and difficult to reproduce. Differential thermal analysis data are shown for those transitions. Data obtained on cooling are shown as solid squares. Supercooling effects on the freezing point of the eutectic mixture are readily apparent. At $ZrCl_4$ concentrations greater than approximately 33%, supercooling of the liquidus transitions was relatively small. Throughout the entire range of concentrations supercooling of the monotectic and eutectic compositions ranged from 10 to 50°C. However, the sharp drop in the melting point of mixtures in the $AlCl_3$-rich side of the eutectic composition and the possibility that the existence of the monotectic may be an artifact has led to several alternative interpretations of the data. These are still under consideration and will be discussed in future reports.

Sparse data reported by B. G. Korshunov et al.[6] for the $AlCl_3$-$ZrCl_4$ system are also shown in Fig. 4.5 as triangles. These parallel cooling data obtained in our studies by thermal analysis which represent supercooled freezing temperatures in the binary liquid mixtures.

In the region of approximately 10 to 100 mole % $ZrCl_4$, complete miscibility of the liquid mixture is postulated, while in the region of approximately 3 to 10 mole % $ZrCl_4$ a narrow two-phase section is shown with a monotectic composition of 10% $ZrCl_4$ at 192°C. An $AlCl_3$-$ZrCl_4$ eutectic is postulated at approximately 2.5% $ZrCl_4$ and 170°C. Table 4.4 lists the data from which the curves are derived together with notes on the observations. The phase diagram appears to be consistent with the trend of data reported in other investigations of binary systems containing $AlCl_3$. For example, the presence of a eutectic of high percentage $AlCl_3$, the sharp initial rise of the liquidus curve, and the presence of two liquid phases appear to be characteristic of a number of such systems.[7]

---

[6]B. G. Korshunov, A. M. Reznik, and I. S. Morozov, "Thermal and Tensimetric Study of $AlCl_3$-$ZrCl_4$ and NaCl Systems," Tr. Mosk. Inst. Tonkoi Khim. Teknol. 7, 127 (1958).

[7]I. N. Belyaev, "The Formation of Two Liquid Phases in Inorganic Systems," Russ. Chem. Rev. (English Transl.) 29, 428 (1960).

Table 4.4. Melting and Freezing Point Temperatures of the $ZrCl_4$-$AlCl_3$ Binary Phase System

Mole % $ZrCl_4$	Transition Temperatures on Heatup, °C			Transition Temperatures on Cooldown, °C	
	I	II	Liquidus	I and II	Liquidus
100			437		435
90	167	191	425	150 (a)	420
80	159		419	144	417
75	160			139	396
67	163		399	144	396
50	162		369	143	366
40	166		350	154 (a)	
33	168	191 (b)	320 (a)	150	317
25	164	198	312 (c)	135	262
20	167	193	291 (c)	130	234
14	163	192	245 (c)	125	
10	170	192	194 (c)	120	
7	170	187 (b)		125	
5	172	188 (b)		127	
4	171	190 (b)		132	
3	178	188 (b)		135	
2	183			160	
1	185			162	
100% $AlCl_3$	193			183	

[a] Vague transition.

[b] Poor resolution of second peak.

[c] By direct visual observation.

Thermodynamic activities of $ZrCl_4$ as a function of temperature were calculated for the $ZrCl_4$-rich part of the phase diagram. Assumptions of constancy of heat capacity and partial molar heat of solution were made in these calculations. Activities were compared to the corresponding concentrations in mole fraction units in two ways: first, as a mixture with dimeric $(AlCl_3)_2$ which is the usual state of the pure liquid; and secondly, as a mixture with monomeric $AlCl_3$. It was found that from about 33 to 100 mole % $ZrCl_4$, the $ZrCl_4$ liquidus curve showed apparent ideal behavior based on a model of a solution of monomeric $AlCl_3$ and $ZrCl_4$.

$AlCl_3$-$ThCl_4$ Phase Studies

Investigation[8] of the $AlCl_3$-$ThCl_4$ system by thermal methods and by direct observation of melting and freezing for concentrations of 100, 90, 75, 50, 25, and 10 mole % $ThCl_4$ in $AlCl_3$ showed no indication of mutual solubility. Some recent Russian work[9] has also suggested that the solubility of $ThCl_4$ in $AlCl_3$ should be much below 10 mole %.

Direct measurement of the solubility of $ThCl_4$ in liquid $AlCl_3$ was obtained by equilibrating 10 mole % mixtures of $ThCl_4$ in $AlCl_3$ at constant temperature. The $ThCl_4$ was separated by settling at temperature, and the system was rapidly frozen. The $AlCl_3$-rich phase was analyzed for thorium content. Measurements were conducted at five temperatures with the following results:

Temperature, °C	210	215	250	300	350
Solubility, mole % $ThCl_4$	0.98	0.96	1.01	0.85	0.88

The solubility over this range is regarded as constant at 1 mole % $ThCl_4$ in $AlCl_3$.

---

[8] A. J. Shor and E. L. Compere, Reactor Chemistry Div. Ann. Progr. Rept. Jan. 31, 1964, ORNL-3591, pp. 56–58.

[9] B. G. Korshunov, V. I. Ionov, T. A. Baklashova, and V. V. Kokorev, "Reaction of Th Chloride with Chlorides of Mg, Ca, Ce, Al, Fe, Nb, and Nb Oxychloride," Izv. Vysshikh. Uchebn. Zavedenii, Tsvetn. Met. 6, 114 (1960).

Protactinium-233 Tracer Experiments

Tracer quantities (2 to 30 μc) of ^{233}Pa were generated in selected mixtures of $ThCl_4$ and $AlCl_3$ by thermal neutron irradiation in the Oak Ridge Research Reactor pool. The salts were contained in an evacuated 9-mm-ID quartz tube, divided into two sections joined by a short 4-mm-ID neck. The tube was sealed under vacuum while the body of the tube was immersed in liquid nitrogen to prevent escape of volatile salts. During attempts to distill the protactinium, the shorter 75-mm region of the tube was used as the salt container section while the longer 125-mm section served generally as the receiver section. In some cases a loose quartz wool plug was placed in the neck section to prevent physical carry over of material.

The relative distribution of protactinium after distillation was measured by moving the quartz tube in 1-cm steps past a slit (approx 1 cm) between two sections of lead shielding, and determining with a G-M tube the collimated radiation.

Starting salt compositions, consisting of 100, 50, 10, and 0.5 mole % $ThCl_4$ in $AlCl_3$ were distilled at salt temperatures ranging from 160 to 275°C. Results are summarized in Table 4.5.

No transfer of protactinium activity to an air-cooled receiver was observed when heating pure $ThCl_4$ or a salt mixture containing 50 mole % $ThCl_4$ in $AlCl_3$ to temperatures as high as 275°C for periods up to 46 hr. With the mixtures containing substantially more $AlCl_3$, an appreciable fraction of the protactinium activity was transferred when the $AlCl_3$ was distilled under these conditions. The retention of the protactinium when 50 mole % $AlCl_3$ or less was used may have been due to retention of protactinium in the interior of the $ThCl_4$ grains or to strong adsorption of protactinium from $AlCl_3$ solution on the relatively abundant surface of the solid $ThCl_4$. Evidence below supports the latter view.

At concentrations of 10 mole % $ThCl_4$ in $AlCl_3$, from 10 to 90% of the protactinium was transferred when one end of tubes containing salt mixtures was heated in the temperature range of 160 to 260°C for 2 to 7 hr and the $AlCl_3$ distilled to the receiver end. The volatilization of such proportions of protactinium, when only 1 mole % $ThCl_4$

Table 4.5. Protactinium-233 Volatilization Experiments with Tubes Containing Irradiated $ThCl_4$-$AlCl_3$ Mixtures

Tube Number	$ThCl_4$ in $AlCl_3$ Mixture (mole %)	Quartz Fiber Filter Present	Time Heated (hr)	Temperature, °C		^{233}Pa Found in "Original Receiver" Region[a] (%)	$AlCl_3$ Found in Receiver Region (%)	Comments
				Original Mixture Region	Original Receiver Region			
3	100	Yes	46	250	60	None		
7	50	Yes	7	275	95	None	All	
9	10	Yes	7	160	55	10	All	
10	10	No	4	212	37	30	All	
11	10	Yes	4	208	32	50	All	
8	10	Yes	4	220	350[d]	90	All	Mostly on quartz fiber
13	0.5	No	4	267	35	40	All	
17	0.5	(b)	4	200	203[d]	45	All	Mostly on quartz fiber in receiver
17	0.5	(b)	4	60	205	45	All	Attempt to transfer back was ineffective
16	0.5	(c)	4	202	60	0	All	Quartz fiber in original mixture
15	0.5	No	1/3	215	60	9.5	56	Quartz container
T 29	0.5	No	1/2	256	118	33	All	Teflon capsule
T 29	0.5	No	2 1/2	267	95	28	All	Teflon capsule

[a]Based on integrated count of entire tube including the material found on "receiver" side of filter at constriction between regions.

[b]Quartz wool in receiver only.

[c]Quartz wool in original mixture only.

[d]Maximum temperature of receiver region. Distillation of $AlCl_3$ doubtless occurred during cooldown, apparently more rapid in receiver.

is soluble in $AlCl_3$, implies that protactinium was leached to a substantial degree from $ThCl_4$ grains, and then volatilized with $AlCl_3$.

The fraction transferred seems substantially affected by adsorption phenomena including an affinity of protactinium for quartz fiber, for $ThCl_4$, and possibly for the quartz tube.

This phenomenon might be the basis of a protactinium separation process; some pertinent observations follow.

In distillation experiments involving 10 mole % $ThCl_4$, the use of quartz fiber in the neck region appeared to result in greater protactinium transfer (Table 4.5). Without the quartz wool 30% of the protactinium was transferred; with quartz wool present 50% was transferred, and a large part of the activity was found in the region of the quartz. With the quartz at high temperature for a time, an even greater quantity was transferred; this material remained fixed to the quartz.

In experiments with 0.5 mole % $ThCl_4$ in $AlCl_3$ in which quartz wool was placed entirely in the receiver region, distillation at 200°C transferred 45% of the protactinium irreversibly to this region. In another experiment, quartz wool in the original mixture region prevented the distillation of protactinium under similar conditions. Though confirmatory experiments (such as percolation) were not included in the present program, it is implied that quartz wool might serve as an effective adsorbent for protactinium from aluminum chloride in either liquid or vapor phase.

Nickel distillation tubes retained protactinium more strongly than did quartz. Most of the retained protactinium was recovered by leaching the nickel with dilute nitric acid or with hydrogen fluoride solution. Some reaction of the salt mixture with nickel seems to have occurred; the salt was found to contain about 200 ppm Ni after the experiment.

In order to study the protactinium volatility phenomena with as little interference as possible from adsorption, two distillations were conducted in mechanically sealed Teflon tubes. Thorium chloride concentrations of 0.5 mole % were used in order to have initially the materials entirely in solution. Distillation of 0.5 mole % $ThCl_4$-$AlCl_3$

mixtures contained in the Teflon tubes in the presence of helium atmosphere (dry glove box ambient) resulted in the transfer of 33% of the protactinium. A reverse distillation of the $AlCl_3$ (not shown in Table 4.5) transferred all of the activity back to the original region. Subsequent redistillation transferred 28% of the protactinium activity to the receiver. Complete transfer in the back distillation implies no interaction between Teflon and protactinium. If this is accepted then the lack of complete forward transfer must be interpreted as being due to the presence of $ThCl_4$. This, in turn, probably indicates adsorption of protactinium on precipitated $ThCl_4$, though complexing with $ThCl_4$ dissolved in the liquid $AlCl_3$ is also possible.

APPENDIX A

Thorium-to-Uranium Ratios and Gas-Release Values Obtained for Every Sol-Gel Batch Prepared During Kilorod Program

Sol-Gel Batch Number (SGB-1)	^{233}U-to-(Th + ^{233}U) Ratio by Analysis	Gas[a] Released (std cm^3/g)	Sol-Gel Batch Number (SGB)	^{233}U-to-(Th + ^{233}U) Ratio by Analysis	Gas Released (std cm^3/g)
Campaign 1					
1 A	2.92	0.018	8 A	2.88	0.038
2 A	3.02	0.013	B	2.92	
B	3.01		C	2.92	
3 A	2.99	0.013	9 A	2.99	0.015
B	3.01		B	3.00	
C	3.01		10 A	3.15	0.034
4 A	3.04	0.004	B	3.07	
B	3.05		C	3.11	
C	3.19		D	3.15	
5 A	2.91		11 A	2.93	0.031
6 A	2.94	0.013	B	2.91	
B		0.018	12 A	2.92	0.038
7 A	2.95	0.005			
Campaign 2					
13 A	2.98	0.050	21 A	3.02	0.021
14 A	3.02	0.019	B	3.01	0.022
15 A	3.03	0.038	22 A	2.94	0.043
16 A	3.03	0.054	23 A	2.99	0.026
17 A	2.94	0.016	24 A	3.01	0.013
B	3.01	0.018	25 A	3.04	0.008
18 A	3.00	0.005	26 A	3.07	0.022
B	3.03		B	3.03	
19 A	3.08	0.010	27 A	3.02	0.010
20 A	3.07	0.036	28 A	3.03	0.033
Campaign 3					
29 A	3.00	0.013	35 A	3.00	0.013
30 A	3.05	0.017	36 A	3.01	0.015
31 A	3.10	0.016	37 A	2.96	0.011
B	3.02		38 A	2.98	0.014
32 A	2.95	0.025	39 A	3.07	0.007
33 A	3.01	0.013	B	3.06	
34 A	2.99	0.020	40 A	3.00	0.012
Campaign 5					
41 A	2.94	0.010	47 A	3.01	0.011
B	2.94		48 A	2.96	0.031
42 A	3.01	0.012	49 A	3.05	0.015
43 A	3.02	0.018	50 A	2.99	0.042
44 A	2.97	0.019	51 A	3.02	0.040
44 B	2.98		52 A	2.98	
45 A	3.02	0.010	53 A	3.09	0.039
B	3.00		B	3.05	
46 A	2.95	0.015			
Campaign 6					
54 A	3.02	0.030	65 A	3.00	0.015
55 A	2.95	0.053	66 A	3.00	0.018
56 A	2.96	0.025	67 A	2.96	0.014
57 A	2.99	0.009	68 A	3.00	0.004
58 A	3.00	0.018	69 A	3.01	0.016
59 A	3.01	0.057	70 A	3.00	0.006
60 A	2.99	0.048	71 A	3.05	0.057
61 A	3.01	0.012	72 A	3.02	0.008
62 A	2.87	0.056	73 A	3.04	0.006
B	2.95		74 A	2.99	0.004
63 A	2.96	0.004	75 A	3.04	0.010
64 A	2.97	0.035	76 A	3.00	0.011
Campaign 7					
77 A	2.93	0.007	92 A	2.95	0.008
B	2.94		93 A	3.04	0.010
78 A	2.99	0.005	94 A	3.05	0.034
79 A	2.95	0.015	B	2.96	
80 A	3.02	0.005	C	2.94	
81 A	3.04	0.019	D	2.97	
82 A	3.00	0.009	95 A	2.95	0.027
83 A	2.93	0.022	B	3.00	
B	2.92		C	2.98	
84 A	2.97	Sample lost	D	2.98	
B	2.94		96 A	2.97	0.071[b]
85 A	3.03	0.008	B	2.96	
86 A	2.98	0.007	97 A	2.95	0.103[b]
87 A	3.03	0.003	B	2.93	
88 A	2.98	0.006	98 A	2.98	0.075[b]
89 A	2.97	0.004	99 A	3.01	0.025
90 A	2.96	0.020	100 A	3.06	0.020
91 A	2.95	0.004	B	3.06	

[a]Obtained by heating sample to 1200°C in vacuum.

[b]Off-gas upset due to furnace test.

ORNL-3831
UC-25 – Metals, Ceramics, and Materials

INTERNAL DISTRIBUTION

1. Biology Library
2–4. Central Research Library
5. Reactor Division Library
6–7. ORNL – Y-12 Technical Library Document Reference Section
8–27. Laboratory Records Department
28. Laboratory Records, ORNL R.C.
29. ORNL Patent Office
30. J. W. Anderson
31. S. E. Beall
32. R. E. Blanco
33. A. L. Boch
34. W. D. Bond
35. G. E. Boyd
36. R. E. Brooksbank
37. K. B. Brown
38. F. R. Bruce
39. W. D. Burch
40. J. M. Chandler
41. S. D. Clinton
42. E. L. Compere
43. F. L. Culler
44. J. E. Cunningham
45. H. P. Danforth
46. F. C. Davis
47. D. A. Douglas, Jr.
48. W. S. Ernst, Jr.
49. D. E. Ferguson
50. L. M. Ferris
51. R. B. Fitts
52. H. A. Friedman
53. J. H Frye, Jr.
54. T. A. Gens
55. H. E. Goeller
56. A. T. Gresky
57. J. C. Griess
58. W. R. Grimes
59. P. A. Haas
60. J. P. Hammond
61. R. L. Hamner
62. W. O. Harms
63. C. C. Haws
64. D. N. Hess
65. M. R. Hill
66. F. J. Hurst
67. A. R. Irvine
68. J. P. Jarvis
69. M. T. Kelley
70. M. J. Kelly
71. A. T. Kleinsteuber
72. C. E. Larson (K-25)
73. R. E. Leuze
74. A. W. Longest
75. A. L. Lotts
76. H. G. MacPherson
77. J. L. Matherne
78. J. P. McBride
79. K. H. McCorkle
80. H. F. McDuffie
81. J. R. McWherter
82. A. B. Meservey
83. F. W. Miles
84. E. C. Miller
85. C. S. Morgan
86. E. L. Nicholson
87. A. R. Olsen
88. J. R. Parrott
89. F. L. Peishel
90. J. J. Perona
91. R. L. Pilloton
92. R. B. Pratt
93. P. E. Reagan
94. J. M. Robbins
95. J. T. Roberts
96. M. W. Rosenthal
97. J. L. Scott
98. H. E. Seagren
99. J. D. Sease
100. C. H. Secoy
101. R. J. Shannon
102. W. A. Shannon
103. D. M. Shepherd
104. A. J. Shor
105. J. W. Snider
106. B. A. Soldano
107. D. B. Trauger

108. J. W. Ullmann
109. J. E. Van Cleve, Jr.
110. J. T. Venard
111. A. M. Weinberg
112. W. J. Werner
113. M. E. Whatley
114. R. G. Wymer
115. G. Young
116. P. H. Emmett (consultant)
117. J. J. Katz (consultant)
118. C.W.J. Wende (consultant)
119. C. E. Winters (consultant)
120. M. B. Bever (consultant)
121. T. A. Read (consultant)
122. J. A. Krumhansl (consultant)
123. A. R. Kaufmann (consultant)

EXTERNAL DISTRIBUTION

124. A. J. Alexander, AEC, Hartford Operations Office
125–126. D. F. Cope, AEC, Oak Ridge Operations Office
127. W. J. Larkin, AEC, Oak Ridge Operations Office
128. R. L. Morgan, AEC, Savannah River Operations
129. R. E. Pahler, AEC, Washington
130. C. W. Richards, AEC, Atomics International, Canoga, Park, California
131. C. L. Storrs, Atomics International, Canoga Park, California
132. W. M. Vannoy, Babcock and Wilcox, Lynchburg, Virginia
133. R. P. Varnes, Combustion Engineering, Windsor, Connecticut
134. Research and Development Division, AEC, ORO
135–450. Given distribution as shown in TID-4500 under Metals, Ceramics, and Materials category (75 copies – CFSTI)